

THE UNIVERSITY OF READING



School of Biological Sciences

**Reptarenavirus prevalence in reptiles sampled in
the UK and related studies**

**A thesis submitted for the degree of Doctor of Philosophy in
microbial sciences**

By

Hasan Alrashedi

**Supervisors: Prof. Ian M. Jones
Dr Geraldine Mulley
Dr Benjamin W. Neuman**

Reading, UK

June 2019

Declaration

I confirm that this is my own work and the use of all material from other sources has been properly and fully acknowledged.

Hasan Alrashedi

Abstract

Arenaviruses are enveloped RNA viruses with a genome of two segments of single stranded RNA which is classified as ambisense in its coding strategy. Arenaviruses within the *Reptarenavirus* genus infect many species of snake and are associated with inclusion body disease (IBD). Reptarenavirus infection of humans has not been reported. In this thesis molecular techniques were utilized for RNA analysis and gene amplification by reverse transcription PCR (RT-PCR) in order to find evidence of reptarenavirus sequences in reptilian samples. Total RNAs were isolated from frozen specimens of snakes and other reptiles followed by an evaluation of RNA integrity. Degenerate primers of ribosomal mitochondrial and reptarenavirus genes were used for quality control of the RNA and for identification of virus sequence respectively, and then the results were confirmed by Sanger sequencing. The mitochondrial RNA was successfully amplified, whereas no reptarenavirus sequences were found in the samples screened. Spiking experiments determined that the cut-off for detection was less than 10^8 copies of virus RNA per sample. Although no evidence for the circulation of reptarenaviruses was found the study serves as a guide for reptarenavirus investigations using the RT-PCR technique in cases where new samples are suspected of having been infected with an existing or novel reptarenavirus.

In addition, a related study investigating the role of replication organelles in the pathogenicity of infectious bronchitis virus (IBV) was performed using Transmission Electron Microscopy (TEM) of infected cells. Further, an assessment was made of the use of the arenavirus L sequence to look for related sequences associated with

currently unknown viruses in the TSA database. Several matches were found which, along with a reasoned approach to their phyla, was used to provide a likelihood score of their zoonotic potential.

Acknowledgments

I would like to acknowledge University of Reading for its support during my academic study. My warmest gratitude to my supervisor Prof. Ian M. Jones for his guidance and support, my thanks also to the second supervisor, Dr Geraldine Mulley and to the external supervisor Dr Benjamin W. Neuman for their support.

My thanks also to Mrs Susie Pritchard and Mr Ross Hayes from quarantine department at Heathrow Animal Reception Centre (HARC) and additional thanks to Mr Edmund Flach and Miss Tilly Dallas at Zoological Society of London (ZSL) at London Zoo for supplying frozen specimens.

I would also like to thank Dr Jussi Hepojoki at University of Helsinki for providing UHV samples. Many thanks to Dr Helena Maier from the Pirbright Institute, UK for providing coronavirus specimens and for her collaboration. Thanks to Dr Peter Harris and Miss Amanipreet Kaur for training me in using the Microtome and Electron Microscope. I am also grateful to the technical staff working in the Knight building at the University of Reading for their assistance during my research.

Finally, I would like to acknowledge Iraqi Ministry of Higher Education and Scientific Researches for sponsorship and Iraqi Culture attaché in London for sponsorship and funding.

Publications and conference presentations

1. Papers:

- Extensive coronavirus-induced membrane rearrangements are not a determinant of pathogenicity

Scientific Reports, volume 6, issue 1, published online 2016

- Infectious Bronchitis Virus Nonstructural Protein 4 Alone Induces Membrane Pairing

Viruses, volume 10, issue 9, published online 2018

- Bioinformatics analysis for L polymerase homology of arenaviruses

Submitted to bioRxiv, 2019

2. 6th European Congress of Virology (ECV2016) from 19-22 October 2016 in Hamburg, Germany.

Poster title: Universal primers to detect emerging reptarenaviruses.

3. Translational Bioinformatics conference from Jun 12, 2017 through Jun 13, 2017. Hosted by Wellcome Genome Campus Advanced Courses and Scientific Conferences, Hinxton, Cambridge, United Kingdom.

Poster title: Bioinformatics for novel arenaviruses.

4. Iraqi Environment and Health Society-UK (IEHS-UK), Degradation of the Environment in Iraq and its Impact on Public Health conference, 18th February 2018, University College London (UCL), London, United Kingdom.

Poster title: Nested Reverse Transcription-PCR for the detection of viral RNA in post mortem snake tissue.

Table of Contents

DECLARATION.....	2
ABSTRACT.....	3
ACKNOWLEDGMENTS.....	5
PUBLICATIONS AND CONFERENCE PRESENTATIONS.....	6
TABLE OF CONTENTS	7
INDEX OF FIGURES	10
INDEX OF TABLES.....	13
ABBREVIATIONS	15
CHAPTER 1 INTRODUCTION.....	18
1.1 TAXONOMY AND PHYLOGENETIC RELATIONSHIPS OF ARENAVIRUS	18
1.2 MOLECULAR BIOLOGY OF ARENAVIRUS.....	21
1.2.1 <i>Physical characteristics of arenavirus</i>	21
1.2.2 <i>Genome organization and replication of arenavirus</i>	23
1.3 ARENAVIRUS PROTEINS	26
1.4 ARENAVIRUS LIFE CYCLE	30
1.4.1 <i>Receptors of the arenavirus</i>	30
1.4.2 <i>Arenavirus entry proteins</i>	34
1.4.3 <i>Arenavirus budding</i>	36
1.5 THE ROLE OF INTERFERON ANTAGONISTS IN ARENAVIRUS INFECTION	40
1.6 EPIDEMIOLOGY OF ARENAVIRUS.....	42
1.1 PATHOGENESIS AND INCLUSION BODY DISEASE OF SNAKE REPTARENAVIRUS	50
1.2 CLINICAL DETECTION OF ARENAVIRUS.....	52
1.3 INHIBITION OF ARENAVIRUS REPLICATION AND ANTIVIRAL THERAPEUTICS.....	55
1.4 SNAKE AND OTHER REPTILIAN VIRUSES	57
1.4.1 <i>Herpesviridae</i>	57
1.4.2 <i>Iridoviridae</i>	59
1.4.2.1 <i>Ranavirus</i>	59
1.4.2.2 <i>Erythrocytic virus</i>	60
1.4.2.3 <i>Iridovirus</i>	60
1.4.3 <i>Poxviridae</i>	61
1.4.4 <i>Adenoviridae</i>	62
1.4.5 <i>Papillomaviridae</i>	62
1.4.6 <i>Parvoviridae</i>	63
1.4.7 <i>Reoviridae</i>	64
1.4.8 <i>Retroviridae and inclusion body disease of boid snakes</i>	64
1.4.9 <i>Arboviruses</i>	65
1.4.9.1 <i>Flaviviridae</i>	66
1.4.9.2 <i>Togaviridae</i>	66
1.4.10 <i>Caliciviridae</i>	67
1.4.11 <i>Picornaviridae</i>	68
1.4.12 <i>Paramyxoviridae</i>	68
CHAPTER 2 MATERIALS AND METHODS.....	71
2.1 OLIGONUCLEOTIDE PRIMER DESIGN	71
2.1.1 <i>Degenerate primers for reptarenavirus proteins</i>	71
2.1.2 <i>Infusion degenerate primers for L polymerase of reptarenavirus</i>	74
2.1.3 <i>Universal primers of ribosomal mitochondrial genes</i>	75
2.2 BUFFERS AND SOLUTIONS	77

2.2.1	<i>Tris-acetate-EDTA (TAE) buffer</i>	77
2.2.2	<i>HEPES and sodium cacodylate buffers</i>	78
2.2.3	<i>Tissue preservation reagent</i>	78
2.3	PLASMIDS AND BACTERIAL STRAINS	79
2.3.1	<i>Plasmids</i>	79
2.3.2	<i>Bacterial strains</i>	79
2.4	ANTIBIOTICS	80
2.5	LURIA BERTANI (LB) AGAR AND BROTH	80
2.6	COMPLEMENTARY DNA (cDNA) AMPLIFICATION OF REPTARENAVIRUS	80
2.7	AGAROSE GEL ELECTROPHORESIS	81
2.8	PCR PURIFICATION AND GEL EXTRACTION	82
2.9	CLONING L POLYMERASE GENES OF UHV INTO pTriEx 1.1 PLASMID VECTOR.....	83
2.9.1	<i>Linearization of pTriEx 1.1 plasmid by restriction digestion</i>	83
2.9.2	<i>PCR amplification of L polymerase from UHV</i>	84
2.9.3	<i>Cloning the UHV L polymerase PCR products into pTriEx 1.1</i>	85
2.10	TRANSFORMATION OF UHV PLASMIDS INTO COMPETENT CELL (<i>E. COLI</i>)	85
2.10.1	<i>Colony PCR (cPCR) of transformants</i>	86
2.10.2	<i>Purification of DNA plasmids</i>	87
2.10.3	<i>Storage of bacterial strain with cloned plasmids</i>	87
2.11	DNA SANGER SEQUENCING	87
2.12	RNA EXTRACTION AND ANALYSIS	88
2.12.1	<i>Reptiles specimens</i>	88
2.12.2	<i>Total RNA extraction</i>	88
2.12.3	<i>Total RNA integrity</i>	89
2.13	REVERSE TRANSCRIPTION PCR (RT-PCR).....	90
2.13.1	<i>Reverse transcription of RNA</i>	90
2.13.2	<i>Detection of specific reptile mitochondrial and reptarenavirus genes by RT-PCR</i>	91
2.14	BIOINFORMATIC ANALYSIS OF L POLYMERASE OF ARENAVIRUSES.....	92
2.14.1	<i>Obtaining L polymerase sequences in GenBank database</i>	92
2.14.2	<i>Identification of open reading frames (ORFs)</i>	93
2.14.3	<i>Protein homology and structure prediction</i>	94
2.14.4	<i>Sequence analysis</i>	94
2.15	FIXATION AND RESIN EMBEDDING OF THE INFECTIOUS BRONCHITIS VIRUS (IBV) SPECIMENS	95
2.15.1	<i>Fixation of IBV specimens</i>	95
2.15.2	<i>Washing of IBV specimens</i>	95
2.15.3	<i>Dehydration of IBV specimens</i>	96
2.15.4	<i>Infiltration of IBV specimens</i>	97
2.15.5	<i>Embedding of IBV specimens</i>	98
2.15.6	<i>Sectioning of embedded IBV specimens by Ultramicrotome</i>	98
2.15.7	<i>Transmission Electron Microscopy (TEM)</i>	99
CHAPTER 3	DESIGN AND VALIDATION OF REPTARENAVIRUS DETECTION PRIMERS.....	100
3.1	INTRODUCTION	100
3.2	RESULTS	104
3.2.1	<i>Protein sequence-based degenerate primer design</i>	104
3.2.2	<i>Identity among proteins of novel snake reptarenavirus</i>	108
3.2.3	<i>Validation of reptarenavirus primers</i>	110
3.2.3.1	Amplification of L polymerase and NP genes from UHV	110
3.2.3.2	Primer test of Z and GPC genes of UHV	112
3.2.4	<i>Transformation of pNP, pZ and pGP of UHV</i>	114
3.2.5	<i>L polymerase gene cloning of UHV</i>	116
3.2.5.1	Digestion of pTriEx 1.1 plasmid.....	116
3.2.5.2	High Fidelity PCR of L polymerase genes of UHV.....	118
3.2.5.3	L polymerase gene cloning and transformation of UHV.....	119
3.2.6	<i>Bioinformatics analysis of University of Helsinki virus (UHV)</i>	122
3.2.6.1	Analysis of University of Helsinki virus (UHV) sequences	122
3.2.6.2	Amplicon alignment of University of Helsinki virus (UHV).....	123

3.2.7	<i>Cloning maps of University of Helsinki virus (UHV)</i>	129
3.3	DISCUSSION.....	134
CHAPTER 4	SPECIMEN PROVENANCE, DISSECTION AND SAMPLE PREPARATION.....	136
4.1	INTRODUCTION	136
4.2	RESULTS	138
4.2.1	<i>Reptile provenance</i>	138
4.2.2	<i>Reptile dissection</i>	140
4.2.2.1	Snake dissection	140
4.2.2.2	Turtle and tortoise dissection	142
4.2.2.3	Chameleons dissection	144
4.2.2.4	Other reptile dissected	145
4.2.3	<i>Internal tissue provenance</i>	146
4.3	DISCUSSION.....	148
CHAPTER 5	TOTAL RNA ANALYSIS AND REVERSE TRANSCRIPTION PCR (RT-PCR) FOR REPTARENAVIRUS'S SEQUENCES	150
5.1	INTRODUCTION	150
5.2	RESULTS	151
5.2.1	<i>RNA extraction</i>	151
5.2.2	<i>Total RNA integrity</i>	152
5.2.3	<i>Reverse transcription for complementary DNA (cDNA) synthesis</i>	156
5.2.4	<i>Identification of mitochondrial 12S and 16S rRNAs genes</i>	160
5.2.5	<i>L polymerase and NP amplification for the presence of reptarenavirus sequences</i>	164
5.3	DISCUSSION.....	170
CHAPTER 6	DISCUSSION AND FUTURE DIRECTION	172
APPENDIX ONE: PUBLISHED PAPERS		177
REFERENCES		260

Index of Figures

Figure 1.1: Phylogenetic analysis of reptarenavirus species in snakes associated with inclusion body disease.	20
Figure 1.2: Arenavirus structure	22
Figure 1.3: Electron microscopy of snake reptarenavirus	23
Figure 1.4: Arenavirus genome structure	25
Figure 1.5: Arenavirus genome replication and gene transcription.....	26
Figure 1.6: Arenavirus proteins interactions.....	30
Figure 1.7: Arenavirus receptors TfR1 and α -DG... ..	34
Figure 1.8: Role of the ESCRT pathway in arenavirus replication.. ..	38
Figure 1.9: Arenavirus budding from infected target cell.....	40
Figure 1.10: The multiple roles of arenavirus Z protein, including interferon antagonism.	42
Figure 1.11: Reptarenavirus antigens of boid inclusion body disease (BIBD) in liver tissue of boid snakes.. ..	52
Figure 2.1: Molecular weight marker, HyperLadder 1kb (Bioline).	82
Figure 2.2: Map of the pTriEx 1.1 vector.....	84
Figure 3.1: Sites of proposed degenerate primers for reptarenavirus.....	108
Figure 3.2: Identity among snake reptarenavirus protein coding regions.. ..	109
Figure 3.3: Gel electrophoresis of L polymerase and NP genes of UHV	111
Figure 3.4: Gel electrophoresis of zinc finger motif protein (Z) and glycoprotein precursor (GPC) genes of UHV	113
Figure 3.5: Gel electrophoresis of NP insert of UHV in pNP amplified by colony PCR	115

Figure 3.6: Gel electrophoresis of Z insert of UHV in pZ amplified by colony PCR ..	115
Figure 3.7: Gel electrophoresis of GP insert of UHV in pGP amplified by colony PCR ..	116
Figure 3.8: Agarose gel of digested pTriEx 1.1 plasmid..	117
Figure 3.9: High Fidelity PCR of L polymerase genes of UHV.....	119
Figure 3.10: Colony PCR of L1 insert of UHV in pL1.....	120
Figure 3.11: Colony PCR of L2 and L3 inserts of UHV in pL2 and pL3 respectively ..	121
Figure 3.12: Alignment of L polymerase fragments of University of Helsinki virus (UHV)..	126
Figure 3.13: Alignment of Z protein fragment of University of Helsinki virus (UHV)..	127
Figure 3.14: Alignment of NP fragment of University of Helsinki virus (UHV).....	127
Figure 3.15: Alignment of GPC fragment of University of Helsinki virus (UHV)..	128
Figure 3.16: Cloning map of L1 fragment of University of Helsinki virus (UHV)..	129
Figure 3.17: Cloning map of L2 fragment of University of Helsinki virus (UHV)..	130
Figure 3.18: Cloning map of L3 fragment of University of Helsinki virus (UHV)..	131
Figure 3.19: Cloning map of Z fragment of University of Helsinki virus (UHV)..	132
Figure 3.20: Cloning map of NP fragment (NP2) of University of Helsinki virus (UHV)..	133
Figure 3.21: Cloning map of GP fragment of University of Helsinki virus (UHV)..	134
Figure 4.1: Dissection of royal python (<i>Python regius</i>) also known as ball python.	141

Figure 4.2: Dissection of Oachita map turtle (<i>Graptemys ouachitensis</i>)..	143
Figure 4.3: Dissection of <i>Chameleon</i> spp..	144
Figure 5.1: Electropherograms of total (eukaryotic) RNAs of snakes	154
Figure 5.2: Gel-like electrophoresis of total RNA (eukaryotic) of snakes showing ribosomal 18S and 28S rRNA subunits.	156
Figure 5.3: Reverse transcription PCR of UHV. A first RT reaction was done with random hexamer primers..	158
Figure 5.4: Gel electrophoresis for determination of the viral load of reptarenavirus by RT-PCR.....	160
Figure 5.5: Mitochondrial 12S rRNA amplification from snake RNA samples.....	162
Figure 5.6: Mitochondrial 16S rRNA amplification from snake RNA samples.....	162
Figure 5.7: Mitochondrial 12S rRNA amplification from reptilian RNA samples..	163
Figure 5.8: Mitochondrial 16S rRNA amplification from reptilian RNA samples..	163
Figure 5.9: Gel electrophoresis of RT-PCR of L polymerase gene (L1)..	165
Figure 5.10: Gel electrophoresis of RT-PCR of L polymerase gene (L1)..	165
Figure 5.11: Gel electrophoresis of RT-PCR of L polymerase gene (L2)..	166
Figure 5.12: Gel electrophoresis of RT-PCR of L polymerase gene (L3)..	166
Figure 5.13: Gel electrophoresis of RT-PCR of L polymerase gene (L3)..	167
Figure 5.14: Gel electrophoresis of RT-PCR of L polymerase gene (L4)..	167
Figure 5.15: Gel electrophoresis of RT-PCR of nucleoprotein gene (NP2)..	168
Figure 5.16: Gel electrophoresis of RT-PCR of nucleoprotein gene (NP2)..	168

Index of Tables

Table 1.1: The motif of Late-domain in arenaviruses and some other viruses.. ...	39
Table 1.1.2: Mammarenavirus species and their host, geographical distribution, origin of the name and diseases.	45
Table 2.1: Degenerate primers for L polymerase of snake reptarenavirus	72
Table 2.2: Degenerate primers for nucleoprotein (NP) of snake <i>reptarenavirus</i> ...	72
Table 2.3: Degenerate primers for zinc finger motif (Z) protein and glycoprotein precursor (GPC) of snake reptarenavirus	73
Table 2.4: Improved degenerate primers for L polymerase of snake reptarenavirus for redundancy	73
Table 2.5: Infusion degenerate primers of L polymerase of snake reptarenavirus.	74
Table 2.6: Universal primers designed for amplification of 12S and 16S rRNAs mitochondrion genes from reptiles.	75
Table 2.7: Mitochondrial ribosomal genes accession number	76
Table 2.8: Plasmids used in this study.	79
Table 2.9: Bacterial strains used in this study.	79
Table 2.10: Protein accession number of arenaviruses and viruses used to root the phylogenetic trees	93
Table 2.11: Dehydration steps of IBV specimens by different concentration of acetone.	96
Table 3.1: Gel electrophoresis analysis of amplicons of L polymerase and NP protein of UHV.	112

Table 3.2: Gel electrophoresis analysis of amplicons of Z protein and GPC of UHV.....	113
Table 3.3: BLAST analysis of cloned genes of University of Helsinki virus (UHV).	123
Table 4.1: Frozen reptiles as collected from Heathrow Animal Reception Centre (HARC).....	138
Table 4.2: Snake species as archived at Zoological Society of London (ZSL) in London Zoo.....	146

Abbreviations

Nucleotide code

A	Adenine	W	A or T
C	Cytosine	K	G or T
G	Guanine	M	A or C
T	Thymine	B	C or G or T
U	Uracil	D	A or G or T
R	A or G	H	A or C or T
Y	C or T	V	A or C or G
S	G or C	N	any base

Amino acid code

A	Alanine	Q	Glutamine	L	Leucine	S	Serine
R	Arginine	E	Glutamine acid	K	Lysine	T	Threonine
N	Asparagine	G	Glycine	M	Methionine	W	Tryptophan
D	Aspartic acid	H	Histidine	F	Phenylalanine	Y	Tyrosine
C	Cysteine	I	Isoleucine	P	Proline	V	Valine

aa Amino acid

Akt Protein kinase B (PKB), known as Akt

bp Base pair

°C Celsius

DC-SIGN Dendritic Cell-Specific Intercellular adhesion molecule-3-Grabbing Non-integrin

dH₂O Distal water

DNA Deoxyribonucleic acid

<i>E. coli</i>	<i>Escherichia coli</i>
E-value	Expect value
EDTA	Ethylenediaminetetraacetic acid
ESCRT	Endosomal sorting complex required for transport
ExpASy	Expert Protein Analysis System
g	gram
<i>g</i>	Gravity
HEPES	4-(2-hydroxyethyl)-1-piperazineethanesulfonic acid
hr	Hour
kb	Kilobase
kV	Kilovolt
L	Litre
LB	Luria broth
LSEctin	Liver and lymph node sinusoidal endothelial cell C-type lectin
M	Molar, molarity
mg	Milligram
min	Minutes
ml	Millilitre
mm	Milimetre
mM	Millimolar
mRNA	Messenger ribonucleic acid
ng	Nanogram
nm	Nanometre
nt	Nucleotide
OD ₂₆₀	Optical density unit

ORFs	Open reading frames
PCR	Polymerase Chain Reaction
pH	Hydrogen potential
RIN	RNA integrity number
RNA	Ribonucleic acid
Rnase	Ribonuclease
RNP	Ribonucleoprotein
rpm	Revolutions per minute
rRNA	Ribosomal ribonucleic acid
S	Svedberg units
SDS	Sodium dodecyl sulfate
sec	Second
SOC	Super Optimal broth with Catabolite repression
TCID ₅₀	Tissue Culture Infectious Dose 50%
Tyro3	Tyrosine-protein kinase 3
uv	Ultraviolet
V	Volt
VLPs	Virus-like particles
VPS4	Vacuolar protein sorting-associated protein 4
vRNA	Viral RNA
w/v	Wight/volume
μg	Microgram
μl	Microlitre
μm	Micromolar

Chapter 1 Introduction

1.1 Taxonomy and phylogenetic relationships of arenavirus

The *Arenaviridae* are a family of viruses within four genera *Mammarenavirus*, *Reptarenavirus*, *Hartmanivirus* and *Antennavirus*, which include 43 species to date (35 species of *Mammarenavirus*, 5 species of *Reptarenavirus*, 1 species of *Hartmanivirus* and 2 species of *Antennavirus*) according to the most recent International Committee on the Taxonomy of Viruses (ICTV) report (Abudurexiti et al. 2019). Mammalian arenaviruses of the genus *Mammarenavirus* are traditionally divided into two serogroups, the Old World arenaviruses which contain the Lassa virus and lymphocytic choriomeningitis virus (LCMV) serogroups and New World arenaviruses that consist of the Tacaribe virus serogroup (Clegg 2002). Arenaviruses in the genus *Reptarenavirus* infect snakes and are associated with inclusion body disease (Bodewes et al. 2013; Hepojoki et al. 2015a; Hetzel et al. 2013). The only reported species of *Hartmanivirus* also infects snakes but does not induce the formation of intracellular inclusion bodies characteristic of reptarenavirus infections (Hepojoki et al. 2018).

It is very possible that speciation in the New World arenaviruses within *Sigmodontine* rodents was associated with long-term co-evolution (Zhou et al. 2015). Other features of the arenaviruses have distinguished them into groups, including important divergence in cross-neutralization and cross-reactivity antigenically, geographical distribution, host species and differences in amino acid sequence. For example, the nucleoprotein sequence differs by at least 12%

between different species of arenaviruses. A similar level of sequence divergence has been found between Lassa virus isolates, leading some researchers to suggest a new classification of current Lassa virus species into a new group within the same complex. As arenaviruses have a segmented genome there is the possibility for reassortment which can lead to inter-species reassortment such as has been observed for Mopeia virus and Lassa virus (Rodas and Salvato 2006).

To date, University of Helsinki virus 1 (UHV-1), Golden Gate virus (GGV), California Academy of Science virus (CASV) and University of Giessen virus (UGV-1, UGV-2, UGV-3) have been classified formally within *Reptarenavirus* (Maes et al. 2018). Recently, Boa virus (Figure 1.1) and Aurora borealis virus (ABV-1, ABV-2) were isolated from snakes and found to group within the *Reptarenavirus* genus but are still waiting formal recognition (Bodewes et al. 2013; Hepojoki et al. 2015b). In recent months many more sequences have been deposited in GenBank pending publication.

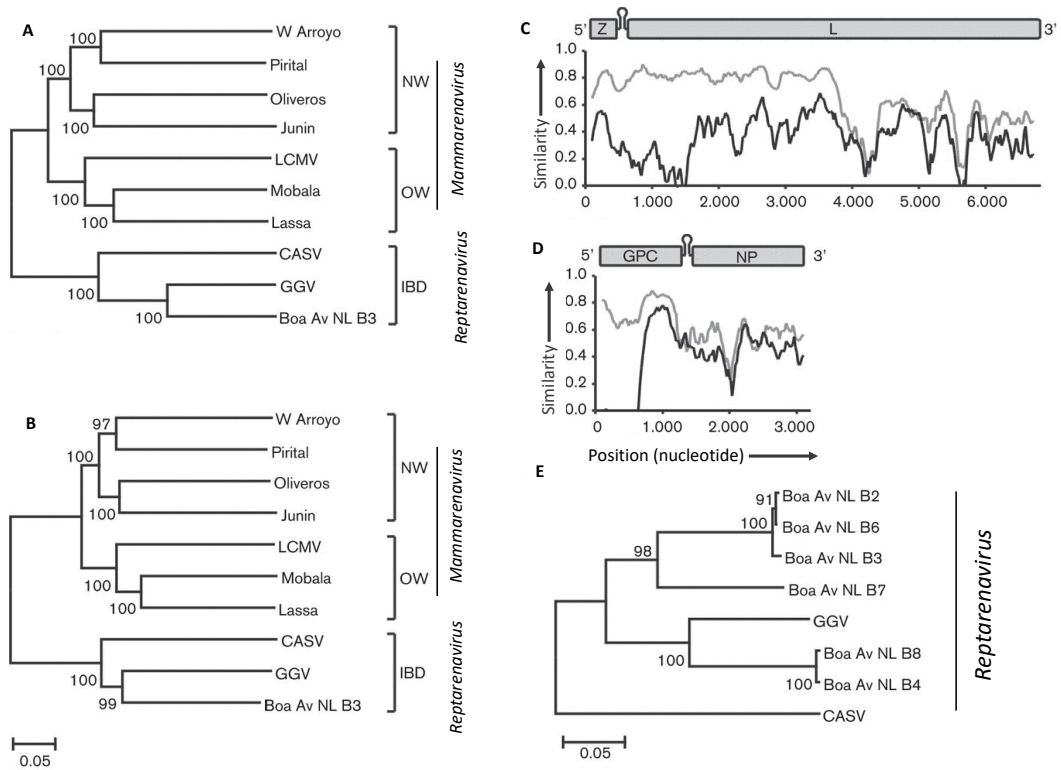


Figure 1.1: Phylogenetic analysis of reptarenavirus species in snakes associated with inclusion body disease. NW: New World, OW: Old World arenavirus, W Arroyo: Whitewater Arroyo virus, LCMV: Lymphocytic choriomeningitis virus, CASV: California Academy of Sciences virus, GGV: Golden Gate virus. The identified sequences of viral RNA dependent RNA polymerase or L polymerase (A) and nucleoprotein (NP) (B) proteins of Boa Av NL B3 in boid snakes with inclusion body disease (IBD) with some selected arenaviruses species were used for designing phylogenetic trees with 1000 bootstrap replicates and p-distance. SimPlot 3.5.1 was used for comparison between nucleotide sequence of ORFs and inter-ORF regions of L (C) and S (D) segments of Boa Av NL B3 with nucleotide sequence of CASV (black line) and GGV (grey line) (Lole et al. 1999). The GenBank accession of Boa Av NL B3 (L) KC508670, Boa Av NL B3 (NP): KC508669, were GenBank accessions (one for each viral segment) of arenaviruses species, W Arroyo: NC_010703.1 and NC_010700, Pirital: AY216505 and AF277659, Oliveros: AY216514 and NC_010248.1, Junin: NC_005080.1, LCMV: M20869.1 and AY847351, Mobala: NC_007904.1 and NC_007903.1, Lassa: NC_004297 and J04324, CASV: NC_018484.1 and NC_018481.1, GGV NC_018483.1 and NC_018482.1. Also, partial sequences of nucleoprotein (NP) of all six Boa virus strain (E) from six boid snakes were used for finding similarity with 1000 bootstrap replicates and p-distance. Were GenBank accession numbers of GGV: NC_018483.1, CASV: NC_018481.1, Boa Av NL B2: KC508664, Boa Av NL B4: KC508665, Boa Av NL B6: KC508666, Boa Av NL B7: KC508667, Boa Av NL B8 KC508668, Boa Av NL B3: KC508669. Figure adapted from (Bodewes et al. 2013).

1.2 Molecular biology of arenavirus

1.2.1 Physical characteristics of arenavirus

Typical arenavirus particles are oval or spherical in shape and about 110-130 nanometres in diameter. There is an electron-dense ribonucleoprotein (RNP) which is found inside viral particles and reaches about 20-50 nanometres in length, and unusually host ribosomes are picked up at the time of budding giving the virus a sandy appearance by TEM, which gave rise to its name. The viral lipid envelope contains club-shape projections that protrude eight to ten nanometres from the surface of the virion (Figure 1.2) (Fields et al. 2013). The lipid bilayer surrounds the ribonucleoprotein which consists of two strands of RNA wound around many copies of the nucleoprotein (NP) and capped by a polymerase protein (L), similar to the ribonucleoprotein of the orthomyxoviruses (Zheng and Tao 2013). Cryo-electron micrographs show that snake reptarenaviruses are similar in appearance to other structurally characterized arenaviruses (Figure 1.3) (Hetzl et al. 2013). Lipids represent about 20% of the total dry weight of arenaviruses and carbohydrates can be present at up to 8% of the dry weight of the virion, attached to Glycoprotein 1 (GP1) and Glycoprotein 2 (GP2) (Buchmeier 2002; Oldstone 1987). Interestingly, arenavirus replication in cell culture is typically non-lytic which may assist arenaviruses in establishing persistent infections in their natural hosts (Buchmeier et al. 2007).

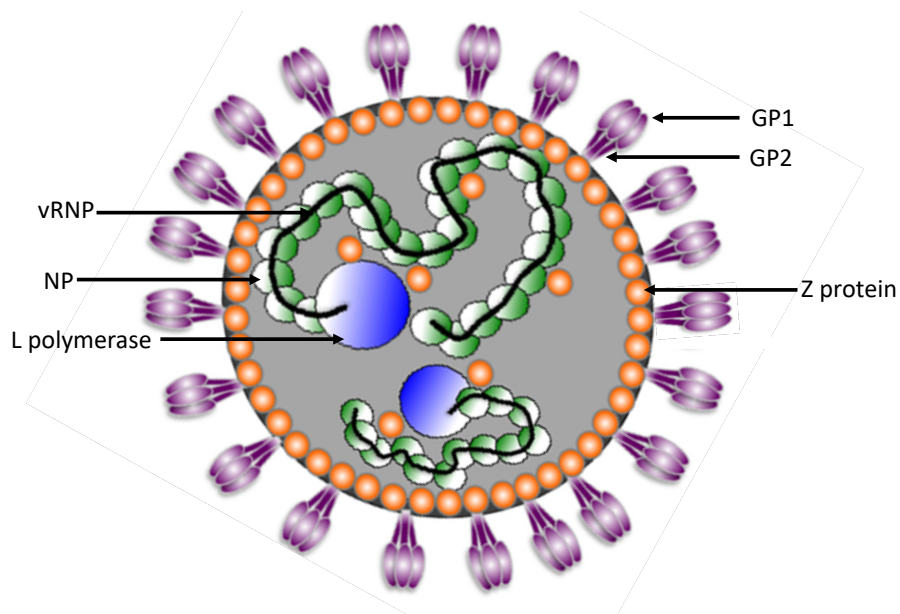


Figure 1.2: Arenavirus structure. The virus is surrounded by a lipid bilayer and contains the receptor binding protein (GP1) and viral fusion protein (GP2). The protein layer underneath the bilayer is composed of Z protein. Viral ribonucleoprotein (vRNP) makes the core of the arenavirus particle and consists of the viral genome, encapsidated by NP protein. L polymerase is associated with vRNP and with NP. Figure adapted from (Martínez-Sobrido and de la Torre 2016).

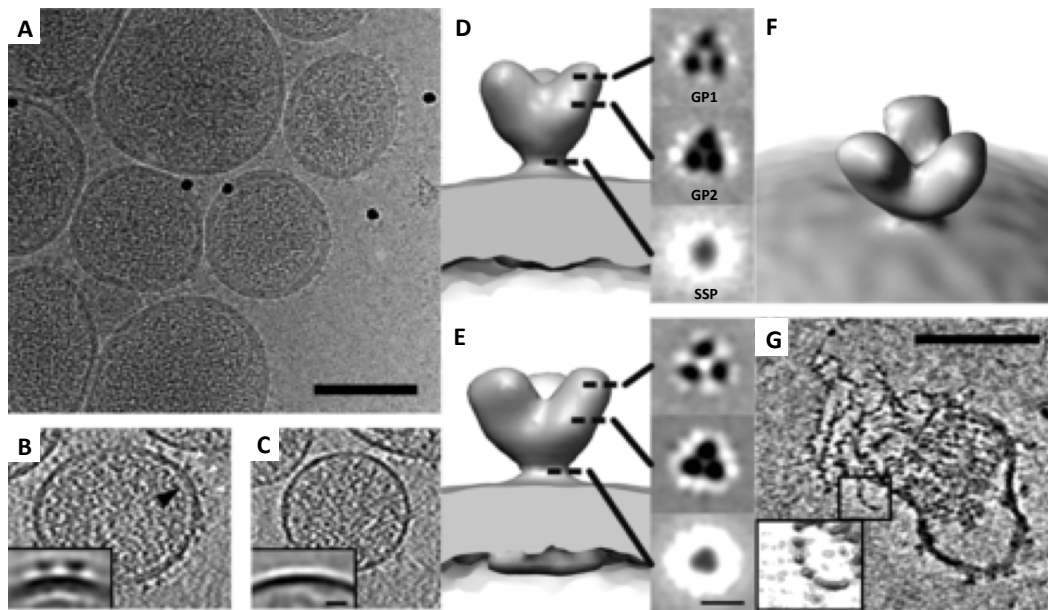


Figure 1.3: Electron microscopy of snake reptaenavirus. A: Cryo-EM image showing University of Helsinki virion embedded in vitrified water. B: Type 1 virion: the inset refers to type 1 virion sections used for subtomographic averaging. C: Type 2 virion: the inset indicates the section of type 2 virion used for tomographic average of the virion surface. D: refers to the virion spike showing the surface of the subtomographic reconstruction without application of symmetry. Section E and F: 3-fold averaged spike, subtomographic reconstructions from the side (E) and oblique to the spectator (F). Panel D and E, there are three levels through the GPC spike that show the domains in the tips and centre which combine close to the virion membrane. Black colour refers to protein density. G: tomographic reconstruction of a broken virion, inset refers to magnified surface of the virion tomogram. Scale bar A: 100 nm, C (inset): 10 nm, D and E: 10 nm, G: 100 nm. Panels A to C and D to E are in same scale, same scale of insets in panels B and C. Figure taken from (Hetzl et al. 2013).

1.2.2 Genome organization and replication of arenavirus

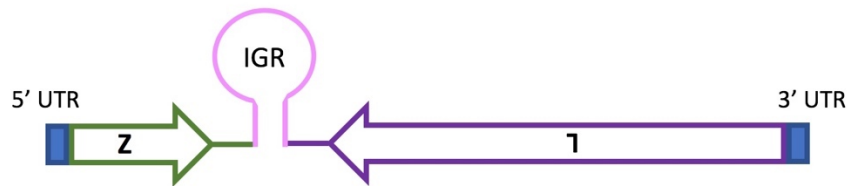
Arenaviruses have a segmented ambisense ssRNA genome, that is, proteins are encoded on both strands, and are typically grouped with negative sense RNA viruses based on polymerase homology and replication strategy (Buchmeier et al. 2007; De La Torre 2009). The genome of arenaviruses consists of large (L) and

small (S) segments (Figure 1.4); the L segment (7.2 kb) encodes the viral RNA-dependent RNA polymerase (RdRp) known as L polymerase and a small zinc finger motif protein (Z). The S segment (3.2 kb) encodes the nucleoprotein (NP) and the glycoprotein precursor (GPC) which consists of two sequences GP1 and GP2 formed by cleavage of the GPC precursor and a stable signal peptide (SSP) (Salvato et al. 1989). The sizes of L polymerase, Z protein, NP and GPC are around 2200 aa, 99 aa, 569 aa and 491 aa respectively (Zapata and Salvato 2013). Each of the arenavirus genomic segments contains two proteins that are separated by an intergenic region (IGR) (Zapata and Salvato 2013), the hairpin structure of which has a role in termination of RNA transcription (Shao et al. 2015). In addition, the two segments of RNA have short terminal untranslated regions (UTRs) (Zapata and Salvato 2013) that are important *cis*-acting signals involved in RNA replication and transcription (Lee et al. 2000; Salvato et al. 1989) and formation of viral nucleocapsid (Shao et al. 2015).

The replication strategy of arenaviruses produces three kinds of RNAs including genomic RNA, antigenomic RNA and mRNA in the cytoplasm of infected cell. Both genomic and antigenomic RNAs are full length RNAs but the mRNA is transcribed from the promoter and then terminated by the IGR. The mRNA of L polymerase and NP can be transcribed from genomic RNA as template. Due to the ambisense nature of the arenaviral genome, the mRNA of Z and GP are only transcribed from antigenomic RNAs (Shao et al. 2015). In addition, the full length complementary antigenomic RNAs of arenavirus are utilized as a template for the production of more arenaviral genomic segments (Martínez-Sobrido and de la Torre 2016) (Figure 1.5). Interestingly, the poly-A tail, a part of mRNA in eukaryotic cells, has been found to

be absent from the mRNAs of arenaviruses through the study of 3' poly-A synthesis, despite the fact that poly-A plays an important role for increasing mRNA stabilization and translation (Flint et al. 2000).

L genomic RNA



S genomic RNA

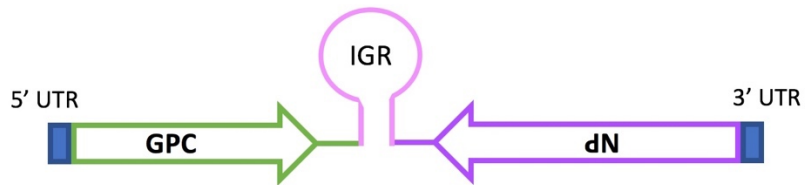


Figure 1.4: Arenavirus genome structure. Arenavirus genome composed from L and S segments. L segment encodes L polymerase (violet colour) and Z protein (green colour), while the S segment (B) encodes nucleoprotein (NP) and glycoprotein (GPC) in light violet and green colour respectively. L and S segments terminate with untranslated regions (UTRs, blue boxes) and each protein coding region separated by intergenic region (IGR, pink colour). Each arenavirus genome is flanked by 5' and 3' UTRs. Figure adapted from (Martínez-Sobrido and de la Torre 2016).

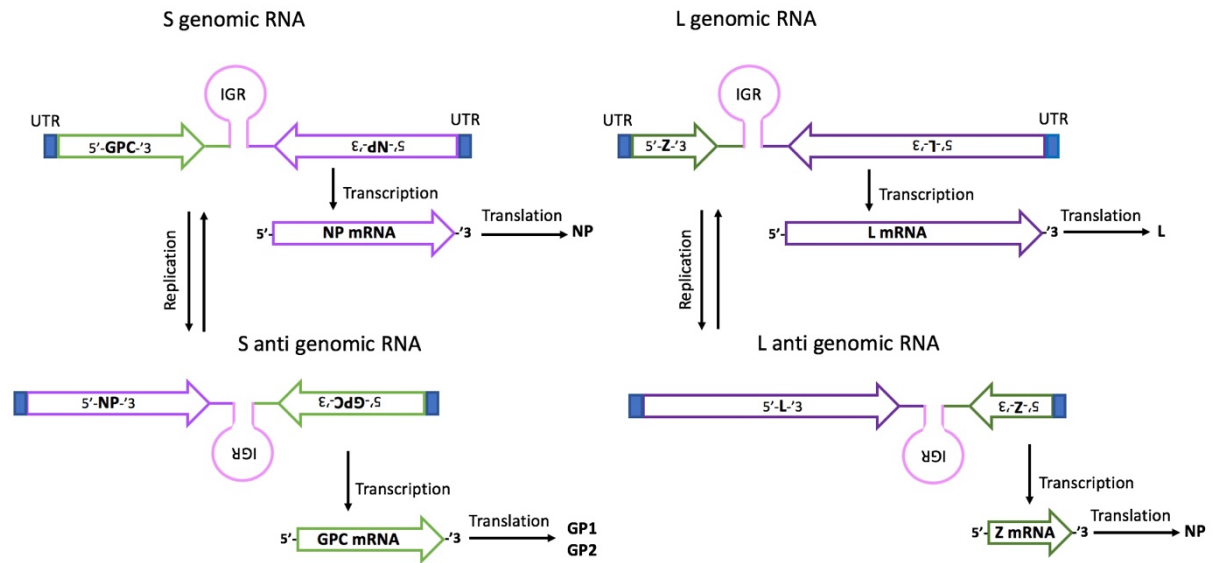


Figure 1.5: Arenavirus genome replication and gene transcription. L polymerase and NP are transcribed from genomic RNA, while Z protein and GP are transcribed from antigenomic RNA. IGR terminate the transcription process. The anti-sense genomic RNA serves as a template for genomic RNA of arenavirus. Figure adapted from (Martínez-Sobrido and de la Torre 2016).

1.3 Arenavirus proteins

There are four structural proteins of arenaviruses, viral RNA-dependent RNA polymerase (RdRp), known as L polymerase, a small zinc finger motif protein (Z), the nucleoprotein (NP) and the glycoprotein precursor (GPC) (Hass et al. 2004; Kerber et al. 2011; Lopez et al. 2002).

The RNA-dependent RNA polymerase (RdRp) or L polymerase is the largest protein in all known arenavirus species. There are many ancillary functions of L polymerase such as binding with RNA templates which leads to the assembly of encapsidated full-length anti-genomes (Müller et al. 1994; Vieth et al. 2004) as well as its essential

function in the replication and transcription of the arenavirus genome (Lopez et al. 2002). Furthermore, L polymerase contains an endonuclease domain which is essential for viral mRNA cap-snatching which occurs during viral RNA transcription. This cap-snatching mechanism is the reason why there are a variety of sequences at the 5'-termini of viral transcripts determined from infected cells. The analysis of secondary structure and the sequences of L polymerases for different species of the related *Bunyaviridae* family show that the N-terminal ends of these virus L proteins have the same endonuclease domain. The application of mutagenesis coupled with assays of endonuclease activity in arenaviruses has confirmed the N-terminus domain of the L polymerase as the cap- domain of L polymerase in all species of arenaviruses (Morin et al. 2010).

The most essential function of L polymerase is as the virus RdRp. The L polymerase structure of a related negative sense, single strand RNA virus (ssRNA), vesicular stomatitis virus (VSV), has been determined recently by electron cryo-microscopy, confirming that the L polymerase has the finger-palm-thumb structure typical of polymerases in general. The catalytic site of the RdRp of VSV is located between the finger and thumb subdomains in a deep channel of the palm, whereas the N terminal domain of the L polymerase, found near one end of the channel, supports the delicate thumb subdomain (Liang et al. 2015). The structure suggested also that VSV L polymerase could be similar with L polymerases found in double stranded RNA viruses (dsRNA) which have been reported to have a cage-like structure (Rahmeh et al. 2010). However, the structure of the capping domain of VSV RdRp is different to the RdRp of dsRNA viruses. The suggested relationship between ssRNA and dsRNA viruses was also apparent through observation of the

appearance of VSV L polymerase by TEM following negative staining (Liang et al. 2015). RdRp activity occurs at the centre of a closed cavity, the catalytic centre, with four surrounding channels including template entrance, template exit, transcript exit and nucleoside triphosphate (NTP) exchange, all necessary for L polymerase to connect with the exterior and fulfil its function in replication the viral genome (Lu et al. 2008).

Arenavirus Z protein is an enlarged RING domain protein and has various functions. Visualized by EM, Z protein forms a matrix layer of electron density between the strata formed of the nucleoprotein NP and lipid membranes of the virus (Neuman et al. 2005). Also, the Z protein has an important role in self-budding and has the ability to trap GP and viral ribonucleoproteins inside virus-like particles (VLPs), in addition to interactions with NP and L polymerase (Perez et al. 2003) (Figure 1.6). Furthermore, the Z protein can lock the L polymerase protein in a catalytically inefficient form, which acts as a regulator of L polymerase function (Kranzusch and Whelan 2011) and inhibits the synthesis of viral RNAs (Cornu and de la Torre 2001) so regulating the replication of the viral genome and transcription. The Z protein of pathogenic arenaviruses also reduces the function of the retinoic acid-inducible gene I product (RIG-1), an innate sensor, so acts as an IFN antagonist (Fan et al. 2009).

The nucleoprotein (NP) of arenaviruses is the most abundant viral protein in both virions and infected cells. There are many roles for the nucleoprotein (NP) such as binding with anti-genomic and genomic RNAs to form the viral nucleocapsids. Besides, during RNA replication NP is required with the L polymerase for viral RNA

synthesis (Brunotte et al. 2011a; Hass et al. 2004; Levingston Macleod et al. 2011). The association of NP with itself can make dimeric and trimeric forms inside mammalian cells during Tacaribe virus (TCRV) infection and these forms of NP are the predominant forms observed also for lymphocytic choriomeningitis virus (LCMV) (Ortiz-Riaño et al. 2012).

The glycoprotein (GPC) of arenaviruses is synthesized first as a protein that acts as an inefficient precursor, preGP-C, where the signal peptide is cleaved co-translationally to give the stable signal peptide (SSP) and GP-C (Eichler et al. 2003). GP-C undergoes post-translational maturation cleavage which occurs by proprotein convertase S1P, also called subtilisin/kexin isozyme-1 (SKI-1), of the host cell (site 1 protease) to allow GP-1 and GP-2 formation (the distal receptor-binding subunit and the transmembrane-spanning fusion competent subunit respectively) (Beyer et al. 2003; Buchmeier and Parekh 1987; Rojek et al. 2008). The stable signal peptide (SSP) is essential for activation of S1P cleavage of GP-C and acts as a trans-acting maturation factor for GP (Lenz et al. 2001) by interaction with a zinc-binding domain in the cytoplasmic tail of GP-2 (Briknarová et al. 2011; Eichler et al. 2004; York and Nunberg 2007). On the arenavirus virion surface, the SSP remains part of a tripartite form of the glycoprotein spike complex with GP-1 and GP-2, to form the arenavirus mature glycoprotein spikes (Eichler et al. 2003; Schlie et al. 2010).

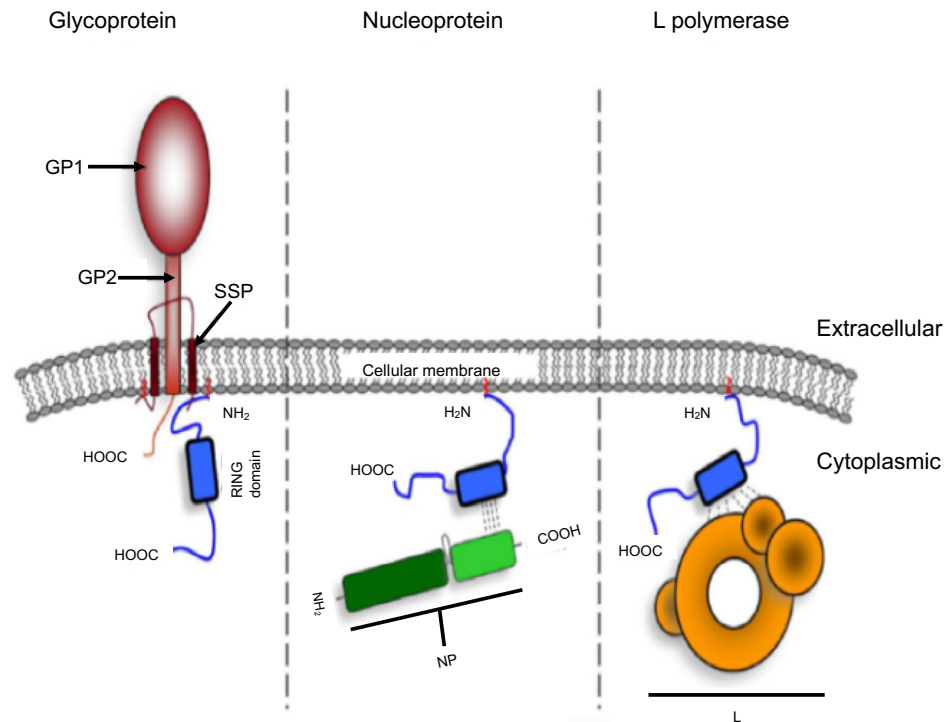


Figure 1.6: Arenavirus protein interactions. The Z protein (blue) interacts with L polymerases (L; orange), nucleoprotein (NP: green) and glycoprotein (GP; red). GP interacts with Z protein at the stable signal peptide (SSP) region, while Z interacts with nucleoprotein NP at its C-terminal domain (light green). Arenavirus Z protein also interacts with L polymerase via amino acids in the Z RING motif and interaction sites located between the polymerase domain and its N-terminus. Figure adapted from (Kranzusch et al. 2010).

1.4 Arenavirus life cycle

1.4.1 Receptors of the arenavirus

The entry of arenavirus into the target cell is initiated by the binding of GP-1 to a cell-surface receptor protein. Pathogenic New World arenaviruses bind human transferrin receptor-1 (TfR1), which is recognized by GP-1 (Flanagan et al. 2008; Radoshitzky et al. 2007). GP-1 binds via the tip of the apical domain (Cheng et al. 2004) and compared crystal structures for GP-1 have revealed that the binding of TfR1 does not stimulate a conformational change following receptor-binding

(Abraham et al. 2010; Bowden et al. 2009). Limitations of host-range can be characterized by the interaction of TfR1-GP1 as, in human, TfR1 with single amino-acid changes can permit cell entry by other species of non-pathogenic arenaviruses such as Tacaribe virus (TCRV) (Abraham et al. 2009).

The transferrin receptor 1 (TfR1) follows an endocytosis route of normal cycling. It transfers inside the target cell to an acidified vesicle where it releases its iron cargo to the cytoplasm after crossing the cell membrane (Andrews et al. 1999). Arenavirus cell entry essentially mimics this process and the pathway is predominantly used by the New World arenaviruses that cause haemorrhagic fever in humans such as (JUNV, MACV, SABV, CHPV, and GTOV) (Flanagan et al. 2008). However, some nonpathogenic arenaviruses such as Tacaribe virus (TCRV) and Amapari virus (AMPV) also utilize TfR1 for cell entry (Abraham et al. 2009) suggesting receptor tropism is not the only reason for pathogenicity.

Old World arenaviruses and New World clade C arenaviruses (Latino and Oliveros viruses) use other cellular receptors such as α -dystroglycan (α DG) for attachment to target cells (Cao et al. 1998; Spiropoulou et al. 2002). The dystrophin-associated glycoprotein dystroglycan (DG) that is cleaved into two-non-covalently associated subunits; α -dystroglycan (α DG) and β -dystroglycan (β DG). α DG comprises the binding sites for arenaviruses and is expressed on many cell types, explaining why arenaviruses, such as the Old World arenaviruses, can have a wide host range (Figure 1.7). β DG plays an important function by connecting dystrophin with the interior part of the cell, specifically the cytoskeletal network. DG is highly expressed on dendritic cells in mice, which are targets for arenavirus infection as their

impairment leads to suppression of the host immune response which naturally assists the life cycle of the virus (Sevilla et al. 2000).

Small amounts of α DG are also present on the surface of B cells, CD4 and CD8 T cells (Sevilla et al. 2000). Laminin, part of the extracellular matrix (ECM), is displaced when the arenavirus attaches to α DG which might unsettle the cell membrane and lead to aberrant cellular signalling and this could participate in the pathogenesis of arenavirus infections (Rojek et al. 2012). The composition of α DG consists of a pair of globular domains separated by a mucin-like domain. The mucin-like domain of α DG contains O-mannosylated glycans which can be recognized by cellular acetylglucosaminyltransferase-like "LARGE" enzymes to function as a glycosyltransferase (bifunctional) with glucuronyltransferase and xylosyltransferase activity leading to the production of repeating units of (-3-xylose-a1, 3-glucuronic acid-b1-) (Inamori et al. 2012). This modification is significant for α DG in order to make interactions with the arenavirus glycoprotein (GP) (Kunz et al. 2005; Rojek et al. 2007). The binding of Lassa virus (LASV) glycoprotein (GP) to α DG can be blocked by laminin in Vero cells. In many cases of LASV infection this does not hinder glycoprotein (GP) binding so there could be other alternative receptors used by arenaviruses (Kunz et al. 2005). Indeed mice that lack a functional LARGE enzyme are still susceptible to lymphocytic choriomeningitis virus (LCMV) infection (Imperiali et al. 2008).

This target cell entry of New World (clade C) and Old World arenaviruses depends on binding of GP-1 with α DG (Cao et al. 1998; Reignier et al. 2006; Spiropoulou et al. 2002) following which the virus takes an endocytic route (Borrow and Oldstone 1994) and transfers to multi-vesicular bodies (MVBs) (Pasqual et al. 2011; Quirin et al. 2008). When the late endosome becomes acidic, fusion of the membranes by the action of the GPCs occurs (Cosset et al. 2009; Klewitz et al. 2007; Pasqual et al. 2011). The complete entry process of arenaviruses is still not fully understood for receptors of the New World arenaviruses clade A (Nunberg and York 2012).

Four further receptors were identified for arenaviruses such as in Lassa virus (LASV) for cellular entry; the proteins Axl, Tyro3 (TAM family), DC-SIGN and LSEctin (C-type lectin family) can act as receptors separately from α DG (Shimojima et al. 2012). Hepatocytes have these receptors and infected cells produce high titres of virus, even though there is limited DG detection (Bedossa et al. 2002; Shibata et al. 2004; Walker et al. 1982). These receptors are also relevant for Ebola virus (Alvarez et al. 2002; Brindley et al. 2011; Gramberg et al. 2005) which shows a similar cellular tropism to arenaviruses for liver, endothelial, macrophage and dendritic cells.

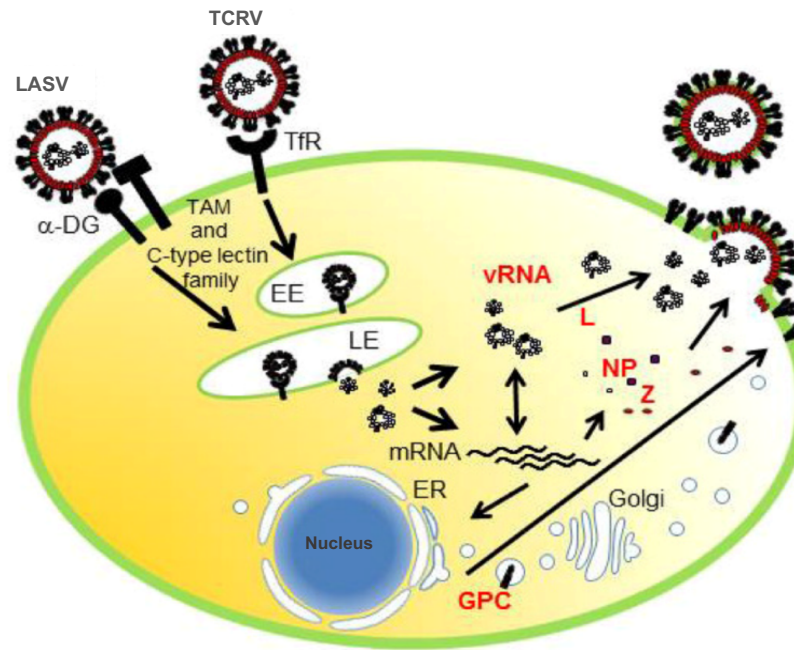


Figure 1.7: Arenavirus receptors TfR1 and α -DG. The TfR1 and α -DG mediate cell entry during arenavirus infection. The human transferrin receptor-1 (TfR1) is used by New World arenaviruses (except clade C) such as Tacaribe virus (TCRV) and the α -DG is used by Old World arenaviruses such as Lassa virus (LASV) for cell entry leading to access the early endosome (EE) and thereby the acidic late endosome (LE). TAM and C-type lectin family receptors are also used by LASV for cell entry. Figure adapted from (Urata and Yasuda 2012).

1.4.2 Arenavirus entry proteins

The arenavirus Z protein plays an important role in regulating the functions of the host cell for viral replication. Arenavirus Z protein interacts with various host factors including the nuclear fraction of the ribosomal protein, promyelocytic leukaemia protein (PML), proline-rich homeodomain protein (PRH) and the eukaryotic translation initiation factor 4E (eIF4E) (Fehling et al. 2012). The promyelocytic leukaemia protein (PML) has the ability to regulate the growth of mammalian cells

and leads to nuclear body formation which is modified by some viral infection and in acute promyelocytic leukaemia (Reineke and Kao 2009). During LCMV infection, the PML protein redistributes to the cytoplasm from the nucleus and locates in Z protein rich large bodies. For example, the Z proteins of LCMV and LASV redistribute the PML protein to the cytoplasm of infected cells and direct interaction between Z and PML proteins *in vitro* has been reported (Borden et al. 1998). These interactions influence infection through processes such as apoptosis because PML protein enhances apoptosis during viral infection (Bernardi et al. 2008), more generally the PML interaction could act as part of the immune evasion strategy of the virus as PML protein has a significant role in antiviral defence (Regad et al. 2001).

The large ribosomal subunit is composed of P0, P1 and P2 proteins that each play a role in ribosomal function. For instant, they make connection with the 28S rRNA and allow binding of aminoacyl-tRNA and eukaryotic elongation factors. The Z protein colocalizes with P0, P1 and P2 during LCMV infection (Borden et al. 1998) causing P1 and P2 down regulation while P0 levels stay constant. These observations suggest ribosomal function is altered by Z-mediated interference. P0 plays a role in nucleic acid processing in the life cycle of LCMV explaining why its level of expression is maintained and not affected by infection as with P1 and P2. The interaction of Z protein with P0 has been suggested as the reason why virions of the arenaviruses have been found to contain ribosomes (Carey et al. 1972).

Eukaryotic translation initiation factor 4E (eIF4E) is a cellular translation factor that expedites ribosomal binding with cellular mRNAs via their 5' cap structures, which then boosts the translation of eIF4E-dependent proteins (Campbell Dwyer et al. 2000; Pestova et al. 2001) and an interaction between eIF4E and Z protein of LASV and LCMV has been shown in transfected and infected cells where Z protein suppresses protein expression (Kentsis et al. 2001). Z protein attaches to eIF4E distal to the cap binding domain but prompts conformational change at the cap binding site (Volpon et al. 2010). This might reduce eIF4E affinity for normal substrates, cellular 5' cap structures, and reduce the synthesis of proteins dependent on eIF4E (Campbell Dwyer et al. 2000). Many of the proteins found to be eIF4E-dependent translation products contribute to innate immunity of the host cell, such as interferon regulatory factor 7 (IRF-7), necessary for the IFN-response and subsequent antiviral state so, as with the redistribution of PML protein, the interaction of Z protein with eIF4E during arenavirus infection could be part of immune evasion, counteracting the interferon (IFN) system of target cells (Fehling et al. 2012).

1.4.3 Arenavirus budding

The cell membrane of the target cell is an important barrier for virus egress and arenaviruses take advantage of natural sorting mechanisms present in the target cell to conquer this physical barrier. For example, in target cells vesicles form inside multi-vesicular bodies (MVBs) constantly and these are enlisted by the virus to enable budding. The endosomal sorting complex required for transport (ESCRT)

machinery of the target cell is targeted by the viruses to get out of cells as has also been shown for many other enveloped viruses (Chen and Lamb 2008).

The ESCRT-system supports cytokinesis steps and formation of multi-vesicular bodies (MVBs) in target cells. The ESCRT-system comprises six proteins (Alix/AIP1, ESCRT-0, -I, -II, -III and Vps4) which are recruited to the location of virus budding. ESCRT-I and ESCRT-II are co-assembled at the cell membrane for bud formation while ESCRT-III has an important role for the last stage of membrane scission by binding with ESCRT-I and/or Alix/AIP1 (Figure 1.8). In the last stage, the AAA-type ATPase Vps4 regulates the disassembly and recycling of the complex (Hurley and Hanson 2010).

The activity of self-budding matrix proteins for many enveloped viruses was first demonstrated for “late domains” which were found within their sequences, e.g. for HIV (Freed 2002; Hurley and Hanson 2010). The sequences of many late domains have now been mapped (Table 1.1), arenavirus Z and NP proteins among them, and shown to contain tetrapeptide motifs such as PT/SAP, PPxY and YxxL, (where x means any amino acid) (Chen and Lamb 2008).

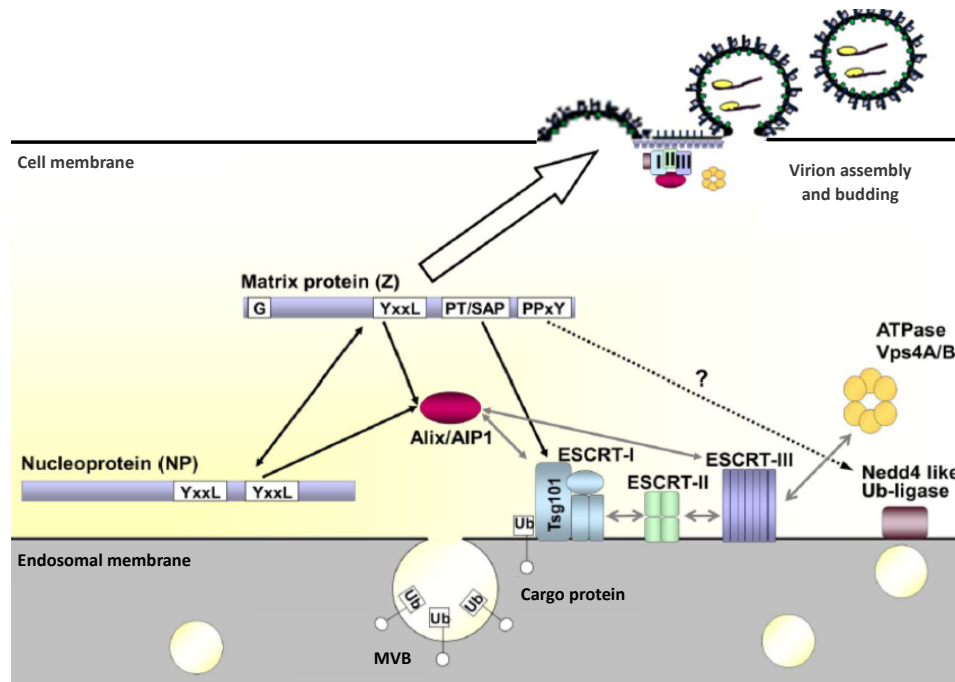


Figure 1.8: Role of the ESCRT pathway in arenavirus replication. The ESCRT maintains the traffic of protein components during multivesicular body formation (MVBs). During arenavirus infection Z protein interacts with the ESCRT pathway, including YxxL and/ or PT/SAP as well as PPxY motifs. Also, there are interactions in Alix/AIP1, Tsg101 and Nedd 4-like ubiquitin ligases. Z protein is myristoylated, which is essential for budding, and the combined action of interaction with ESCRT and myristoylation leads to virion release from the cell membrane. Finally, the recycling and disassembly of the entire complex is regulated by Vps4A/B. Figure adapted from (Wolff et al. 2013).

Table 1.1: The motif of Late-domain in arenaviruses and some other viruses. Where x: Amino acid, θ : Hydrophobic amino acids, * not important for budding. Table adapted from (Wolff et al. 2013).

Motif	Interacting proteins	References
YxxL	<i>Arenaviridae</i> (NP, Z) <i>Retroviridae</i> (Gag) <i>Paramyxoviridae</i> (C, M)	(Irie et al., 2007; Shtanko et al., 2011)
PPxY	<i>Arenaviridae</i> (Z) <i>Filoviridae</i> (VP40) <i>Retroviridae</i> (Gag) <i>Rhabdoviridae</i> (M)	(Kikonyogo et al. 2001; Strecker et al. 2003)
PT/SAP	<i>Arenaviridae</i> (Z) <i>Filoviridae</i> (NP, VP40) <i>Retroviridae</i> (Gag) <i>Rhabdoviridae</i> (M)*	(Dolnik et al. 2010; Irie et al. 2007)
θ PxV	<i>Paramyxoviridae</i> (M)	(Schmitt et al. 2005)

In summary, as shown in Figure 1.9, the complete infection cycle of arenaviruses starts when the virus penetrates the host cell membrane using α DG or TfR1 as receptors. Secondly, the endocytosis pathway allows the virus to enter the target cell resulting in an acidified vesicle. Then, pH dependent membrane fusion allows viral ribonucleoprotein (vRNP) to be released into the cytoplasm by the action of the glycoprotein (GP-2). Next, transcription, replication and gene expression occur in the cytoplasm of the target cell resulting in assembly of progeny viruses at the host cell membrane. Late in this process glycoprotein 1 (GP1), glycoprotein 2 (GP2) and stable single peptide (SSP) are cleaved from the glycoprotein precursor (GPC). Arenavirus assembly and budding occurs at the outer membrane of the target cells. Finally, the new arenaviruses detach from the infected cell to infect other cells (McLay et al. 2013).

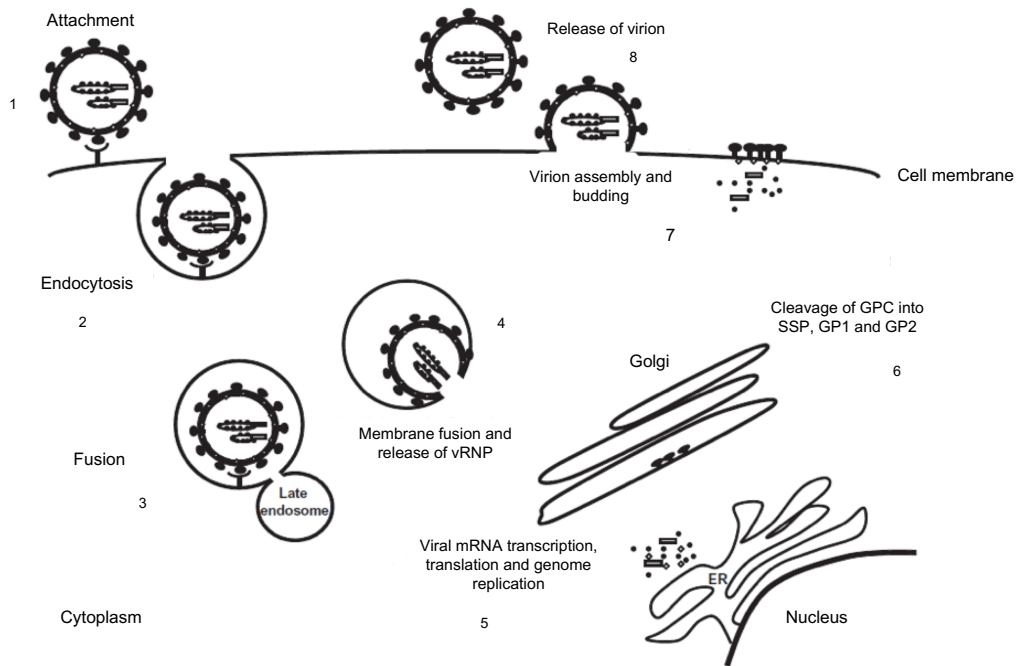


Figure 1.9: Arenavirus budding from infected target cell. 1: Virus-cell receptor attached. 2: Endocytosis. 3: Fusion with late endosome (Low pH). 4: release of viral ribonucleoprotein (vRNP). 5: Gene expression including transcription, translation and genome replication. 6: GPC cleavage either in Golgi apparatus or endoplasmic reticulum (ER). 7: Virus assembly and budding. Figure adapted from (McLay et al. 2013).

1.5 The role of interferon antagonists in arenavirus infection

Many species of arenaviruses evade the induction of cellular immunity by encoding antagonists of the interferon (IFN) type 1 response. The two types of interferon 1 (IFN- α/β) are mediators of the immune system in vertebrates that reduce virus spreading and so curtail the life cycle. It has been reported that arenaviruses inhibit the synthesis of IFN in cell culture (Carnec et al. 2011; Groseth et al. 2011; Martínez-Sobrido et al. 2007) and that the nucleoprotein (NP) acts as an inhibition factor for IFN synthesis via inhibition of the nuclear translocation of IRF-3. The NP of Junin virus (JUNV), Machupo virus (MACV) and Tacaribe virus (TCRV) have been shown

to inhibit IFN production (Martínez-Sobrido et al. 2007). NP activity as an IFN antagonist relies on its capacity of binding RNA (double-stranded) that is otherwise an effective IFN inducer (Brunotte et al. 2011; Hastie et al. 2011). Moreover, the NP of many species of arenaviruses reacts with I κ B-kinase epsilon (IKK ϵ), IKK ϵ which is an intermediate in the signalling pathway for IFN-3 (Fehling et al. 2012; Pythoud et al. 2012). NP is therefore a fundamental interferon antagonist for arenaviruses (Fehling et al. 2012).

The Z protein of arenaviruses also represses interferon type 1 (IFN1) as it interacts with the retinoic acid-inducible gene I product (RIG-I) (Fan et al. 2009), a cytosolic sensor of viral RNA via the Mitochondrial Antiviral Signalling (MAVS) signal transducer (Figure 1.10). The Z protein prevents the RIG-I – MAVS interaction which leads to inhibition of downstream signalling and production of IFN- β (Fan et al. 2009). The literature to date suggests this mechanism for only some species of arenaviruses such as JUNV, GOTV, SABV, TCRV and MACV while there is no evidence for Z protein-RIG-I interaction in the case of LCMV and LASV. The suppression of IFN induction is significant for the viral life cycle as it has been noted that the IFN- α induced cellular factor tetherin (a membrane-associated protein) suppresses the spreading of arenaviruses. Tetherin plays an important role in the control of enveloped viruses and inhibits LASV Z-induced VLPs synthesis (Sakuma et al. 2009) during LASV and MACV infection (Radoshitzky et al. 2010) decreasing the efficiency of virus transmission (Fehling et al. 2012).

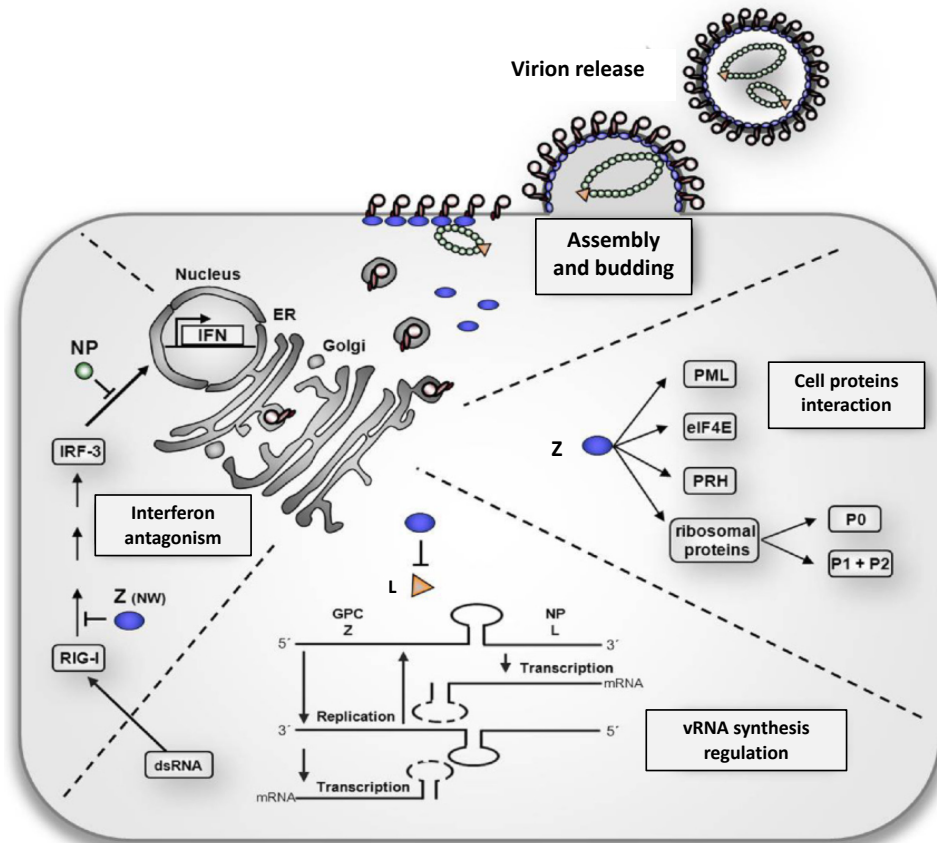


Figure 1.10: The multiple roles of arenavirus Z protein, including interferon antagonism. The Z protein of New World arenaviruses antagonises interferon (IFN) production (left of figure). The nucleoprotein (NP) also acts as an antagonist by inhibition of the nuclear translocation of IRF-3. The general role of Z in interactions with host cell proteins which may also impact innate pathways, is also shown (right of figure). Figure adapted from (Fehling et al. 2012).

1.6 Epidemiology of arenavirus

Arenaviruses are distributed worldwide and cause diseases in both humans and animals (Buchmeier et al. 2007). Arenaviruses of the genus *Mammarenavirus* cause febrile diseases in humans and animals (Table 1.2). Old World arenaviruses are responsible for human febrile diseases, especially in African countries (McCormick and Fisher-Hoch 2002). Most species of New World

arenaviruses are not associated with any symptoms in humans or animals, with the exception of clade B viruses that cause febrile diseases in South America regions, such as Guanarito virus (GTOV), Machupo virus (MACV), Junin virus (JUNV), and Sabia virus (SABV) (Peters 2002). However, the first known outbreak of arenaviruses was recorded in 1933, when lymphocytic choriomeningitis virus (LCMV) caused disease in both humans and animals (Armstrong and Lillie 1934). Emerging arenavirus haemorrhagic fevers are an international cause for concern following deadly outbreaks of Chapare virus in Bolivia and Lujo virus in South Africa (Briese et al. 2009; Delgado et al. 2008). In fact, Lassa virus (LASV) causes as many as 5000 deaths per year, is endemic in West Africa, and is a worldwide cause for concern because it can be spread by air although the endemic area for LASV is normally considered to be restricted to Sierra Leone, Liberia, Nigeria and Guinea (Ehichioya et al. 2010). Human infection with LASV is confirmed by serological tests and isolation of the virus has been reported from Mali, Central African Republic, Ivory Coast, Ghana and Senegal (Fichet-Calvet and Rogers 2009; Safronetz et al. 2010). Therefore, viruses of the LASV-complex viruses are probably endemic in a much larger area of West Africa. There are around 220 million people currently living in countries where LASV is endemic (Kitching et al. 2009), a figure which is supported by the study of arenavirus epidemiology (Zapata and Salvato 2013).

Mammarenaviruses are carried by a variety of rodents, and infection with these viruses is often asymptomatic in the natural host (Emonet et al. 2009). In fact, rodents from the family *Muridae*, subfamily *Sigmodontinae* are commonly infected with New World arenaviruses (Charrel et al. 2003). While rodents are the

most common source of mammarenavirus, fruit-eating bats of the genus *Artibeus* are a natural reservoir for Tacaribe virus (Emonet et al. 2009). More recently, it was discovered that a highly divergent group of arenaviruses, reptarenavirus and hartmanivirus are carried by snakes. It was found that in some European countries such as Netherlands, Finland and Germany, some species of snakes with associated inclusion body disease were infected with reptarenavirus (Aqrawi et al. 2015; Bodewes et al. 2013; Hepojoki et al. 2015b). Recent findings reveal that reptarenavirus infection is also confirmed in the United States (Chang et al. 2016). Currently, there is no evidence of zoonotic transmission of snake reptarenavirus to humans; their discovery represents only a potential threat to human health because of their prevalence of the infected animals and the fact that many snakes are kept as pets (Zapata and Salvato 2013).

Generally, the transmission of mammarenaviruses to humans has many potential routes but foremost among them is inhalation of virus contaminated aerosols from patients or from rodent excretions. Another mode of transmission occurs when rodent meat is used as a source of protein for human consumption in some countries such as Guinea (Ter Meulen et al. 1996). Furthermore, transmission can occur during blood transfusion, organ transplantation or direct contact with contaminated blood or other body fluid of patients, each of which has been implicated in nosocomial outbreaks with human to human transmission of arenavirus haemorrhagic fevers such as Lujo virus (Kernéis et al. 2009).

Table 1.2: Mammarenavirus species and their host, geographical distribution, origin of the name and diseases. Mammarenaviruses include New World (NW) and Old World (OW) serogroups. The NW arenaviruses or Tacaribe serocomplex consist of South American and North American groups. The South American group is further divided into three clades (A, B and C) while the North American group has one phylogenetic clade (A). Table adapted From (Zapata and Salvato 2013).

Old World arenaviruses or LASV-LCMV serocomplex						
Virus	Host	Distribution	Disease	Year	Origin of name	Reference
Lymphocytic choriomeningitis virus (LCMV)	House mouse (<i>Mus musculus</i>) and (<i>Mus domesticus</i>) and Syrian hamster (<i>Mesocricetus auratus</i>)	World wide	Flu like symptoms, meningitis, encephalitis, congenital abnormalities, abortion, multisystem organ failure in transplanted patients	1933	Disease	(Armstrong and Lillie 1934)
Lassa virus (LASV)	Multimammate mouse (<i>Mastomys</i> genus)	West Africa	Haemorrhagic fever	1969	Town, Nigeria	(Frame et al. 1970)
Mopeia virus (MOPV)	Multimammate mouse (<i>Mastomys natalensis</i>)	Southern Africa	Not associated with human disease	1977	Town, Mozambique	(Wulff et al. 1977)
Merino Walk virus	Karoo rat (<i>Myotomys unisulcatus</i>)	Eastern Cape	Unknown pathogenicity for humans	1985	Farm, Merino Walk	(Palacios et al. 2008; Zapata et al. 2013)
Mopeia/Lassa Reassortant (ML29)	Laboratory virus. Passage in Vero E6 and BHK cells	Russia	Vaccine candidate against LHF	1992	M/L reassortant clone 29	(Lukashevich 1992)
Morogoro virus	Multimammate mouse (<i>Mastomys natalensis</i>)	East Africa, Tanzania	Unknown pathogenicity for humans	2009	City, Tanzania	(Günther et al. 2009)
Mobala virus (MOBV)	Soft-furred rat (<i>Praomys</i> sp.)	Central African Republic	Not associated with human disease	1983	Region, DR of Congo	(Gonzalez et al. 1983)
IPPY (IPPYV)	Nile grass rat (<i>Arvicanthis</i> sp.)	Central African Republic	Not associated with human disease	1985	Town, Central African	(Swanepoel et al. 1985)
Lujo virus (LUJV)	Unknown	Southern Africa	Haemorrhagic fever	2009	Lusaka, Zambia Johannesburg, South Africa	(Paweska et al. 2009)

Luna virus (LUNV)	Multimammate mouse (<i>Mastomys natalensis</i>)	Southern Africa, Zambia	Unknown pathogenicity for humans	2009	Lusaka-Namwala, Zambia	(Ishii et al. 2011)
New World arenaviruses or Tacaribe serocomplex (South American group)						
Clade A						
Virus	Host	Distribution	Disease	Year	Origin of name	Reference
Pichinde virus (PICV)	Tome's rice rat (<i>Oryzomys albigularis</i>)	South America, Colombia	Not associated with human disease	1965	Valley, Colombia	(Trapido and Sanmartín 1971)
Parana virus (PARV)	Paraguayan rice rat (<i>Oryzomys buccinatus</i> , <i>Oryzomys angouya</i>)	South America, Paraguay	Not associated with human disease	1965	River Paraguay, Brazil, Argentina	(Webb et al. 1970)
Flexal virus (FLEV)	Tome's rice rat (<i>Oryzomys albigularis</i> , <i>Nephelomys albigularis</i>), Paraguayan rice rat (<i>Oryzomys angouya</i> , <i>Oryzomys buccinatus</i>)	South America, Brazil	Febrile illness associated with nonfatal laboratory-acquired infection	1975	South America, Brazil	(Carlton et al. 2012)
Pirital virus (PIRV)	Alston's cotton rat (<i>Sigmodon alstoni</i>)	South America, Venezuela	Not associated with human disease	1995	Community, Venezuela	(Fulhorst et al. 1997)
Allpaahuayo virus (ALLV)	Arboreal rice rats (<i>Oecomys bicolor</i> and <i>Oecomys paricola</i>)	South America, Peru	Unknown pathogenicity for humans	1997	National reserve, Peru	(Moncayo et al. 2001)
Clade B						
Virus	Host	Distribution	Disease	Year	Origin of name	Reference
Tacaribe virus (TCRV)	Fruit-eating bat (<i>Artibeus</i> sp.)	Caribbean Sea, Trinidad	Associated only with single, nonfatal, laboratory-acquired infection	1956	Beach, Trinidad	(Downs et al. 1963)
Junin virus (JUNV)	Corn mouse, drylands vesper mouse (<i>Calomys masculinus</i>), grass field mouse (<i>Akodon azarae</i>), dark field mouse (<i>Bolomys obscurus</i>)	South America, Argentina	Haemorrhagic fever	1958	Town, Argentina	(Parodi et al. 1959)

Chapter One: Introduction

Candid#1	Passaged in guinea pigs (GP2), then mouse (MB44), followed by clonal selection in fetal rhesus monkey lung cells (FRhL19)	South America, Argentina	Live-attenuated vaccine strain against Argentinian haemorrhagic fever	1985	Argentina	(Barrera and KT Jr 1991)
Machupo virus (MACV)	Large vesper mouse (<i>Calomys callosus</i>)	South America, Bolivia	Haemorrhagic fever	1962	River, Bolivia	(Johnson et al. 1965)
Amapari virus (AMAV)	Rice rat (<i>Oryzomys goeldii</i>), bristly mouse (<i>Neacomys guianae</i>)	South America, Brazil	Not associated with human disease	1964	Amapá region, Brazil	(Pinheiro et al. 1966)
Cupixi virus (CPXV)	Large-headed Rice Rat (<i>Oryzomys capito</i>)	South America, Brazil	Not associated with human disease	1970	Town, Brazil	(Charrel et al. 2002)
Guanarito virus (GTOV)	Cane mouse (<i>Zygodontomys brevicauda</i>)	South America, Venezuela	Haemorrhagic fever	1989	Region, Venezuela	(Salas et al. 2017)
Sabia virus (SABV)	Unknown (suspected rodent)	South America, Brazil	Haemorrhagic fever, haemorrhagic fever associated with nonfatal laboratory-acquired infection	1990	Town, Brazil	(Coimbra et al. 1994)
Chapare virus (CHPV)	Unknown	South America, Bolivia	Haemorrhagic fever	2005	Town, Bolivia	(Delgado et al. 2008)

Clade C						
Virus	Host	Distribution	Disease	Year	Origin of name	References
Latino virus (LATV)	Large vesper mouse (<i>Calomys callosus</i>)	South America, Bolivia and Brazil	Not associated with human disease	1965	Bolivia	(Rowe et al. 1970)
Oliveros virus (OLVV)	Not associated with human disease	South America, Argentina	Dark bolo mouse (<i>Bolomys obscurus</i>)	1990	Town, Argentina	(Bowen et al. 1996)
Pampa virus (PAMV)	Dark bolo mouse (<i>Bolomys sp.</i>)	South America, Argentina	Not associated with human disease	1997	Region, Argentina	(Lozano et al. 1997)
New World arenaviruses or Tacaribe serocomplex (North American group)						
Clade A						

Virus	Host	Distribution	Disease	Year	Origin of name	Reference
Tamiami virus (TAMV)*	Hispid cotton rat (<i>Sigmodon hispidus</i>)	North America, Florida	Not associated with human disease	1964	Everglades, USA	(Calisher et al. 1970)
Whitewater Arroyo virus* (WWAV)	White-throated woodrat (<i>Neotoma albigula</i>)	North America, New Mexico	Febrile infection, Respiratory distress syndrome	1993	Whitewater Creek	(Fulhorst et al. 1996)
Catarina virus (CTNV)	Southern Plains Woodrat (<i>Neotoma micropus</i>)	North America, Texas	Unknown pathogenicity for humans	1999	Town, USA	(Cajimat et al. 2007)
Skinner Tank virus (SKTV)	Mexican woodrat (<i>Neotoma Mexicana</i>)	North America, Arizona	Unknown pathogenicity for humans	2002	Reservoir, USA	(Cajimat et al. 2008)
Big Brushy Tank virus (BBTV)	White-throated woodrat (<i>Neotoma albigula</i>)	North America, Arizona	Unknown pathogenicity for humans	2008	USA	(Milazzo et al. 2008)
Tonto Creek virus (TTCV)	White-throated woodrat (<i>Neotoma albigula</i>)	North America, Arizona	Unknown pathogenicity for humans	2008	Creek, USA	(Milazzo et al. 2008)
Bear Canyon virus (BCNV)*	California mouse (<i>Peromyscus californico</i>), Large-eared woodrat (<i>Neotoma macrotis</i>)	North America, California	Unknown pathogenicity for humans	2002	Trailhead, USA	(Fulhorst et al. 2002)

* Represents recombinant viruses (Charrel et al. 2003).

1.1 Pathogenesis and inclusion body disease of snake reptarenavirus

An inclusion body is an amphophilic, amorphous, eosinophilic and intracytoplasmic body found during histological examination which contains a predominant protein (Wozniak et al. 2000). Boid inclusion body disease (BIBD) was observed in 1970 and causes high mortality among captive snakes (Schumacher et al. 1994). BIBD can affect several genera of boid species such as green anaconda (*Eunectes murinus*), boa constrictor (*Boa constrictor*), Haitian boa (*Epicrates striatus*), garden tree boa (*Corallus hortulanus*), ringed tree boa (*Corallus annulatus*), Burmese python (*Python molurus*), ball python (*Python regius*), Australian pythons (*Morelia spilota variegata* and *Morelia spilota spilota*) (Carlisle-Nowak et al. 1998) and reticulated python (*Python reticulatus*). Similar clinical signs have also been recognized in other species of snakes like Corn snakes (*Elaphe guttata*) (Fleming et al. 2018), Californian king snake (*Lampropeltis getula*), and some species of viperids such as captive palm vipers (*Botriechis marchi*) (Raymond et al. 2001). Clinical signs of inclusion body disease in *Boa* species include intermittent regurgitation, anorexia and central nervous system signs such as opisthotonus (stargazing), head tremor and anisocoria (different eye pupil sizes) (Schilliger et al. 2011). Clinical signs in pythons has included observations that disease can progress to neurological symptoms which cause death after a few weeks of infection. Infected snakes can also be infected with other microorganisms such as *Salmonella* spp., *Aspergillus* spp. and species of amoeba, which might cause septicaemia associated with pneumonia, encephalitis, enteritis or osteomyelitis, hepatitis and lymphomas that lead to snake death (Chang and Jacobson 2010;

Vancraeynest et al. 2006). Historically BIBD was suggested to be associated with several viral infection such as by arenaviruses, retroviruses or paramyxoviruses (Ariel et al. 2010; Huder et al. 2002; Pees et al. 2010; Raymond et al. 2001).

Studies have revealed that BIBD causes immunosuppression (Chang and Jacobson 2010; Wozniak et al. 2000) due to the suppression of white blood cells (WBCs), red blood cells (RBCs) and myelopoietic cell functions as well as the development of the typical inclusion bodies (IB) (Chang and Jacobson 2010; Vancraeynest et al. 2006). Immunosuppression can lead to the death of snakes within weeks or months after infection or, in other cases, the snakes can be asymptomatic carriers (Chang and Jacobson 2010; Vancraeynest et al. 2006). BIBD spreads between animals rapidly but there has been little direct study of horizontal transmission from one animal to another. Many species of snakes can be infected when infested with the snake mite (*Ophionyssus natricis*) (Chang and Jacobson 2010) which might represent one route of transmission. BIBD can be recognized from liver biopsy and blood smears by using light microscopy and it follows infection by purified virus, fulfilling Koch's postulates for the primary infectious agent. Reptarenavirus antigens were isolated and identified from boid snakes with BIBD by using immunohistochemistry (IHC) (Hetzl et al. 2013) (Figure 1.11).

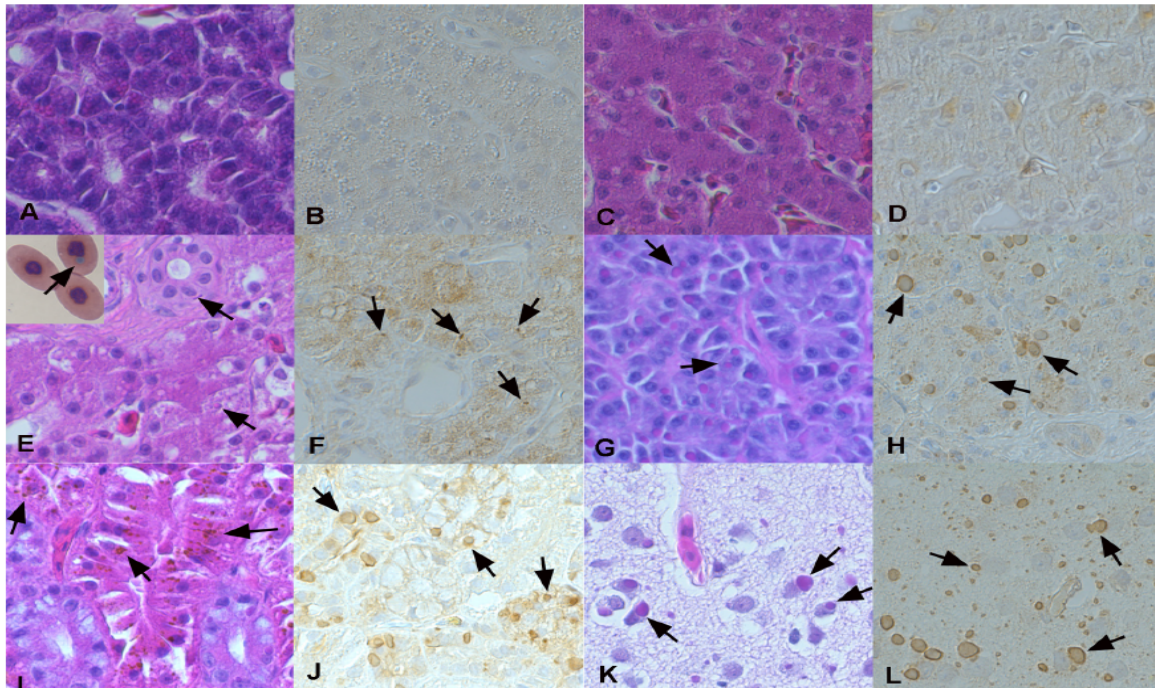


Figure 1.11: Reptarenavirus antigens of boid inclusion body disease (BIBD) in liver tissue of boid snakes. BIBD-negative (A to D) and BIBD-positive (E to L) snakes were analysed by haematoxylin and eosin staining (A, C, E, G, I and K) and by immunohistochemistry (B, D, F, H, J and L) with an antibody raised against UHV. Visible inclusion bodies are indicated by arrows. Figure adapted from (Hetzl et al. 2013).

1.2 Clinical detection of arenavirus

There are many methods for the detection of arenaviruses. Detection of antibodies in serum can give evidence of past infections but is not a useful method for detecting ongoing infections in reservoir animals. In mammalian hosts, the antibody response can also vary depending on the virus strain. However, serology tests can be important tools in determining the host and geographic range of arenavirus infections (Bowen et al. 1996; Lozano et al. 1997). CD4⁺ and CD8⁺ T lymphocyte responses can also be used to detect arenavirus infection and are used for vaccine efficacy tests (Bui et al. 2007; Meulen et al. 2004). Infection by arenaviruses also

results in altered interferon signalling but these responses are general markers of infection and are not useful for diagnosis (Teijaro et al. 2013).

Methods of intermediate specificity are also available. Mass spectrometry (mass spectrometry of proteins only) and transcription profiles of genes expressed more abundantly during arenavirus infection (Zapata et al. 2013) and Toll-like receptor activation patterns can suggest the organs where the viruses replicate (Oldstone 1987). Most arenaviruses can be cultured in BHK-21 cells or Vero-E6 cells. Another more recent technique is microarrays, used for viral detection and based on printing many thousands of oligonucleotides on a slide with dimensions 70 mm × 20 mm (Palacios et al. 2007). High-throughput methods, based on pyrosequencing technology have also been used for virus detection (Palacios et al. 2008). In a number of cases where infections with arenavirus occur in specific regions there is a need to improve the techniques used for detection such as by using primer techniques (Bowen et al. 1996; Lozano et al. 1997). Primers and reverse transcription PCR (RT-PCR) have been used for discovering novel arenaviruses, for example, Morogoro virus and Kodoko virus were identified using this technique (Lecompte et al. 2007; Vieth et al. 2007). RT-PCR is a highly sensitive technique due to exponential amplification of the RNA template, and it also gives fast virus detection within a few hours (Sellner and Turbett 1998). As suggested by these publications, degenerate primers for the discovery of snake reptarenavirus were designed for finding evidence of reptarenavirus infection in snakes and other reptiles in this study.

Arenavirus ongoing infection can be detected by real time PCR (RT-PCR) and this can be rapid diagnosis for some species of arenavirus such as Junin virus. Many reports shown the success of real time PCR using only 0.5 TCID₅₀ of virus (Vieth et al. 2005). A real time SYBRGreen assay improved the original PCR assay and is used for testing human samples that could contain a pathogen (Drosten et al. 2002; Vieth et al. 2005). The specimens must be collected with positive samples (internal control) in order to ensure the efficacy of the enzymatic reaction and serial dilution of the samples is necessary in order to avoid enzymatic reaction inhibition by mammalian tissue factors (Charrel et al. 2008).

Immunohistochemical (IHC) staining is another technique that is used in the diagnosis of viruses infections and is characterised by high specificity and sensitivity. Antibodies react with specific viral antigen(s) in the tissue (Ramos-Vara et al. 2008). In the case of reptarenavirus, IHC staining makes use of a reaction between a defined monoclonal antibody (MAb) and the inclusion body disease protein (IBDP) in preserved tissue samples (Chang et al. 2013). Recently, multiple arena-like viruses were isolated through the use of polyclonal antibody recognized IBDP (Hetzl et al. 2013; Stenglein et al. 2012).

1.3 Inhibition of arenavirus replication and antiviral therapeutics

Arenaviruses cause many diseases for humans and animals globally, and yet there are currently no effective treatments for arenavirus infections. Compounds that have been shown to block specific stages of the arenavirus replication cycle *in vitro* include PPMOs, siRNA, T705 (McLay et al. 2013). Ribavirin is the only commercially available antiviral that can be used for arenavirus infections but it has been shown to only be effective if used in the very early stages of Lassa fever infection (McCormick and Fisher-Hoch 2002). Immune plasma therapy has been shown to be effective for some species of arenaviruses such as Junin virus infection, reducing mortality from 30 % to 1 % (Maiztegui et al. 1979), but it is clear that novel antivirals are required to combat arenavirus infections.

Many studies have aimed to develop antiviral drugs based on a complete understanding of the viral morphogenesis pathway in order to identify potential targets for effective antivirals. These targets include viral protein interactions such as Z and NP proteins described previously, as well as interactions between target cell components and arenavirus components. Tetherin, also known as bone marrow stromal antigen 2 (BST-2), is an IFN-inducible membrane protein which has a negative effect on HIV-1 release (Neil et al. 2008; Van Damme et al. 2008). Experiments using Lassa virus-like particle systems suggest that tetherin prevents the release of arenaviruses (Radoshitzky et al. 2010; Sakuma et al. 2009). Tetherin therefore has the potential to be used as a novel antiviral with activity against a range human and animal viruses including arenaviruses, but excluding filoviruses (Radoshitzky et al. 2010).

An alternative approach is to target post-translational processing of viral components. In arenaviruses, the Z protein is myristoylated and this is required for the release of viruses from the cell. The inhibition of myristoylation in Old World arenaviruses such as LCMV, MOPV and LASV and New World arenaviruses like TCRV and JUNV by using an inhibitor or by mutation of the essential Glycine at residue 2 inhibits virus production (Casabona et al. 2009; Sakuma et al. 2009; Shtanko et al. 2011; Strecker et al. 2006). Alternatively, other cell signalling pathways such as the phosphatidylinositol 3-kinase and serine/threonine kinase (PI3K/AKT) interaction (Franke 2008) which play an important role in arenavirus budding (Linero and Scolaro 2009; Sun et al. 2008; Urata and Yasuda 2012) offer potential targets. As noted above, cellular vesicular trafficking is required for arenavirus budding and is controlled by PI3K/Akt signalling so its inhibition could negatively affect arenavirus replication (Urata and Yasuda 2012; Wolff et al. 2013). Where tested however, inhibition in PI3K/Akt signalling did not reduce viral RNA synthesis (Linero and Scolaro 2009).

1.4 Snake and other reptilian viruses

1.4.1 *Herpesviridae*

Members of the *Herpesviridae* infect primarily mammalian and avian hosts. Herpesviruses typically cause a latent infection, only causing clinical signs that appear when the infected animal is exposed to stress (Hoff and Hoff 1984). In tropical water areas, marine turtles are infected by chelonid fibropapilloma-associated herpesvirus (CFPHV) which causes fibromas and fibropapillomas, infecting the epidermis on the plastron, carapace and eyes, as well as causing serosal lesions in internal organs (D'Amato and Moraes-Neto 2000). Juvenile green turtles have shown a high mortality rate in the waters around Florida and Hawaii as a result of infection with CFPHV (Foley et al. 2005; Lu et al. 2003). Also, fibropapillomatosis herpesvirus can show oncogenic potential, as demonstrated by studies on infected marine turtles (Greenblatt et al. 2005; Lu et al. 2003; Quackenbush et al. 2001). Many co-infections and abiotic environmental factors such as algal blooms also correlate with disease in wild turtle species (Bicknese et al. 2010; Herbst et al. 2009; Stacy et al. 2008; Van Houtan et al. 2010).

Another disease is the lung-eye-trachea disease-associated virus (LETV) known as Chelonid herpes virus 6 which infects young green turtles and causes lesions in the respiratory system and eyes. LETV has been cultured using cells derived from turtle kidneys and has been observed by electron microscopy. The growth of LETV in cell culture has made it possible to develop serological techniques to identify other herpes viruses that infect turtle (Jacobson et al. 1986).

Additionally, 90-100% of cultured green turtle hatchlings may be infected with Grey Patch Disease (GPD) which causes a mortality rate of 5-20%. GPD is characterized by skin lesions which amalgamate into diffuse grey lesions with epidermal necrosis. Infected epidermal cells can show intranuclear enveloped particles of 160-180 nm with 105-120 nm electron dense cores under EM, consistent with tentative identification with a herpesviruses (Rebell et al. 1975).

Some loggerhead turtles such as *Caretta caretta* are infected with two herpesviruses, which were detected by PCR (Stacy et al. 2008). Loggerhead genital-respiratory herpesvirus (LGRV) and loggerhead orocutaneous herpesvirus (LOCV) are used as names of the viruses depending on the infected tissue used to detect them. Tortoises are also infected with four different species of herpesvirus (THV1-4) (Bicknese et al. 2010; Johnson et al. 2005). Herpesvirus infection in tortoises causes lesions in different parts of the body and can lead to stomatitis, hepatitis, central nervous system involvement, conjunctivitis and respiratory system infection (Muro et al. 1998; Origgi et al. 2004).

The Siamese cobra species *Naja naja kaouthia* can be infected with Indian cobra herpesvirus, also called Elapid herpesvirus which infects the venom gland and causes focal necrosis and degeneration of glandular epithelial cells resulting in reduced venom synthesis (Simpson et al. 1979). Lizards can also be infected with herpesviruses. For example, green lizards are infected by green lizard herpesvirus that causes papillomas in infected tissue. Another example is stomatitis in lizards,

which is associated with gerrhosaurid herpesviruses 1-3 or varanid herpesvirus 1 isolated from the heart, spleen and kidney (Clark and Karzon 1972).

1.4.2 Iridoviridae

1.4.2.1 Ranavirus

The genus *Ranavirus* (family *Iridoviridae*) infect frogs and aquatic animals. Frog virus 3 (FV3) is the most often related with frog viral infection but fish and amphibians can also be infected with ranaviruses that cause contagious diseases such as epizootic hematopoietic necrosis virus (EHNV) of fish (Anonymous 2008). Ranavirus infection is found worldwide and causes high mortality in reptiles (Ariel et al. 2010; Hyatt et al. 2002; Pallister et al. 2007) and can rarely also infect some species of tortoise such as the gopher tortoise (*Bopherus polyphemus*) (Westhouse et al. 1996), Hermann's tortoise (*Testudo hermanni*) and the spur-tailed Mediterranean land tortoise (Heldstab and Bestetti 1982). Similarly, ranaviruses have been shown to infect red-eared sliders (*Trachemys scripta elegans*) and the Burmese Star tortoise producing similar clinical signs in both animals. Detection of ranaviruses is done by one of many methods. Electron microscopy (EM) was used for diagnosis of the virion within infected cells (Johnson et al. 2007) and many reptilian organs such as liver, kidney, spleen stomach, lungs and oesophagus are infected (De Voe et al. 2004; Hyatt et al. 2002; Johnson et al. 2008). Intracytoplasmic inclusion bodies are associated with these infections and can be seen clearly in cell lines (Ariel et al. 2009). The Polymerase Chain Reaction (PCR) technique is the most effective method used for detection as the viral genome is DNA, so relatively robust, and can be combined with immune assays for detection based on the polymerase and capsid proteins of the virus (Holopainen et al. 2009;

Hyatt et al. 2002). Co-infections occur and in the Leopard tortoise both chelonid herpes virus and ranavirus viruses were isolated by using swabs from oral and pharyngeal areas of infected tortoises (Holopainen et al. 2009; Jancovich et al. 2003).

1.4.2.2 Erythrocytic virus

Fish, amphibians and other reptiles have long been hosts for erythrocytic viruses which is a disease characterized by cytoplasmic inclusion lesions in erythrocytes, identified by electron and light microscopy (Johnsrude et al. 1997). Researchers have shown that the clinical signs are not always apparent, but in animals with severe infections it might progress to anaemia (Wellehan et al. 2004). Phylogenetic analyses of DNA-dependent DNA polymerase sequence from a ribbon snake with erythrocytic inclusions suggest erythrocytic viruses may belong to a separate genus of *Iridoviridae* (Wellehan et al. 2009).

1.4.2.3 Iridovirus

Viruses in the genus *Iridovirus* (family *Iridoviridae*) cause many serious diseases in invertebrates, while in reptiles the infection is only present occasionally and is not a serious infection (Just et al. 2001). Not classified for many years, molecular techniques have been used to identify iridoviruses which could be considered a new genus of *Iridoviridae* (Wellehan et al. 2004). Iridoviruses were isolated from reptiles after infected breeding crickets that were used to feed lizards and it found that these viruses infected the reptiles (host) as well as replicating in cells of the cricket.

Terrapin Heart (TH-1) and Viper Heart (VH-2) are the cell cultures were used for growing iridoviruses in order to isolate it from some species of chameleons such as *Chamaeloe Hoehnelii*. These viruses cause lesions on the chameleon and the studies have concluded that iridoviruses prefer reptiles as invertebrate reservoirs (Weinmann et al. 2007).

1.4.3 Poxviridae

Poxviruses can cause lesions on the skin of alligatorid crocodilians including *Caiman crocodilus fuscus* and *Caiman sclerops* (Villafane et al. 1996), *Crocodilus porosus*, *Crocodilus johnstoni* and *Crocodylus niloticus* (Buenviaje et al. 1992). Hermann tortoise species such as *Testudo hermanni* infected with poxviruses cause broncho-pneumonia (Orós et al. 1998). Furthermore, the tegu lizard (*Tupinambis teguixin*) (Stauber and Gogolewski 1990) and flap-necked chameleon (Jacobson and Telford 1990) have a dermatitis disease caused by poxviruses (Stauber and Gogolewski 1990). There are eosinophilic intracytoplasmic inclusions associated with hypertrophied epithelial cells. Electron microscopy (EM) observation of the inclusions show pox-like virions of about 100-200 nm in diameter, which it is somewhat smaller than insect and other vertebrate poxviruses. There is a low mortality rate among susceptible species (Orós et al. 1998) and the infection is generally limited to only some areas in the world (Ariel 2011). Molecular analysis classified the poxvirus (pathogenic poxvirus in Nile crocodiles) into a new genus related to the *Chordopoxvirinae* (Afonso et al. 2006).

1.4.4 Adenoviridae

Many species of vertebrates are infected by adenoviruses that cause respiratory system infections. Adenovirus was also been isolated from snakes (Papp et al. 2009; Schumacher et al. 1994), Corn snake (Ahne and Juhasz 1995), turtles (Farkas and Gál 2009; McArthur et al. 2004) crocodiles, (Huchzermeyer et al. 1994) and lizards (Jacobson et al. 1996; Papp et al. 2009). Also, the terrapin turtle can be infected with chelonian adenovirus and the virus was isolated from these animals (Farkas and Gál 2009), although they are not completely similar with other adenovirus family members (Ariel et al. 2009). The genera of *Aviadenovirus* and *Mastadenovirus* cause infection for avian and mammalian species (Benkö et al. 2005), while *Ictadenovirus* infect fish, such as White sturgeon adenovirus 1.

Many molecular techniques are used for adenovirus diagnosis like PCR followed by sequencing, with the specimen taken by swab of the infected organs (Wellehan et al. 2004) or in formalin fixed tissue (Perkins et al. 2001). The adenoviruses that infect Sulawesi tortoises (*Indotestudo forsteni*) were characterized by using sequence analysis to be of the genus *Siadenovirus* (a novel adenovirus) and classified as a unique reptile virus within this genus (Davison and Harrach 2011; Rivera et al. 2009).

1.4.5 Papillomaviridae

Members of the *Papillomaviridae* family infect different species of reptile and cause distinct lesions. Green lizard (*Lacerta viridis*) is infected with papillomaviruses were associated with papilloma, the more highly keratinized areas containing virions

(Raynaud and Adrian 1976). Papilloma-like particles from lung-washings of a Horsfield Russian tortoise were identified as papillomavirus (Drury et al. 2001). Moreover, the green turtle (*Chelonia mydas*), sea turtles and loggerhead turtle (*Caretta caretta*) are also infected with papillomavirus cause fibropapillomatosis (Manire et al. 2008; Stacy et al. 2008). There are many techniques for papillomavirus detection. One of the most common techniques is histopathological detection which confirms the hyperplasia and hyperkeratosis associated within acanthosis but does not give evidence of inclusion bodies. Electron microscopy (EM) is used for observing the hexagonal particles that occur in intranuclear crystalline arrays and have a 42 nm diameter, similar to papilloma virions found in wart lesions in mammals (Jacobson et al. 1982).

1.4.6 Parvoviridae

The infection by parvovirus is usually associated with another virus infection in reptiles as some parvoviruses, dependoviruses, which require other viruses such as adenovirus to complete their replication cycle. For instance, the intestinal epithelium of some species of snakes and lizards (bearded dragon and species of *Pogona vitticeps*) are infected with parvovirus and adenovirus and the virus was observed in both the liver and intestinal tracts of infected reptiles (Farkas and Gál 2009; Frye et al. 1994; Wozniak et al. 2000). A parvovirus-like serpentine adeno-associated virus was also isolated and identified from an infected ball (royal) python (Farkas and Gál 2009).

1.4.7 *Reoviridae*

Reptiles can be infected with members of the *Reoviridae* and the infection is associated with obvious symptoms such as neurological disorder and pneumonia (Wellehan et al. 2009). The Oribund python (*Pythonregius*) is infected with reovirus, and reovirus was also isolated from the brain of a rattlesnake that suffered from neurological disorder (Vieler et al. 1994). Vero cells and Iguana cells (IgH2) are used for growing the virus and cytopathic effect (CPE) of syncytial giant cell formation was present after reovirus infection (Ahne et al. 1987; Corcoran and Duncan 2004). Reovirus was isolated from two non-living elapid snakes as well as the black rat snake (*Elaphe obsoleta*). Moreover, the causative agent was re-isolated and gave similar clinical signs with other species of black rat snake that were infected (Lamirande et al. 1999).

1.4.8 *Retroviridae* and inclusion body disease of boid snakes

Snakes, turtles, crocodiles and the Komodo dragon lizard can be at risk of retrovirus infection (Martin et al. 2002; Van Regenmortel et al. 2000) and in snakes the infection is associated with tumours in many cases (Jacobson et al. 1980). For instant, in captive snakes, inclusion body disease (IBD) is a common infection of boid snakes but there is often no evidence of a causative agent (Chang and Jacobson, 2010; Hder et al., 2002). However, many clinical signs appear such as regurgitation of food, neurological disorders, tumours, stomatitis and pneumonia. In epithelial cells of all main infected organs of the bodies there are eosinophilic intracytoplasmic inclusion bodies and the infection might develop to meningoencephalitis (Johnson et al. 2005). Inoculation of primary cell cultures

derived from the kidney of an infected boa constrictor into young Burmese pythons (*Python molurus bivittatus*) leads to inclusion body disease (IBD) (Schumacher et al. 1994). Retroviruses in reptiles were diagnosed by using advance molecular procedures (Huder et al. 2002).

1.4.9 Arboviruses

Arboviruses are classified as arthropod borne viruses which replicate in both arthropod vectors and vertebrate hosts (Shortridge et al. 1975). Most species of arbovirus cause serious diseases in human, while in amphibians and reptiles the viruses cause some signs of infection (Jacobson et al. 2005). Arboviruses of many virus families including togaviruses, flaviviruses, bunyavirus and rhabdoviruses infect reptiles. For instance, lizards (*Ameiva ameiva*) can be infected with rhabdoviruses such as Marco virus, Timbo virus and Chaco virus (Causey et al. 1966). These arboviruses grow in cell lines with an optimal temperature of 30°C and have no serological cross-reactivity with other species of rhabdoviruses (Monath et al. 1979). A new classification of a virus that infected some species of turtles such as *Trionyx spinifer emoryi*, was found to be part of the *Bunyamwera* and was isolated from turtles in 1970 during the Texas reptile survey. There are often no clear symptoms in reptiles during infection with arboviruses, however, reptiles can play an important role as reservoirs and can transmit the viruses to humans and animals (Ariel 2011).

1.4.9.1 *Flaviviridae*

Japanese encephalitis virus (JEV) and Saint Louis encephalitis virus (SLEV) are two of many arboviruses within the family *Flaviviridae* that cause disease in humans. Snakes and turtles can be infected with these viruses as confirmed by antibody detection (Shortridge et al. 1975). Japanese encephalitis Virus (JEV) was isolated from a Chinese rat snake (*Elaphe rufodorsata*) (Lee et al. 1972), and flavivirus was also isolated from a tortoise in 2001 (Drury et al. 2001). Flaviviruses play a significant role in human and animal disease. To illustrate, West Nile virus (WNV) is classified as a zoonotic virus as a new strain of West Nile fever reached the America continent in 1999 and subsequently spread nationwide suggesting that WNV had found new species of reptiles as reservoirs more than any other type of animal (Ariel 2011). Researchers have detected West Nile fever virus (WNV) in American alligators in Louisiana, wild alligators in Florida and farmed crocodiles in Mexico (Farfán-Ale et al. 2006; Jacobson et al. 2005; McNew et al. 2007). Infection with WNV causes serious disease with high mortality rate in some areas such as Florida, Georgia and Louisiana (Jacobson et al. 2005; Miller et al. 2003).

1.4.9.2 *Togaviridae*

Western equine encephalitis virus (WEEV), Eastern equine encephalitis virus (EEEV) and Venezuelan equine encephalitis are arboviruses within the family *Togaviridae* that cause zoonotic viral diseases (Shortridge and Oya 1984). Many togaviruses are known to infect species of snake, crocodile, lizard, turtle and tortoise (Hoff and Trainer 1973; Lunger and Clark 1978). Typically these viruses cause a

mild infection in the reptile hosts but can act as reservoirs (Lunger and Clark 1978). Snakes and tortoises tend to be highly susceptible (Hayes et al. 1964) with signs of viraemia during experimental infection, and this susceptibility reaches a peak from 3 to 105 days after infection depending on the temperature (Bowen 1977). Togaviruses were isolated from blood samples in most infections (Shortridge and Oya 1984) and during three years of collection of blood samples from reptiles in an endemic area in Alabama it was found that 75% of these specimens contained EEEV (Cupp et al. 2004; Wozniak et al. 2000). The transmission of Western equine encephalitis virus (WEEV) to garter snakes could be due to biting by the *Culex tarsalis* mosquito (Gebhardt et al. 1966) and 31% of mosquitoes can be infected with WEEV after sucking blood from infected snakes even with a low level of viraemia. Vertical transmission is an additional mode of transmission reported for WEEV from infected garter snake mothers to their offspring (Gebhardt et al. 1964).

1.4.10 Caliciviridae

Aruba Island rattlesnakes (*Crotalus unicolor*), rock rattlesnake (*Crotalus lepidus*), eyelash viper (*Bothrops schlegeli*) and Bell horned frogs (*Ceratophrys orata*) can be infected with caliciviruses. The infection causes necrosis in different body parts of the reptiles and Vero cells was used at 37°C for isolation of the causative *Caliciviridae* family members (Barlough et al. 1998).

1.4.11 *Picornaviridae*

Reptiles can be infected with the picornaviruses. The boa constrictor infected with picornavirus shows clinical signs such as central nervous system disorder and gastrointestinal disease. Cell necrosis and inclusion bodies (intranuclear) are present throughout the liver, spleen, pancreas and intestinal tract. Electron Microscopy (EM) was used for virion visualization, and the virus was isolated from the spleen and duodenum of infected snakes and confirmed as picornavirus (Heldstab and Bestetti 1984).

1.4.12 *Paramyxoviridae*

Many species of snakes can be affected by paramyxovirus infections. There is some evidence from farmed Fer-de-lance snakes (*Bothrops atrox*) in Switzerland that cause respiratory symptoms with mortality rate > 87% in the endemic area (Fölsch and Leloup 1976). The outbreak extended to some other reptiles such as rock rattlesnakes, viper species, non-viper species (Homer et al. 1995; Jacobson et al. 1980; Just et al. 2001) and lizards. The clinical findings are pneumonia and respiratory tract disorder (Jacobson et al. 2001) in lizard, while infected snakes suffer from nervous symptoms (Jacobson et al. 2001; West et al. 2001). Paramyxoviruses were also isolated from *Testudo hermannii* and farmed Nile crocodiles using faecal samples (Marschang et al. 2009) although the virus could have been associated with the infected chickens used to feed the crocodiles (Homer et al. 1995).

Paramyxovirus infection are detected using immuno-histochemical survey with main lesions found on respiratory organs (Homer et al. 1995). Vero cell lines, cobra eggs, gecko embryo, rattlesnake fibroma and viper heart are the most used cell lines for paramyxovirus isolation with samples taken from brain and lung of infected snake (Richter et al. 1996). Virus growth at 28°C rather than at 37°C could assist syncytium production and cell layer destruction (Blahak 1995).

Finally, there are many genetic differences between paramyxoviruses of reptiles and those of other animals (Franke et al. 2001; Kurath et al. 2004). Genomic analysis indicates the relationship between paramyxoviruses that infected reptiles and those of snake and lizard, researches shown that the paramyxovirus of the tortoise had a different genetic structure (Marschang et al. 2009).

Aims of study

As detailed in the introduction, amphibian and reptilian viruses are numerous and rather general in their clinical symptoms. Many induce inclusion body formation in infected tissues but have been characterized only poorly in the past by limited serological and microscopic examination. In some cases, there is a clear zoonotic threat represented by infected animals while for others the threat is only theoretical. As a result, there is a clear need for rapid specific tests to detect suspected viruses in pathological samples as well as rational methods, such as bioinformatics, to gauge the likelihood of a zoonotic transfer. Clearly, most viruses have strict tropisms and do not represent zoonotic threats, but the very widespread nature of amphibian

and reptilian viruses suggest they may be a special case for consideration and that more routine virus screening could be useful. To that end and using the examples of emerging snake reptarenavirus associated with inclusion body disease in boid snakes as the test case, studies are presented that seek to address the screening issue.

Bioinformatics is used to deduce primers that could act as universal primers for the amplification of reptarenavirus sequences in test tissue even if the virus was a drifted variant. Primers are validated using cloned examples and then used to screen a number of test tissues, all uniquely sourced.

Bioinformatics is also used more generally to identify reptarenavirus relatives in the unannotated databases of deposited sequences. The case for zoonotic potential is considered after phylogeny and species biology is taken into account.

Chapter 2 Materials and Methods

2.1 Oligonucleotide primer design

2.1.1 Degenerate primers for reptarenavirus proteins

Degenerate primers were designed for snake reptarenavirus species to amplify regions containing the 1) RNA dependent RNA polymerase (RdRp) known as L polymerase; 2) nucleoprotein (NP); 3) small zinc finger motif protein (Z); and 4) glycoprotein precursor (GPC) open reading frames. The sequence data for these four reptarenavirus proteins were obtained from the National Center for Biotechnology Information (NCBI) sequence repository (<https://www.ncbi.nlm.nih.gov>) for the reptarenavirus species Golden Gate virus (GGV), Boa virus, California Academy of Science virus (CASV) and University of Helsinki virus 1 (UHV-1). Multiple sequence alignments (MSA) were performed using Clustal Omega version (1.2.4) (McWilliam et al. 2013) available on (<http://www.ebi.ac.uk/Tools/msa/clustalo/>) in order to design degenerate primers (Table 2.1, 2.2 and 2.3). A further set of primers to amplify L polymerase (Table 2.4) was designed using GGV, Boa virus, CASV, UHV-1 and two additional reptarenavirus sequences in the MSA: Aurora borealis virus 1 (ABV-1) and Aurora borealis virus 2 (ABV-2) in order to improve redundancy. All oligonucleotide primers were ordered from Integrated DNA Technologies (IDT) and diluted with nano-pure dH₂O to 100 mM then preserved at -20°C.

Table 2.1: Degenerate primers for L polymerase of snake reptarenavirus. Four L polymerase sequences of Golden Gate virus (GGV), Boa virus, California Academy of Science virus (CASV) and University of Helsinki virus 1 (UHV-1) were aligned and then using for designing degenerate primers. L polymerase accession number of GGV: NC_018482.1:c6830-630, Boa virus: NC_023762.1:c6819-622, CASV: NC_018484.1:c6656-516 and UHV-1: NC_023765.1:c6850-632. Degenerate nucleotide codes are included in the List of abbreviations.

Primer	Primer sequence	Length (Bases)	GC %	Tm (°C)	Expected size (bp)
L4087F	WAKYWCNATGAAYACATC	18	33.3	43.5	1012
L5099R	CCACARACCCAATCRCCAA	19	52.6	55.7	
L1017F	TYCCAAGTG TSAAYGACAGA	20	45	53.8	527
L1544R	AATGCYTTYTGWCCTTCACC	20	45	53.2	
L5081F	TTGGYGATTGGGTYTGTGG	19	52.6	58.9	235
L5316R	ARYTCCATTTCRGGTCTWAC	20	42.5	50.9	

Table 2.2: Degenerate primers for nucleoprotein (NP) of snake reptarenavirus. The sequences of NP protein of Golden Gate virus (GGV), Boa virus, California Academy of Science virus (CASV) and University of Helsinki virus 1 (UHV-1) were aligned and then using for design degenerate reptarenavirus primers. Nucleoprotein (NP) accession number of GGV: NC_018483.1:c3391-1616, Boa virus: NC_023761.1:c3322-1568, CASV: NC_018481.1:c3177-1423 and UHV-1: NC_023766.1:c3345-1597. Degenerate nucleotide codes are included in the List of abbreviations.

Primer	Primer sequence	Length (Bases)	GC %	Tm (°C)	Expected size (bp)
NP332F	TDGAVVKDATMAAGAAAAA	19	26.3	43.6	605
NP937R	TTRTAYAAVADRTCTTCAAA	20	22.5	42.9	
NP173F	GDYTRAGRAARGAGACAAA	19	38.6	47.7	389
NP562R	GMDGGTGADGTHCCAAACTG	20	52.5	54.8	

Table 2.3: Degenerate primers for zinc finger motif (Z) protein and glycoprotein precursor (GPC) of snake reptarenavirus. The sequence of Z and GPC protein of Golden Gate virus (GGV) and University of Helsinki virus 1 (UHV-1) were used for design degenerate reptarenavirus primers. Z protein accession number of GGV: NC_018482.1:121-471, UHV: NC_023765.1:121-471, while GPC protein accession number of GGV: NC_018483.1:161-1444, UHV-1: NC_023766.1:71-1342. Degenerate nucleotide codes are included in the List of abbreviations.

Primer	Primer sequence	Length (Bases)	GC %	Tm (°C)	Expected size (bp)
Z40F	ATCTCCATAATAACATTCAT	20	50	52.5	309
Z349R	ATGGTTTCGGGGAGKGTGTCCC	21	64.3	62.7	
GP895F	GAACATGTGACTGAYGCCA	19	50	54.1	388
GP1283R	CCAGCTGCAAACAAAMCA	18	47.2	52.8	

Table 2.4: Improved degenerate primers for L polymerase of snake reptarenavirus for redundancy. The L polymerase sequences of six species of reptarenavirus including Golden Gate virus (GGV), Boa virus, California Academy of Science virus (CASV) and University of Helsinki virus 1 (UHV-1), Aurora borealis virus 1 (ABV-1) and Aurora borealis virus 2 (ABV-2) were aligned and then using for designing degenerate primers. L polymerase accession number of GGV, Boa virus, CASV were described in Table 2.1. Accession number of L segment of ABV-1: KR870021.1, ABV-2: KR870033.1 were used for redundancy primer. Degenerate nucleotide codes are included in the List of abbreviations.

Primer	Primer sequence	Length (Bases)	GC %	Tm (°C)	Expected size (bp)
L3480F	WRAHRTHDSAGMASKTWTGDT	21	34.9	50.1°C	319
L3799R	WYRWKWKGHMCDAHYTCAGA	20	40	50.6	

2.1.2 Infusion degenerate primers for L polymerase of reptarenavirus

Infusion degenerate primers were designed for cloning L polymerase genes of University of Helsinki virus (UHV). Six degenerate primer sequences of L polymerase were selected from Table 2.1 and then the pTriEx 1.1 vector sequence (AGGAGATATA and GATGGTGGTG) plus *Nco*I (CCATGG) and *Xho*I (CTCGAG) restriction sites were added to the 5' end of each primer sequence (Table 2.5). The infusion primers were ordered from Integrated DNA Technologies (IDT) and used to prepare to amplify L segments of UHV. The infusion primers were diluted with nano-pure dH₂O to 100 mM then preserved at -20°C as before.

Table 2.5: Infusion degenerate primers of L polymerase of snake reptarenavirus. The sequence of infusion degenerate primers to amplify the L polymerase of reptarenavirus University of Helsinki virus (UHV). The sequence homologous to the to the pTriEx 1.1 vector are highlighted in green, and the *Nco*I and *Xho*I restriction sites are highlighted in blue. The size of the amplicon was as described in Table 2.1.

Primer	Primer sequence	Length (Bases)	GC %	TM (°C)
Inf. L4087F	AGGAGATATACCATGGWAKYWCNATGAAYACATC	34	38.2	58.8
Inf. L5099R	GATGGTGGTGCTCGAG CCACARACCCAATCRCCAA	35	57.1	69.3
Inf. L1017F	AGGAGATATACCATGGTYCCAAGTGTSAAYGACAGA	36	44.4	63.6
Inf. L1544R	GATGGTGGTGCTCGAGAATGCYTTYTGWCCTTCACC	20	45	53.2
Inf. L5081F	GGAGATATACCATGGTTGGYGATTGGGTGTGTGG	34	50	64.1
Inf. L5316R	GATGGTGGTGCTCGAGARYTCCATTTTCRGGTCTWAC	36	51.4	65.3

2.1.3 Universal primers of ribosomal mitochondrial genes

Universal primers of ribosomal mitochondrial genes including 12S and 16S rRNAs genes of reptiles were designed and used for RT-PCR. The methods used to design universal degenerate primers for 12S and 16S rRNAs (Table 2.6) were carried out as stated in section 2.1. Accession number of mitochondrion genes of the reptiles are listed in Table 2.7. The universal primers were ordered from Integrated DNA Technologies (IDT), diluted with nano-pure dH₂O to 100 mM and then preserved at -20°C.

Table 2.6: Universal primers designed for amplification of 12S and 16S rRNAs mitochondrion genes from reptiles. Degenerate nucleotide codes are stated in the List of abbreviations.

Primer	Primer sequence	Length (Bases)	GC %	Tm (°C)	Expected size (bp)
12S rRNA.16429F	TRWRAAAGGAACTMRGCAA	20	35	49.4	495
12S rRNA.16924R	TGTTATCCCTGGRGTARCTTG	21	47.6	54	
16S rRNA.4199F	GTGCCAGCVRCCGCGGTTA	19	69.3	64.2	486
16S rRNA.4685R	GYTACRCCTYGACCTGAC	18	58.3	59.7	

Table 2.7: Mitochondrial ribosomal genes accession number. The sequence data for mitochondrion were obtained from the National Center for Biotechnology Information (NCBI) sequence repository (<https://www.ncbi.nlm.nih.gov>).

Species	12S rRNA	16S rRNA	Species	Mitochondrion DNA (complete genome)
<i>Stoliczkaia borneensis</i>	AF544779.1	AF544808.1	<i>Acrochordus granulatus</i>	AB177879.1
<i>Aplopeltura boa</i>	AF544761.1	AF544787.1	<i>Protobothrops dabieshanensis</i>	NC_022473.1
<i>M.euryxanthus</i>	Z46433.1	Z46483.1	<i>Protobothrops dabieshanensis</i>	NC_022473.1
<i>Azemiops feae</i>	L01763.1	L01764.1	<i>Heosemys depressa</i>	JQ266017.1
<i>Compsophis albiventris</i>	FJ404149.1	AY188050.1	<i>Mauremys megalcephala</i>	HM132059.1
<i>Aparallactus capensis</i>	FJ404129.1	AY188045.1	<i>Platysternon megacephalum</i>	NC_007970.1
<i>Atractaspis bibronii</i>	FJ404131.1	AY188047.1	<i>Chelonia mydas</i>	NC_000886.1
<i>Lamprophis capensis</i>	FJ404201.1	FJ404162.1	<i>Chelydra serpentina</i>	EF122793.1
<i>Pythonodipsas carinata</i>	FJ404189.1	AY188075.1	<i>Chelodina longicollis</i>	KJ713173.1

Species	12S rRNA	16S rRNA	Species	Mitochondrion DNA (complete genome)
<i>Prosymna janii</i>	FJ404193.1	FJ404222.1	<i>Apalone ferox</i>	FJ890514.1
<i>Aspidura sp.</i>	KC347307.1	KC347342.1	<i>Carettochelys insculpta</i>	FJ862792.1
<i>Geochelone sulcata</i>	AY081787.1	AY081788.1	<i>Abronia graminea</i>	NC_005958.1
<i>Emys orbicularis</i>	AB090021.1	AB090049.1		
<i>Staurotypus triporcatatus</i>	AB090018.1	AB090046.1		
<i>Eseya georgesii</i>	AF095894.1	AF113628.1		
<i>Phrynops geoffroannus</i>	U40647.1	AF113635.1		

2.2 Buffers and solutions

2.2.1 Tris-acetate-EDTA (TAE) buffer

TAE buffer was used for agarose gel electrophoresis. The amount of 242 g of Tris-base (Thermo Fisher) was dissolved in 0.7 L dH₂O. The volume of 57.1 ml absolute glacial acid and 100 ml 0.5 M EDTA disodium salt (pH 8.0) were mixed with Tris-base solution, and the final volume was completed to 1 L by L dH₂O to produce 50x TAE buffer. The pH of the final TAE buffer was adjusted to 8.5 using 1 M NaOH.

To prepare 1x TAE buffer for agarose gel electrophoresis, 20 ml of 50x TAE buffer was completed to 1 L by dH₂O. The final concentration of 1x TAE buffer was: 40 mM Tris-base, 20 mM glacial acid, 1 mM EDTA. The buffer was stored at room temperature.

2.2.2 HEPES and sodium cacodylate buffers

HEPES and/or sodium cacodylate buffers 0.1 M were used for washing and dehydration of specimens used in Transmission Electron Microscopy (TEM). To prepare 0.1 M HEPES buffer, 23.83 g of HEPES (Sigma) was dissolved in 1 L of dH₂O. To prepare 0.1 M sodium cacodylate buffer, 13.79 g of sodium cacodylate (Sigma) was dissolved in 1 L of dH₂O. The pH of the buffers was adjusted to 7.4 by 1 M NaOH before use and stored at 4°C.

2.2.3 Tissue preservation reagent

Tissue preservation reagent known as RNAlater was used to preserve tissue specimens prior to total RNA extraction. A 0.5 M EDTA stock was prepared by dissolving 18.61 g EDTA (Sigma) in 100 ml dH₂O and the pH was adjusted to 8.0 with 1 M NaOH. A 1 M of sodium citrate stock was also prepared by dissolving 29.4 g sodium citrate (Thermo Fisher) in 100 ml dH₂O. To prepare the tissue preservation reagent, 4 ml of 0.5 M EDTA pH 8.0, 2.5 ml of 1 M Tri-Sodium citrate and 70 g ammonium sulphate (Sigma) were mixed, and then 93.5 ml dH₂O were added to the solution. The components were mixed using a magnetic stirrer on low heat until the salt completely dissolved. Then, the pH was adjusted to 5.2 with 1 M H₂SO₄. Finally,

the reagent was filtered using 0.22 µm syringe filter (Millex) for sterilization and then stored at room temperature.

2.3 Plasmids and Bacterial strains

2.3.1 Plasmids

The plasmids used in this study are listed in Table 2.8.

Table 2.8: Plasmids used in this study.

Plasmid	Description	Source
pTriEx 1.1	Insect, bacterial, and mammalian vector for expressing proteins with a C-terminal HSV-8xHis cassette	Novagen
pL1	PCR product (L1, 1012 bp) of L polymerase of UHV was cloned into pTriEx 1.1, the total size of the plasmid is 6173 bp	This work
pL2	PCR product (L2, 527 bp) of L polymerase of UHV was cloned into pTriEx 1.1, the total size of the plasmid is 5688 bp	
pL3	PCR product (L3, 235 bp) of L polymerase of UHV was cloned into pTriEx 1.1, the total size of the plasmid is 5396 bp	
pZ	ORFs of Z protein of UHV that was cloned into pFastBac/HBM TOPO vector	Dr J. Hepojoki
pNP	ORFs of NP protein of UHV that was cloned into pFastBac/HBM TOPO vector	
pGP	ORFs of NP protein of UHV that was cloned into pFastBac/HBM TOPO vector	

2.3.2 Bacterial strains

Bacterial strains used in this study are listed in Table 2.9.

Table 2.9: Bacterial strains used in this study.

Strain	Description	Source
Stellar competent cells (<i>E. coli</i> HST08)	F ⁻ , endA1, supE44, thi-1, recA1, relA1, gyrA96, phoA, Φ80d lacZΔ M15, Δ(lacZYA-argF) U169, Δ(mrr-hsdRMS-mcrBC), ΔmcrA, λ ⁻	Clontech

2.4 Antibiotics

The antibiotic ampicillin was used when required to select transformants and maintain plasmids in *E. coli* at a working concentration of 100 µg/ml. To prepare a stock solution of ampicillin (100 mg/ml), 1 g of sodium ampicillin (Sigma-Aldrich) was completely dissolved in 10 ml dH₂O. A 0.22 µm sterile filter (Millex) was prewashed by dH₂O and then used to sterilize the antibiotic solution, before storage at -20°C.

2.5 Luria Bertani (LB) agar and broth

LB broth and agar were used for routine culture of *E. coli*. To prepare LB broth, 10 g Tryptone, 5 g yeast extract and 5 g NaCl were dissolved in 1 L dH₂O. The final mixture was sterilized by autoclaving at 115°C for 15 min.

The LB agar was also prepared by adding 15 g bacteriological agar (Miller) to the LB broth recipe in 1 L dH₂O as stated and mixed using a magnetic stirrer. The LB agar was sterilized in the autoclave at 115°C for 15 min.

2.6 Complementary DNA (cDNA) amplification of reptarenavirus

Complementary DNA (cDNA) of University of Helsinki virus (UHV) was kindly provided by Dr Hepojoki at University of Helsinki in Finland. The cDNA of UHV was used as a template in conventional polymerase chain reaction (PCR) with CloneAmp HiFi PCR Premix (Clontech) or DreamTaq DNA Polymerase (Thermo

Scientific). Each reaction of PCR contain mixture from these materials: cDNA of UHV, Hifi PCR premix or DreamTaq DNA Polymerase master mix and degenerate primers of reptarenavirus (Table 2.1, 2.2 and 2.3). The PCR mixture was put in a SensoQuest Basic Thermal Labcycler (Geneflow) and run according to the conditions: 1 cycle of Initial denaturation at 95°C for 3 min, 30 cycles of denaturation at 95°C for 30 sec, annealing at 54°C for 30 sec, extension at 72°C for 90 sec, followed by a final extension at 72°C for 5 min.

2.7 Agarose gel electrophoresis

1% agarose gels (w/v) were prepared by mixing 1 g agarose (Bioline) in 100 mL TAE buffer and boiling in a microwave until fully dissolved. 2 µl GelRed (Biotium) was added to molten agarose solution to a final concentration of 1x. DNA samples were electrophoresed in 1% agarose gels for either 45 min/120 V or 60 min/100 V immersed in 1x Tris-acetate-EDTA (TAE) buffer. The size of the DNA fragment was estimated using HyperLadder 1kb (Bioline) (Figure 2.1). In addition, agarose gel contains 0.1% sodium dodecyl sulfate (SDS) (Thermo Scientific), was used for visualized mitochondrial 18S and 28S rRNAs of the total RNA. The DNA was visualized using the G: Box Chemi XL 1.4 (Syngene) with GeneSys (Syngene) software.

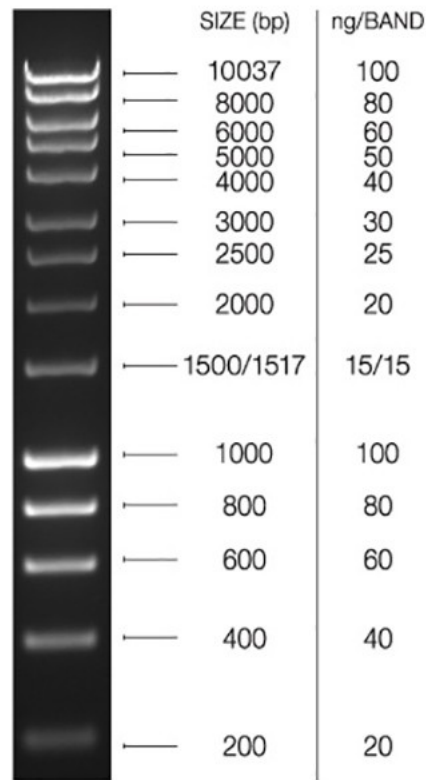


Figure 2.1: Molecular weight marker, HyperLadder 1kb (Bioline).

2.8 PCR purification and gel extraction

The PCR amplicons and DNA fragments in the 1% agarose gel were purified using a PCR clean-up, gel extraction kit (Macherey-Nagel). The agarose gel was visualized using a DR46B transilluminator (Clare Chemical). The section of gel containing the desired DNA was excised and cut into small pieces using a clean, sterile scalpel and then collected into 1.5 ml Eppendorf tubes. After, the gel extraction procedure was carried out according to the manufacturer's instructions of the kit. The concentration of the eluted product was determined by ND-1000 Nanodrop spectrophotometer (Thermo Fisher) and stored at -20°C.

2.9 Cloning L polymerase genes of UHV into pTriEx 1.1 plasmid vector

2.9.1 Linearization of pTriEx 1.1 plasmid by restriction digestion

Plasmid pTriEx 1.1 (Novagen) (Figure 2.2) was used for cloning the L polymerase genes for University of Helsinki virus (UHV). Double digestion of the vector was carried out according to the manufacturer's instructions (Clontech). The volume of 2 μ l from the vector (1 μ g) was digested with 5 μ l 10x green buffer (Thermo Fisher), 1 μ l of each restriction enzyme, *Xho*I and *Nco*I (Thermo Fisher), were used for cutting the target sites of the vector to produce linearized vector. Then, the volume was completed to 50 μ l by nuclease free water. The reaction mixture was incubated at 37°C for 30 min. Finally, the mixture was electrophoresed in 1% agarose gel for 1 hr/100 V as mentioned in section 2.7. The linear pTriEx1.1 plasmid was then extracted from the agarose gel as stated in section 2.8. Finally, the concentration of digested pTriEx 1.1 plasmid was measured using a ND-1000 Nanodrop spectrophotometer (Thermo Fisher) and preserved at -20°C.

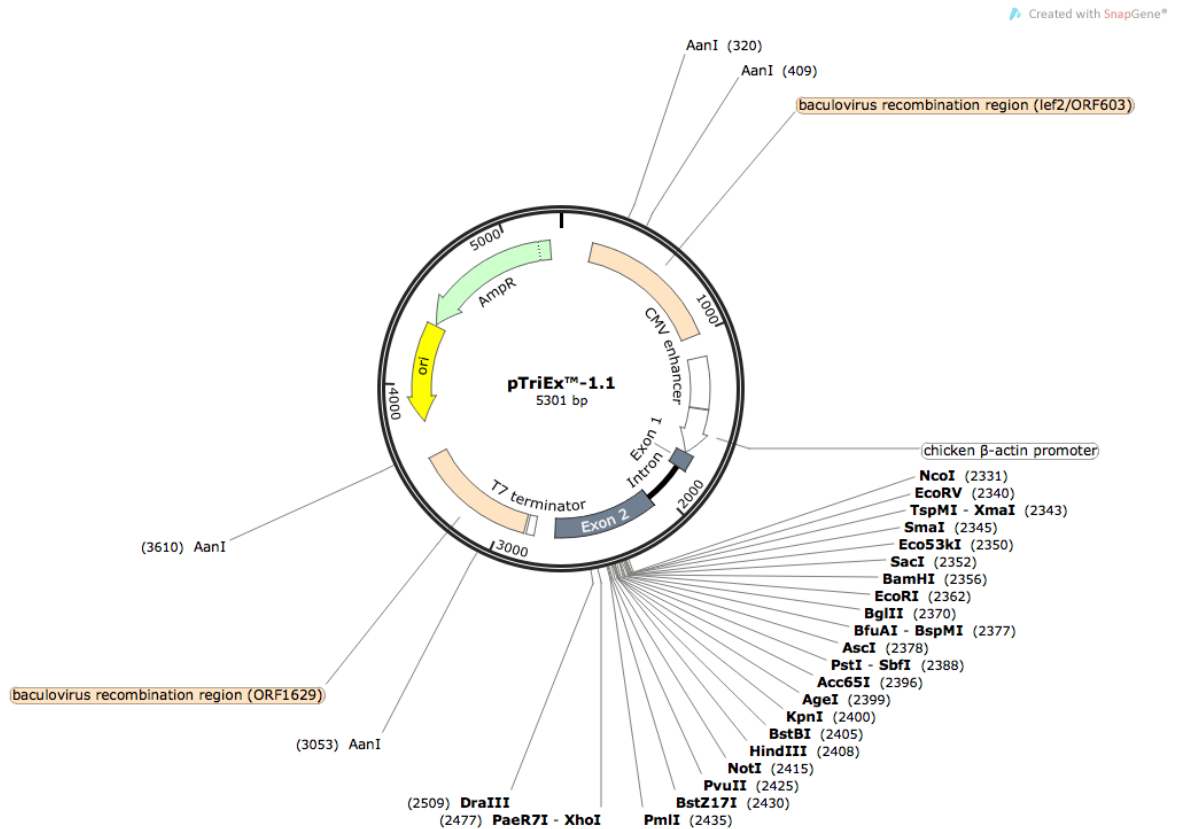


Figure 2.2: Map of the pTriEx 1.1 vector. The figure was created using SnapGene 2.8.3 software (GSL Biotech; available at snappgene.com).

2.9.2 PCR amplification of L polymerase from UHV

High Fidelity PCR was used to amplify the three regions (L1, L2 and L3) of L polymerase from University of Helsinki virus (UHV). Each PCR reaction contained 25 µl CloneAmp HiFi PCR Premix (Clontech), 2.5 µl for each forward and reverse infusion degenerate primers (Table 2.5), and 2.5 µl purified L polymerase gene fragments of UHV. At this time, the mixture was completed to 50 µl by nuclease free dH₂O. Then, the Thermal cycler (Geneflow) was run with the following conditions: 1 cycle of initial denaturation at 95°C for 2 min, 35 cycles of denaturation at 95°C for 1 min, annealing at 55°C for 1 min, extension at 72°C for 1 min, followed by a final

extension at 72°C for 10 min. Lastly, the PCR products were purified as stated in section 2.8 and stored at -20°C.

2.9.3 Cloning the UHV L polymerase PCR products into pTriEx 1.1

Three L polymerase genes of University of Helsinki virus (UHV) were cloned into linearized pTriEx 1.1 vector. The volume of both L polymerase inserts (L1, L2 and L3) obtained in section 2.9.2 and linearized pTriEx 1.1 vector using In-Fusion® Molar Ratio Calculator specifying a 1:3 molar ratio of insert to vector, available at (<http://bioinfo.clontech.com/infusion/molarRatio.do>). The cloning procedures were carried out according to the manufacturer's protocol (Clontech). Each fragment L1, L2 and L3 of UHV was mixed with linearized pTriEx 1.1 vector and 2 µl of 5x In-Fusion HD Enzyme Premix (Clontech). The concentration of insert and vector depended on molar ratio calculator result. Then, the final volume of the mixture was completed to 10 µl using nano-pure dH₂O. Finally, the reaction was incubated at 50°C for 15 min to be ready for transformation into *E. coli*.

2.10 Transformation of UHV plasmids into competent cell (*E. coli*)

The Infusion cloning reactions produced in section 2.9.3 (pL1, pL2 and pL3) were transformed into chemically Stellar™ Competent Cells (*E. coli* HST08 strain) (Clontech). The pNP, pZ and pGP plasmids within pFastBac/HBM-TOPO vector were kindly supplied by Dr Jussi Hepojoki at University of Helsinki and were also transformed into Stellar™ Competent Cells (*E. coli* HST08 strain) (Clonetch). 200

ng/ μ l of each plasmid was transformed into chemically *E. coli* HST08 strain (Clonetch) according to supplied protocols. 1 μ l plasmid DNA was added to 25 μ l competent cells, and then incubated in ice for 30 min. Then, the cells were heat shocked by incubating at 42°C for 45 sec. Afterwards, the cells were put in ice for 2 min. Pre-warmed 125 μ l SOC medium (Clontech) was then added to the plasmid-competent cells mixture and incubated in shaker at 37°C/200 rpm for 1 hr. During this time, LB plates containing ampicillin 100 μ g/ml were prepared and after incubation 50 μ l and 100 μ l of the final mixture were spread on the plates. The plates were incubated at 37°C over night.

2.10.1 Colony PCR (cPCR) of transformants

In order to corroborate that the target plasmids (Table 2.8) of University of Helsinki virus (UHV) were correct, single colonies were transferred from transformation plates using a sterile micropipette tip into a mixture containing 5 μ l from DreamTaq DNA Polymerases (Thermo Scientific), 1 μ l from each forward and reverse degenerate primers (Table 2.1, 2.2 and 2.3). Then, the final volume was completed to 10 μ l by adding 3 μ l from nano-pure dH₂O. The cPCR reactions was put in Thermal Labcycler (Geneflow) and then run under the following condition: 1 thermal cycle for initial denaturation at 95°C for 10 min, 30 thermal cycles for denaturation at 95°C for 45 sec, annealing at 54°C for 45 sec, extension at 72°C for 1 min, followed by a final extension at 72°C for 5 min. Ultimately, the cPCR products were loaded into 1% agarose gels for gel electrophoresis at 120 V/45 min as stated in section 2.7.

2.10.2 Purification of DNA plasmids

Transformants that were confirmed by cPCR to contain the UHV ORFs in the pTriEx1.1 (pL1, pL2 and pL3) and pFastBac/HBM-TOPO vectors (pNP, pZ and pGP) were selected for purification. The Maxiprep purification was carried out by using GeneJET Plasmid Maxiprep kit (Thermo Scientific) according to the manufacturer's instructions. In the end, around 500 µl of the product was eluted and the concentration was measured by ND-1000 Nanodrop spectrophotometer (Thermo Fisher) and then the plasmids were preserved at -20°C.

2.10.3 Storage of bacterial strain with cloned plasmids

Colonies with the cloned plasmids contains inserts of UHV were taken from LB plates and added to 10 ml LB broth with ampicillin (100µg/ml). Then, the broth was incubated in shaker 37°C/200 rpm for overnight. Next, 700 µl of incubated broth mixed with 300 µl of 50% glycerol. Lastly, the plasmids were preserved in -80°C.

2.11 DNA Sanger sequencing

Purified PCR amplicons and plasmids of UHV were sequenced at Source BioScience laboratory service. The sequencing was carried out using 10 µl each DNA amplicons (10 ng/µl) or plasmid (100 ng/µl) and 10 µl (10 uM) degenerate specific primers. Each amplicons/plasmids and primers were in separate tubes and were sent to the company for Sanger sequencing.

2.12 RNA extraction and analysis

2.12.1 Reptiles specimens

Internal organs including liver, spleen and kidney were dissected from different species of reptiles including snakes, turtles and tortoises, chameleons, lizard and fire skink. The frozen animals were collected from Heathrow Animal Reception Centre (HARC) and then the animals were dissected using sterilized blades and forceps. The dissection was carried out in isolated area. In addition, snake's liver specimens were collected by collaboration with Zoological Society of London (ZSL) at London Zoo. All specimens were collected into tubes contains tissue preservation reagent and preserved at -80°C for total RNA isolation.

2.12.2 Total RNA extraction

Total RNA was isolated from small pieces of tissue ≤ 25 mg stored in tissue preservation reagent using the RNeasy Mini kit (Qiagen), while ≤ 5 mg tissue was used for total RNA isolation by peqGOLD MicroSpin Total RNA kit (peqlab). The tissue was collected in RNase free 2ml Eppendorf tubes and mixed with lysis buffer. The mixture was then transferred to 2 ml Lysing Matrix D tube (MP Biomedicals) containing ceramic spheres to homogenize the specimens and destroy the cell wall and release the RNA. The tubes were placed in a FastPrep-24™ homogenizer (MP Biomedicals) for either once at speed 6.5 for 45 sec or twice at speed 6.5 for 30 sec with a 5 min rest on ice in between. The homogenized samples were kept on ice for 5 min, and then centrifuged at 12000 rpm for 10 min at 4°C. The supernatant was

mixed with 75% ethanol (one volume) (Note: 50% ethanol was used for liver samples to increase RNA yield). The mixture was then added to a spin column placed in 2 ml collection tube and centrifuged for 15 sec. Then, the DNA contamination was removed either by DNA column or Dnase I digestion treatment (Peqlab) according to the manufacturer's instructions. Followed by two washing steps, the first with 700 µl of RW1 buffer which contains a small amount of guanidine thiocyanate to denature RNases, the second wash with 500 µl of RPE buffer (contains 96-100% ethanol) to remove traces of salts. Finally, 25-30 µl total RNA was eluted with RNase free water and the product was quantified using a ND-1000 Nanodrop spectrophotometer and preserved at -80°C.

In addition, a sample of UHV RNA in triazole was kindly provided by Dr Jussi Hepojoki at University of Helsinki was also purified using the peqGOLD MicroSpin total RNA Kit (Peqlab) according to the manufacturer's instructions for use as a positive control in RT reactions.

2.12.3 Total RNA integrity

Total RNA (eukaryotic) was analysed using an RNA 600 Nano kit (Agilent), which is designed for use with an 2100 Bioanalyzer (Agilent). The kit components were equilibrated at room temperature for 30 min. First, the RNA 6000 Nano Gel Matrix was prepared by pipetting 550 µl into a spin filter and centrifuged at 13000 rpm for 10 min at room temperature. Second, 65 µl of the filtered RNA 6000 Nano Gel Matrix was mixed and vortexed with 1 µl RNA 6000 Nano Dye and centrifuged for 10 min at 13000 rpm. Next, a new RNA chip was placed on the chip priming station, and 9

μ l RNA 6000 Nano gel-dye mixture was loaded into the bottom of the three 'G' wells. The plunger was set to 1 mL and then secured in the chip priming station until held by the clip, before the plunger was pressed. After 1 min, the plunger was released and after a 5 sec wait, the plunger was pulled back to the 1 ml position again. Then, 9 μ l RNA 6000 Nano gel-dye mixture was loaded in the top two 'G' wells. 5 μ l RNA 6000 Nano Marker was then loaded in to the 12 sample wells and the ladder well, followed by loading 1 μ l RNA 6000 NanoLadder in ladder well. Finally, 1 μ l purified RNA sample was loaded in to each sample well and the chip was vortexed horizontally at 2400 rpm for 1 min using IKA vortex (Agilent). Each chip was run on the 2100 Bioanalyzer within 5 min after samples were loaded using Eukaryotic total RNA Nano Assay. The electropherogram shows total RNA (eukaryotic) with 18S and 28S ribosomal RNAs peaks, and the RNA integrity number (RIN) calculation is given for each RNA sample.

2.13 Reverse transcription PCR (RT-PCR)

2.13.1 Reverse transcription of RNA

Total RNA extracts of snakes and other reptiles were reverse transcribed using TaqMan® Reverse Transcription Reagents (Applied Biosystems). Total RNA extracts and purified RNA of UHV (positive control) were used as a template for reverse transcription (RT) reaction. Each RT reaction column contained final concentration of 1 μ l from each MultiScribe™ RT reaction (2.5 U/ μ L), RNase Inhibitor (1.0 U/ μ l), 100 mM dithiothreitol (DTT), 4 μ l from 10 mM dNTP mix, 1.4 μ l 25 mM MgCl₂ and 2 μ l 1x RT Buffer in a final reaction completed to 20 μ l using

DEPC- treated dH₂O. Then, 1 µl from 50 µM random hexamers primer was mixed with the reaction. Finally, 1-7 µl RNA sample (up to 1 µg/µl) was added to the final RT reaction. In addition, 1 µl (50 µM) from each Oligo(dT) and random hexamers primers (Applied Biosystems) were mixed and then used to monitor the RT reaction. A spiked RT reaction was carried out using RNA extract mixed with the UHV RNA positive control. The RT reactions were run in SensoQuest Basic Thermal Labcycler (Geneflow) according to the conditions: Primer extension at 25°C for 10 min, DNA polymerization at 37°C for 30 min and enzyme deactivation at 95°C for 5 min. The cDNA products were preserved at -20°C.

2.13.2 Detection of specific reptile mitochondrial and reptarenavirus genes by RT-PCR

cDNA was used as template to amplify the mitochondrial ribosomal genes (12S and 16S rRNAs) and reptarenavirus genes (L and NP) in the second step of RT-PCR. The RT-PCR mixture contained 6.5 µl DreamTaq DNA Polymerase (Thermo Scientific), 1.5 µl cDNA template and 1 µl (10 uM) of each forward and reverse primer. Then, the final volume was completed to 12.5 µl by adding 2.5 µl nano-pure dH₂O. The primers used are specific of mitochondrial genes (Table 2.6), L polymerase and nucleoprotein (Table 2.1, 2.2 and 2.4). The PCR was run in SensoQuest Basic Thermal Labcycler (Geneflow) according to the conditions: 1 cycle of initial denaturation at 95°C for 3 min, 35 cycles of denaturation at 95°C for 30 sec, annealing at 55°C for 30 sec, extension at 72°C for 90 sec, followed by a final extension at 72°C for 5 min. The annealing temperature was at 47°C when the degenerate primers of L polymerase (Table 2.4) were used. RT-PCR reactions

containing UHV cDNA were used as a positive control. The expected amplicon was electrophoresed in 1% agarose gel (Bioline) and then extracted as stated in section 2.7 and 2.8 respectively. The eluted products were sent for Sanger sequencing as described in section 2.11.

2.14 Bioinformatic analysis of L polymerase of arenaviruses

2.14.1 Obtaining L polymerase sequences in GenBank database

The database on National Centre for Biotechnology Information (NCBI) was used to obtain protein sequences of arenaviruses and some other viruses. L polymerase sequences of four species of both mammarenavirus and reptarenavirus including Tacaribe virus (TCRV), lymphocytic choriomeningitis virus (LCMV), Golden Gate virus (GGV), California Academy of Science virus (CASV) were utilized for finding similarity with arenaviruses in GenBank database. In addition, RNA dependent RNA polymerase sequences of other viruses were used to root the phylogenetic trees (Table 2.10).

Table 2.10: Protein accession number of arenaviruses and viruses used to root the phylogenetic trees. The accession numbers of the amino acids were obtained from the National Centre for Biotechnology Information (NCBI) sequence repository (<https://www.ncbi.nlm.nih.gov>).

Virus	Accession Number
Tacaribe virus (TCRV)	NP_694848.1
Lymphocytic choriomeningitis virus (LCMV)	NP_694845.1
Golden Gate virus (GGV)	YP_006590089.1
California Academy of Science virus (CASV)	YP_006590093.1
Hantaan virus (HTNV)	NP_941982.1
Bunyamwera virus (BUNV)	NP_047211.1
Rice stripe virus (RSV)	AFM93820.1
Tomato spotted wilt virus (TSWV)	AIA24440.1
Vesicular stomatitis virus (VSV)	AAA48442.1
Citrus psorosis virus (CPsV)	Q6DN67.1
European mountain ash ringspot-associated virus (EMARaV)	Q6Q305.2
Lettuce big-vein associated virus (LBVaV)	Q8B0U2.1
Influenza A virus	P03433.2
Midway nyavirus (MIDWV)	YP_002905331.1
Borna disease virus (BDV)	CEK41892.1
Zaire ebolavirus (EBOV)	AAG40171.1
Human metapneumovirus (hMPV)	All17600.1

2.14.2 Identification of open reading frames (ORFs)

The amino acids sequence of L polymerase of four arenavirus species (Table 2.10), Tacaribe virus (TCRV), lymphocytic choriomeningitis virus (LCMV), Golden Gate virus (GGV) and California Academy of Science virus (CASV) were used for searching the translated nucleotide database (transcribed RNA) on GenBank database. The query sequence of the L polymerase was entered in fasta format in translated blast (tBLASTn) on National Center for Biotechnology Information (NCBI). The database searching was allocated at Transcriptome Shotgun Assembly (TSA), while maximum target sequencing assigned to one hundred at algorithm parameters and followed by running the tBLASTn. Target sequence data of transcribed RNA was collected where E-values were less than 1. Then, the translate tool (ExpASy)

was used to find the open reading frames (ORFs) in the transcribed RNA sequences (Gasteiger et al. 2003) (available on <http://web.expasy.org/tools/translate/>). Compact choice was selected as output format for translation protein. One or two of the largest open reading frames were selected for further bioinformatic analysis.

2.14.3 Protein homology and structure prediction

The bioinformatic tool kit HHpred version HHsuite-2.0.16mod (Söding et al. 2005) (available on <https://toolkit.tuebingen.mpg.de/hhpred>) was used for detecting protein homology and predicting structure using a known structural protein. The largest one or two open reading frames that were identified by translate tool (ExpASy) in section 2.14.2 were entered in to protein homology database searching on HHpred online facility. The parameters with lowest E-value and high score were selected and saved for further bioinformatics analysis.

2.14.4 Sequence analysis

MrBayes version v3.2.6 (Ronquist et al. 2011) is a command line programme that was used in phylogenetic analysis in parallel mode (Huelsenbeck and Dyer 2004). Partial sequencing of arenavirus L polymerase, ORFs determined in section 2.14.2 and RNA dependent RNA polymerase (RdRp) sequence of rooted viruses (Table 2.10) were used for Bayesian analysis. These sequences were aligned by multiple sequence alignments (MSA) using Clustal Omega version (1.2.4) (McWilliam et al. 2013) and the alignment file (.nexus) was entered as command-line in mb of the

MrBayes program. Then, the posterior distribution of model parameters was estimated by Markov chain Monte Carlo (mcmc) command. The sump and sumt commands were used to build consensus trees (.trprobs) (Hall 2018; Ronquist et al. 2011). Finally, the phylogenetic trees were viewed and edited by FigTree v1.4.3 software (<http://tree.bio.ed.ac.uk/software/figtree/>).

2.15 Fixation and resin embedding of the infectious bronchitis virus (IBV) specimens

2.15.1 Fixation of IBV specimens

The pellets of CK, TOCs and DF1 cells that are mock infected and infected with infectious bronchitis virus (IBV) strains in 0.1 M sodium cacodylate buffer were kindly provided by Dr Helena Maier from the Pirbright Institute, UK. The samples were rinsed from the 0.1 M sodium cacodylate buffer and the pellets were then fixed by adding 1 ml osmium tetroxide 1% (w/v) in 0.1 M sodium cacodylate. The samples were left for 1-3 hr at room temperature until the samples turned black in colour.

2.15.2 Washing of IBV specimens

IBV samples were washed with either 0.1 M sodium cacodylate buffer or HEPES buffer. The osmium tetroxide 1% (w/v) / 0.1 M cacodylate buffer was discarded from the pellets and 1 ml from the 0.1 M sodium cacodylate/ HEPES buffer was added to the samples and centrifuged at high speed (13000 rpm) for 1 min. Then, the samples were left for 15 min immersed in buffer. The buffer was discarded, and fresh buffer

was added. The washing protocol was repeated three times on each sample in preparation for the dehydration steps (Davies 1999).

2.15.3 Dehydration of IBV specimens

The samples of IBV were dehydrated by using absolute acetone:cacodylate/HEPES buffer (0.1 M) in different concentration and incubation period (15-30 min). The concentration and the incubation time of dehydration are described in Table 2.11. The buffer from final step of washing was discarded and 1 ml 30% absolute acetone:cacodylate/HEPES (0.1 M) buffer was added to each sample and incubated at room temperature for 15 min. Subsequently, increasing concentrations of acetone were used in the dehydration protocol until complete dehydration was achieved after 3 steps using 100% absolute acetone steps (Davies 1999).

Table 2.11: Dehydration steps of IBV specimens by different concentration of acetone. The final dehydration step by absolute acetone was repeated three time.

Volume/ acetone: buffer	Acetone concentration	Time
3:7	30%	15 min
1:1	50%	15 min
7:3	70%	30 min
8:2	80%	30 min
Absolute acetone (Three times)	100%	30 min

2.15.4 Infiltration of IBV specimens

The infiltration protocol was carried out directly after the final steps of dehydration were finished. An agar 100 resin kit (Agar Scientific) was used for infiltration according to manufacturer's instructions. The kit components, cylinder and conical flask were warmed to 60°C before preparing the final mixture. The IBV blocks can be soft, medium or hard depending on the volume of the kit components used, which include Agar 100 epoxy resin, Dodecenylsuccinic anhydride (DDSA), Methyl nadic anhydride (MNA) and Benzyldimethylamine (BDMA). The hard block IBV samples were prepared by adding 20 ml of pre-warmed Agar 100 epoxy resin, 9 ml of DDSA (hardener) and 12 ml of MNA (hardener) into the warm conical flask, then the component was mixed and gently shaken. 1.2 ml BDMA (accelerator) was added to the component and mixed gently for 1-2 min. To begin with, the infiltration steps started when absolute 100% acetone was discarded from the final step of samples dehydration. 1:3 resin:acetone was added to each sample and sealed using parafilm and left on a rotator for 3-6 hr. Subsequently, the infiltration procedure was repeated using 1:1 and then 3:1 resin:acetone. The resin:acetone mixture was discarded, and 1 ml 100% resin was added to the IBV samples, which were sealed and put on the rotator for 3-6 hr. The last infiltration step with 100% resin was performed twice (Davies 1999).

2.15.5 Embedding of IBV specimens

The IBV specimens were embedded using 100% fresh resin (Agar Scientific) according to manufacturer's instructions. The embedding was carried out directly after finishing the incubation period of the last step of the infiltration procedure. The old resin from the final step of infiltration was discarded and fresh 100% resin (hard in density) and new polypropylene moulds were prepared. The volume of the final 100% resin depended on how many samples that were used. IBV samples (black pellet) were transferred to the bottom of the new polypropylene moulds. Then, the 100% resin was added until close to the edge of the moulds. Finally, the samples were named and put it in an oven at 60°C for 2-3 days for hardening.

2.15.6 Sectioning of embedded IBV specimens by Ultramicrotome

IBV specimens were sectioned using a Reichert-Jung Ultracut E Ultramicrotome. The IBV blocks containing polymerized resin were removed from the moulds. Then, the site of interest (end of the blocks containing black embedded samples) were trimmed to a pyramid shape using a clean, sharp razor blade, as the size of trapezoid should be no more than 0.5 mm in width. The sample blocks were polished initially using a class knife, followed by a diamond knife for final IBV sections. Each section ranged between 60-80 nm in thickness, the silver colour of the section indicating it was adequate for examination by Transmission Electron Microscopy (TEM). A few floating silver sections were collected on copper grids (300 mesh) and then stained using 0.5-2% (w/v) uranyl acetate (Davies 1999). The grids were left for 2-3 hr at room temperature until completely dry.

2.15.7 Transmission Electron Microscopy (TEM)

The stained grids of IBV were screened and photographed using Transmission Electron Microscopy (Philips CM20) at 80-200 kV with a charged-coupled device (CCD) camera. Many images for each grid with different TEM focusing were analysed and saved.

Chapter 3 Design and validation of reptarenavirus detection primers

3.1 Introduction

Arenaviruses are single stranded RNA viruses with a genome composed of 2 segments, large (L) and small (S). The L RNA segment encodes the L polymerase or viral RNA dependent RNA polymerase (RdRp) and a zinc finger-like motif protein (Z), while the S RNA segment encodes the nucleoprotein (NP) and glycoprotein (GPC) (Zapata and Salvato 2013). The open reading frames (ORFs) of arenaviruses are ambisense, that is to say their coding capacity is arranged in opposite directions (Bishop 1990) and separated by an intragenic region (or non-coding region) (Romanowski 1993; Salvato 1993). As both L polymerase and NP are conserved functionally, arenaviruses have conserved sequences in their L and S RNA segments that can be used for cDNA synthesis by degenerate primers and such primers have been designed and validated for gene amplification using reverse transcription PCR (RT-PCR) (Auperin et al. 1982; Vieth et al. 2007). Many arenaviruses from many target species have been isolated and diagnosed using such PCR approaches (Lozano et al. 1997; Paweska et al. 2009) or by real time PCR (Cordey et al. 2011). Both PCR techniques are based on using specific gene primers for conserved regions for screening for the existence of novel but related arenaviruses in human and animal samples (Lozano et al. 1997).

Reverse transcription PCR is the method of choice used for arenavirus diagnosis through the use of degenerate oligonucleotide primers for arenavirus genes (Demby et al. 1994; Vieth et al. 2007). Using degenerate primers coupled with the RT-PCR technique has proved successful for the detection of novel and existing arenaviruses.

RT-PCR detection based on the viral RNA dependent RNA (RdRp) have been carried out during investigation of arenavirus haemorrhagic fever and/or to discover novel arenaviruses in infected and suspected specimens. For instance, Morogoro and Kodoko viruses were identified by detection of the conserved regions of the L polymerase and infections by these viruses subsequently confirmed by sequencing (Lecompte et al. 2007; Vieth et al. 2007) which indicated a high degree of accuracy for the use of RT-PCR for virus detection and diagnosis (Palacios et al. 2008). Also, the L polymerase gene of the Lassa virus was detected by RT-PCR using specific gene primers providing evidence for Lassa infection in both cell culture and patients in the last decade (Vieth et al. 2007). Lassa virus nucleoprotein (NP) and glycoprotein (GPC) genes were also detected in suspected specimens by RT-PCR (Ter Meulen et al. 1998). Similarly, arenaviruses including Lassa virus was detected in serum and urine specimens from human patients using RT-PCR by amplifying conserved regions of the NP and GPC genes (Lunkenheimer K, Hufert FT 1990). Therefore, many cases of arenavirus infection have been detected by variants of the PCR technique (Bowen et al., 1996; Lozano et al., 1997).

Real time PCR can also be used for arenavirus detection. Real time PCR was used for arenavirus detection in cases that were only suspected of arenavirus infection because of suspected spreading in an endemic area or when testing clinical or environmental situations (Cordey et al. 2011). On the other hand, arenaviruses have been isolated from suspected specimens including human samples using real time SYBR Green PCR rather than ordinary real time PCR and such tests have been approved for use by clinicians in epidemics (Drosten et al. 2002). For example, real time PCR was used as a diagnostic technique for Argentine haemorrhagic fever (AHF) caused by Junin virus (Trombley et al. 2010). In general, techniques for arenavirus detection have been improved considerably by using molecular detection (Bowen et al. 1996; Lozano et al. 1997; Trombley et al. 2010). An advantage of the procedure is that quantitation is possible as demonstrated by the determination of arenavirus infectious titre associated with cytopathic effects (CPE) in tissue culture (Vieth et al. 2005).

The objective of the study described in this chapter was to design degenerate oligonucleotide primers for detecting reptarena-like viruses by RT-PCR. To do this, degenerate primers were designed based on conserved genes, the viral RNA-dependent RNA polymerase (L), nucleoprotein (NP), small zinc finger motif protein (Z) and glycoprotein precursor protein (GPC) from snake reptarenavirus, including Golden Gate virus (GGV), Boa virus, California Academy of Science virus (CASV) and University of Helsinki virus 1 (UHV-1). The function of the degenerate primers was established using DNA as template using total viral cDNA of UHV. Specific products were amplified from each of the four UHV genes using the newly designed

degenerate primers and the products of the L polymerase gene amplification were cloned and sequenced for use as an L-specific PCR standard.

In parallel, to assess if these primers could bind to unknown reptarenavirus sequences, bioinformatics was used to compare them to all available reptarenavirus sequences. The bioinformatics tools and databases used were those of the European Bioinformatics Institute (EMBL-EBI). EMBL-EBI provides analysis tools such as FASTA, NCBI BLAST and Clustal Omega for multiple sequence alignments (MSA). The tool kits and programming languages used are described in the guides and tutorials that are available (McWilliam et al. 2013). Jalview 2.9 (Waterhouse et al. 2009) and SnapGene 3.1.2 (GSL Biotech; available at snapgene.com) were also used throughout. Recently, it was found that Aurora borealis virus 1 (ABV-1) and Aurora borealis virus 2 (ABV-2) were associated with snake inclusion body disease (Hepojoki et al. 2015b) and these reptarenavirus sequences were also included in this analysis. In all, to perform the sequence analysis, the L polymerase and nucleoprotein (NP) coding regions of six reptarenavirus isolates including Golden Gate virus (GGV), Boa virus, California Academy of Science virus (CASV), University of Helsinki virus 1 (UHV-1) and Aurora borealis virus (ABV-1 and ABV-2) were used. In addition, the sequences of the cloned genes of UHV were aligned with the sequence of UHV-1 and ABV-1 available in the GenBank database to ensure no errors induced by the amplification and cloning procedures. The sequences of the cloned amplicons derived from L, Z, NP and GPC genes of UHV were also compiled in their respective cloning vectors to provide standard cloning maps.

3.2 Results

3.2.1 Protein sequence-based degenerate primer design

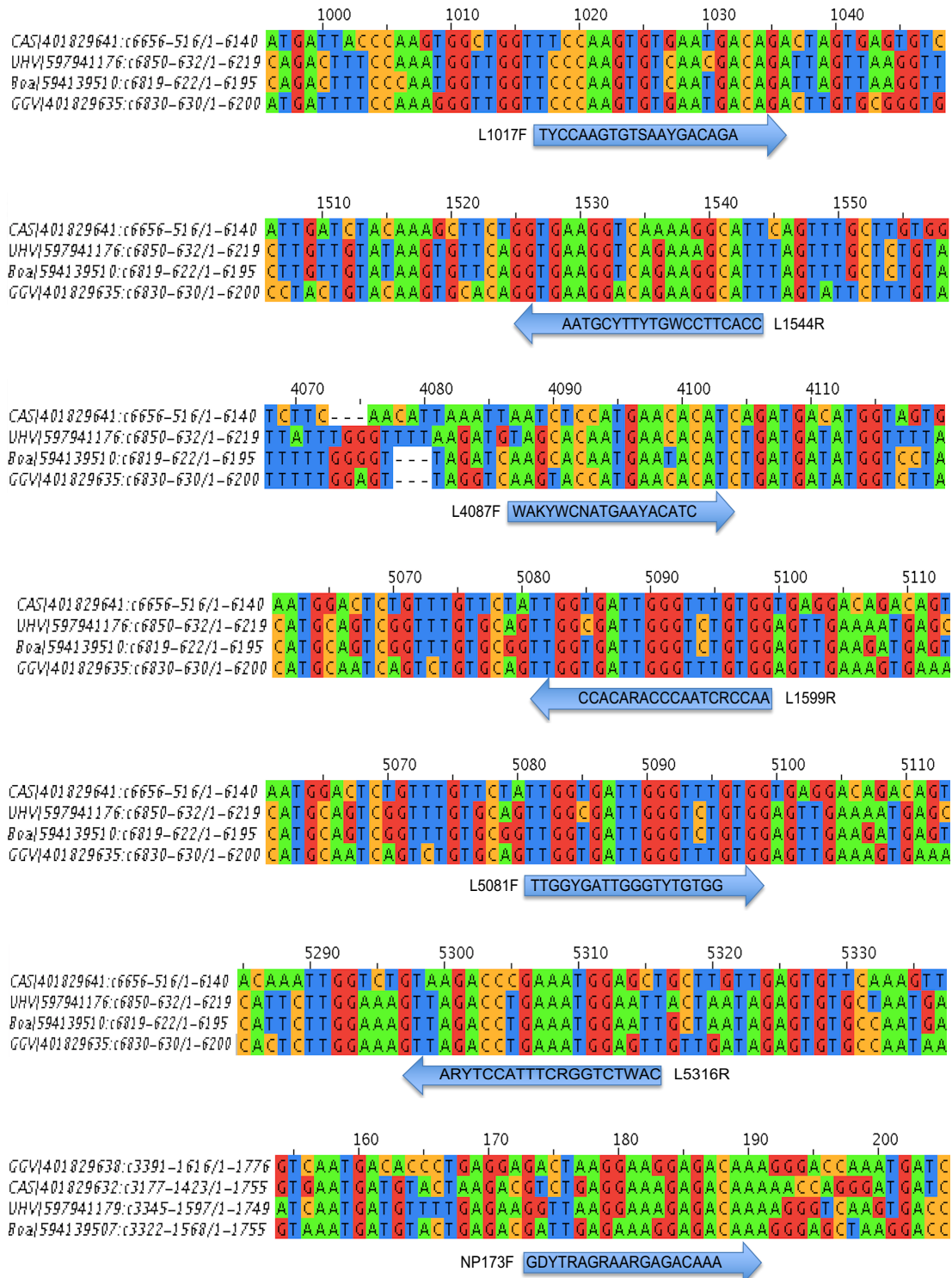
A protein BLAST search (Stephen et al. 1990) of the National Centre for Biotechnology Information non-redundant protein sequence database with the Z, NP, GPC and L proteins of CASV and GGV was performed in order to collect reptarenavirus sequences for analysis. Protein sequences with more than 90% amino acid identity to each other were selected for alignment of GGV, Boa, CASV and UHV-1 which was carried out using Clustal Omega version 1.2.4 (Sievers et al. 2014). The results of the alignment were viewed and edited using Jalview 2.9 software (Waterhouse et al. 2009). Conserved amino acid sequences were identified manually and converted back to nucleotide sequences using uncertainty codes to include each of the possible codons that could encode a particular amino acid. For example, a conserved valine could be encoded by GUA, GUC, GUG or GUU codons, which can be summarized as the sequence GUN, where N stands for any of the four nucleotides. International Union of Pure and Applied Chemistry (IUPAC) conventions were used where a mixture of nucleotides was required in the primer design.

Regions of 6-7 universally conserved amino acids were selected manually from the sequence alignments in order to design primers of approximately 18-21 nt. Potential primer binding sites were evaluated and identified by looking for clusters of amino acids encoded by the fewest possible nucleotide combinations. For example, amino acids encoded by one or two codons, such as methionine (1 codon) or tryptophan (1 codon) were preferred to amino acids encoded by more than four codons, such

as leucine and serine. Comparison of the cDNA sequences within the selected regions for each degenerate primer is shown in Figure 3.1. A similar analysis was performed using a mix of mammarenavirus and reptarenavirus sequences, but did not yield any useful primer pairs, suggesting that arenaviruses could likely only be detected using genus-specific degenerate primer sets. As a result of their higher amino acid conservation, multiple primer sets could be designed for the L polymerase and NP genes, while only one primer set could be successfully designed for each of the Z and GPC genes. This is in keeping with the literature where many species of arenaviruses, including novel sequences for Lassa virus, LCMV, Ippy virus, Mobala virus and Mopeia virus as well as Pichinde virus and Tacaribe virus, were determined by using RT-PCR for the L polymerase gene (Vieth et al. 2007) while only Lassa virus was detected using primers for the NP and GPC genes (Lunkenheimer K, Hufert FT 1990). Both L polymerase and NP proteins are important for viral transcription and replication (Pinschewer et al. 2003) so change little for reasons of structural constraint on their function. Additionally, they occur inside the virus particle so are not subject to immune pressure. By contrast, the GPC protein is a single polypeptide consisting of peripheral membrane protein (GP1) and transmembrane protein (GP2) that are created from the original GP1/GP2 precursor during posttranslational processing by the cellular SKI-1/S1P subtilase (Beyer et al. 2003; Eichler et al. 2006; Lenz et al. 2001). As GP1/GP2 occur on the outside of the virus particle they can vary as a result of antibody driven selection. The Z protein carries L domains (Freed 2003) required for the formation of the budded virus (Strecker et al. 2003; Wang et al. 2012) but despite this functional restraint Z gene sequences vary significantly, possibly as a result of their interactions with multiple host cell proteins (Grande-Pérez et al. 2016).

Chapter Three: Degenerate primers and bioinformatics analysis

The analysis here revealed several highly conserved regions found in snake reptaenavirus species, which could potentially be used for detection of novel reptaenavirus sequences in specimens of snakes and other reptiles.



Chapter Three: Degenerate primers and bioinformatics analysis

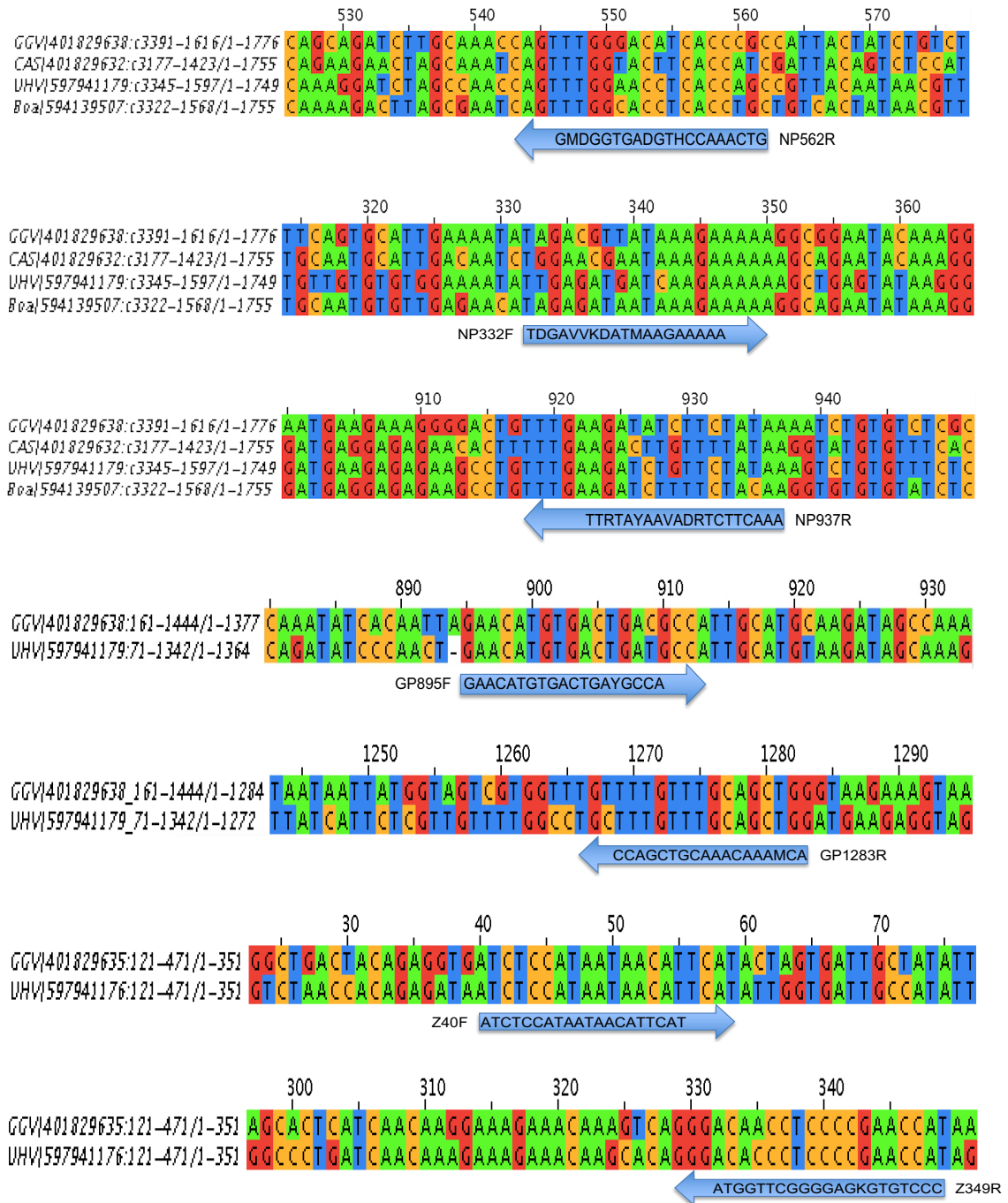


Figure 3.1: Sites of proposed degenerate primers for reptarenavirus. Degenerate primers complementary to the arrow regions of between (18-21 bp) are shown. The image was created using Jalview 2.9 software (Waterhouse et al. 2009). Accession number for L polymerase, Z protein, NP and GPC of UHV-1, Boa virus, GGV and CAS virus were mentioned in Table 2.1, 2.2, and 2.3.

3.2.2 Identity among proteins of novel snake reptarenavirus

Arenaviruses are characterized by re-assortment among their segments so the question of the origin of the genes present in any new isolate arises; is a newly identified virus truly original or is it a recombinant derived from existing viruses that may have re-assorted. To address this question the protein coding regions of two strains, ABV-1 and ABV-2, were aligned with other characterized snake reptarenavirus including CAS, Boa, GGV and UHV-1 and the conserved regions identified in the same way as that described for the design of degenerate primers of reptarenavirus. It was found that some conserved parts of these viruses were almost identical at the sequence level suggesting that these regions could be used to design further degenerate oligonucleotides (Table 2.4) for screening unknown samples to identify new variants and to contribute to phylogenetic studies and the molecular characterization of snake reptarenaviruses (Figure 3.2).

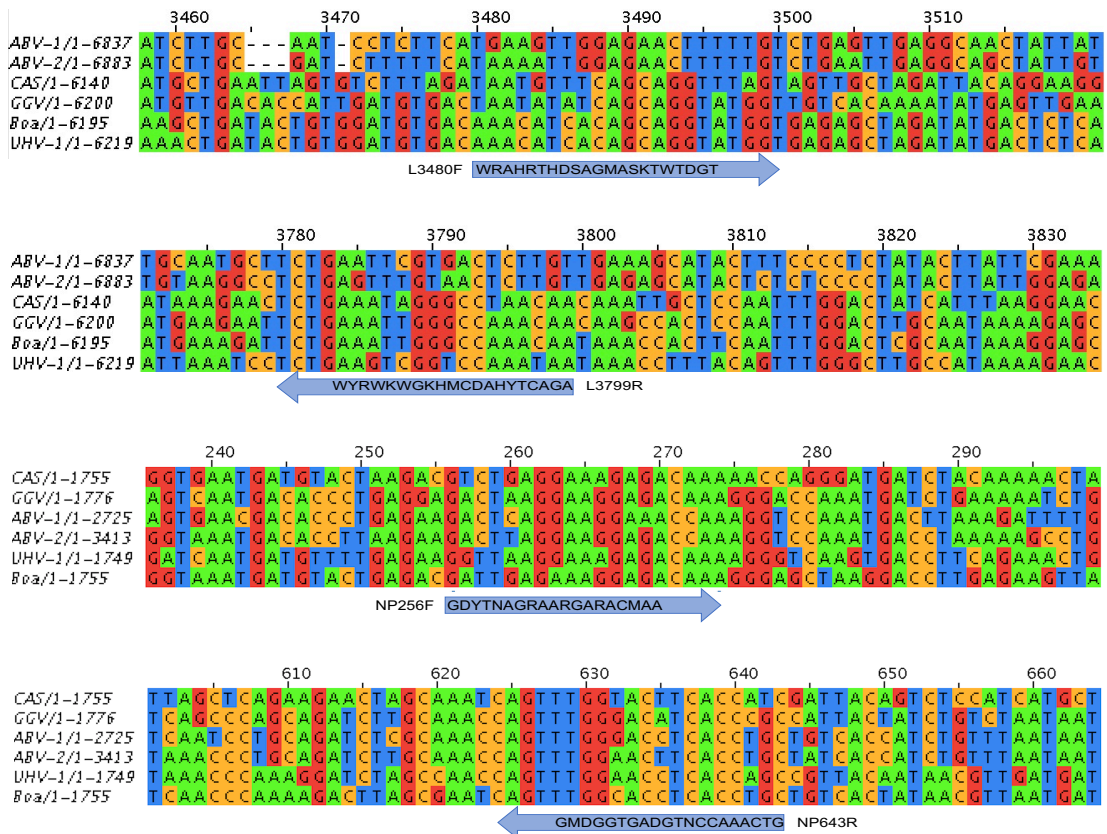


Figure 3.2: Identity among snake reptarenavirus protein coding regions. The two snake reptarenavirus proteins (L and NP) were used for alignment using Clustal Omega (1.2.4) and 18-21 bp were selected from observing the parts that has obvious similarity. Arrows show the nucleotide sequences for snake reptarenavirus detection primers. Accession number for L polymerase and NP of UHV-1, GGV, Boa virus and CASV were described (Table 2.1). Accession number of L segment of ABV-1: KR870021.1, ABV-2: KR870033.1, accession number of S segment of ABV-1: KR870010.1, ABV-2: KR870018.1(Waterhouse et al. 2009).

From the analysis shown in Figure 3.1 and Figure 3.2, it is observed that the L polymerase coding region has a greater number of identical regions followed by NP protein sequence, while Z and GPC protein have less similarity, consistent with other studies (Zapata and Salvato 2013). That the L polymerase and NP proteins are more identical among snake reptarenavirus than the other proteins is not unexpected as they are either enzymes whose function is highly conserved or are internal structural proteins that are not subject to antibody mediated selection

(Lopez et al. 2002; Vieth et al. 2007). The GPC genes, encoding the surface glycoproteins, inevitably vary with strain (Schlie et al. 2010) and the multifunctional Z protein antagonizing the host innate immune response and variation in relation to these different functions in different species may be expected (Fan et al. 2009). From this analysis two further sets of degenerate primers were designed to amplify regions of the L polymerase gene and NP genes. These primers were designed to be able to amplify all reptarenavirus known at the time of the study.

3.2.3 Validation of reptarenavirus primers

3.2.3.1 Amplification of L polymerase and NP genes from UHV

In order to validate the oligonucleotide primers designed, a basic PCR was used with target DNA and target sequences in the viral RNA-dependent RNA polymerase (RdRp) (L polymerase) and nucleoprotein (NP) of UHV were tested for amplification with primers L4087F, L5099R, L1017F, L1544R, L5081F, L5316R, NP332F, NP937R, NP173F and NP562R (Table 2.1 and 2.2). The PCR reactions were prepared using CloneAmp HiFi PCR Premix (Clontech) and cDNA of UHV as PCR template and the program was completed as described in section 2.6. The PCR products were analysed by agarose gel electrophoresis and visualized on a UV imager (G:Box, Syngene). L polymerase and NP fragments of the expected size were amplified from the UHV cDNA template (Figure 3.3) and (Table 3.1) and the amplicon sizes were in agreement with those predicted when compared to the HyperLadder 1kb marker (Bioline). These degenerate reptarenavirus primers thus successfully amplify UHV and provisionally could be used for an investigation of the

presence of established or novel reptarenaviruses in snakes and other reptiles (Demby et al. 1994; Paweska et al. 2009; Vieth et al. 2007) as will be described in chapter five.

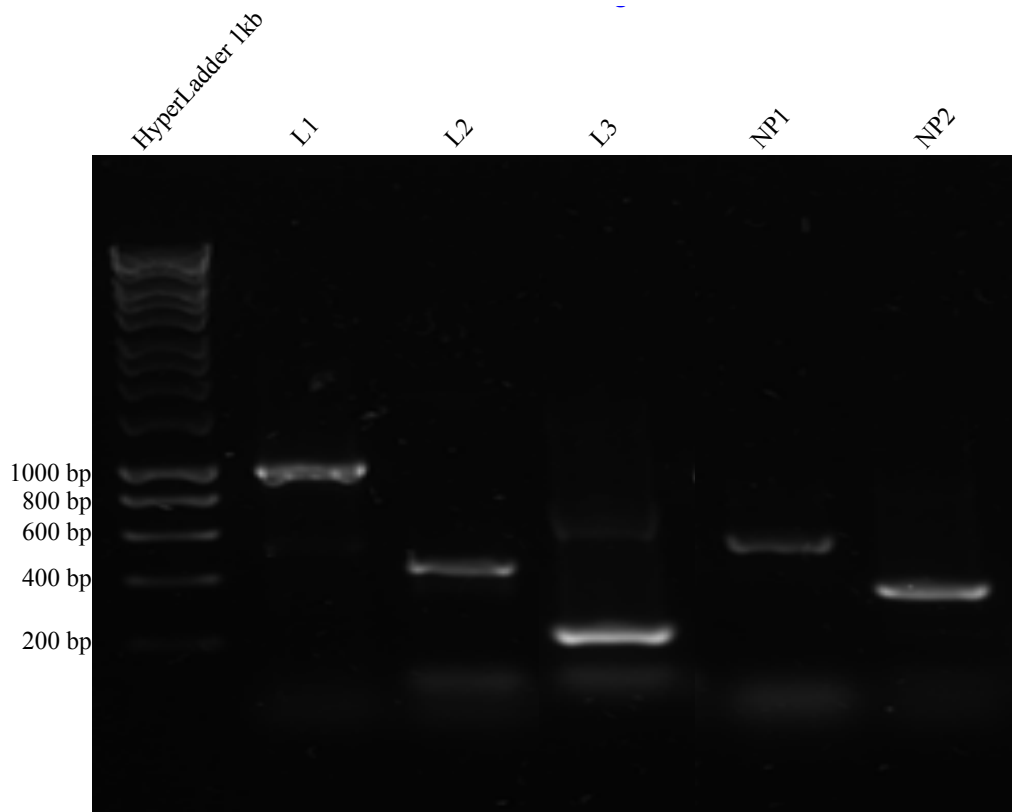


Figure 3.3: Gel electrophoresis of L polymerase and NP genes of UHV. Complementary DNA (cDNA) of UHV was used as PCR template. Three degenerate primers sets of L polymerase and two degenerate primers sets of NP (Table 1.1 and Table 1.2) were used in PCR reactions. The three L polymerase amplicons (L1, L2 and L3) and the two NP amplicons (NP1 and NP2) were amplified as shown. The size of the target amplicons was as expected, and the PCR was run according to the conditions described in 2.6. The marker is HyperLadder 1kb (Bioline).

Table 3.1: Gel electrophoresis analysis of amplicons of L polymerase and NP of UHV.

Protein	Amplicon	Primer	Expected size (bp)
L	L amplicon (L1)	L4087F, L5099R	1012
	L amplicon (L2)	L1017F, L1544R	527
	L amplicon (L3)	L5081F-L5316R	235
NP	NP amplicon (NP1)	NP332F, NP937R	605
	NP amplicon (NP2)	NP173F, NP562R	389

All sets of degenerate primers were successful in generating reptarenavirus amplicons, termed L1, L2, L3, NP1 and NP2, when cDNA of UHV, provided by Dr Jussi Hepojoki at University of Helsinki, was used as a DNA template and the size of the UHV fragments was as expected, *i.e.* L1: 1012 bp, L2: 527 bp, L3: 235, NP1: 605 bp, NP2: 380 bp (Table 3.1). The data also agree with other studies which have detected arenaviruses by using primers to both viral RNA dependent RNA polymerase (RdRp) (Keller et al. 2017; Vieth et al. 2007) and nucleoprotein (NP) (Ter Meulen et al. 1998).

3.2.3.2 Primer test of Z and GPC genes of UHV

Two primers complementary to the small zinc finger motif protein (Z) and glycoprotein precursor (GPC) proteins were designed based on the alignment of two species of reptarenavirus, UHV-1 and GGV, and named Z40F, Z349R, GP895F, and GP1283R (Table 2.3). As before, in order to confirm whether the primers were able to amplify cDNA of the appropriate size from UHV cDNA the primers were tested by conventional PCR using CloneAmp HiFi PCR Premix (Clontech), Z and GPC primers and the provided cDNA of UHV as described in section 2.6. Following

agarose gel electrophoresis, the sizes of UHV fragments were determined according to HyperLadder 1kb (Figure 3.4). The amplified bands of Z and GPC sequence were of the expected size when compared with the primer design (Table 3.2).

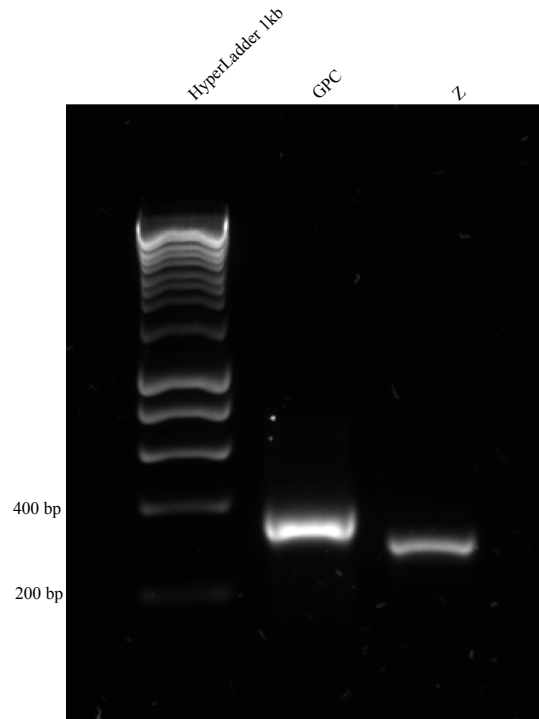


Figure 3.4: Gel electrophoresis of zinc finger motif protein (Z) and glycoprotein precursor (GPC) genes of UHV. Complementary DNA (cDNA) of UHV was used as PCR template. Degenerate primers of Z and GPC (Table 2.3) were used in PCR reactions. Both Z and GPC amplicons were amplified, and the size was as expected. The PCR was run according to the conditions described in 2.6 and the marker is HyperLadder 1kb (Bioline).

Table 3.2: Gel electrophoresis analysis of amplicons of Z protein and GPC of UHV.

Protein	Amplicon	Primer	Expected size (bp)
Z	Z amplicon	Z40F, Z349R	309
GPC	GPC amplicon	GP895F, GP1283R	388

Successful amplification of GPC and Z gene fragments by these primers could be used later for screening for novel/existing reptarenaviruses. However, previous research has concluded that amplifying conserved regions of both glycoprotein (GPC) and Z protein of arenaviruses is not adequate for definitive virus identification and diagnosis for the reasons of less sequence conservation previously discussed (Strecker et al. 2003). Therefore, for the investigation to be completed in this study the conserved regions of L polymerase and NP will be targeted primarily although the GPC and Z primers will be assessed also (Lunkenheimer K, Hufert FT 1990; Vieth et al. 2007).

3.2.4 Transformation of pNP, pZ and pGP of UHV

The plasmids pNP, pZ and pGP of UHV as received from Dr Jussi Hepojoki were transformed into Stellar™ Competent Cells (*E. coli* HST08 strain) as described in section 2.10. Colony PCR (cPCR) was used to screen the transformants with gene specific primers of NP (Table 2.2), GPC and Z (Table 2.3). A colony PCR (cPCR) was performed using the cPCR conditions in section 2.10.1 and the amplified products were analysed by gel electrophoresis as before. Contrary to expectations, some transformants appeared negative (Figure 3.5, 3.6 and 3.7), possibly due to insufficient bacterial mass used as a cPCR template. However, many amplified fragments were of the predicted amplicon size and the plasmids therein were subsequently extracted as described in section 2.10.2, and then confirmed by Sanger sequencing.

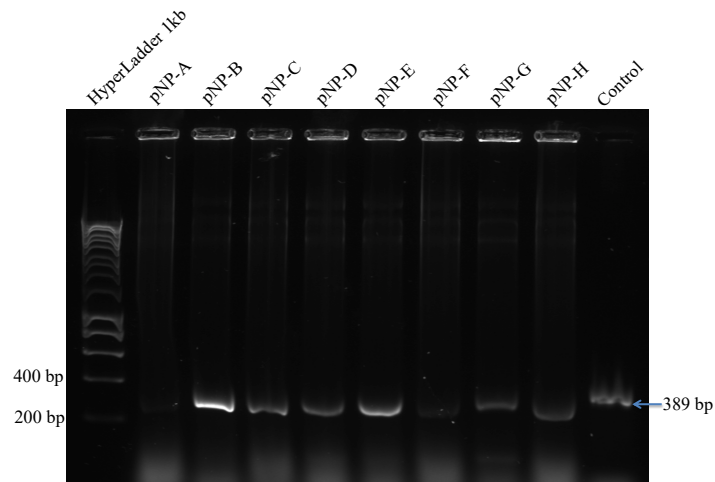


Figure 3.5: Gel electrophoresis of NP insert of UHV in pNP amplified by colony PCR. Transformants pNP A-H of *E. coli* HST08 strain, selected on LB agar plates containing ampicillin, were screened for presence of the cloned NP insert (NP2, 389 bp) within the pFastBac/HBM-TOPO vector. A small amount of each colony was used as the cPCR template with degenerate NP primers NP173F and NP562R (Table 2.2). Complementary DNA of UHV was used as a template in the positive control. The cPCR was run according to conditions described in section 2.10.1. The size of the inserts in transformants pNP-B, -C, -D, -E, -G and -H was as expected for NP2. Marker: HyperLadder 1kb (Bioline).

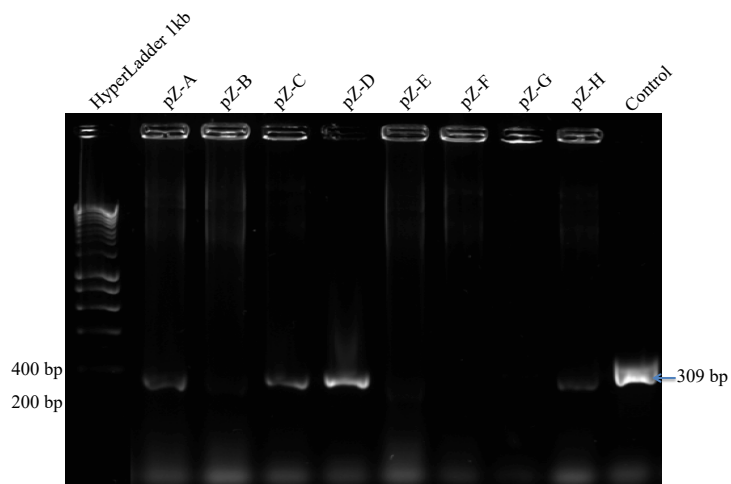


Figure 3.6: Gel electrophoresis of Z insert of UHV in pZ amplified by colony PCR. Transformants pZ A-H of *E. coli* HST08 strain, selected on LB agar plates containing ampicillin, were screened for presence of the cloned Z protein insert (Z, 309 bp) within the pFastBac/HBM-TOPO vector. A small amount of each colony was used as the cPCR template with degenerate Z protein primers Z40F and Z349R (Table 2.3). Complementary DNA of UHV was used as a template in the positive control. The cPCR was run according to conditions described in section 2.10.1. The size of the inserts in transformants pZ-A, -C and -D was as expected for Z. Marker: HyperLadder 1kb (Bioline).

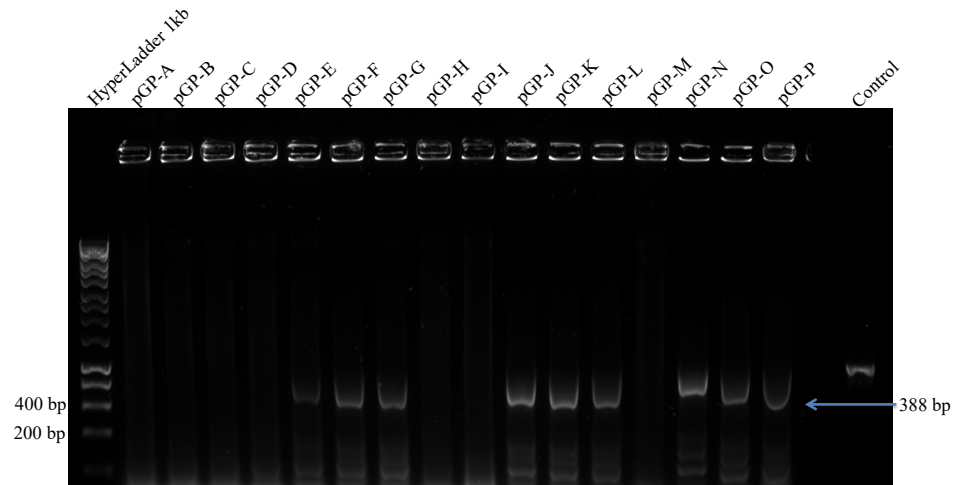


Figure 3.7: Gel electrophoresis of GP insert of UHV in pGP amplified by colony PCR. Transformants pGP A-P of *E. coli* HST08 strain, selected on LB agar plates containing ampicillin, were screened for presence of the cloned GP insert (GP, 388 bp) within the pFastBac/HBM-TOPO vector. A small amount of each colony was used as the cPCR template with degenerate GP primers GP895F and GP1283R (Table 2.3). Complementary DNA of UHV was used as a template in the positive control. The cPCR was run according to conditions described in section 2.10.1. The size of the amplified inserts was as expected in transformants pGP-F, -G, -J, -K, -L, -N, -O and -P. Marker: HyperLadder 1kb (Bioline).

3.2.5 L polymerase gene cloning of UHV

3.2.5.1 Digestion of pTriEx 1.1 plasmid

Unlike the other UHV gene sequences the sequence encoding the L protein was gifted as a cDNA preparation amplified from virus RNA. The L polymerase gene encodes the viral polymerase, which is normally the most conserved gene across RNA viruses (Morin et al. 2010). For further use as a positive control, fragments of the L polymerase gene of UHV were amplified and cloned into a vector. To this end, the three demonstrated amplicons, L1, L2 and L3 (Table 3.1 and Figure 3.3) were cloned into pTriEx-1.1 (Novagen). The pTriEx 1.1 plasmid was prepared by

digestion with restriction enzymes *XhoI* and *NcoI* and analysed by agarose gel electrophoresis (Figure 3.8). The larger band representing linearized vector with the polylinker removed was purified by using a gel extraction kit from Macherey-Nagel (MN) and quantified as 430.2 ng/ul by ND-1000 Nanodrop spectrophotometer.

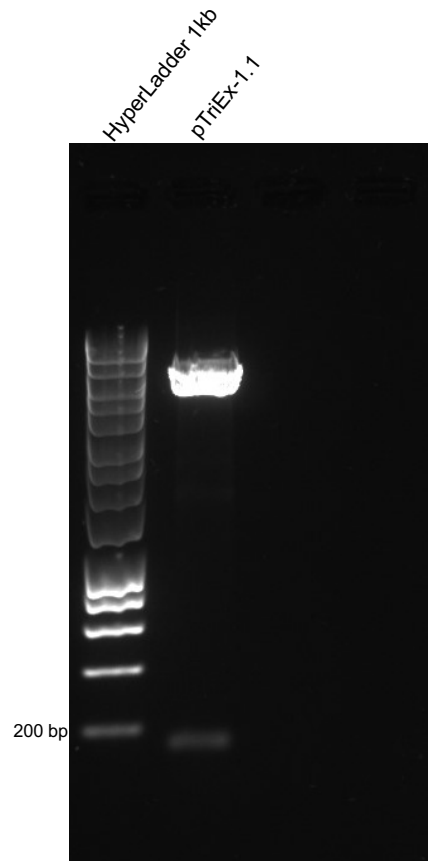


Figure 3.8: Agarose gel of digested pTriEx 1.1 plasmid. The plasmid was digested by *XhoI* and *NcoI* to produce a linear vector of 5301 bp and fragment of 146 bp. HyperLadder 1kb (Bioline) was used for determination the size.

3.2.5.2 High Fidelity PCR of L polymerase genes of UHV

High Fidelity PCR was performed to prepare the L1, L2 and L3 inserts for cloning via the infusion method. Infusion primers of L polymerase of UHV Inf. L5081F, Inf. L5316R, Inf. L1017F, Inf. L1544R, Inf. L4087F and Inf. L5099R (Table 2.5) were used with purified L polymerase amplicons of UHV as template. The reaction used CloneAmp HiFi PCR Premix (Clontech) for high fidelity PCR and was run according to the High-Fidelity PCR condition described in section 2.9.2. The CloneAmp HiFi PCR Premix has an exceptionally low error rate (12 mismatched bases per 542,580 total bases) and quick priming and extension (5 sec/kb) enable fast PCR reactions according to the manufacturer's instruction. The reaction products were visualized by agarose gel electrophoresis and compared to the marker HyperLadder 1kb (Bioline). The three amplicons of UHV L were successful amplified (Figure 3.9) and were purified using PCR clean up kit (Macherey-Nagel) and quantified, L1: 271.9 ng/ μ l, L2: 225 ng/ μ l and L3: 245.9 ng/ μ l. The infusion primers used included sequences of the pTriEx1.1 vector flanking the restriction sites were used to provide the homology arms for rapid cloning using the infusion protocol.

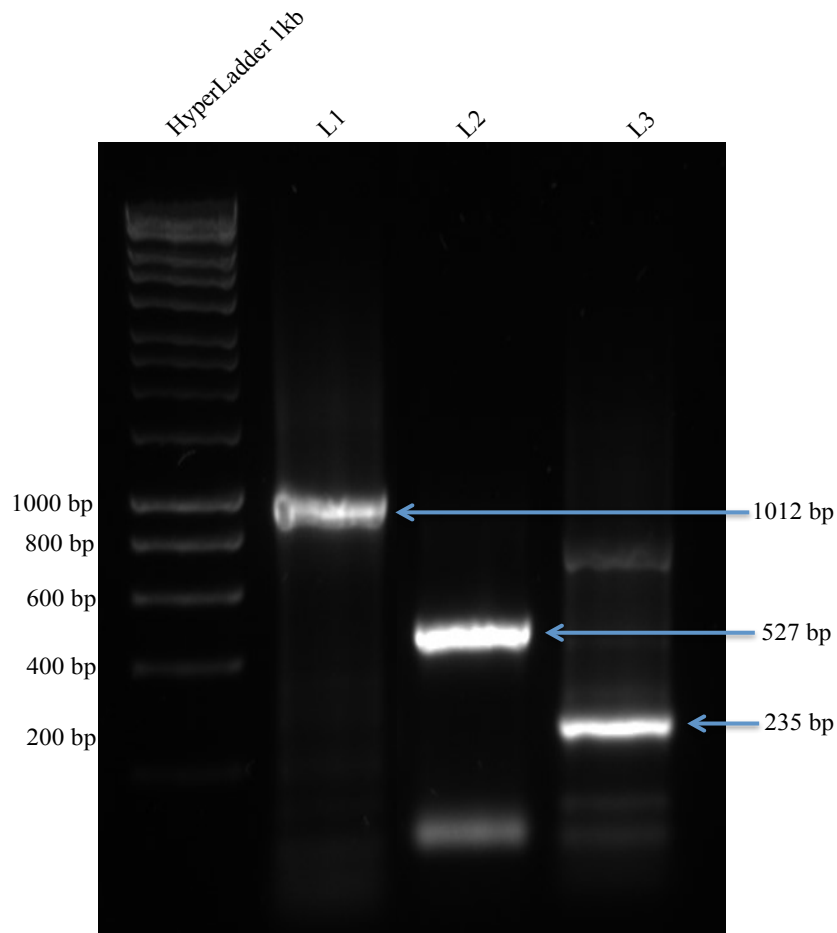


Figure 3.9: High Fidelity PCR of L polymerase genes of UHV. Purified L polymerase genes (L1, L2 and L3, Table 3.1) of UHV were used as a template for High Fidelity PCR. Infusion primers of UHV L polymerase (Table 2.5) were used in PCR reaction. The PCR was run according to the conditions described in section 2.9.2. The size of L1 (1012 bp), L2 (527 bp) and L3 (235 bp) amplicons was as expected. Marker: HyperLadder 1kb (Bioline).

3.2.5.3 L polymerase gene cloning and transformation of UHV

The amplicons of L polymerase of UHV were infusion cloned within the appropriate digested pTriEx 1.1 at a ratio of 1:3 of L insert to plasmid vector. The L1, L2, L3 and double digested pTriEx 1.1 vector were mixed with 5x In-Fusion HD Enzyme Premix (Clontech) and the final mixture was transformed into StellarTM Competent Cells (*E. coli* HST08 strain) as described in section 2.9.3 and 2.10. Transformants were

screened for the presence of the correct inserts by colony PCR (cPCR) as before using the L polymerase gene primers described above, L4087F, L5099R, L1017F, L1544R, L5081F and L5316R (Table 2.1). The reactions were analysed by gel electrophoresis (Figure 3.10 and 3.11) and plasmids present in the positive colonies were extracted as described in section 2.10.2. Following DNA Sanger sequencing positive transformants of UHV, and then L1, L2 and L3 were preserved in 50% glycerol and stored at -80°C . The three inserts of L polymerase of UHV were successfully cloned into pTriEx1.1 vector to be used as positive controls for later screening of samples for the presence of snake reptaenaviruses.

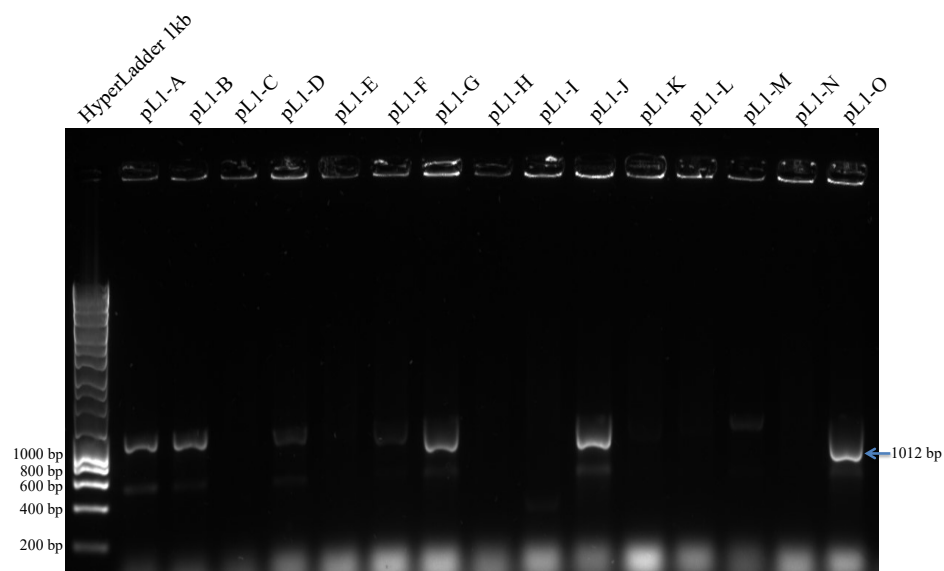


Figure 3.10: Colony PCR of L1 insert of UHV in pL1. Transformants pL1 A-O of *E. coli* HST08 strain, selected on LB agar plates containing ampicillin, were screened for presence of the cloned L polymerase insert (L1, 1012 bp) within the pTriEx 1.1 vector were used as cPCR template. A small amount of each colony was used as the cPCR template with degenerate L primers L4087F and L5099R (Table 2.1). The cPCR was run according to conditions described in section 2.10.1. The size of the amplified inserts was as expected for transformants pL1-A, -B, -G, -J and -O. Marker: HyperLadder 1kb (Bioline).

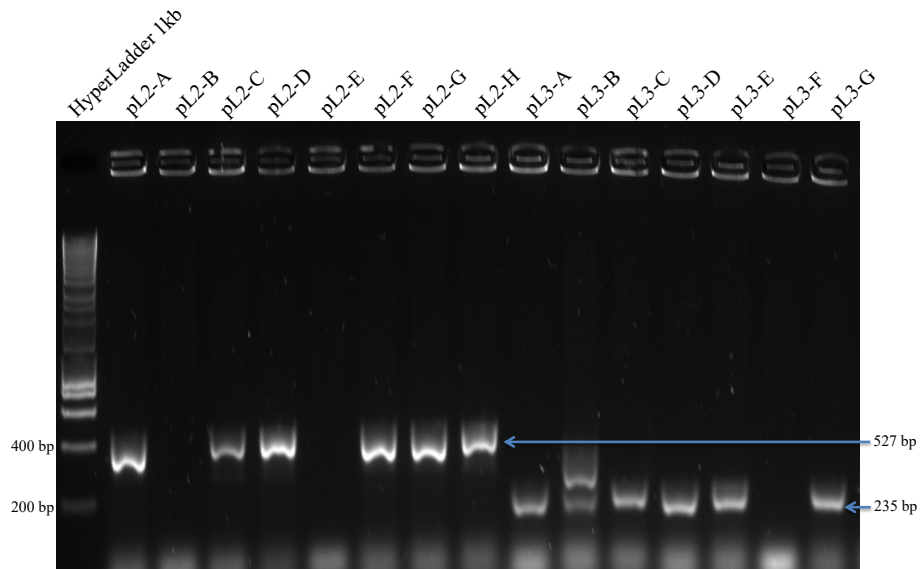


Figure 3.11: Colony PCR of L2 and L3 inserts of UHV in pL2 and pL3 respectively. Transformants pL2 A – H and pL3 A-G of *E. coli* HST08 strain, selected on LB agar plates containing ampicillin, were screened for presence of the cloned L polymerase insert L2 (527 bp) or L3 (235 bp) within the pTriEx 1.1 vector. A small amount of each colony was used as the cPCR template with degenerate L primers L1017F and L1544R for L2, or L5081F and L5316R for L3 (Table 2.1). The cPCR was run according to conditions described in section 2.10.1. The size of the amplified amplicons was as expected for transformants L2-A, -C, -D, -F, -G and -H, and L3-A, -C, -D, -E and -G. Marker: HyperLadder 1kb.

3.2.6 Bioinformatics analysis of University of Helsinki virus (UHV)

3.2.6.1 Analysis of University of Helsinki virus (UHV) sequences

The positive controls for these studies were provided as gifts of University of Helsinki virus (UHV). It was necessary therefore to confirm that the transformed and cloned segments of UHV were indeed identical with the protein coding regions of snake reptarenavirus available in the GenBank database. Accordingly, the raw sequence data provided by Source BioScience was read by the program FinchTV 1.4 and trimmed to dependable text sequence, especially at the extremities of the reads. Then, the nucleotide BLAST (BLASTn) (Stephen et al. 1990) option on the NCBI website (<https://blast.ncbi.nlm.nih.gov/blast.cgi>) was used for matching the cloned sequence with other reptarenavirus genes in the online database. The cloned sequences were found to have identity with other snake reptarenavirus proteins in specific cases (Table 3.3). The results confirm the cloned sequences as snake reptarenavirus and show very high homology with UHV-1 and ABV-1 and other reptarenaviruses supporting the original design considerations that regions selected for primer design are highly conserved among these viruses.

Table 3.3: BLAST analysis of cloned genes of University of Helsinki virus (UHV). The BLAST was carried out using the sequence of transformed amplicons of UHV in BLASTn on NCBI. The table shows the similarity between transformants and other reptarenavirus in GenBank database.

Virus segment	Virus protein	Transf-ormant	Virus identity	Query cover	Identity	Accession number	
L	L	L1	ABV-1	%100	%100	KR870021.1	
			Boa	%99	%91	KC508670.1	
			ABV-2	%99	%87	KR870033.1	
			UHV-1	%93	%79	KF297881.1	
		L2	ABV-1	%100	%100	KR870021.1	
			GGV	%98	%82	JQ717263.1	
		L3	ABV-1	%100	%100	KR870021.1	
			UHV-1	%100	%100	KF297881.1	
			Boa	%100	%95	KC508670.1	
			ABV-2	%96	%93	KR870033.1	
		Z	Z	ABV-1	%100	%100	KR870021.1
				UHV-1	%100	%100	KF297881.1
ABV-2	%100			%89	KR870033.1		
S	GPC	GPC	UHV-1	%100	%100	KF297880.1	
	NP	NP	UHV-1 *	%100	%100	KR870011.1	

* Identity was only with UHV-1 as no similarities with other reptarenaviruses found.

3.2.6.2 Amplicon alignment of University of Helsinki virus (UHV)

For the identity of the cloned fragments of University of Helsinki virus (UHV) with other snake reptarenavirus genes available in the GenBank database nucleotide BLAST (BLASTn) (Stephen et al. 1990) on NCBI was used as before, as was Clustal Omega version (1.2.4) (McWilliam et al. 2013) and Jalview 2.9 (Waterhouse et al. 2009). Using this workflow, the six inserts of UHV (fragments L1, L2, L3, Z, NP and GPC) were successfully aligned with both the original UHV-1 sequence and the sequence of ABV-1. Analysis by BLASTn showed similarities with other reptarenaviruses. It was somewhat expected that the transformants of UHV had full identity with the fragments in the L and S segments of ABV-1 and UHV-1. However, detailed analysis showed that L1 and L2 aligned with ABV-1 while L3 aligned better

with UHV-1 and ABV-1. The alignment for L1 with ABV-1 was from 3877 bp to 4822 bp, a conserved region of 946 bp, while the L2 fragment alignment with ABV-1 was from 1075 bp to 1487 bp with a conserved region of 413 bp. The L3 alignment to UHV-1 is from 4988 bp to 5175 bp with a conserved segment of 188 bp. The alignments of L transformants showed 100% nucleotide identity with UHV-1 and ABV-1 in these regions (Figure 3.12).

For the Z gene fragment the alignment with UHV-1 starts at 292 bp to 468 bp, encompassing a region of 177 bp and the nucleotide identity between the cloned gene and the Z protein of UHV-1 in that region is 100% (Figure 3.13).

For the NP gene sequence, the alignment starts from 377 bp to 601 bp with a 100% nucleotide identity to UHV-1 of 225 bp (Figure 3.14), and for the GPC gene the match occurs from 992 bp to 1270 bp of the database copy of GPC, a fragment of 279 bp (Figure 3.15).

The results of these alignments support the observation of the raw protein sequence alignments of UHV composed from UHV-1 and ABV-1 sequences in GenBank database.

Chapter Three: Degenerate primers and bioinformatics analysis

UHV,cloned_segment,L1/1-946 1 ATGGGGATGATGACCAAAAGGACAAACTGCTTCTGATCACTAATTTCT 48
ABV-1,L_segment/3877-4822 3877 ATGGGGATGATGACCAAAAGGACAAACTGCTTCTGATCACTAATTTCT 3924

UHV,cloned_segment,L1/1-946 49 TGTGCTTAGTGTGAACTGTTTGAACAAACACATCTCACCCAAAGTTTT 96
ABV-1,L_segment/3877-4822 3925 TGTGCTTAGTGTGAACTGTTTGAACAAACACATCTCACCCAAAGTTTT 3972

UHV,cloned_segment,L1/1-946 97 GTTGTAGCCCACTTGTGGGGAATTCAAATCACATTTTGAAGTTGAAG 144
ABV-1,L_segment/3877-4822 3973 GTTGTAGCCCACTTGTGGGGAATTCAAATCACATTTTGAAGTTGAAG 4020

UHV,cloned_segment,L1/1-946 145 CCACAATGGTCCCTCTATTACAAAATTTTTTGCAGCTTCAATCAACA 192
ABV-1,L_segment/3877-4822 4021 CCACAATGGTCCCTCTATTACAAAATTTTTTGCAGCTTCAATCAACA 4068

UHV,cloned_segment,L1/1-946 193 ATTTCAAGATGTAAAACACCGATGGAGCTCTTCAACACGTGTGATGCCA 240
ABV-1,L_segment/3877-4822 4069 ATTTCAAGATGTAAAACACCGATGGAGCTCTTCAACACGTGTGATGCCA 4116

UHV,cloned_segment,L1/1-946 241 TTGTTGAACAAGGAATTTGCAACGGTATGTCCCTAAAATTAGCTGATT 288
ABV-1,L_segment/3877-4822 4117 TTGTTGAACAAGGAATTTGCAACGGTATGTCCCTAAAATTAGCTGATT 4164

UHV,cloned_segment,L1/1-946 289 CACTGAAAGGTAAGATGGTTGAAATGTTGGGCTGGTTAGGATATGTTG 336
ABV-1,L_segment/3877-4822 4165 CACTGAAAGGTAAGATGGTTGAAATGTTGGGCTGGTTAGGATATGTTG 4212

UHV,cloned_segment,L1/1-946 337 GCGATCCTTTAAATGAAGCCTGTAGTGTCAAGACAACAAGATTGGTTGG 384
ABV-1,L_segment/3877-4822 4213 GCGATCCTTTAAATGAAGCCTGTAGTGTCAAGACAACAAGATTGGTTGG 4260

UHV,cloned_segment,L1/1-946 385 AAGGCTGTCTTTCTTATAGAAAAGTTAGGTCAGTAGAGAGTTGGTTGA 432
ABV-1,L_segment/3877-4822 4261 AAGGCTGTCTTTCTTATAGAAAAGTTAGGTCAGTAGAGAGTTGGTTGA 4308

UHV,cloned_segment,L1/1-946 433 TGGACATGGGGATAGAGAAAATTAAAGCTTGAAAGTACTGAAGCTTGAGC 480
ABV-1,L_segment/3877-4822 4309 TGGACATGGGGATAGAGAAAATTAAAGCTTGAAAGTACTGAAGCTTGAGC 4356

UHV,cloned_segment,L1/1-946 481 TGTAAAAAGTAAATTAAGAAATTAAGAGAAATCATCATTAGCACCATCTG 528
ABV-1,L_segment/3877-4822 4357 TGTAAAAAGTAAATTAAGAAATTAAGAGAAATCATCATTAGCACCATCTG 4404

UHV,cloned_segment,L1/1-946 529 TAGCATATAAAAAAGATGGTGGAAAATAAGTCTGATTGGAAC TAGGAGAAA 576
ABV-1,L_segment/3877-4822 4405 TAGCATATAAAAAAGATGGTGGAAAATAAGTCTGATTGGAAC TAGGAGAAA 4452

UHV,cloned_segment,L1/1-946 577 TTAACCTGTGGTTCCCTACACTCAATGGGAGTTCAAAC TATTGTTA 624
ABV-1,L_segment/3877-4822 4453 TTAACCTGTGGTTCCCTACACTCAATGGGAGTTCAAAC TATTGTTA 4500

UHV,cloned_segment,L1/1-946 625 GGAGCAAACTCAATTTAGGTACTACAATAAATGAAACGTGTGAGAAC 672
ABV-1,L_segment/3877-4822 4501 GGAGCAAACTCAATTTAGGTACTACAATAAATGAAACGTGTGAGAAC 4548

UHV,cloned_segment,L1/1-946 673 TGTGATTAAAAAGTTGATTAAACCATTACTCCAGATATTCAAAGCAA 720
ABV-1,L_segment/3877-4822 4549 TGTGATTAAAAAGTTGATTAAACCATTACTCCAGATATTCAAAGCAA 4596

UHV,cloned_segment,L1/1-946 721 GCCTTGGCTTGTAAATTGCAGAGGGGCTTGAAAGGTCTGCTTTCCAAA 768
ABV-1,L_segment/3877-4822 4597 GCCTTGGCTTGTAAATTGCAGAGGGGCTTGAAAGGTCTGCTTTCCAAA 4644

UHV,cloned_segment,L1/1-946 769 GTTCAGTGGTAACTGGGTTCAATGGTTTGAAGCATTAGCTTATCAGGCC 816
ABV-1,L_segment/3877-4822 4645 GTTCAGTGGTAACTGGGTTCAATGGTTTGAAGCATTAGCTTATCAGGCC 4692

UHV,cloned_segment,L1/1-946 817 CATGTGTGAGGAAGGGTGTGGCACGTTCTTAACTCTGAGGGAATCCA 864
ABV-1,L_segment/3877-4822 4693 CATGTGTGAGGAAGGGTGTGGCACGTTCTTAACTCTGAGGGAATCCA 4740

UHV,cloned_segment,L1/1-946 865 AAAC TGAATCAAACCAAGTTGCTGAACTTTTCCCCTCCTTAGTCATGC 912
ABV-1,L_segment/3877-4822 4741 AAAC TGAATCAAACCAAGTTGCTGAACTTTTCCCCTCCTTAGTCATGC 4788

UHV,cloned_segment,L1/1-946 913 AGTCGGTTTGTGCAGTTGGCGATTGGGCTGTGG 946
ABV-1,L_segment/3877-4822 4789 AGTCGGTTTGTGCAGTTGGCGATTGGGCTGTGG 4822

Chapter Three: Degenerate primers and bioinformatics analysis

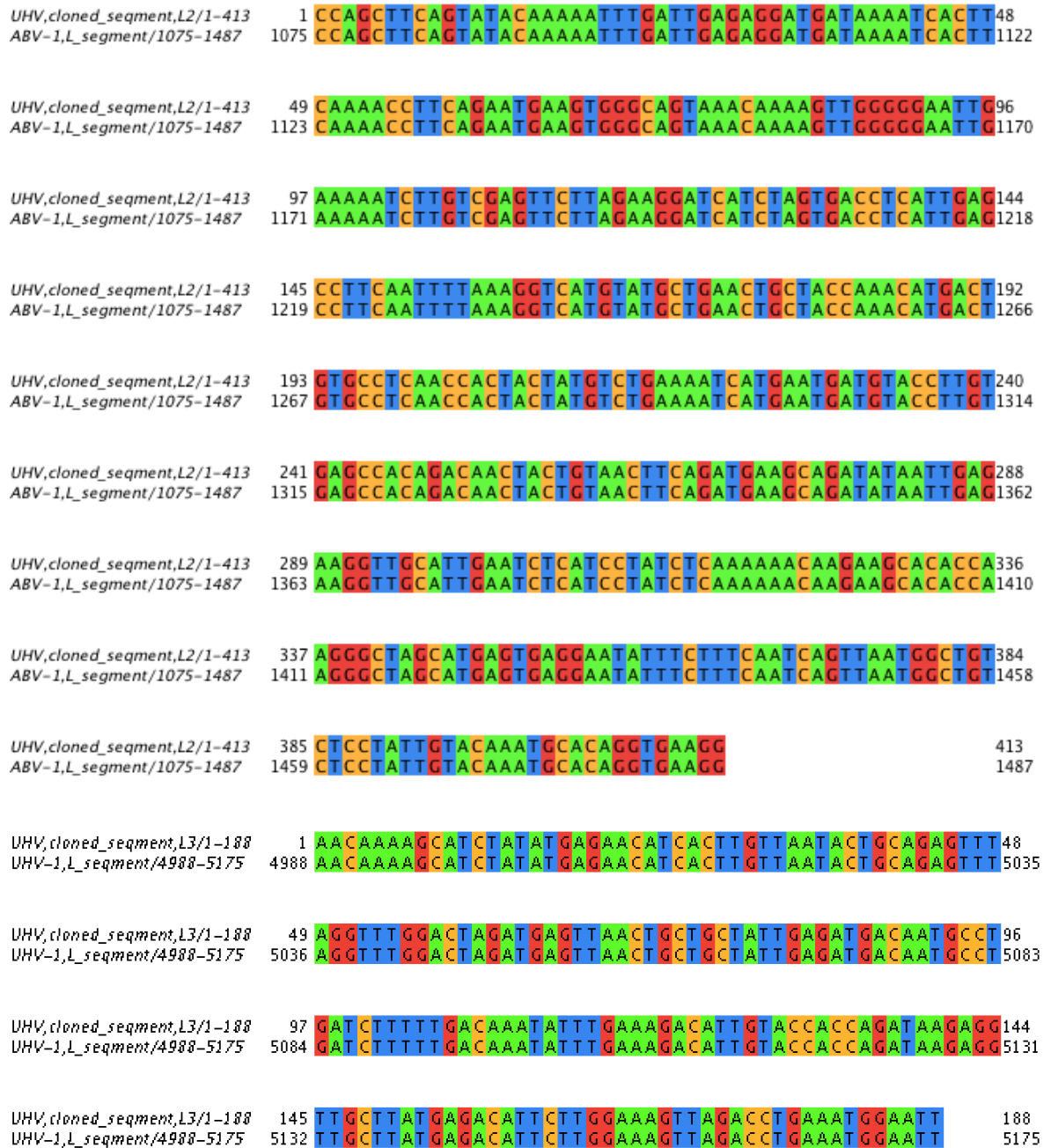


Figure 3.12: Alignment of L polymerase fragments of University of Helsinki virus (UHV). Three-cloned amplicons of L protein of UHV (L1, L2 and L3) were aligned with UHV-1 and ABV-1 on NCBI to show similarity. The alignments were created using Jalview 2.9 program. Accession number of segment L (contains L polymerase) of UHV-1: KF297881.1, ABV-1: KR870021.1.



Figure 3.13: Alignment of Z protein fragment of University of Helsinki virus (UHV). The transformed amplicon of Z protein of UHV was aligned with UHV-1 located on NCBI. Jalview 2.9 was used for presenting final alignment. Accession number of L segment (contains Z protein) of UHV-1: KF297881.1.

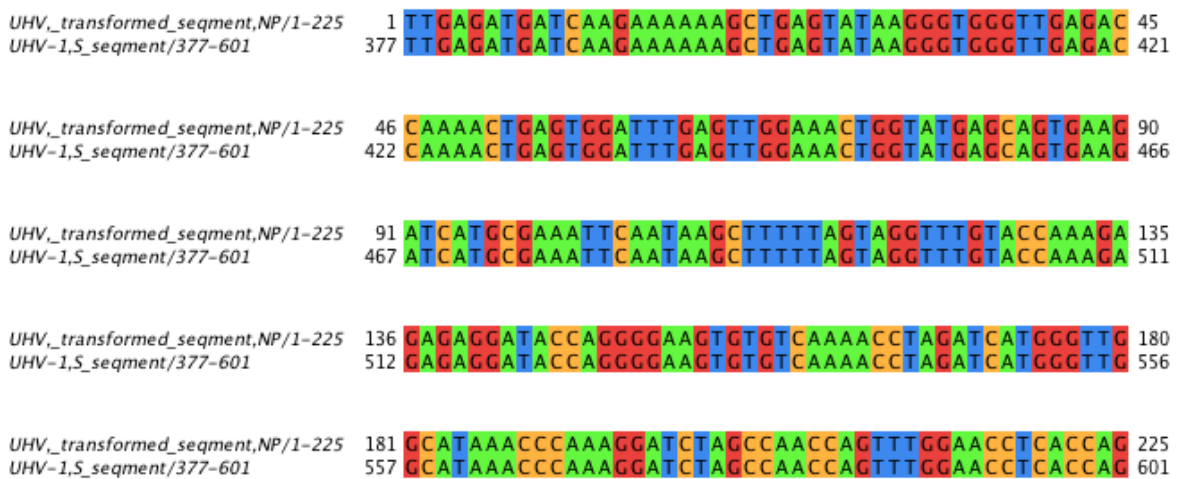


Figure 3.14: Alignment of NP fragment of University of Helsinki virus (UHV). Transformed NP amplicon of UHV was aligned with UHV-1 on NCBI database. Jalview 2.9 was used for final presenting of similarity. Accession number of S segment (contains NP protein) of UHV-1: KF297880.1.

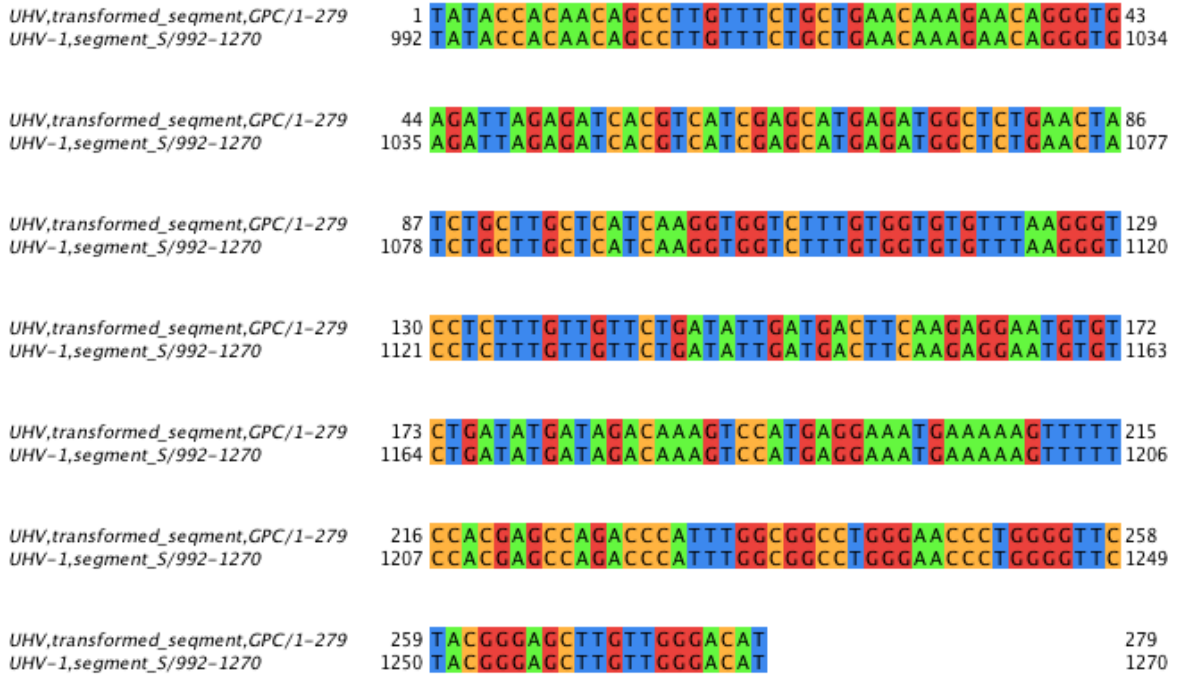


Figure 3.15: Alignment of GPC fragment of University of Helsinki virus (UHV). Transformed amplicon of GPC protein of UHV was aligned with UHV-1 on NCBI with 100% identity. Jalview 2.9 was used for the final alignment. Accession number of S segment (contains GPC protein) of UHV-1: KF297880.1.

As shown in Figure 3.12 to 3.15, the cloned sequences of the UHV L polymerase, NP, Z protein and GPC show regions of 100% nucleotide identity with regions of the UHV-1 and/or ABV-1 sequences in the GenBank database. This finding confirms previous findings that have shown close sequence similarities between UHV and other related reptarenaviruses (Hepojoki et al. 2015b). Phylogenetically, based on nucleotide homology, it seems that the cloned UHV sequences are more closely related to ABV-1 based on the L polymerase sequence, but more closely related to UHV-1 based on the Z protein, NP and GPC sequences. These finding could assist in the design of primers to detect highly conserved regions within more distantly-related reptarenaviruses in future investigations using RT-PCR.

3.2.7 Cloning maps of University of Helsinki virus (UHV)

To establish standard operating procedures for tissue screening that may be transferred to other sites and investigators, full cloning maps of the plasmids generated by cloning the inserts of UHV were generated. That is, the sequences of the L polymerase gene of UHV (L1, L2 and L3) within the pTriEx 1.1 vector (Novagen) and the Z, GPC and NP genes of UHV as already cloned in pFastBac/HBM TOPO. The cloning maps also include landmark restriction enzymes (*XhoI*, *NcoI* and *KpnI*) and were created with SnapGene 3.1.2 (GSL Biotech; available at snapgene.com). The six fully annotated maps were compiled as detailed in Figures 3.16-3.21 and serve as repository information for all subsequent investigations in this thesis.

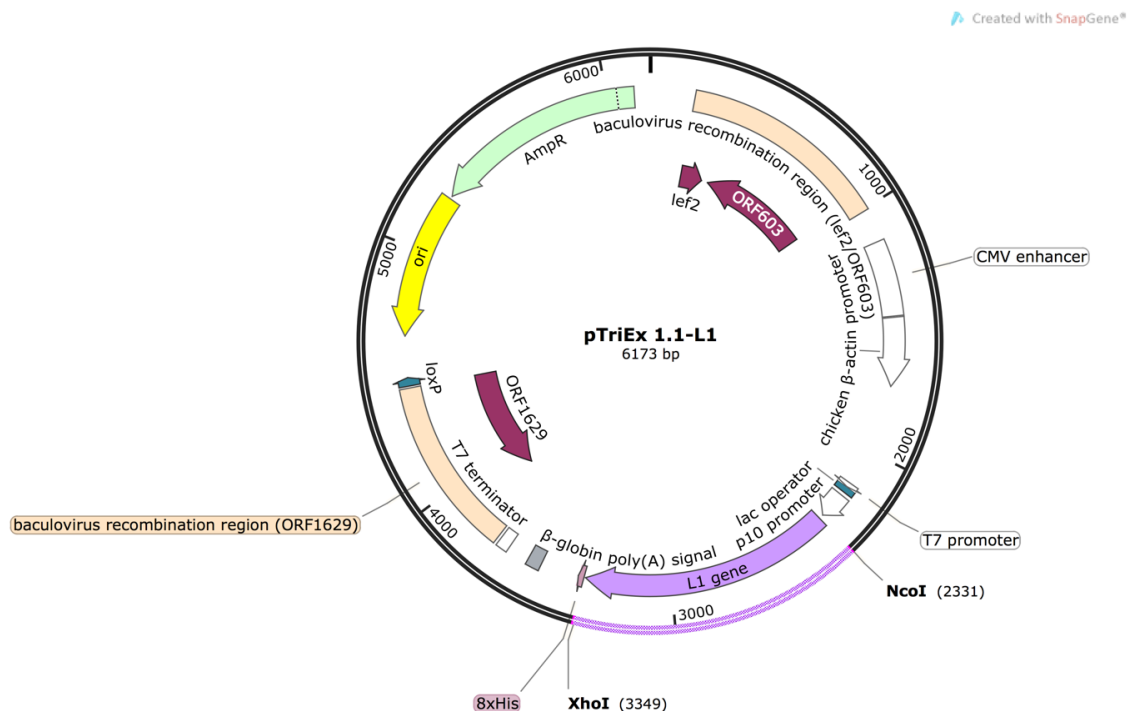


Figure 3.16: Cloning map of L1 fragment of University of Helsinki virus (UHV). Purple colour: the insert (L1 gene, 1012 bp) as a part of L polymerase of UHV located between two restriction enzyme sites for *XhoI* and *NcoI* (magenta colour) start from 2331 bp to 3349 bp within the pTriEX 1-1 vector. The total size of the cloning map is 6173 bp. The map was created using SnapGene 3.1.2 software.

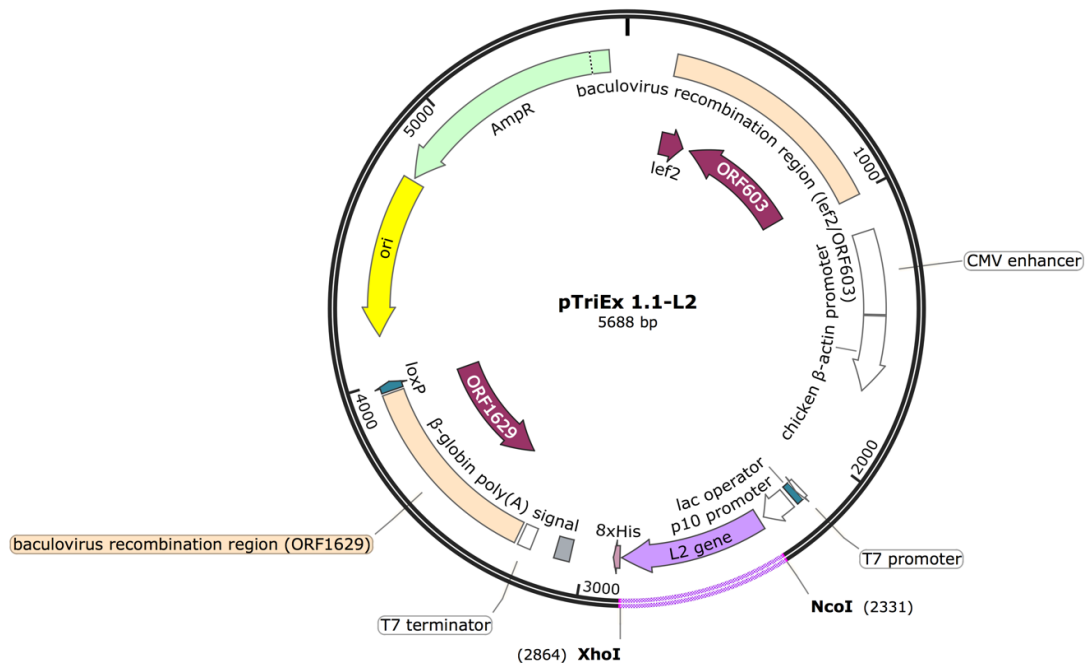


Figure 3.17: Cloning map of L2 fragment of University of Helsinki virus (UHV). Purple colour refers to the insert (L2 gene, 527 bp) of L polymerase of UHV, magenta colour refers to restriction enzyme *NcoI* and *XhoI* boundaries and start from 2331 bp to 2864 bp. L2 is located between these enzymes within the pTriEX 1-1 vector. The total size of the cloning map is 5688 bp. The map was created using SnapGene 3.1.2 software.

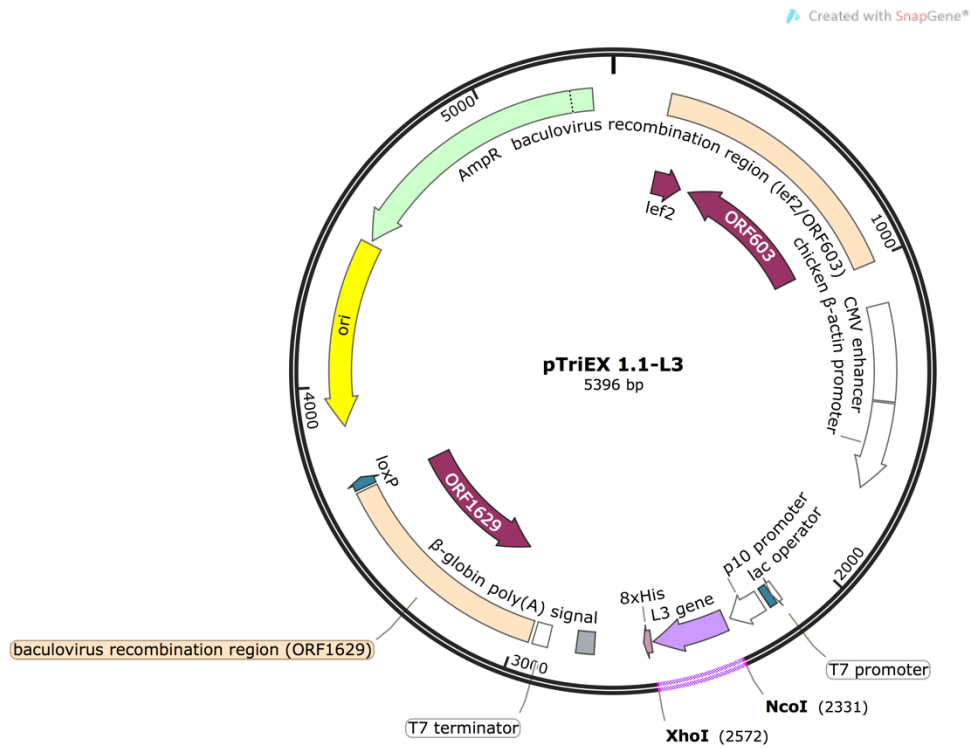


Figure 3.18: Cloning map of L3 fragment of University of Helsinki virus (UHV). Purple colour: The insert (L3 gene, 235 bp) of L polymerase of UHV (235 bp) is located between two restriction enzyme sites *NcoI* and *XhoI* (magenta colour) from 2331 bp to 2572 bp in pTriEX 1-1 vector. The total size of cloning map reaches to 5396 bp. The map was created by SnapGene 3.1.2 software.

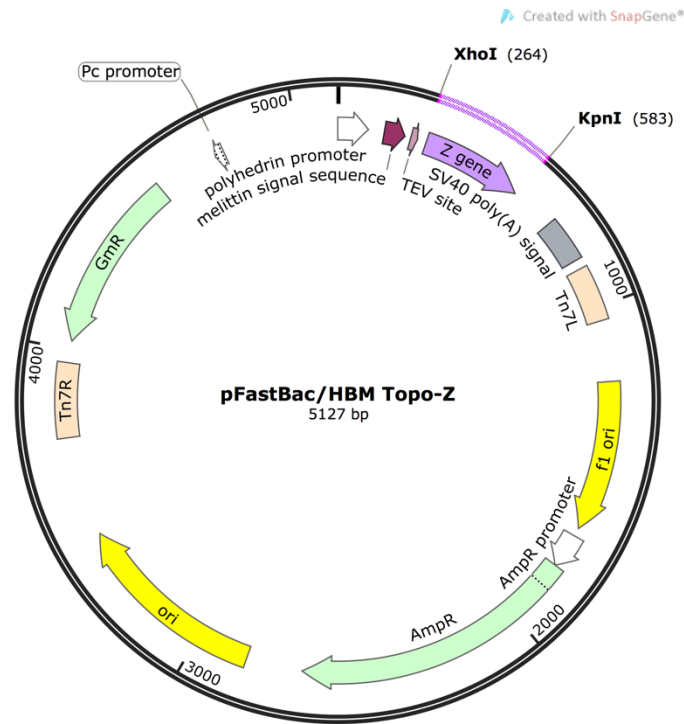


Figure 3.19: Cloning map of Z fragment of University of Helsinki virus (UHV). Purple colour: Transformed Z gene (309 bp) of Z protein of UHV. Z gene located between restriction enzyme sites *XhoI* and *KpnI* (magenta colour) from 264 bp to 583 bp within pFastBac/HBM TOPO vector. The total size of the vector is around 5127 bp. The map was created by SnapGene 3.1.2 software.

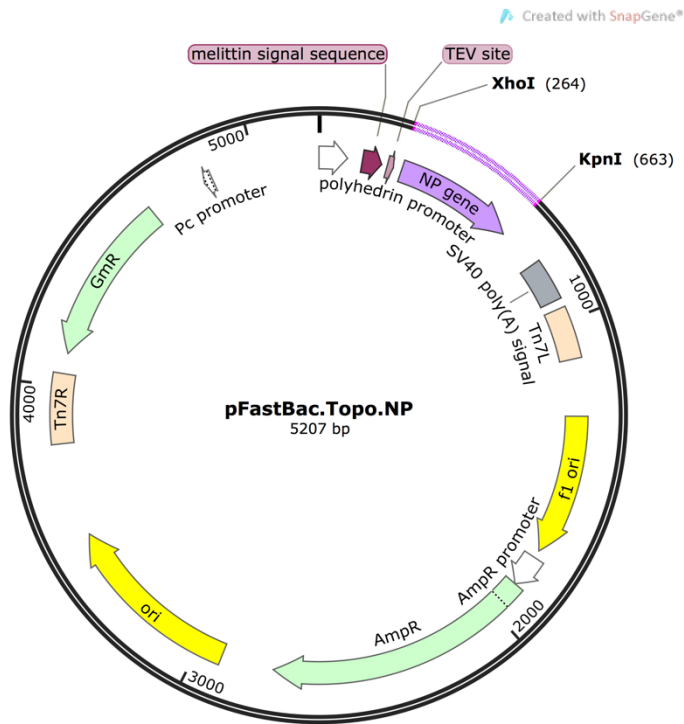


Figure 3.20: Cloning map of NP fragment (NP2) of University of Helsinki virus (UHV). Purple colour refers to the insert of NP gene (389 bp) of NP protein of UHV, magenta colour refers to restriction enzyme sites (*XhoI* and *KpnI*) and occurs from 264 bp to 663 bp were the NP gene is located in the pFastBac/HBM TOPO vector. The total size of the vector is 5207 bp. SnapGene 3.1.2 software was used for creating the map.

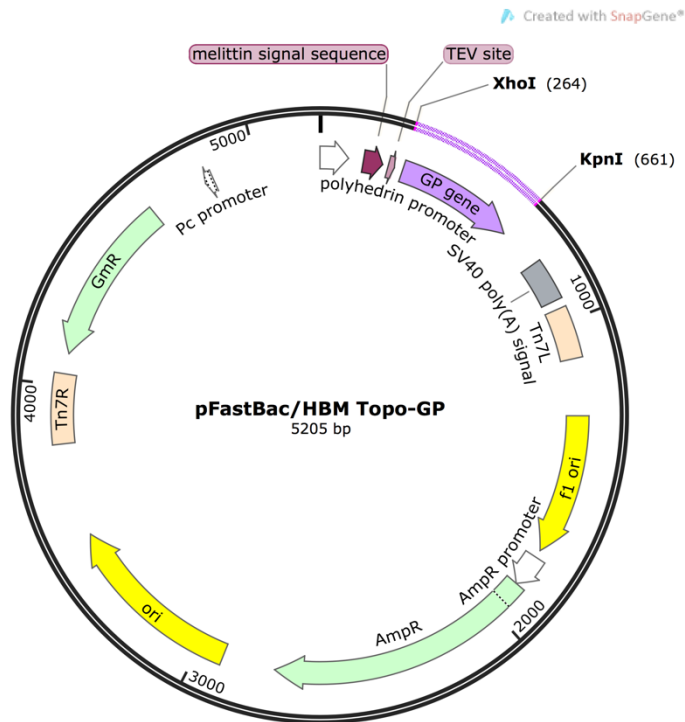


Figure 3.21: Cloning map of GP fragment of University of Helsinki virus (UHV). Purple colour: GPC gene (388 bp) insert of UHV, magenta colour: restriction enzymes (*XhoI* and *KpnI*). The GPC gene located between restriction enzymes start from 264 bp to 661 bp within the pFastBac/HBM TOPO. The total sizes of cloning map around 5205 bp. The map was created by SnapGene 3.1.2 software.

3.3 Discussion

In this chapter, degenerate primers (specific gene primers) for reptarenaviruses were designed and tested using gifted cDNA of UHV as a template. Four genomes of reptarenavirus including Golden Gate virus (GGV), Boa virus, California Academy of Science virus (CASV) and University of Helsinki virus 1 (UHV) were used for designing degenerate primers, the L polymerase, nucleoprotein (NP), small zinc motif protein (Z) and glycoprotein (GPC). Three set of L polymerase primers, two

sets of NP primers and one set for both Z and GPC primers of reptarenavirus were designed and were shown to successfully amplify the cDNA of UHV. In principle these primers could be used in molecular approaches such as RT-PCR for finding novel/existing reptarenavirus species in tissue samples from snakes and other reptiles (Iserte et al. 2013).

Multiple sequence alignment (MSA) confirmed that sequence identity with the amplicons occurs in various reptarenavirus even though they were isolated from different species of snakes. Particular identity occurred with University of Helsinki virus 1 (UHV-1) as expected but also with ABV-1 and ABV-2.

All control target genes, the nucleoprotein (NP), small zinc finger motif protein (Z), and glycoprotein precursor (GPC) genes of UHV, as gifted from the University of Helsinki, were confirmed following sequence analysis and the L polymerase gene fragments, generated by amplification from cDNA, were cloned for use as positive controls in subsequent studies. All plasmids were transformed successfully into *E. coli* and verified by DNA sequence prior to storage.

The molecular biology procedures of the project were facilitated by the completion of SnapGene vector maps. Together, the tools and sequence information of snake reptarenaviruses required for subsequent study were verified by the work in this chapter, demonstrating their suitability for the work in the chapters that follow.

Chapter 4 Specimen provenance, dissection and sample preparation

4.1 Introduction

Recently, it has been reported that some species of snake with inclusion body disease carry reptarenaviruses. Researchers in several European countries such as Netherlands, Finland, and Germany isolated reptarenavirus from snakes associated with inclusion body disease (Aqrabi et al. 2015; Bodewes et al. 2013; Hepojoki et al. 2015b) and reptarenavirus infection in Corn snakes was also confirmed in the United States (Chang et al. 2016). Most recently, reptarenaviruses were identified in pythons, Corn snakes and Madagascar tree boa in Australia (Hyndman et al. 2019). In the UK the situation is unclear as there is little documented evidence of reptarenavirus infection in snakes and other reptiles. The likelihood that snakes carry a reptarenavirus with the potential to infect other reptiles is therefore unknown. In consequence, the probability of virus transmission to humans as a zoonotic infection, which is a concern as many reptiles including snakes, chameleons and turtles are bred and housed as pets, cannot be assessed. In this study, to address the question of the level of reptarenavirus carriage by a variety of reptiles, frozen samples of snake and other reptiles such as turtles, chameleons and lizards were collected with the kind collaboration of the quarantine department at Heathrow Animal Reception Centre (HARC) and additional frozen specimens of snake organs were sampled via a collaboration with the Zoological Society of London (ZSL) at London Zoo. Whenever possible, under instruction from the author, collaborators agreed to store liver, kidney and spleen samples from these reptiles

in tubes containing the RNA stabilization reagent (RNAlater) followed by preservation at -80°C. In some cases however, the time between the animal being frozen and the subsequent dissection was variable. In other cases, the time between death and freezing was also not available, particularly for frozen animals collected from HARC. This variability in sample source was unavoidable but wherever the specimen appeared intact, the liver of snakes and reptiles were dissected and collected, again in RNA stabilization reagent, for subsequent RNA purification. The liver of the reptiles is a main internal target organ for the investigation of reptarenaviruses as it was found that hepatocytes express high virus titres (Shibata et al. 2004) and reptarenaviruses have been detected in liver of snakes (Hetzl et al. 2013; Hyndman et al. 2019; Keller et al. 2017; Stenglein et al. 2017).

As a consequence of the sample sourcing a number of liver, kidney and spleen samples of snakes, turtles and tortoises, chameleons and other reptiles, like lizard and fire skink were successfully isolated. All dissection was done in a safety cabinet to prevent any disease agent transmission. Furthermore, the dissection tools such as scalpels, forceps and pins were sterilized by heat so as to avoid any sample contamination by RNase enzymes that could affect RNA integrity. The internal reptile organs collected were all preserved in RNAlater and either processed immediately or re-frozen prior to RNA purification and an investigation of the presence of reptarenavirus sequences.

4.2 Results

4.2.1 Reptile provenance

Frozen reptiles as shown in Table 4.1 were kindly provided by collaboration with Heathrow Animal Reception Centre (HARC). These reptiles had either died at the centre for some reason or they had arrived dead. In these cases, standard practice was for the cadavers to be routinely moved to a freezer at the quarantine centre for long term preservation. The frozen animals sourced are listed in Table 4.1 and were collected piecemeal over a period of about 2 years from the HARC quarantine centre for dissection purposes.

Table 4.1: Frozen reptiles as collected from Heathrow Animal Reception Centre (HARC).

Animal common name	Scientific name	Quantity	Organs	Date of death	Date of dissection
Baby king cobra	<i>Ophiophagus hannah</i>	1	Liver, kidney	Unknown	07-08-2015
Red eared Slider	<i>Trachemys scripta elegans</i>	1	Liver and kidney	10-09-2014	11-08-2015
Royal python	<i>Python regius</i>	2	Liver, kidney and body fluids	Unknown	04-02-2016
Oachita map turtle (Sabine map turtle)	<i>Graptemys ouachitensis</i>	8	Liver	18-08-2014	25-02-2016
Flap-necked chameleon	<i>Chamaeleo dilepis</i>	1	Liver	05-07-2005	31-03-2016
Graceful chameleon	<i>Chamaeleo gracilis</i>	1	Liver	25-04-2005	31-03-2016
Von Höhnel's chameleon	<i>Trioceros hoehneli</i>	1	Liver	12-09-2003	31-03-2016
Fischer's Chameleon	<i>Kinyongia fischeri</i>	1	Liver	18-07-2003	31-03-2016
Rudis chameleon	<i>Trioceros rudis</i>	1	Liver	Unknown	31-03-2016
Flap-necked chameleon	<i>Chamaeleo dilepis</i>	1	Liver	30-06-2005	31-03-2016
Chameleon spp.	Unconfirmed	2	Liver	11-12-2004	31-03-2016

Animal common name	Scientific name	Quantity	Organs	Date of death	Date of dissection
Flap-necked chameleon	<i>Chamaeleo dilepis</i>	1	Liver	12-02-2004	31-03-2016
Chameleon incounutos	Unconfirmed	1	Liver	20-12-2001	31-03-2016
Chameleon rudis	<i>Trioceros rudis</i>	1	Liver	19-01-2003	31-03-2016
Common chameleon (Mediterranean chameleon)	<i>Chamaeleo chamaeleon</i>	1	Liver	04-01-2001	31-03-2016
Side Striped Chameleon	<i>Chamaeleo bitaeniatus</i>	1	Liver	28-01-2003	31-03-2016
Jackson's chameleon	<i>Trioceros jacksonii</i>	1	Liver	28-03-2008	31-03-2016
Chameleon spp.	Unconfirmed	2	Liver	Unknown	31-03-2016
Rudis chameleon	<i>Trioceros rudis</i>	1	Liver	05-01-2004	18-07-2016
Flap-necked chameleon	<i>Chamaeleo dilepis</i>	1	Liver	15-02-2004	18-07-2016
Graceful chameleon	<i>Chamaeleo gracilis</i>	1	Liver	12-02-2005	18-07-2016
Red eared terrapin (Slider)	<i>Trachemys scripta elegans</i>	1	Liver	07-05-2011	18-07-2016
Red eared terrapin (Slider)	<i>Trachemys scripta elegans</i>	1	Liver and spleen	13-05-2015	18-07-2016
Spur-thighed tortoise (Greek tortoise)	<i>Testudo graeca</i>	1	Liver	Unknown	18-07-2016
False mississippi map turtle	<i>Graptemys pseudogeographica kohni</i>	1	Liver	11-08-2014	18-07-2016
Chinese river turtle	<i>Rafetus swinhoei</i>	2	Liver	02-03-2011	18-07-2016
House gecko	<i>Hemidactylus spp.</i>	2	Liver	08-04-2014	19-07-2016
Spiny-tailed Iguanas	<i>Ctenosaura spp.</i>	1	Liver	25-09-2015	19-07-2016
Dwarf yellow-headed gecko	<i>Lygodactylus luteopicturatus</i>	1	Liver	26-03-2015	19-07-2016
Turquoise dwarf gecko	<i>Lygodactylus williamsi</i>	2	Liver	26-03-2015	19-07-2016
Turquoise dwarf gecko	<i>Lygodactylus williamsi</i>	2	Liver	08-04-2015	19-07-2016
Yellow headed gecko	<i>Gonatodes albogularis</i>	1	Liver	24-03-2015	19-07-2016
Turquoise dwarf gecko	<i>Lygodactylus williamsi</i>	1	Liver	29-03-2015	19-07-2016
Dwarf yellow-headed gecko	<i>Lygodactylus luteopicturatus</i>	1	Liver	29-03-2015	19-07-2016
Turquoise dwarf gecko	<i>Lygodactylus williamsi</i>	4	Liver	Unknown	19-07-2016
Fire skink (Togo fire skink)	<i>Lepidothyris fernandi</i>	1	Liver	Unknown	19-07-2016
Soft shell turtle	<i>Trionychidae</i>	1	Liver	23-07-2015	19-07-2016
Garden tree boa	<i>Corallus hortulanus</i>	1	Liver, kidney	19-01-2017	09-02-2017

In Table 4.1., the different species of reptile including 4 species of snake were collected and dissected over a two years period. All animals were frozen at HARC quarantine which should minimize the risk of RNA degradation. However, the different death data for the cadavers could have an effect on RNA isolation, since there is a likelihood of RNA degradation for samples that were preserved for longer than ten years, such as the chameleons. The postmortem can give some indication of whether the samples are suitable for reptarenavirus investigation or not, offering an expectation for RNA integrity.

4.2.2 Reptile dissection

4.2.2.1 Snake dissection

Four frozen snakes, including one baby king cobra (*Ophiophagus Hannah*), two royal pythons (*Python regius*) (Figure 4.1) and one garden tree boa (*Corallus hortulanus*) as shown in Table 4.1 were collected from Heathrow Animal Reception Centre (HARC) and dissected in a disinfected and cleaned cabinet (0.5% SDS) to minimize the opportunity for disease transmission and sample cross-contamination. The dissection was carried out through the abdominal surface to facilitate the observation and collection of the internal organs. Surgical tools such as scalpels, scissors and forceps were sterilized to avoid any contamination with ribonuclease (RNase) that could affect RNA quality (Vennemann and Koppelkamm 2010). Liver and kidney samples from four snakes were successfully dissected and added directly to tubes contain RNA stabilization solution and then preserved at -80°C. The remaining cadaveric parts were discarded in yellow clinical waste bags and sent for incineration.

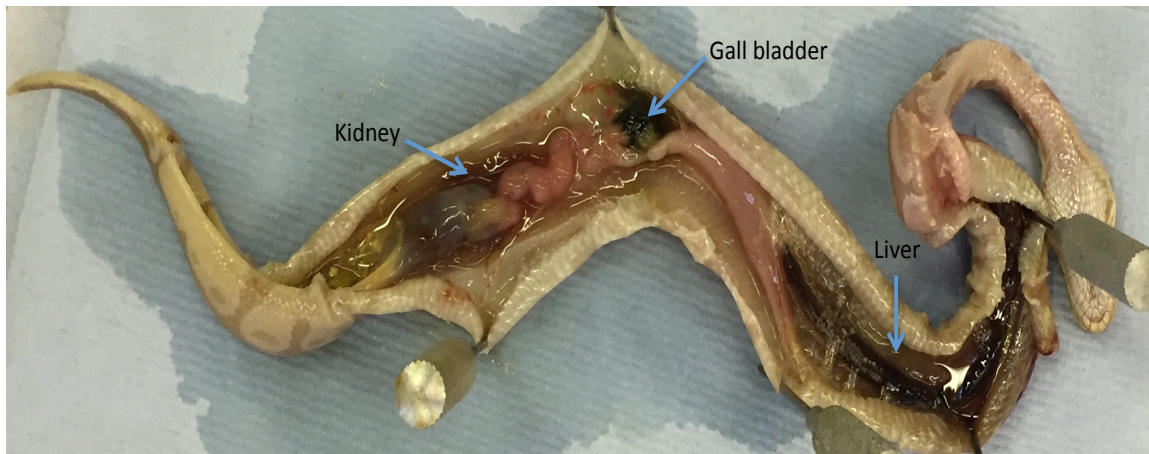


Figure 4.1: Dissection of royal python (*Python regius*) also known as ball python. The dissection was carried out in a controlled, disinfected environment using sterilized tools such as forceps and blades. The postmortem suggested the snake may have died because of infection as there was body fluid found in most parts of the snake. The liver was enlarged and dark brown in colour, while the kidneys were normal in size and colour. Liver and kidney samples were collected into tubes containing RNAlater and stored at -80°C for RNA isolation.

As shown in Figure 4.1, the liver of the snake is elongated and located from ventral to caudal sides, from two thirds of the lung until the end of the stomach, while on both sides the kidneys are thin, elongated and found on the caudal side of the digestive tract, the left kidney being cranial to the right (Orosz 2006). The organs are normal in shape and colour, but there was body fluid in one of the snakes. The reasons of the aggregation of body fluid was unconfirmed but could be related to some pathogen infection or oedema. Moreover, it was observed that in the royal python sample, the contents of the bile had been secreted, perhaps because the snake was exposed to some physical stress. On the other hand, the dissection of the baby king cobra confirmed that the internal organs such as liver and kidney had dried, and this could affect the integrity of the RNA. In contrast, no pathological changes were apparent in the liver and kidneys of the tree garden boa. All tissue

specimens were preserved in tubes containing RNAlater at -80°C with snake name, organ and date of dissection recorded on it.

4.2.2.2 Turtle and tortoise dissection

Around fifteen frozen species of turtles and one species of Spur-thighed (Greek) tortoise (*Testudo graeca*) were collected from (HARC) for liver dissection (Table 4.1). The cause of death of these reptiles was not available when they were collected as frozen cadavers in boxes from the HARC freezer. Next, the animals were dissected in a cabinet with sterilized surgical equipment including scalpels, forceps and scissors as before. Notably in these cases, the carapace (dorsal shell) of the turtle and tortoise was separated from the plastron (ventral shell) by cutting the bridge bone between them using a hacksaw or scissors. Later, the plastron was removed, and the liver was detached from the other organs using a new blade (Wyneken 2001). The liver was immersed directly in a tube containing RNAlater and animal name, organ and date of dissection were recorded, and the sample was preserved at -80°C.



Figure 4.2: Dissection of Oachita map turtle (*Graptemys ouachitensis*). Eight turtles were dissected using sterilized forceps and blades on a sanitized bench. The postmortem showed that the internal organs such as liver were normal in size and colour. The reason for the death of the turtles is unknown. Liver samples collected in tubes containing RNAlater were preserved at -80°C for RNA isolation.

The livers seemed normal in colour and size (Figure 4.2) with the exception of some animals that had been kept in unsuitable conditions where the livers were darker in colour, which could affect RNA integrity. The specimens showed differences in organ size, depending on the species and age of the animals, but that should not affect RNA isolation as ≤ 25 mg of tissue is required for a virus investigation. Thus, most specimens were successfully dissected and preserved in RNAlater, apparently in a suitable form for RNA isolation.

4.2.2.3 Chameleons dissection

Many species of chameleon as noted in Table 4.1 were dissected. Frozen chameleons were collected from the Heathrow Animal Reception Centre (HARC) in a thermal box and the dissection was carried out in a sanitized cabinet with the surgical tools sterilized to avoid any cross-contamination. The liver was detached from the rest of the body through a slit in the skin on the left hand side of the animal (Greek 2002). As before the livers were immersed in tubes contain RNAlater and animal species, organ and date of animal dissection were recorded, and the sample preserved at -80°C . Several different species of chameleons were successfully dissected in this way to provide samples for the analysis.



Figure 4.3: Dissection of *Chameleon* spp. The arrows indicate the liver organs; the dissection procedure was carried out in a sanitized cabinet and the liver collected in sterile tubes containing RNAlater and preserved at -80°C ready for RNA isolation.

Generally, the liver samples were normal in size but most were dark in colour rather than the reported reddish purple colour (Greek 2002) as demonstrated in Figure 4.3. This could refer to the date of the animal's death as it was found that most of the chameleons had been dead for at least a decade. In addition, there was no evidence for the cause of chameleon death. Of all the samples sourced, the change of colour in these samples was most indicative of an effect on RNA integrity and it was considered unlikely that intact RNA could be isolated from these organs. Nevertheless, the dissected livers were preserved in tubes containing RNAlater as for all other samples.

4.2.2.4 Other reptile dissected

The dissection of livers was expanded and carried out on other reptiles that could act as potential hosts for reptarenaviruses, one Togo fire skink (*Lepidothyris fernandi*) and several different species of lizard were used for this purpose. The animals were collected from the HARC centre and in a cleaned cabinet, sterilized scalpels and forceps were prepared for dissection. Next, the livers were placed in tubes containing RNAlater with the specimen's details and preserved in -80°C. Thus, the livers of many species of lizard and one fire skink as shown in Table 4.1 were dissected for the reptarenavirus investigation.

In these cases, the dissected livers presented as dark in colour rather than brown consistent with previous studies (Wyneken 2001), which described lizards' livers as dark and larger than the other organs. Accordingly, livers of the lizards and fire skink were considered to be suitable for the RNA isolation described in the next chapter.

4.2.3 Internal tissue provenance

In addition to the samples gifted by the HARC centre, several specimens of snake liver were collected via a collaboration with the Zoological Society of London (ZSL) at London Zoo. Unlike the HARC samples, most animals were dissected within one day or less of the snake's death as shown in Table 4.2 and the specimens stored at -80°C. The frozen livers of different species of snakes from ZSL were placed directly into tubes containing RNAlater with the specimen details recorded.

Table 4.2: Snake species as archived at Zoological Society of London (ZSL) in London Zoo. The liver was sample from the whole organ into a 1.5 ml Eppendorf tube contain RNAlater and preserved at -80°C.

Snake common name	Scientific name	Date of death	Date of dissection
March's palm pit viper (1)	<i>Bothriechis marchi</i>	02/02/17	03/02/17
Rhinoceros rat snake (1)	<i>Rhynchophis boulengeri</i>	11/01/17	12/01/17
Rhinoceros rat snake (2)	<i>Rhynchophis boulengeri</i>	04/08/16	04/08/16
Pueblan milk snake	<i>Lampropeltis triangulum campbelli</i>	20/07/16	21/07/16
False water cobra	<i>Hydrodynontes gigen</i>	27/05/16	27/05/16
Emerald tree boa	<i>Corallus caninus</i>	05/05/16	10/05/16
Mangshan pit viper (1)	<i>Protobothrops mangshanesis</i>	11/04/06	12/04/06
Mangshan pit viper (2)	<i>Protobothrops mangshanesis</i>	11/04/06	12/04/06
Mangshan mountain viper (1)	<i>Protobothrops mangshanesis</i>	11/04/06	12/04/06
Mangshan mountain viper (2)	<i>Protobothrops mangshanesis</i>	11/04/06	12/04/06
Marches palm pit viper (2)	<i>Bothriechis marchi</i>	24/03/16	24/03/16
Corn snake (1)	<i>Pantherophis guttatus</i>	09/03/16	10/03/16
Rhinoceros viper	<i>Bitis nasicornis</i>	26/02/16	01/03/16
Mangshan viper (3)	<i>Protobothrops mangshanensis</i>	20/12/15	21/12/15
Mangshan viper (4)	<i>Zhaoermia mangshanesnsis</i>	04/12/15	04/12/15
Red-tailed rat snake	<i>Gonyosoma oxycephala</i>	14/09/15	17/09/15
Jamaica boa	<i>Epicrates subflavus</i>	05/09/15	14/09/15

Snake common name	Scientific name	Date of death	Date of dissection
European long-nosed viper	<i>Vipera ammodytes</i>	27/08/15	28/08/15
Black mamba (1)	<i>Dendroaspis Polylepis</i>	05/06/15	09/06/15
Black mamba (2)	<i>Dendroaspis Polylepis</i>	05/06/15	09/06/15
Boelen's python	<i>Morelia boeleni</i>	03/06/15	04/06/15
Corn snake (2)	<i>Elaphe guttata</i>	20/05/15	21/05/15
Tiger rat snake	<i>Spilotes pullatus</i>	28/01/15	29/01/15
Cave rat snake (1)	<i>Elaphe taeniura ridleyi</i>	21/08/14	22/08/14
Cave rat snake (2)	<i>Elaphe taeniura ridleyi</i>	21/08/14	22/08/14
Emerald monitor	<i>Varanus prasinus</i>	21/07/14	21/07/14
Mangshan viper (5)	<i>Protobothrops mangshanensis</i>	22/05/14	22/05/14
Burmese rock python	<i>Python molurus bivittatus</i>	21/04/14	22/04/14
Cave rat snake (3)	<i>Elaphe taeniura ridleyi</i>	13/04/14	14/04/14
Dumeril's ground Boa	<i>Acranthophis dumerili</i>	Unknown	04/2014
Corn snake (3)	<i>Elaphe guttata</i>	31/03/14	02/04/14
Rhinoceros snake	<i>Rhynchophis boulengeri</i>	07/03/2014	07/03/2014
Blood python	<i>Python brongersmei</i>	25/02/2014	25/02/2014
Mangrove snake	<i>Boiga dendrophila</i>	05/02/2014	06/02/2014

As shown in Table 4.2, the livers were taken from many species of snakes that had been dissected originally for postmortem purposes. The liver is a target organ for reptarenaviruses isolation rather than other organs, as previously mentioned, hepatocytes express high viral titres (Shibata et al. 2004) and reptarenaviruses have been isolated using liver specimens (Hetzl et al. 2013; Hyndman et al. 2019; Keller et al. 2017; Stenglein et al. 2017). As a result, the expectation of these studies was that reptarenavirus isolation from snakes might be more facile than that from other reptiles, based on previous studies carried out by researchers who isolated reptarenavirus from snakes associated with inclusion body disease (Chang et al. 2016; Hepojoki et al. 2015b). Overall, around half the samples that were used in this study were from snake species, but as other reptiles could potentially be infected

with reptarenavirus these samples were also sourced as and when they were available, even if their condition was less than ideal. Notably, the snake samples were dissected soon after the animal's death and were deemed suitable for RNA isolation, although their RNA integrity needed to be confirmed by analytical procedures before attempting cDNA synthesis.

4.3 Discussion

The purpose of the current study is to obtain specimens of wild animals in order to investigate the possible occurrence of reptarenavirus sequences in reptile samples in the UK. To this end, snakes and some other reptiles that were potentially infected with an infectious agent were sourced and used. Whenever the sample allowed it, liver, kidney and spleen were detached from the reptile's other organs to be used for RNA isolation. There were many provenances for the specimens used as "the UK" as the study was enabled by collaborations with the Heathrow Animal Reception Centre (HARC) and the Zoological Society of London (ZSL) at London Zoo. In all, around 4 species of snakes, 16 species of turtles and tortoise, 19 species of chameleon, 11 species of lizard and one species of fire skink, as shown in Table 4.1, were collected from the HARC and 34 livers of snakes as shown in Table 4.2 were collected from ZSL, all for RNA isolation. In all cases the dissection was carried out in way that aimed to avoid any sample cross contamination or exposure to ribonuclease (RNase) enzyme, which could affect RNA integrity.

Thanks to the willingness of HARC and ZSL to assist in this study a large number of samples were sourced as suitable for RNA isolation. While, in some cases, there

was some obvious physical change in the internal organs examined, such as a change in colour due to the age and conditions under which the specimen had been stored, generally the quality of the samples appeared good, at least at the level of a physical examination of the animal. Exactly what quality of RNA could be achieved for the reptarenavirus sequence investigation was determined by measuring the RNA integrity number (RIN) as described in the next chapter.

Chapter 5 Total RNA analysis and reverse transcription PCR (RT-PCR) for reptarenavirus's sequences

5.1 Introduction

As described, arenaviruses are classified as negative sense ssRNA viruses and their genomes encode four proteins, the most conserved of which are the RNA dependent RNA polymerase (RdRp) also known as L polymerase and the nucleoprotein (NP). Tissue samples were described in the previous chapter (Table 4.1 and 4.2) as deriving from snakes and some other reptiles and were used in this study for total RNA purification, analysis and an investigation of the presence of reptarenavirus sequences. In general, RNA can be easily degraded into small fragments by RNase and other physical factors such as light and humidity (Vennemann and Koppelkamm 2010). Thus, total (eukaryotic) RNA isolation was carried out in an isolated and disinfected area and the equipment was sterilized to ensure that no contamination with RNase could have affected RNA quality. Total RNA quality was tested by gel electrophoresis and then by analysed on a 2100 Bioanalyzer (Agilent Technologies). Then, reverse transcription (RT) was performed in order to prepare viral cDNA. The final RT reaction was evaluated for mitochondrial 12S and 16S rRNAs using universal primers to mitochondrion RNA to ensure intactness. In addition, the limit of detectible viral load of reptarenavirus was calculated by serial dilution of purified UHV genomic RNA. UHV RNA was also used as a positive control for the RT-PCR reactions in this study, alone and following "spiking" experiments in which it was added to extracted RNA samples.

RT-PCR was used to screen for sequences of the L polymerase and the NP genes of reptarenavirus using the degenerate primers described chapter three. In all, in this chapter isolated total RNA was tested and analysed for its suitability for cDNA synthesis. Subsequently, the cDNA templates were used in RT-PCR technique for finding evidence of reptarenavirus sequences in tissue specimens of different species of snakes and other reptiles.

5.2 Results

5.2.1 RNA extraction

Total (eukaryotic) RNA was isolated from tissues of snakes and other reptiles. As described above, two sources of tissue specimens were used for total RNA isolation including Heathrow Animal Reception Centre (HARC) (Table 4.1) and London Zoo (ZSL) (Table 4.2). Dissected tissue samples were preserved in RNAlater at -80°C prior to use for total RNA extraction. The RNA isolation protocol was carried out on a disinfected bench and the equipment was also disinfected. The samples were homogenized, centrifuged and then the supernatant was used for total RNA extraction as mentioned in section 2.12.2 . Initially, the RNA extracts were evaluated by 260/280 nm and 260/230 nm values in a Nanodrop spectrophotometer. Any contamination in the RNA, including protein and/or organic components is reflected in the absorbance ratio values at 260/280 nm and 260/230 nm respectively. Values of more than 1.8 in the 260/280 ratio were considered suitable for RNA purity (Clements et al. 2006).

5.2.2 Total RNA integrity

RNA is a highly sensitive molecule that can be degraded by many factors including enzymes such as RNase and environmental factors such as high temperature, humidity and light (Vennemann and Koppelkamm 2010). All of these factors influence RNA integrity, in particular the integrity of mRNA (Partemi et al. 2010). RNase is the most significant factor and has a direct impact on RNA integrity due to its endonucleolytic and exonucleolytic activities (Farrell 2017). Also, in some cases RNase is able to enter cells via endocytosis where it can lead to RNA degradation before RNA extraction (Chao and Raines 2011) although in the cases described here the samples came from preserved dead tissue where this concern was minimal. The integrity of the extracted total RNA was therefore an essential measure of quality prior to RT-PCR.

Ribosomal RNA (rRNA) including 18S and 28S ribosomal RNAs forms about 85% of the total RNA in eukaryotic cells (Larson et al. 1991) and can be separated by gel electrophoresis or 2100 Bioanalyzer (Agilent Technologies) electropherogram, which also generates a virtual gel image. In this study, total RNA integrity was evaluated initially by electrophoresis on 0.1% SDS agarose gels, run at 100v for 60 min. In addition, RNA integrity values based on the 18S and 28S rRNAs ratio were determined by using the Agilent RNA 600 Nano kit on a 2100 Bioanalyzer (Agilent Technologies). The 18S and 28S rRNAs appear as two distinct peaks on the electrophoretogram (Figure 5.1) which can also be visualised as a gel-like image (Figure 5.2). Total RNA degradation changes the 18S and 28S rRNA subunits peaks by broadening them, with the addition of many small segments of degraded RNA

which results in an increase in the background of the electrophoretogram (Schroeder et al. 2006).

The Bioanalyzer results give an RNA integrity number (RIN) and the concentration of the sample (Schroeder et al. 2006). The RIN number refers to a ratio calculation for the 18S and 28S rRNAs peaks and has a range from 1 to 10, where a value=1 conforms to completely degraded RNA and a value=10 conforms to totally intact RNA. Total RNA with a RIN value in the range between 8-10 is classified as high quality total RNA, values between 5-8 indicate partially degraded RNA, while values of RIN number below 5 are considered not to be suitable for use as a RT-PCR template (Fleige et al. 2006). Therefore, the higher RIN number samples of intact RNA are considered for cDNA analysis and RT-PCR.

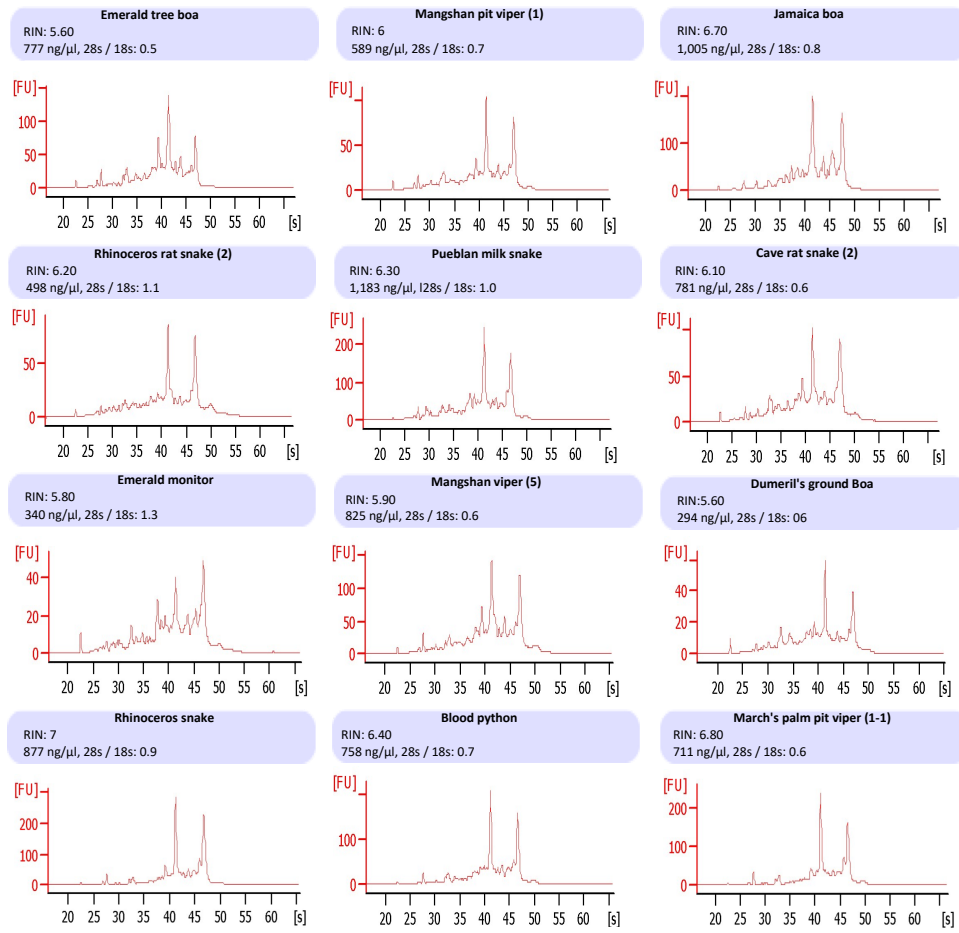


Figure 5.1: Electropherograms of total (eukaryotic) RNAs of snakes. Extracted total RNA from a liver of different species of snakes (Table 4.2) were used for Eukaryotic total RNA Nano Assay by 2100 Bioanalyzer. Each electropherogram consists name of specimen, RNA integrity number (RIN), RNA concentration and 28S/18S rRNA ratio. Total RNA purity is represented by the two prominent peaks of ribosomal 18S and 28S rRNAs. The image was created by Agilent 2100 Bioanalyzer (Agilent Technologies) and manually edited.

As shown in Figure 5.1, there is a partial degradation in the total RNA extracted from snake samples from London Zoo (ZSL) as their RNA integrity number (RIN) ranged from 5-7. The finding is consistent with previous studies suggesting that RNA degradation is commonplace in such preparations (Chao and Raines 2011). The degradation of total RNA during RNA extraction should have been limited as the protocol was carried out on treated bench with ether 0.5% SDS or RNAZap (Sigma)

and filtered tips were used throughout. However, degradation could have occurred at the time of sampling or in subsequent handling. In any event as RNA with RIN number ranges around 5-7 is acceptable for gene expression analysis these samples were included in the subsequent analysis. Other total RNA extracts from the London Zoo (ZSL) snakes had RIN values ranging from 2 to <5 which is less than the RIN value recommended for analysis. In all, the total RNA analysis of the ZSL samples indicated that the highest intact RNA was isolated from the Rhinoceros snake (RIN=7) whereas the lowest intact total RNA (RIN < 5) was isolated from the Corn snake (3), Burmese rock python and Cave rat snake (3) samples (RIN=2.4, 2.60 and 3.60 respectively). The concentration of the RNA extracted ranged from ~ 300 ng/ μ l to 1 ug/ μ l. The data also showed that the size of the ribosomal 18S and 28S rRNAs varied slightly between snake species (Figure 5.2), possibly due to RNA degradation (Schroeder et al. 2006). The highest degradation, lowest RIN and lowest concentration values were found in the total RNAs that were extracted from the Heathrow Animal Reception Centre (HARC) samples (RIN < 3). Thus, despite variability, the RNAs extracted from the ZSL samples had a better integrity than the HARC samples, which might reflect the fact that the ZSL samples were relatively fresh and well persevered while those from the HARC varied considerably in state and age.

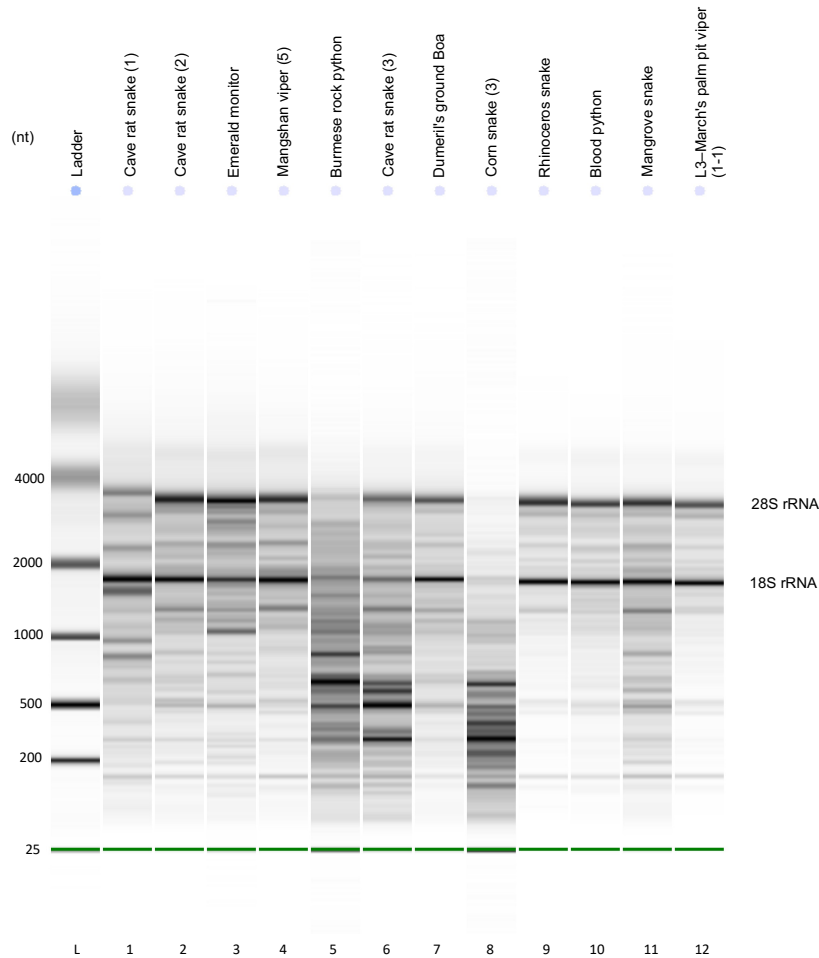


Figure 5.2: Gel-like electrophoresis of total RNA (eukaryotic) of snakes showing ribosomal 18S and 28S rRNA subunits. Total RNA of liver specimens of different species of snakes (Table 4.2) were used by the Eukaryotic Total RNA Nano Assay by 2100 Bioanalyzer. The electropherogram was created by Agilent 2100 Bioanalyzer (Agilent Technologies) and manually edited.

5.2.3 Reverse transcription for complementary DNA (cDNA) synthesis

Complementary DNA (cDNA) was synthesized using a TaqMan® Reverse Transcription Kit (Applied Biosystems) with the template of the total RNAs isolated as described from reptiles (Table 4.1 and 4.2). Gifted genomic RNA of UHV was used as a positive control for the RT reaction. The cDNA was first generated with a random hexamer primer and the total cDNA derived was then used as a template

for PCR using reptarenavirus primers. In addition, spiked RT reaction were done using the RNA of UHV mixed with two total RNA extracts of different species of snakes. Spiked RT-PCR experiments were done to assess the level of any contaminants present in the samples that might have inhibited the initial RT reaction (Liu et al. 2016). Different cDNA synthesis approaches were also evaluated during the study using UHV genomic RNA as template. The effect of Oligo(dT) primers on the RT reaction was investigated in addition to the use of random hexamer primers alone and combined with an Oligo(dT) prime. This was done as Oligo(dT) primers were included as part of the kits used yet were not appropriate for the amplification of reptarenavirus genome or message as these are not polyadenylated. A theoretical risk was considered wherein the Oligo(dT) amplification of cellular message, also present in the total RNA extracts, would consume kit components and so limit the ability to detect reptarenavirus sequences. Thus, reactions with and without Oligo(dT) was done to formally test this possibility. RT reactions were then tested as substrates for PCR using L polymerase and NP primers. The degenerate specific primers for L polymerase were L1017F and L1544R and those for NP were NP173F and NP562R, all as described earlier. The results showed that L polymerase and NP gene fragments were amplified in both RT reactions, confirming that cDNA is generated from the reptarenavirus RNA template even if an Oligo(dT) primer is present in the RT reactions (Figure 5.3). The spiked controls showed no inhibition in RT-PCR reactions, so it can be concluded that there is no significant influence of Oligo(dT) presence on the RT step. The possibility that this would dominate priming and that the viral genome would be difficult to detect is shown not to be the case in the cDNA synthesis done here and the presence or not of an

Oligo(dT) primer in the RT kit did not detrimentally affect the detection of the UHV RT product.

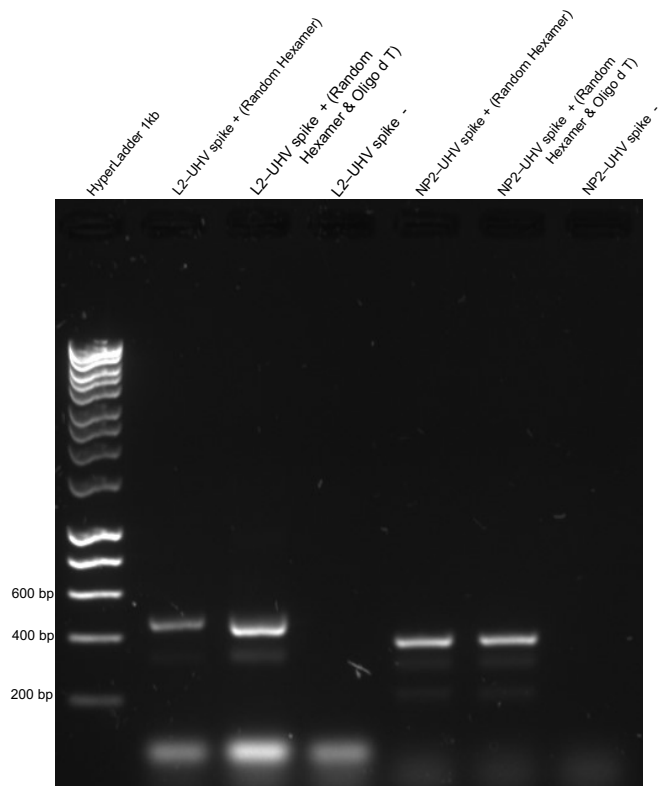


Figure 5.3: Reverse transcription PCR of UHV. A first RT reaction was done with random hexamer primers. The second RT reaction was run with a mixture of random hexamer and oligo(dT) primers. The reaction contains spike RT-PCR (contains RNA of UHV) and negative controls. The degenerate gene specific primers used for fragments of L polymerase and NP were L1017F, L1544R, NP173F and NP562R (Table 2.1 and 2.2). The amplicons L2 (527 bp) and NP2 (389 bp) are as expected. Marker: HyperLadder 1kb (Bioline).

Within this study the minimum viral load detectable for reptarenavirus was determined through detection of UHV by RT-PCR in a dilution series. The number of UHV copies were determined by either using the copy number calculator of single strand RNA available online on (<http://scienceprimer.com/copy-number-calculator-for-realtime-pcr>) or manually using the formula:

$$\text{Number of the RNA copy} = \frac{\text{Amount of the RNA (ng)} * 6.022 \times 10^{23}}{\text{Length of the RNA (bp)} * 1 \times 10^9 * 340}$$

Where 6.022×10^{23} molecules/mole is Avogadro's number and 340 is the average mass of an RNA nucleotide.

A serial dilution from 10^{-1} to 10^{-6} of purified positive RNA (16 ng/ μ l) of UHV was used as a template in the RT reaction. The second step PCR was done with primers for the L polymerase, L1017F and L1544R, and gel electrophoresis was used for visualization of the target amplicons (Figure 5.4). It is apparent from the data that an amount of 1.6 ng/ μ l of RNA sample, i.e. a 10^{-1} dilution of the stock in a 20 μ l RT reaction was the minimum required for reptarenavirus detection by RT-PCR. The calculated UHV copies in 1 microlitre (the assay addition) of 1.6 ng/ μ l RNA was 2.673×10^8 . This number of viral RNA copies is appropriate for the sensitivity of the assay based on typical viral load values in infected tissue (Caliendo et al. 2004). In fact, the detectable limit maybe lower as it is likely that the purified UHV RNA sample also contained cellular RNA which would have contributed to the OD₂₆₀ unit used for the calculation of concentration.

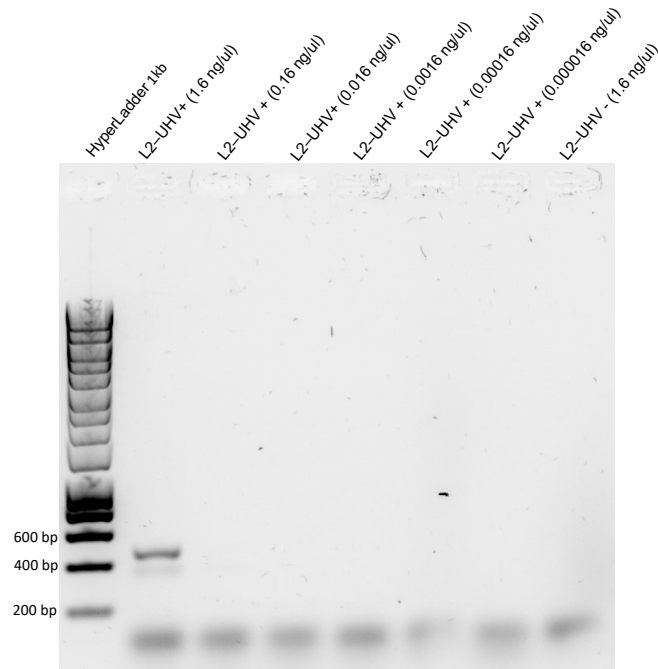


Figure 5.4: Gel electrophoresis for determination of the viral load of reptarenavirus by RT-PCR. Serial dilution of genomic RNA of UHV was used for reverse transcription and then the final reaction was used for RT-PCR. The final RT-PCR reaction was run using gen specific primers for L polymerase L1017F and L1544R (Table 2.1) of reptarenavirus. The size of the target amplicon is 527 bp was as expected. Negative control was also used. Marker: HyperLadder 1kb (Bioline).

5.2.4 Identification of mitochondrial 12S and 16S rRNAs genes

Eukaryotic cells including mammalian cells of human and animal origin contain mitochondria that have their own gene expression system. The genome of the mitochondrial comprises around 1 to 2% of total cellular DNA and has a total size of 16.5 kb. Mitochondrial DNA (mtDNA) encodes several oxidative phosphorylation subunits and two ribosomal genes (rRNA), the 12S and 16S rRNAs. Mitochondrial 12S and 16S are key to mitochondrial ribosomes, each being part of the small and large ribosomal subunits respectively, and so have a significant role in mitochondrial protein synthesis (Pirger et al. 2009; Wallace 1999).

In this study, total RNA extracts of reptiles were evaluated for mitochondrial 12S and 16S rRNAs as a functional measure of RNA quality. Universal oligonucleotide primers for 12S and 16S rRNAs (Table 2.6) were used to amplify the mitochondrial sequences by RT-PCR using the RNA of different species of snakes and reptiles as sample (Table 4.1 and 4.2). Positive mitochondrial 12S and 16S rRNAs PCR products were extracted from the gel and subjected to Sanger sequencing to confirm their sequence. The results showed that the RT-PCR products of mitochondrial gene amplification were around 495 bp for 12S rRNA and around 486 bp for 16S rRNA genes (Figure 5.5, 5.6, 5.7 and 5.8). The tests confirmed that universal primers for 12S and 16S rRNAs were able to amplify mitochondrial genes from a wide range of reptile species including snakes, turtles and chameleons and that the extracted RNAs were able to act as a function RT-PCR template. A high degree of degradation in the total RNA of the *Chameleon incounutos* and *Chamelon rudis* samples prevented amplification of the 12S rRNA although weak amplification of the 16S rRNA was possible (Figure 5.8). In all the analysis showed that 12S and 16S rRNAs could be amplified using universal primers from most samples, even those with a lower RNA integrity, e.g. the mitochondrial 12S and 16S rRNAs of the cave rat snake (3) sample were amplified even though the RIN number of the total RNA was only 3.60.

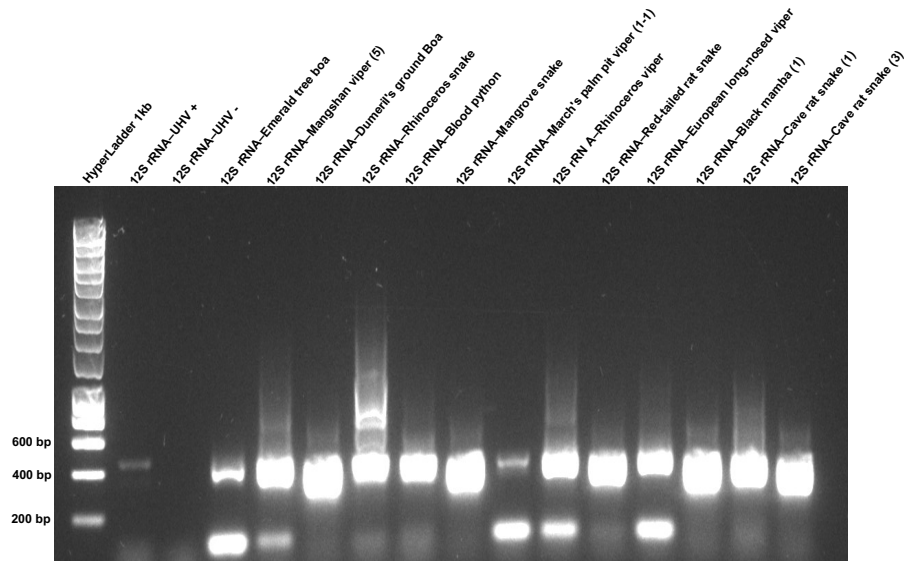


Figure 5.5: Mitochondrial 12S rRNA amplification from snake RNA samples. The cDNA of different species of snakes was used for mitochondrial 12S rRNA amplification by RT-PCR. Universal primers including 12S rRNA.16429F and 12S rRNA.16924R were used in the RT-PCR reaction. The amplified fragments (495 bp) were compared to HyperLadder 1kb (Bioline). Positive and negative controls of 12S rRNA of UHV were used as shown. London Zoo (ZSL) was the source of the snakes' specimens.

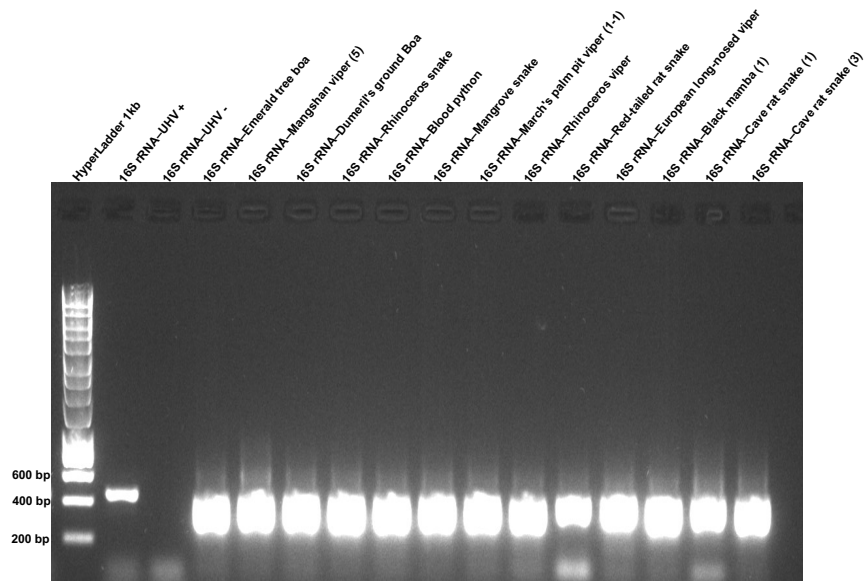


Figure 5.6: Mitochondrial 16S rRNA amplification from snake RNA samples. The cDNA of different species of snakes was used for mitochondrial 16S rRNA amplification by RT-PCR. Universal primers of 16S rRNA including 16S rRNA.4199F and 16S rRNA.4685R were used in the RT-PCR reaction. The amplified amplicons (486 bp) were compared to HyperLadder 1kb (Bioline), positive and negative controls of 16S rRNA of UHV were used as shown. London Zoo (ZSL) was the source of the snakes' specimens.

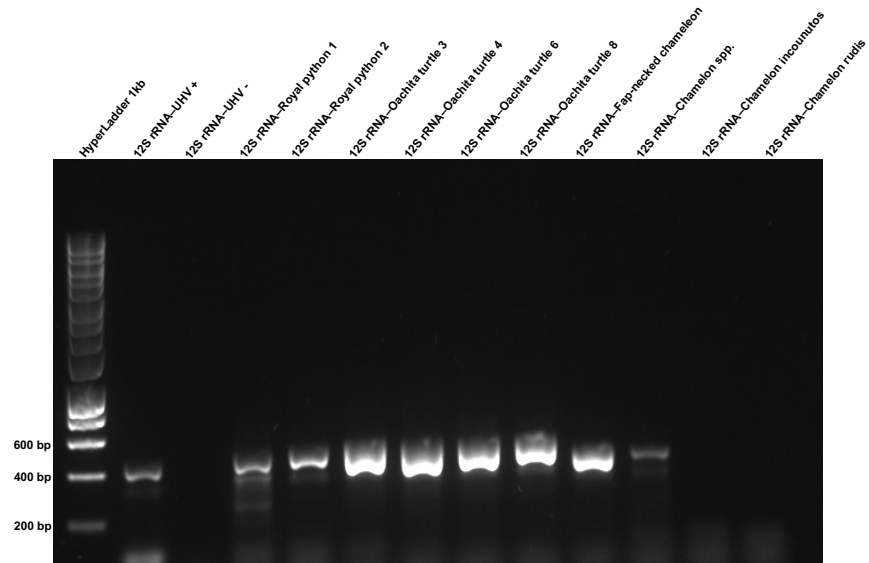


Figure 5.7: Mitochondrial 12S rRNA amplification from reptilian RNA samples. The cDNA of reptiles including snakes, turtles and chameleons was used for mitochondrial 12S rRNA amplification by RT-PCR. Universal primers of 12S rRNA including 12S rRNA.16429F and 12S rRNA.16924R was used in RT-PCR reaction. The size of amplified amplicons (495 bp) were compared to HyperLadder 1kb (Bioline). 12S rRNA positive and negative controls of UHV were used as shown. Heathrow Animal Reception Centre (HARC) was the source of the reptiles' specimens.

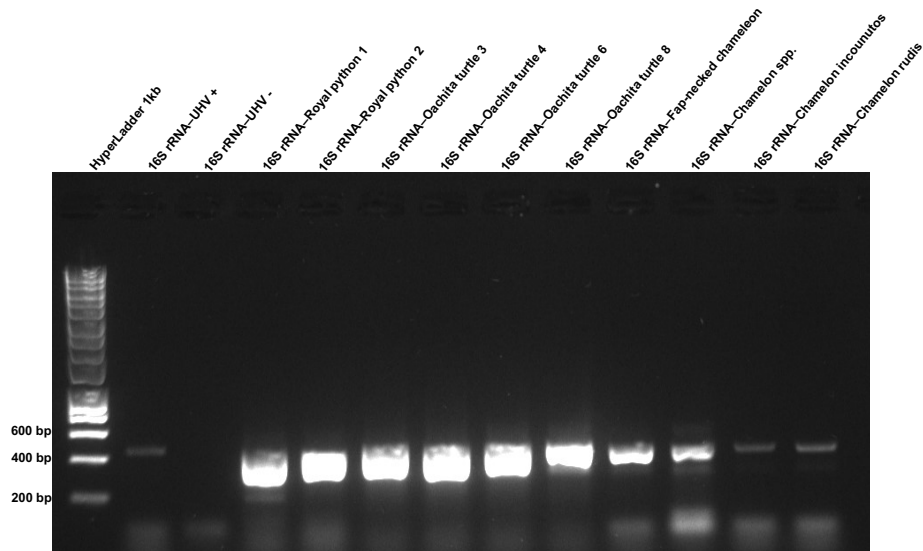


Figure 5.8: Mitochondrial 16S rRNA amplification from reptilian RNA samples. The cDNA of snakes, turtles and chameleons were used for 16S rRNA amplification by RT-PCR. Universal primers of 16S rRNA including 16S rRNA.4199F and 16S rRNA.4685R were used in RT-PCR reaction. The amplified amplicons (486 bp) were compared to HyperLadder 1kb (Bioline), 16S rRNA positive and negative controls of UHV were used as shown. Heathrow Animal Reception Centre (HARC) was the source of the reptiles' specimens.

5.2.5 L polymerase and NP amplification for the presence of reptarenavirus sequences

Reverse transcription PCR (RT-PCR) was used for reptarenavirus identification in boa constrictors, pythons (Aqrawi et al. 2015; Hyndman et al. 2019), boid snakes (Abba et al. 2016) and Corn snake (Hyndman et al. 2019). In this study, a two-step RT-PCR was used to find evidence of L polymerase and NP reptarenavirus sequence in reptile specimens (Table 4.1 and 4.2). Degenerate primers for L polymerase and NP (Table 2.1, 2.2 and 2.4) were used to amplify hexaprimed reverse transcribed viral RNA. For these reactions, positive and negative and spiked PCR reactions were used as controls for L polymerase and NP primers and the size of any expected fragments (L1, L2, L3, L4 and NP2) was judged following electrophoresis by comparison to the HyperLadder 1kb (Bioline) marker. The spiked RT-PCR ensured no inhibitory materials were present in the reaction mixes. The final products were analysed by 1% agarose gel electrophoresis and any reptarenavirus amplicons imaged using a G-Box (Figure 5.9, 5.10, 5.11, 5.12, 5.13, 5.14, 5.15 and 5.16). Any fragments deemed possible amplicons with a size expected for the primers used were extracted from the gel and confirmed by Sanger sequencing.

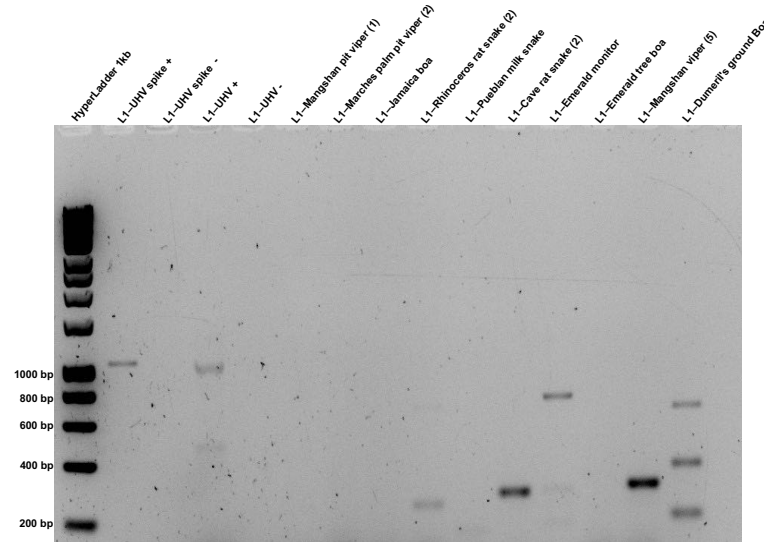


Figure 5.9: Gel electrophoresis of RT-PCR of L polymerase gene (L1). Hexaprimed complementary DNA (cDNA) from liver samples of snakes (Table 4.2) was utilized as the RT-PCR template. Positive, negative and spiked RT-PCR of UHV were used as controls. One set of L polymerase primers (Table 2.1) L4087F and L5099R were used for the RT-PCR reaction. The second step RT-PCR was run according to the conditions described in section 2.13.2. The size of the target amplicon is expected to be 1012 bp. Marker: HyperLadder 1kb (Bioline).

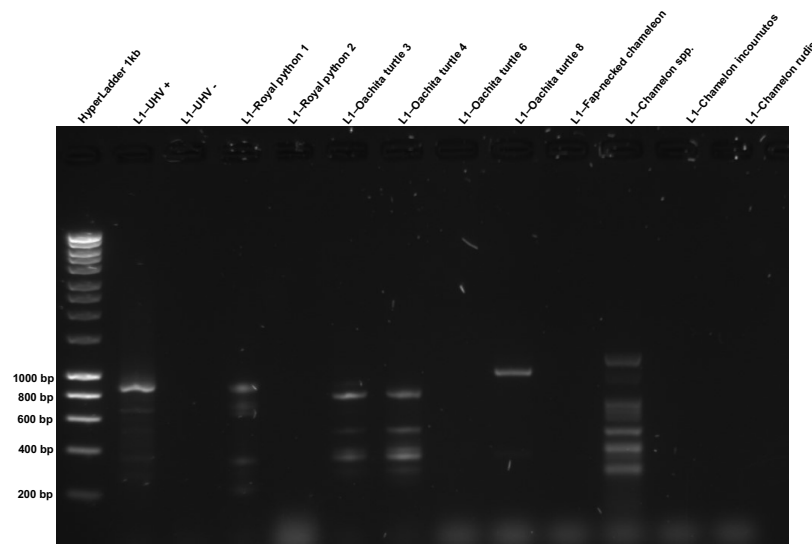


Figure 5.10: Gel electrophoresis of RT-PCR of L polymerase gene (L1). Complementary DNA (cDNA) was synthesised from kidney samples of pythons, and liver samples of turtles and chameleons (Table 4.1). Positive, negative and spiked RT-PCR of UHV were used as controls. One set of L polymerase primers (Table 2.1) L4087F and L5099R were used for reaction. The second step RT-PCR was run according to the conditions described in section 2.13.2. The size of the expected target amplicon is 1012 bp. Marker: HyperLadder 1kb (Bioline).

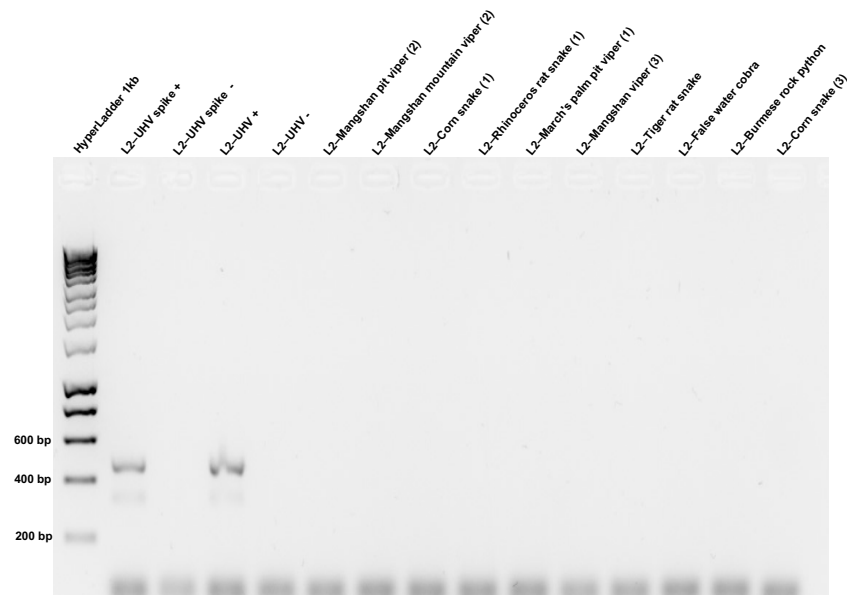


Figure 5.11: Gel electrophoresis of RT-PCR of L polymerase gene (L2). Synthesized cDNA from liver of snakes (Table 4.2) were utilized as a RT-PCR template. Positive, negative and spiked RT-PCR of UHV were used as controls. One set L polymerase primers (Table 2.1) L1017F and L1544R were used for the RT-PCR reactions. The second step RT-PCR was run according to the conditions described in section 2.13.2. The expected size of the target amplicon is 527 bp. Marker: HyperLadder 1kb (Bioline).

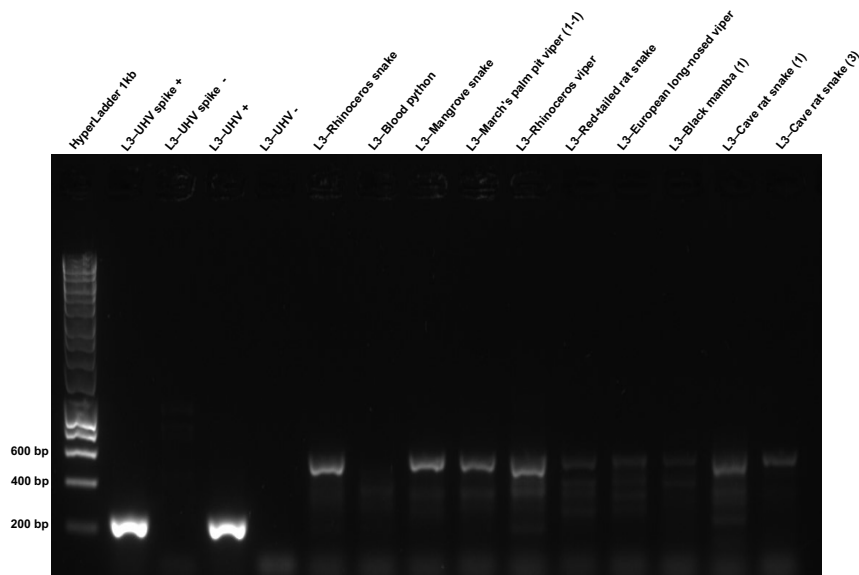


Figure 5.12: Gel electrophoresis of RT-PCR of L polymerase gene (L3). Synthesized cDNA from liver of snakes (Table 4.2) were used as a RT-PCR template. Controls of RT-PCR reaction (positive, negative and spike RT-PCR of UHV) were used in the reactions. Primers of L polymerase (Table 2.1), L5081F and L5316R were used for RT-PCR. The second step RT-PCR was run according to the conditions described in section 2.13.2. The expected size of the target amplicon is 235 bp. Marker: HyperLadder 1kb (Bioline).

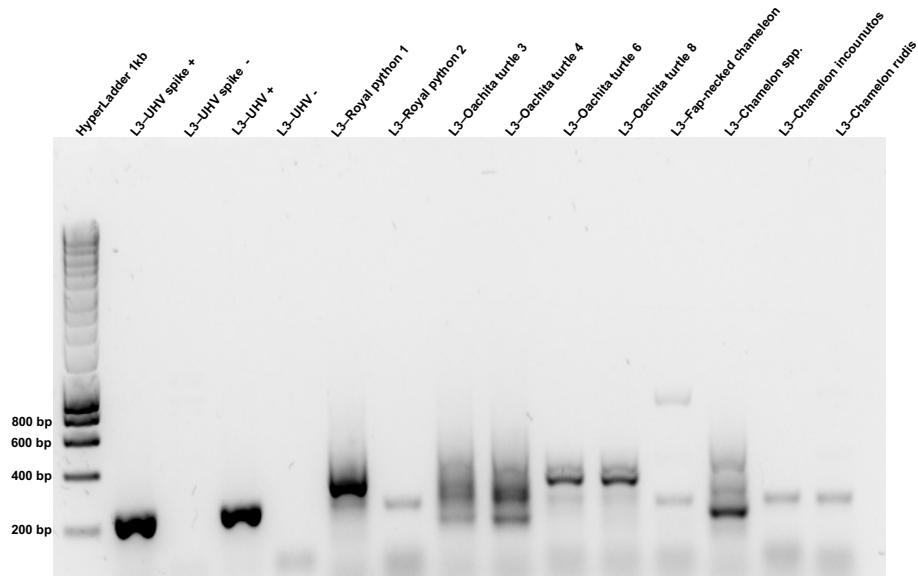


Figure 5.13: Gel electrophoresis of RT-PCR of L polymerase gene (L3). Complementary DNA (cDNA) was synthesized from kidney of pythons, liver of both turtles and chameleons (Table 4.1). The cDNA was used as a RT-PCR template. Positive, negative and spike RT-PCR of UHV were used as controls. One set of L polymerase primers (Table 2.1), L5081F and L5316R were used for reaction. The second step RT-PCR was run according to the conditions described in section 2.13.2. The size of the expected target amplicon is 235 bp. Marker: HyperLadder 1kb (Bioline).

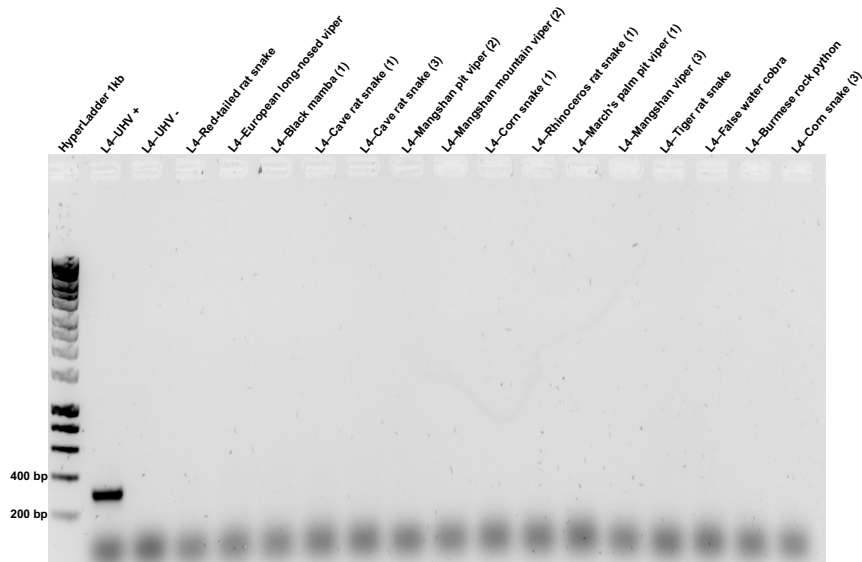


Figure 5.14: Gel electrophoresis of RT-PCR of L polymerase gene (L4). Synthesized cDNA from the liver of snakes (Table 4.2) were used as a RT-PCR template. Positive and negative controls of UHV were used in the RT-PCR reactions. One set of primers of L polymerase (Table 2.4), L3480F and L3799R were used for RT-PCR. The second step RT-PCR was run according to the conditions described in section 2.13.2. The size of the expected target is 319 bp. Marker: HyperLadder 1kb (Bioline).

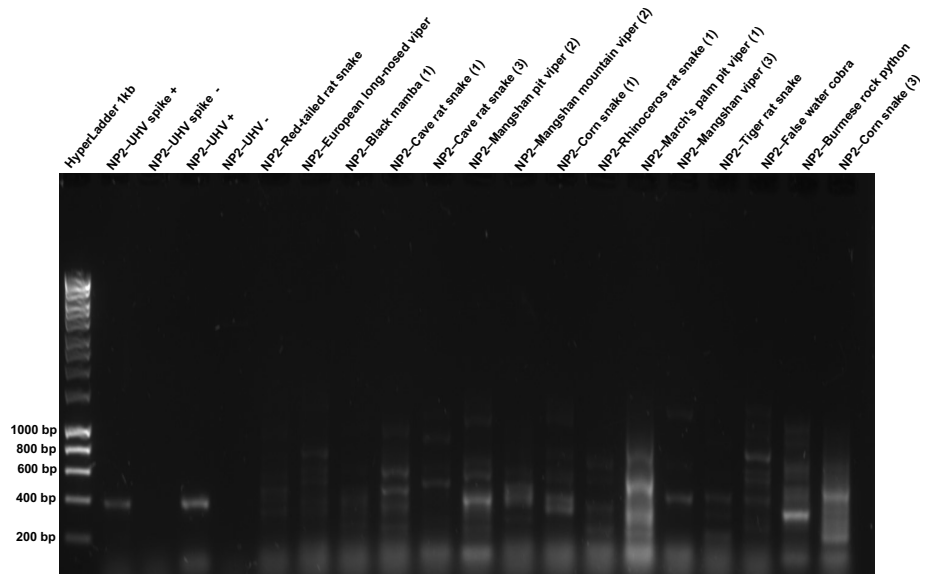


Figure 5.15: Gel electrophoresis of RT-PCR of nucleoprotein gene (NP2). Complementary DNA (cDNA) from the liver of snakes (Table 4.2) were used as a RT-PCR template. Positive, negative and spike RT-PCR of UHV were used as controls. One set NP primers (Table 2.2) including NP173F and NP562R were used for RT-PCR reaction. The second step RT-PCR was run according to the conditions described in section 2.13.2. The expected size of the target fragment is 389 bp. Marker: HyperLadder 1kb (Bioline).

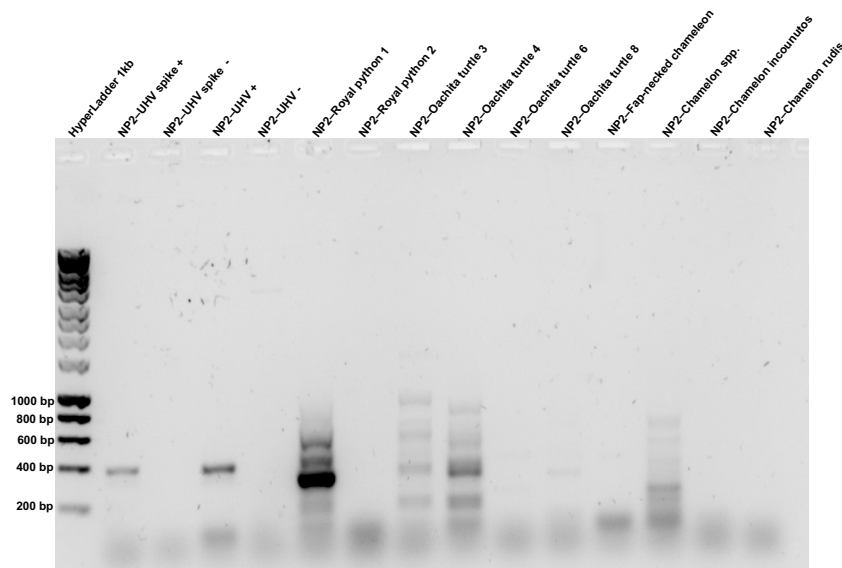


Figure 5.16: Gel electrophoresis of RT-PCR of nucleoprotein gene (NP2). Complementary DNA (cDNA) was synthesized from the kidney samples of pythons, and liver samples of turtles and chameleons (Table 4.2) and used as a RT-PCR template. Positive, negative and spike RT-PCR of UHV were used as RT-PCR controls. One set of NP primers (Table 2.2), NP173F and NP562R were used for RT-PCR reaction. The expected size of the target fragment is 389 bp. The second step RT-PCR was run according to the conditions described in section 2.13.2. Marker: HyperLadder 1kb (Bioline).

Based on the results obtained, it is clear that the positive control for reptarenavirus (UHV) sequence was amplified using both L polymerase and NP primer sets as designed, while the spiked RT-PCR confirmed that the components of the reaction were compatible with the cDNA synthesis of virus sequences if they were present in the reaction. The spiked RT-PCR also confirmed the efficiency of the RT-PCR reaction and the negative controls confirmed no virus genomic contamination of the test samples. Several DNA fragments, as shown in the gel analysis, approximating to the size of the target amplicons for the amplification of the L polymerase fragments (L1 and L3) (Figure 5.9, 5.10, 5.12 and 5.13) and NP gene (NP2) (5.15 and 5.16) were generated. For example, compare the RT-PCR products to the positive controls and the spiked RT-PCR amplicons in Figures 5.11 and 5.14. However, as no fragments were generated by RT-PCR of the L2 and L4 regions, the result was inconsistent with the presence of a complete virus template. To address the identity of these bands the fragments concerned were eluted and sequenced by the Sanger method and the sequences obtained compared to those in the databases by BLASTn analysis. Despite the observation of similar size, the sequence analysis showed that, in fact, these bands were random background fragments of non-specific sequence that by chance were close in size to the positive controls of the L polymerase and NP genes. No similarity was found with any reptarenavirus gene when the BLASTn output was examined. These findings confirmed the data obtained by RT-PCR for the L2 and L4 targets, that is, no confirmation of the presence of any reptarenavirus sequence in the samples tested. The bands derived by RT-PCR for L1, L3 and NP2 genes were spurious, likely endogenous fragments in the reaction that were amplified by the extreme conditions of the RT-PCR reaction (35 cycles). Overall there was no evidence of reptarenavirus

in any of the samples collected, at least as detected by RT-PCR of the tissue samples used in this study with a sensitivity calculated as described.

5.3 Discussion

This chapter seeks to detect emerging or extant reptarenaviruses in snakes and other reptiles. There are two aims of this study, first, to extract total RNAs from internal tissues of reptiles including snakes and ascertain that the extracted RNAs are of sufficient quality for use in RT-PCR. The second aim is to find sequences of L polymerase and NP genes of transcribed RNAs by using a two step RT-PCR. The study started with total RNA isolation from dissected organs (Table 4.1) and separately, snake liver specimens (Table 4.2). The study showed that the isolated total RNA was variable in purity and RNA integrity number, as measured by 18S and 28S rRNAs ratios. The RIN number and yield data supported the discussion in the previous chapter, which described how the animals were handled in ways that were not suitable to protect the RNA from degradation, e.g. time between death and dissection, speed of storage, variability in temperature and humidity. These differences are consistent with RNA degradation before RNA extraction as caused by RNase (Chao and Raines 2011). Evidence of RNA degradation during the RNA work was limited or absent since all equipment was RNase free during handling, dissection and isolation of RNA. Although many samples proved to be suitable for 12S and 16S rRNAs detection, only the higher intact RNA samples with RIN number were considered for virus cDNA synthesis (Fleige et al. 2006). The tests also showed that the RNA extraction was functionally clean as the RT-PCR amplification of spiked controls suggested no inhibitory materials present (Liu et al. 2016).

The study found that the presence of Oligo(dT) primers did not lead to predominant reverse transcription of host mRNA and that viral RNA could be amplified by hexamer primers in the presence or absence of Oligo(dT) primers. Mitochondrial 12S and 16S rRNAs were identified using RT-PCR technique indicating that the isolated total RNA from cadavers of reptiles was appropriate for specific sequence detection. It is interesting to note that the universal primers used for 12S and 16S rRNAs (Table 2.6) could detect a wide range of mitochondrial rRNA sequences from reptilian species including snakes, turtles and chameleons.

Reverse transcribed viral RNA samples from reptiles and the positive control of UHV RNA were used as template for RT-PCR for the presence of the conserved regions of the L polymerase and NP genes of reptarenavirus. The positive controls confirmed the utility of the different sets of degenerate primers for L and NP designed previously but despite this, and a suitably low threshold of detection, the RT-PCR experiments did not detect any evidence of L or NP reptarenavirus sequences in either the frozen animals or the snake liver specimens that were collected and dissected as described. Such bands that were amplified by some L polymerase primers were shown not to be reptarenavirus related. Thus, from this study there is little evidence for widespread infection by reptarenaviruses, at least for animals confiscated at entry into the UK or those kept at ZSL.

Chapter 6 Discussion and future direction

As discussed, reptarenaviruses, within the *Arenaviridae*, are viruses infecting snakes with inclusion body disease around the world (Radoshitzky et al. 2015). As described in Chapters 3-5 of this thesis, specific primers capable of the detection of reptarenavirus sequence were developed and combined with reptilian specimens including snakes and many others of various provenance and used to test for the presence of reptarenavirus or closely related virus sequences gave no evidence for the presence of reptarenavirus in the samples tested. Bands that were consistent with the expected amplicon sizes were tested by Sanger sequencing and were not bona fide virus sequence. However, some limits to the study have to be recognised. Although designed using the available reptarenavirus database sequences and shown to recognize UHV, whether the primer designs were capable of amplifying distant related sequences remains subject to test. Given the conservation among the current reptarenavirus members it seems unlikely that unknown circulating virus would be very divergent, but it is a possibility. A further limitation was the available samples for analysis as, as shown, their suitability for RNA isolation varied. There are many different places of quarantine in the UK and elsewhere and they could have been contacted for collaboration and a much larger and better controlled reptarenavirus investigation study undertaken. Other internal organ samples including lung and brain could have been used for the reptarenavirus investigation by RT-PCR (Keller et al. 2017) although it seems likely that they too would suffer the limitation of dead snake specimens, the lack of fresh tissue specimens and the consequent RNA degradation. In future reptarenavirus investigations, it might be possible to use fresh samples, including blood samples, able for the investigation

rather than stored tissue specimens. Not only more convenient but also potentially more fruitful as some novel reptarenavirus have been isolated from the blood samples of snakes (Chang et al. 2016; Keller et al. 2017). Reptarenavirus have been confirmed in boa constrictor and ball python via RT-PCR and/or immunohistochemistry on blood cells (Hetzl et al. 2013; Keller et al. 2017; Stenglein et al. 2017) but the range of tested snakes remains limited. In future work, different approaches for reptarenavirus detection include quantitative RT-PCR (qRT-PCR) (Stenglein et al. 2017) and isolation by the cell line technique (Abba et al. 2016). Reports have shown that reptarenavirus can grow in African Monkey kidney (Vero), Rat Embryonic Fibroblasts (REF) (Abba et al. 2016) and arthropod cells (Keller et al. 2017). A future investigation might include attempted virus isolation and amplification on such cell lines.

Reptarenavirus infections could potentially cross from current infected snakes to other new species although transmission to the human has never been reported. Future searches for reptarenavirus sequences, confirmed in snakes with BIBD, should include other species in the UK and other regions in cases where there is suspected transmission of infection. New and more widely sourced specimens from HARC and ZSL or samples from other UK quarantine centres should be studied and the degenerate primers designed here should be assessed in other parts of the world. The precise mode of transmission and the incubation period for reptarenaviruses in snakes is unknown although vector-mediated transmission by *Ophionyssus natricis* (snake mite) or via direct contact have been reported (Chang and Jacobson 2010; Hepojoki et al. 2015a). Vertical transmission of BIBD has been confirmed between snakes and their offspring during the egg laying stages and at the live-bearing stage

(Chang and Jacobson, 2010; Keller et al., 2017), in both cases by use of next generation sequencing (NGS). More studies of this nature could better clarify the possibility of reptarenavirus transmission between snakes of different species and between snakes and their offspring.

Recently, several sequences of which have been isolated and archived as novel reptarenavirus species. A BLAST analysis using the amplified genes of University of Helsinki virus (UHV) against the Genbank database matched reptarenavirus identified according to the BLASTn of L gene fragments and the results included novel species of reptarenavirus including ROUT virus (accession YP_009019197.1), Suri Vanera virus (AKN10698.1), tavallinen suomalainen mies virus (APX61223.1), Hans Kompis virus (AKN10706.1) and University of Giessen virus (AKN10708.1). Also, some of these viruses were found using BLASTn with the amplified nucleoprotein gene of UHV, such as ROUT virus (YP_009019195.1), tavallinen suomalainen mies virus (APX61209.1) and University of Giessen virus (AKN10674.1). These viruses are archived as reptarenaviruses although some of these viruses are pending formal classification as *Reptarenavirus*. Some other viruses of the genus *Mammarenavirus* such as Okahandja mammarenavirus (YP_009141006.1), Latino mammarenavirus (AKG54820.1) and Tamiami mammarenavirus (ACC99353.1) also showed homology to the NP gene of reptarenavirus when analysed via the BLASTn facility. As a result of this growing recognition of a diversity of snake reptarenavirus there is the possibility that further examples exist and that designing further universal primers for reptarenavirus would allow for amplification of target fragments of novel/ existing isolates through RT-PCR as was done in the work described here.

Interestingly, protein homology between reptarenavirus and some other viruses from a different family were also reported recently (Rosenthal et al. 2017). Historically, in the *Arenaviridae*, a cap binding domain was not identified in the RNA dependent RNA polymerase, as discovered in influenza virus (Plotch et al. 1981). However, some semblance of cap-snatching endonucleases has been found in the N-terminus of the L proteins of mammarenavirus. In reptarenavirus, the structure of a C-terminal fragment of the L protein of California Academy of Sciences virus (CASV) has been solved by X-ray crystallography revealing individual domains in the C-terminal fragment of CASV L that matched the structure to the cap binding and adjacent domains of influenza virus polymerase, despite not being identified earlier by biochemical study or sequence homology (Thierry et al., 2016; Rosenthal et al., 2017). So, domain homology was found between arenaviruses and other viruses in a different family suggesting that the same fold maybe widely used within the RNA virosphere.

Protein secondary structure predication (PSSP) can be also useful for analysis of reptarenavirus proteins (Jiang et al. 2017) and for understanding their biological function (Wang et al. 2017) and a reasonable protein 3-dimensional (3D) structure can be determined when the accuracy of secondary structure predication for a protein is >80% (Al-Lazikani et al. 2001). Indeed secondary structure prediction of the C-terminus of CASV L protein (Edgar 2004; McWilliam et al. 2013; Simossis and Heringa 2005) with its crystal structure and the secondary structure of Influenza polymerase were utilized for the sequence alignment reported by Rosenthal et al. (Rosenthal et al. 2017).

Finally, the evolutionary history of a virus can be deduced by a phylogenetic network (Hall 2018) and it may be possible to use a phylogenetic network for the analysis of the evolution history among different genes in reptarenavirus species and between genes in same species.

Appendix one: Published papers

Doyle, N., Neuman, B., Simpson, J., Hawes, P., Mantell, J., Verkade, P., **Alrashedi, H.**, Maier, H., 2018. Infectious Bronchitis Virus Nonstructural Protein 4 Alone Induces Membrane Pairing. *Viruses* **10**, 477.

Maier, H.J., Neuman, B.W., Bickerton, E., Keep, S.M., **Alrashedi, H.**, Hall, R., Britton, P., 2016. Extensive coronavirus-induced membrane rearrangements are not a determinant of pathogenicity. *Scientific Reports* **6**, 27126.

Alrashedi, H., Jones, A., Mulley, G., Neuman, B.W., 2019. Bioinformatics analysis for L polymerase homology of arenaviruses. *BioRxiv*.

Introduction

From the outset of this thesis the intention was to work on emerging or re-emerging virus infections with a view to either better describe a current situation or to contribute to understanding emerging virus biology. The main body of the thesis described the work done on the former topic, the current situation of emerging reptarenavirus infections. However, at the start of the project no samples for analysis had been sourced and it was unclear how many samples and of what quality might be obtainable. The scale of the study possible was therefore unclear. It was considered that, in addition to the unique study on arenavirus occurrence in reptilian samples, contributing to an ongoing project on another class of emerging viruses, coronaviruses, might be useful as, if novel reptarenaviruses were discovered, some of the techniques developed for coronavirus study might be reasonably applied to them. For example, analysis of the ultrastructure of the infected reptilian cells following fixation, section and transmission electron microscopy might be possible assuming the tissue samples were of sufficient quality. As a result, a lesser but still significant part of this thesis details the coronavirus studies done, both of which have now been published and are bound here as the formatted complete publications.

In these studies, a quantitative assessment was made of the occurrence of replication organelles in coronavirus infected cells. Transmission Electron Microscopy (TEM) was used for visualised the replication organelles including double membrane vesicles (DMVs), zippered endoplasmic reticulum (zER) and spherules (tethered vesicles) of infections bronchitis virus (IBV) in various cell types.

Using IBV strains that included pathogenic lab (M41), apathogenic lab (Beau-R), pathogenic field (D1466, 4/91 and Italy02) and vaccine strain (H120) variants fixation and resin embedding of the specimens was carried out followed by ultramicrotome sectioning and TEM examination as described in section 2.15. The studies showed that while membrane rearrangements vary considerably with cell type and strain they appear not to be markers of pathogenicity. In a subsequent study, the initial phase of DMV formation, membrane pairing, was shown to be induced by expression of nsp4 only although full DMV formation required the expression of other coronavirus proteins in addition to nsp4.

A third paper, which returns to emerging arenaviruses, has been deposited as an initial draft on bioRxiv. In this study, stimulated by initial considerations in preparation for the reptarenavirus study, conserved arenavirus gene sequences were used to screen the unannotated transcripts deposited in the Transcriptome Shotgun Assembly (TSA) sequence database at NCBI for related content. A surprisingly diverse set of fragments were discovered suggesting that arenavirus-like agents may be circulating in a number of other organisms. Initial hits are followed up and the basis of the homology is determined to be core conserved regions within the L polymerase. Despite their relatedness to described arenaviruses it is concluded that there is little evidence to suppose that any of the discovered hits derive from viruses that could be considered a threat.

Paper one:

Extensive coronavirus-induced membrane rearrangements are not a determinant of pathogenicity

Helena J. Maier¹, Benjamin W. Neuman², Erica Bickerton¹, Sarah M. Keep¹,
Hasan Alrashedi², Ross Hall¹ & Paul Britton¹

¹The Pirbright Institute, Pirbright, Surrey, UK.

²School of Biological Sciences, University of Reading, Reading, Berkshire, UK.

*Correspondence Author:

H.J.M.

Published in Scientific Reports volume 6, 2016

Abstract

Positive-strand RNA (+RNA) viruses rearrange cellular membranes during replication, possibly in order to concentrate and arrange viral replication machinery for efficient viral RNA synthesis. Our previous work showed that in addition to the conserved coronavirus double membrane vesicles (DMVs), Beau-R, an apathogenic strain of avian *Gammacoronavirus* infectious bronchitis virus (IBV), induces regions of ER that are zippered together and tethered open-necked double membrane spherules that resemble replication organelles induced by other +RNA viruses. Here we compared structures induced by Beau-R with the pathogenic lab strain M41 to determine whether membrane rearrangements are strain dependent. Interestingly, M41 was found to have a low spherule phenotype. We then compared a panel of pathogenic, mild and attenuated IBV strains in *ex vivo* tracheal organ culture (TOC). Although the low spherule phenotype of M41 was conserved in TOCs, each of the other tested IBV strains produced DMVs, zippered ER and spherules. Furthermore, there was a significant correlation for the presence of DMVs with spherules, suggesting that these structures are spatially and temporally linked. Our data indicate that virus induced membrane rearrangements are fundamentally linked to the viral replicative machinery. However, coronavirus replicative apparatus clearly has the plasticity to function in different structural contexts.

Introduction

All positive-strand RNA (+RNA) viruses studied to date induce the rearrangement of cellular membranes during infection to facilitate viral RNA synthesis and assembly of RNA synthesis machinery into replication-transcription complexes (Denison 2008; Harak and Lohmann 2015; Miller and Krijnse-Locker 2008; Paul 2013). The types of membrane structures that are induced varies between different families of +RNA viruses but includes single membrane and double membrane vesicles, contiguous vesicles, convoluted membranes (CM), paired membranes and spherules. The source of rearranged membranes also varies between different families of +RNA viruses and can be from intracellular vesicles, endoplasmic reticulum, mitochondria and the plasma membrane. It has long been observed that *Betacoronaviruses* induce the formation of double membrane vesicles (DMVs) during infection of a host cell, along with a reticular network of membranes called convoluted membrane (David-Ferreira and Manaker 1965; de Wilde et al. 2013; Goldsmith et al. 2004; Gosert et al. 2002; Knoops et al. 2008; Snijder et al. 2006; Stertz et al. 2007; Ulasli et al. 2010). During SARS-coronavirus (SARS-CoV) infection, both of these structures were shown to be derived from and linked to cellular ER, as well as linked to each other (Knoops et al. 2008). More recently, comparable structures were also found in cells infected with *Alphacoronaviruses* (Orenstein et al. 2009). The *Coronavirinae* subfamily is divided into four genera, with an ancestral split giving rise to one progenitor for the *Alpha*- and *Beta*- genera and a second progenitor for the *Gamma*- and *Delta*- genera. Interestingly, in our recent work studying avian *Gammacoronavirus* infectious bronchitis virus (IBV), subtle, but potentially significant, differences in the nature of virus induced membrane

rearrangements were reported. Specifically, CM was not observed to any great extent and instead regions of ER were found to become zippered together and tethered to this were pinched out spherules with a neck and channel connecting the spherule interior to the cytoplasm (Maier et al. 2013b). Consistent with observations from other coronaviruses, IBV infection also induced the formation of DMVs. Although detailed understanding of the function of rearranged membranes in the replication of coronaviruses and numerous other +RNA viruses remains to be determined, the conserved process of membrane rearrangement for the whole virus class, and the close association of replicase proteins and products of RNA synthesis with rearranged membranes strongly supports the hypothesis that they play a key role in viral RNA synthesis. Therefore, further study of these likely critical structures and developing understanding of their role in virus replication will provide insight into this central stage of the virus life cycle.

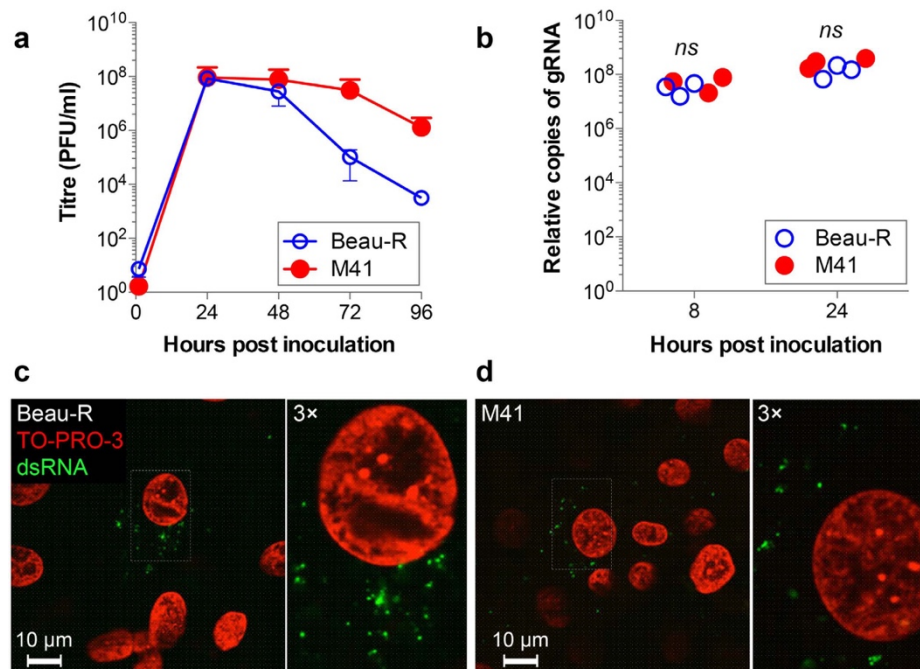


Figure 1. Replication of Beau-R and M41 are comparable in CK cells. (a) CK cells were infected with Beau-R (open circles) or M41 (closed circles) at an MOI of 0.005. Release of progeny virus was determined by plaque assay. Mean and standard error of three independent experiments are shown. (b) Genomic RNA levels were measured by two-step RT-qPCR at 8 and 24 hours after inoculation of CK cells with 20 pfu per cell of Beau-R or M41. Results from three independent experiments are shown. Non-significant differences by t-test are indicated (ns). CK cells were inoculated with (c) Beau-R for 4 hours or (d) M41 for 3 hours. Cells were fixed with 4% paraformaldehyde and labelled with anti-dsRNA (green) and nuclei were labelled with TO-PRO-3 (red).

IBV is a highly important pathogen of poultry, causing animal welfare problems and extensive economic losses to poultry industries globally. There are numerous strains and serotypes of IBV that cause a broad spectrum of disease ranging from mild respiratory symptoms to nephropathy to severe pathology of the

reproductive organs (Benyeda et al. 2009; Cook et al. 2012; de Wit et al. 2011; Gelb et al. 2013). In addition, live-attenuated vaccine strains are commonly used to protect poultry from virus infection (for example Nobilis IB (MSD Animal Health), Poulvac IB (Zoetis) and Cevac (Ceva)). Finally, laboratory adapted strains, capable of replicating in cell culture are used to study viral pathogenesis, the mechanism of virus replication and interaction with the host (Armesto et al. 2009; Casais et al. 2001). Previous studies investigating the nature of coronavirus induced membrane rearrangements have utilised a limited range of virus strains or have compared wild type and mutant viruses of the same strain to study any involvement of membrane rearrangements in virus replication or viral fit-ness in cell culture. Indeed, our previous work was performed using an apathogenic lab strain of IBV and recombinants of this virus (Maier et al. 2014, 2013b).

Therefore, we undertook a study to characterise IBV induced membrane rearrangements in more detail to determine whether virus strain, genotype, degree of pathogenicity or the process of virus adaptation to allow replication in cell culture resulted in changes in the nature of membrane rearrangements. Initially, a comparison of apathogenic Beau-R and pathogenic M41, demonstrated that M41 presented a low spherule phenotype, although replication dynamics were comparable. A further panel of pathogenic, apathogenic, lab adapted, field and vaccine strains of IBV was selected and replication and induction of membrane rearrangements was assessed. We found that there were no significant differences in membrane rearrangements induced by the virus panel. Only IBV strain M41 presented a low spherule phenotype.

Materials and Methods

Ethics statement. Primary chick kidney (CK) cells and *ex vivo* tracheal organ cultures (TOCs) were prepared by The Pirbright Institute microbiological services department from chickens produced in the Institute's poultry production unit. Sacrifice of chickens and embryos was performed by trained staff under a schedule 1 procedure, in accordance with local rules. This procedure does not fall under any UK Home Office licence requirements as procedures were not carried out on live animals. However, studies were carefully considered for animal welfare and ethical implications and were approved via institutional processes. The kidneys were removed from the sacrificed chickens for preparation of the primary CK cells and trachea were removed from the sacrificed chickens or embryos for preparation of *ex vivo* TOCs. All work was performed in a designated establishment, The Pirbright Institute, Compton Laboratory.

Cells, viruses and antibodies. Primary CK cells were produced from 2–3 week-old specific pathogen free (SPF) Rhode Island Red (RIR) chickens (Hennion and Hill 2015). TOCs were produced from 19 day old SPF embryos (Cook et al. 1976; Jones and Hennion 2008), or 2–3 week-old SPF RIR chickens, using the same procedure. The murine DBT astrocytoma cell line was used to grow the *Betacoronavirus* MHV-A59 as described previously (Neuman et al. 2006). The apathogenic molecular clone of IBV, Beau-R, has been described previously (Maier et al. 2014). The pathogenic lab adapted strain of IBV, described elsewhere as M41-CK but here called M41, is a derivative of M41 (Darbyshire et al. 1979). The vaccine strain H120 (Bioral, Merial Sanofi) and field isolates 4/91, Italy02 and D1466 (kindly provided by Prof R. Jones and Dr K. Ganapathy, University of Liverpool) were also

used. The characteristics of these IBV strains are summarised in Table 1. Anti-tubulin was purchased from Sigma-Aldrich. Anti-dsRNA J2 was purchased from English and Scientific Consulting Bt. Goat anti-mouse secondary antibodies were purchased from Life Technologies.

Viral growth kinetics in CKCs. CK cells were infected with Beau-R or M41 at an MOI of 0.005. After 1 hour incubation at 37 °C, cells were washed and fresh 1x BES (MEM, 0.3% tryptose phosphate broth, 0.2% bovine serum albumin, 20 mM N,N-Bis(2-hydroxyethyl)-2-aminoethanesulfonic acid (BES), 0.21% sodium bicarbonate, 2 mM L-glutamine, 250 U/ml nystatin, 100 U/ml penicillin, and 100 U/ml streptomycin) added. Cell supernatant was harvested at 1, 24, 48, 72 and 96 hpi. Presence of progeny virus was determined by plaque assay on CK cells.

Two-step RT-qPCR to analyse viral RNA levels. CK cells were mock infected or infected with either Beau-R or M41 at an MOI of 20. After 1 hour, cells were washed twice with PBS and fresh 1x BES added. Cells were harvested at 2, 8 and 24 hpi using RLT buffer and total RNA extracted using a TissueLyser II (Qiagen) and an RNeasy kit (Qiagen), according to the manufacturer's protocol. RNA was reverse transcribed using Superscript III (Invitrogen), using 600 ng RNA and primers specific for the 5' UTR. Quantitative PCR was then performed as described in (Maier et al. 2013b). Absolute quantitation of cDNA copies was performed using a plasmid standard followed by normalisation against the mock sample from each time point. Finally, the 8 and 24 hpi samples were normalised against input present in the 2 hpi sample.

Immunofluorescence labelling. CK cells were mock infected or infected with Beau-R or M41 and incubated for 1 hour at 37 °C. Cells were then washed and fresh 1x BES added. Cells were fixed at 3 and 4 hpi using 4% paraformaldehyde in PBS for 30 minutes at room temperature. Cells were then washed once with PBS and permeabilised in 0.1% triton X-100 for 20 minutes. Cells were blocked for 1 hour at room temperature in 0.5% BSA in PBS, and then incubated for 1 hour at room temperature with anti-dsRNA diluted 1:1000 in blocking buffer. After three washes in PBS, cells were incubated for 1 hour at room temperature with goat anti-mouse IgG2a Alexa 568 diluted 1:200 in blocking buffer. Finally cells were washed three times in PBS and nuclei stained with TO-PRO-3 iodide (Life Technologies) diluted in water.

TOCs produced from 19 day old SPF embryos were mock infected or infected with 5×10^5 PFU Beau-R, M41 or H120, or 500 μ l D1466, 4/91 or Italy02 grown in SPF eggs, diluted 1:10. TOCs were incubated for 1 hour at 37 °C and fresh medium added. After 24 hours, TOCs were washed with PBS and fixed in 4% paraformaldehyde. TOCs were labelled with anti-dsRNA as described above. Anti-tubulin antibody was diluted 1:1000 and goat anti-mouse IgG1 Alexa 488 was diluted 1:200. Nuclei were stained with 4',6-diamidino-2-phenylindole (DAPI) diluted in water. Labelled TOCs were mounted onto cavity well microscope slides in mounting medium.

Transmission electron microscopy of chemically fixed cells. CK cells in 6 well plates were infected with Beau-R or M41 and incubated for 1 hour at 37 °C when fresh 1x BES medium was added. At 24 hpi, cells were washed once in 0.9% saline and scraped into the buffer. Cells were pelleted at 500 \times g for 5 minutes at 4 °C and

then 500 µl 2% glutaraldehyde in 0.1 M sodium cacodylate. Then, the procedure was carried out as stated in material and method chapter, section 2.15. 60–395 cell sections were imaged per sample.

TOCs produced from 19 day old SPF embryos were mock infected or infected with 5×10^5 PFU Beau-R, M41 or H120, or 500 µl D1466, 4/91 or Italy02 grown in SPF eggs, diluted 1:10. TOCs were incubated for 1 hour at 37 °C and fresh medium added. After 24 hours, TOCs were fixed in 2.5% glutaraldehyde, 4% paraformaldehyde in 0.1 M sodium cacodylate for 1 hour at room temperature and then 4 °C overnight. Then, the procedure was carried out as stated in material and method chapter, section 2.15. 76-84 cell sections were imaged per sample.

DBT cells were inoculated with 3 PFU of MHV-A59 per cell and maintained at 37 °C. Infected cells were fixed in electron microscopy-grade 4% glutaraldehyde (Sigma) in 0.1 M cacodylate buffer, scraped from the plate, and then the procedure was carried out as stated in material and method chapter, section 2.15. 205–604 cell sections were imaged per sample. Cell sections used here each contained a single visible nucleus, with intact nuclear and plasma membranes.

Analysis of membrane structures and statistics. Pixel size for each image was calculated from images of a calibration grid that were recorded at each of the magnifications used to image infected cells. Intracellular features were measured using the boxer module of EMAN (Ludtke et al. 1999) following the procedure previously described for measuring MHV DMVs (Al-Mulla et al. 2014). The longest and shortest diameters of each DMV, spherule and intracellular virus particle were measured twice each, with a standard deviation of about 2 pixels on average, which equated to approximately 4–10 nm at the level of the specimen. Since most virus-

induced intracellular features had elliptical profiles, size was calculated by dividing Ramanujan's first approximation of perimeter length by π to approximate diameter. Size and shape distributions were compared using Welch's *t*-test with Bonferroni correction for multiple comparisons. The intracellular abundance of virus-induced features in individual cell-sections was compared using Fisher's exact test. Linear Pearson correlations between the number of visible DMVs, spherules or intracellular virions in a given cell section were calculated as a way to examine spatial and temporal covariance in IBV-induced features

Results

Apathogenic IBV strain Beau-R and pathogenic M41 exhibit comparable replication characteristics in primary chick kidney cells. In our previous work we characterised the progress of different aspects of replication of apathogenic IBV Beau-R. To begin to understand the relationships between pathogenicity, virus replication and virus induced membrane rearrangements, a comparison was made between Beau-R and M41 infection of primary chick kidney (CK) cells. Initially, viral growth kinetics were analysed. CK cells were infected with either Beau-R or M41 and release of progeny virus assessed over a 96 hour period (Fig. 1a). It can be seen that growth kinetics of both viruses are broadly comparable with a peak of progeny virus release at 24 hours post infection (hpi). It can be noted that the titre of Beau-R decreases after 24 hours to a greater extent than M41, where viral titre plateaus. This may be as a result of the more severe cytopathic effect induced by

Beau-R compared to M41. However, both IBV strains are able to replicate to comparable titres within CK cells.

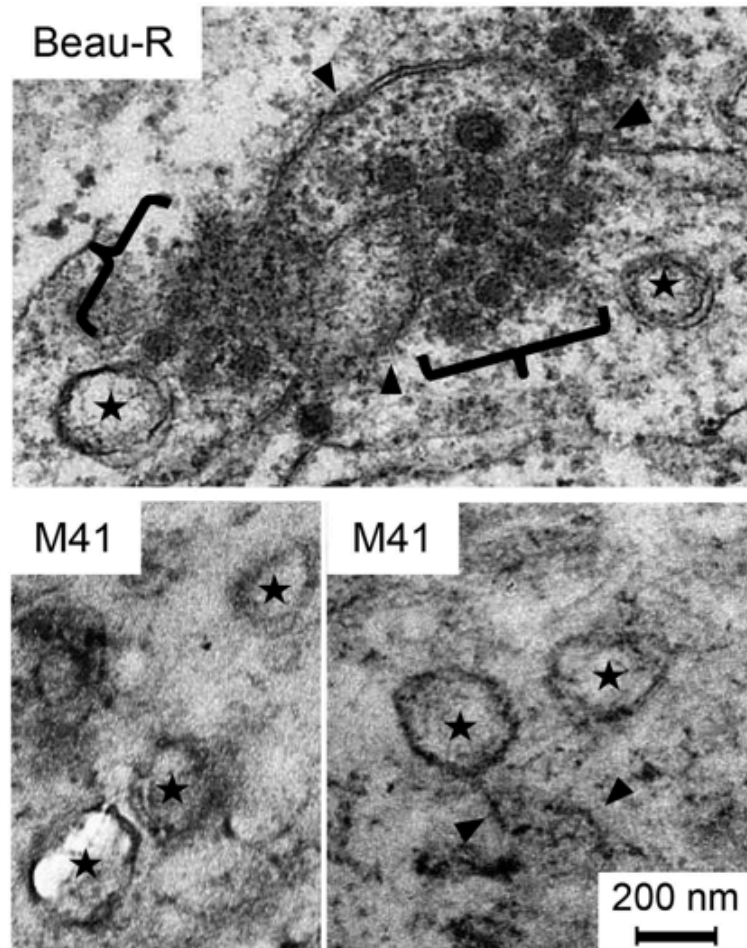


Figure 2. M41 has a low spherule phenotype in CK cells. Primary CK cells were infected with Beau-R or M41. After 24hours, cells were chemically fixed and visualised by TEM. DMVs are indicated with a star, zippered ER is indicated with a black arrowhead and spherules with black brackets.

Membrane rearrangements are thought to play an important role in assembly of viral replication complexes, responsible for synthesising viral RNA. Therefore, the total amount of viral genomic RNA (gRNA) was determined in cells infected with either Beau-R or M41. CK cells were infected or mock infected and total cellular RNA

harvested at 8 and 24 hpi. The amount of gRNA was then assayed by two-step RT-qPCR using a primer/probe set specific for genome length sequence (Fig. 1b). This analysis showed that the total level of viral gRNA was not significantly different in cells infected with either Beau-R or M41.

Finally, the onset of dsRNA accumulation in infected cells was analysed. Virus associated dsRNA has historically been used as a marker for sites of viral RNA synthesis. Although the reliability of this has increasingly come into question in recent years (Hagemeyer et al. 2012; Knoop et al. 2008; Maier et al. 2013b), accumulation of dsRNA still provides an indication of the onset of viral RNA synthesis and the formation of virus induced membrane rearrangements. Therefore, CK cells were infected with Beau-R or M41, fixed at hourly intervals post infection and labelled with an anti-dsRNA antibody. Analysis by confocal microscopy (Fig. 1c–d) showed that dsRNA accumulation during Beau-R infection could be detected in cytoplasmic puncta from 4 hpi, consistent with previous data (Maier et al. 2013b). By comparison, dsRNA accumulation in cells infected with M41 could be detected earlier, at 3 hpi, again in characteristic cytoplasmic puncta. These data suggest that kinetics of replication of Beau-R and M41 are comparable in primary CK cells, and that M41 may initiate RNA synthesis earlier during infection than Beau-R.

M41 presents a low spherule phenotype in CK cells. To further characterise differences in virus replication and virus-host cell interaction of Beau-R and M41, virus induced membrane rearrangements were analysed. Primary CK cells were infected with either Beau-R or M41, or mock infected, and after 24 hours were fixed and analysed by TEM. In agreement with our previous observations (Maier et al. 2013b), Beau-R was found to induce the formation of zippered ER and spherules,

surrounded by an electron dense region (Fig. 2). In addition, DMVs were identified. In comparison, in CK cells infected with M41, although DMVs and intracellular virus particles were easily identifiable and zippered ER could be recognised, very few spherules were observed (Fig. 2). Indeed, 34 M41 cell sections with visible signs of infection including virions, zippered ER and DMVs were imaged and only 10 spherules were identified, compared to 133 spherules identified from 52 Beau-R infected cell sections. Therefore, in CK cells, M41 exhibits a low spherule phenotype, despite having replication characteristics that were comparable to Beau-R.

Strain	Genotype	Designation	Strain information	Refs
H120	Massachusetts	Vaccine	Nobilis IB H120 vaccine strain produced by serial egg passage - not pathogenic in infected birds	(Bijlenga et al. 2004)
Beau-R	Massachusetts	Apathogenic lab	Molecular clone of IBV-Beaudette-CK, which was attenuated by serial egg and CK cell passage - not pathogenic in infected birds	(Casais et al. 2001; Cavanagh et al. 1986)
M41	Massachusetts	Pathogenic lab	Adapted for growth in CK cells by serial passage - severe respiratory symptoms in infected birds	(Armesto et al. 2009; Darbyshire et al. 1979)
D1466	D212	Pathogenic field	First isolated in Holland in 1960s -early isolates minimally pathogenic, but recent isolates like this one cause cystic ovaries and nephritis	(Davelaar et al. 1984; Domanska-Blicharz et al. 2012)
4/91	4/91	Pathogenic field	First isolated in UK in 1991 -respiratory symptoms and nephritis	(Armesto et al. 2011; Cook et al. 1996; Sumi et al. 2012)
Italy02	Italy02	Pathogenic field	First isolated in Italy in 2002 -respiratory symptoms and nephritis in young birds, egg drop in adult birds	(Dolz et al. 2012; Jones et al. 2005)

Table1. Description of IBV strains used in this study.

Pathogenic and apathogenic strains of IBV replicate in *ex vivo* tracheal organ cultures. To determine whether the low spherule phenotype observed for M41 is more broadly associated with IBV pathogenicity in general, the range of pathogenic and apathogenic field and vaccine strains available were utilised. In addition to Beau-R and M41, the selected viral strains were vaccine strain H120 and pathogenic field strains D1466, 4/91 and Italy02 (Table 1). Tracheal organ cultures (TOCs) were found to be useful for the isolation and replication of field isolates of IBV that do not replicate in primary cell culture, as an alternative to embryonated chickens eggs (Cook et al. 1976). Replication of IBV within TOCs results in the inhibition of ciliary activity (Cook et al. 1976). As a first step to assess whether IBV-induced membrane rearrangements differ according to viral genotype, degree of pathogenicity or laboratory adaptation, ability of the selected viruses to replicate within *ex vivo* tracheal organ cultures (TOCs) was investigated. TOCs were infected with the selected strains of IBV and loss of ciliary activity was measured over a 96 hour period (Fig. 3a). The mock infected TOCs show a fairly stable level of ciliary activity. However, although the overall dynamics seem to alter, TOCs that had been infected with any of the selected strains of IBV show a gradual reduction in ciliary activity over the course of the experiment with complete ciliostasis by 96 hpi.

To further confirm viral replication with TOCs, individual TOCs were mock infected or infected with each virus strain, fixed at 24 hpi and labelled with an anti-dsRNA antibody to visualise infected cells (Fig. 3b) or were labelled with anti-dsRNA and anti-tubulin (Fig. 3c). Confocal microscopy analysis revealed that no virus infection could be detected in the mock infected TOCs. However, virus infection could be detected in all other TOCs. Overall, these data confirmed that all of the selected

strains of IBV were capable of infecting and replicating within cells in TOCs, and virus replication resulted in ciliostasis.

All strains of IBV induce zippered ER, spherules and DMVs. After confirmation that the selected strains of IBV replicated within TOCs and induced ciliostasis as expected, the ability of each virus to induce membrane rearrangements was assessed. TOCs were infected with each strain of virus and after 24 hours were chemically fixed and analysed by TEM. Again, Beau-R infection was found to result in the formation of DMVs, zippered ER and spherules (Fig. 4). When TOCs were infected with a second apathogenic strain, vaccine strain H120, comparable structures, zippered ER, spherules and DMVs, were all observed. Three pathogenic field strains (D1466, 4/91 and Italy02) also induced zippered ER, spherules and DMVs in infected TOCs. Finally, TOCs infected with the pathogenic laboratory adapted IBV strain, M41, were then assessed. Consistent with earlier observations in CK cells, DMVs, zippered ER and intracellular virus particles were easily detected (see Supplementary Fig. S1) but very few spherules were visible (Fig. 4c). Several examples of images of Beau-R (Fig. 4b) or M41 (Fig. 4c) infected TOCs are shown to demonstrate the absence of spherules in M41 infected cell sections. Therefore, apathogenic, pathogenic, laboratory adapted and field isolates can all induce a full range of membrane rearrangements.

Some physical characteristics of spherules and DMVs were then measured to determine whether the structures induced by the different viral strains were comparable. Firstly, spherule diameters were classed within 2 nm brackets ranging from 50 nm to 110 nm. The percentage of spherules found in cells infected with each IBV strain that fit into these brackets was determined (Fig. 5a). The spread of

spherule diameter and the peak diameters were comparable for all IBV strains tested. In addition, DMV diameters were classed within 10 nm brackets from 100 nm to 420 nm. The percentage of DMVs found in cells infected with each IBV strain that fit into each bracket was determined (Fig. 5b). The spread of DMV diameters and the peak DMV diameter were also comparable across all IBV strains. This demonstrates that the size and structure of spherules and DMVs is not altered by viral strain.

Samples were further analysed for the percentage of total cells that presented any signs of infection; either DMVs, spherules or intracellular virus (Table 2). Beau-R showed the highest level of infection with 52% of cell sections showing markers for infection. The remaining viral strains had infection rates of between 23% and 11%. When infection markers were analysed individually, again, Beau-R showed the highest percentage of cell sections containing DMVs, spherules and intracellular virus. The remaining viral strains showed varying levels of presence of infection markers, consistent with the total percentage cell sections that showed any sign of infection.

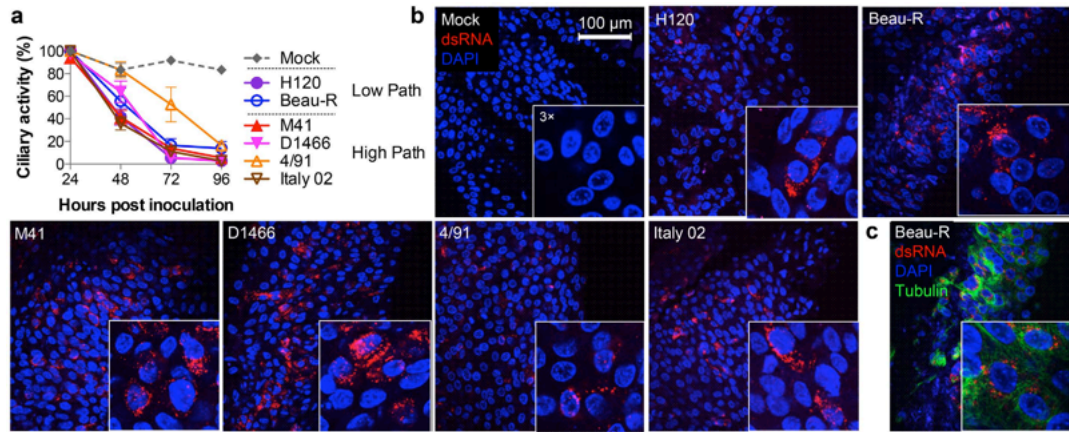


Figure 3. Pathogenic and apathogenic viruses replicate in tracheal organ culture resulting in ciliostasis. (a) TOCs were mock infected or infected with H120, Beau-R, M41, D1466, 4/91 or Italy02. Ciliary activity was assessed and scored at 24hour intervals. The mean and SEM of three independent experiments are shown. (b) TOCs were mock infected or infected with H120, Beau-R, M41, D1466, 4/91 or Italy02. After 24hours, cells were fixed with 4% paraformaldehyde and labelled with anti-dsRNA (red) and anti-tubulin (green, c). Nuclei are stained with DAPI (blue).

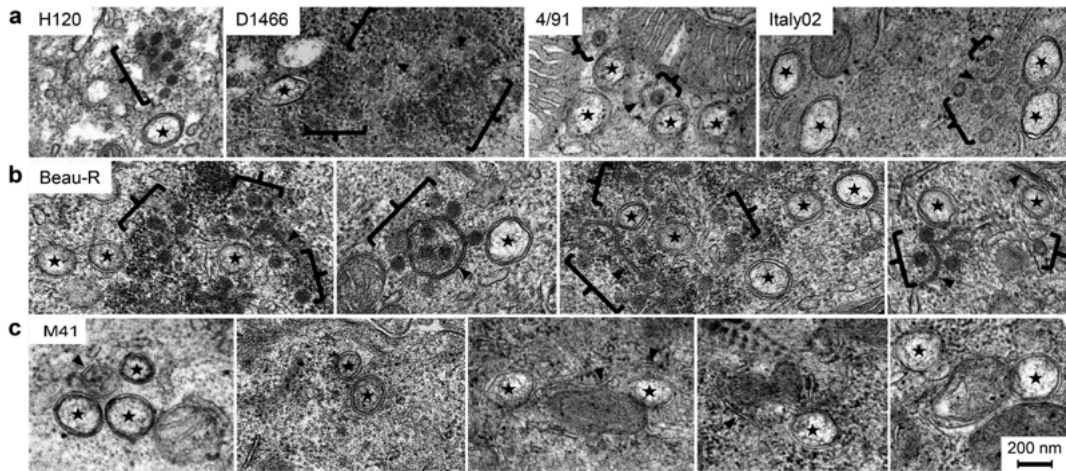


Figure 4. Pathogenic and apathogenic strains of IBV induce zippered ER, spherules and DMVs. TOCs were mock infected or infected with (a) H120, D1466, 4/91 or Italy02, (b), Beau-R or (c) M41. After 24hours, cells were chemically fixed. DMVs are indicated by a star, zippered ER with black arrowheads and spherules with black brackets.

Subsequently, cell sections that had been classified as infected were analysed for the number of DMVs, spherules or intracellular virus. Numbers of DMVs per cell section varied from 2 to 4, number of intracellular virus particles ranged from D1466 with 27 (± 7) to 4/91 with 11 (± 4) and finally number of spherules per cell section ranging from 1 to 4, with the exception of M41. M41 infected cell sections only contained an average of 0.1 spherules (± 0.1). To extend the comparison of Beau-R and M41, images of infected CK cells from Figure 2 were also analysed (Table 2). The percent of CK cell sections showing markers of infection was 37% for Beau-R and 39% for M41. The percentage of cells that showed individual signs of infection were also similar, except for the percentage of M41 infected cells where spherules could be detected, with 2% compared to 14% in Beau-R infected cell sections. Again, the number of different markers of infection found per cell section classified as infected was determined. Indeed, 53 M41 cell sections with visible signs of infection were imaged and only 7 spherules were identified, compared to 248 spherules identified from 69 Beau-R infected cell sections. The most significant observation showing that Beau-R infected cell sections contained an average of 3 spherules (± 1) whilst M41 infected cell sections contained an average of only 0.3 spherules (± 0.2). Finally, the percentage of infected TOC cell sections that contained at least 1 DMV, spherule or intracellular virus particle was determined (Table 2). When compared with vaccine strain H120, there were no significant differences in the percentage of infected cells that contained at least 1 DMV or at least 1 virion. Furthermore, the percentage infected cell sections containing at least 1 spherule was not significantly different for any viral strain (range 24–54%) except M41 with only 6% ($p = 4 \times 10^{-6}$). When the same calculations were performed for Beau-R and M41 infected CK cells, similar results were found with 40% Beau-R

infected cell sections containing at least 1 spherule and only 9% M41 infected cell sections ($p = 1 \times 10^{-3}$).

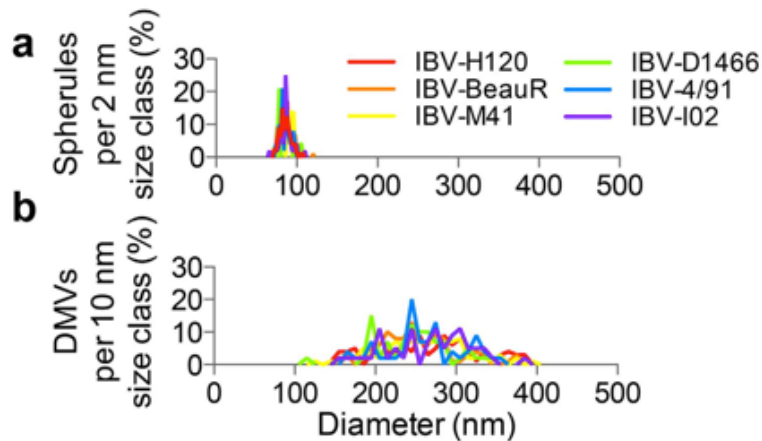


Figure 5. Spherule and DMV diameters are not altered by virus strain. Spherule (a) and DMV (b) diameters were measured and divided into 2nm (spherules) or 10nm (DMV) size classes. The number of spherules or DMVs in each size class is shown for each of the viral strains.

These data indicate that the low spherule phenotype of M41 is characteristic of this viral strain and is not dependent on cell type as comparable observations were made between infection of primary CK cells and *ex vivo* TOCs. However, the observations also demonstrate that spherule formation is not associated with viral pathogenicity, and rather is a unique characteristic of the M41 strain. Therefore, this indicates that DMVs, zippered ER and spherules are typical for IBV infection and are neither associated with viral genotype, level of pathogenicity nor laboratory adaptation.

DMVs and either zippered ER with spherules or convoluted membranes are closely correlated during replication of diverse coronaviruses. During SARS-CoV infection, DMVs have been shown to appear from 2 hpi with CMs appearing at 3 hpi (Knoops et al. 2008). Both structures are derived from and connected to the ER, with connections also detectable between CMs and DMV outer membranes. In our previous work, IBV induced membrane rearrangements were not detectable until 7 hpi, when both DMVs and zippered ER with spherules were found. Zippered ER is clearly contiguous with ER and an example of a connection between the ER and a DMV was also identified. However, no connections were observed between IBV induced zippered ER and DMVs. To determine how related these structures are to one another during replication of diverse coronaviruses, in addition to data already described in this study, DBT, L929, 17Cl-I or MEF cells were infected with mouse hepatitis virus (MHV) strain A59. At the indicated times post infection, cells were chemically fixed and analysed by TEM. Examples of IBV Beau-R infected TOCs (Fig. 6a) and MHV-A59 infected DBT cells (Fig. 6b) are shown with additional panels where DMVs are highlighted in blue, spherules are highlighted in purple and zippered ER or CMs highlighted in red. Enlarged images of IBV Beau-R induced structures (Fig. 6c) and MHV-A59 induced structures (Fig. 6d) are also shown for ease of comparison. Finally, the presence of different markers of infection within IBV or MHV-A59 visibly-infected cell sections was calculated (Fig. 6e). Firstly, for IBV infected cells, the presence of DMVs and spherules, DMVs and intracellular virus or spherules and intracellular virus was quantified using data generated in Figs 2 and 4. Samples were categorised into TOCs infected with either apathogenic IBV or pathogenic IBV (excluding M41) and CK cells infected with Beau-R. Data on the number of virus-induced features per cell was used to look for linkages between

production of coronavirus DMVs, spherules, convoluted membranes and intracellular virus particles, following the hypothesis that features that were spatially and temporally linked would be more likely to co-occur in ultrathin sections of randomly-oriented cells such as these. Statistically significant correlations were observed between the number of IBV DMVs and spherules per infected cell section, but the number of intracellular virions was not significantly correlated with spherule or DMV abundance (Fig. 6e). The correlation between IBV DMV and spherule abundance was statistically significant in both primary and continuous cells regardless of the pathogenic potential of the strains tested. Similarly, strong correlations were observed between the number of MHV DMVs and convoluted membrane clusters per infected cell, but the number of intracellular MHV virions was not significantly correlated with the abundance of DMVs or convoluted membrane clusters (Fig. 6e). The correlation between MHV DMVs and convoluted membrane abundance was significant for all four conditions tested. Together, these data suggest that both IBV spherules and MHV convoluted membranes commonly co-occur with DMVs in infected cells as part of a double-membrane replicative organelle (V'kovski et al. 2015) that is distinct from the site of virus assembly.

Table 2. Quantitation of markers of infection in cells infected with different IBV strains. V=vaccine, L=lab adapted, F=field, AP=apathogenic, P=pathogenic. The intracellular abundance of virus-induced features in individual cell-sections was compared to H120 using Fisher's exact test.

Virus	Cell	Type	Total Cells	Visibly infected cell sections				Per visibly infected cell section			Infected cell sections	Infected cell sections with one or more					
				DMV	Spherule	IV	Any	DMV	Spherule	IV		DMV		Spherule		IV	
H120	TOC 24 hpi	V-AP	n = 210	7%	6%	9%	11%	4 ± 1	4 ± 1	15 ± 5	n = 24	63%	–	54%	–	79%	–
Beau-R		L-AP	n = 63	29%	17%	46%	52%	3 ± 1	4 ± 1	18 ± 4	n = 69	58%	ns	54%	ns	78%	ns
M41		L-P	n = 395	8%	1%	12%	13%	2 ± 1	0.1 ± 0.1	19 ± 4	n = 53	62%	ns	6%	$p = 4 \times 10^{-6}$	92%	ns
D1466		F-P	n = 157	9%	3%	13%	13%	2 ± 1	1 ± 1	27 ± 5	n = 21	67%	ns	24%	ns	95%	ns
4/91		F-P	n = 79	15%	10%	18%	23%	2 ± 1	2 ± 1	11 ± 4	n = 21	67%	ns	48%	ns	76%	ns
Italy02		F-P	n = 60	10%	5%	10%	18%	3 ± 1	3 ± 2	17 ± 5	n = 16	50%	ns	31%	ns	63%	ns
Beau-R	CK cell 24 hpi	L-AP	n = 76	14%	14%	33%	37%	2 ± 1	3 ± 1	35 ± 11	n = 52	42%	–	40%	–	90%	–
M41		L-P	n = 84	19%	2%	37%	39%	1 ± 0.3	0.3 ± 0.2	21 ± 4	n = 34	50%	ns	9%	$p = 1 \times 10^{-3}$	94%	ns

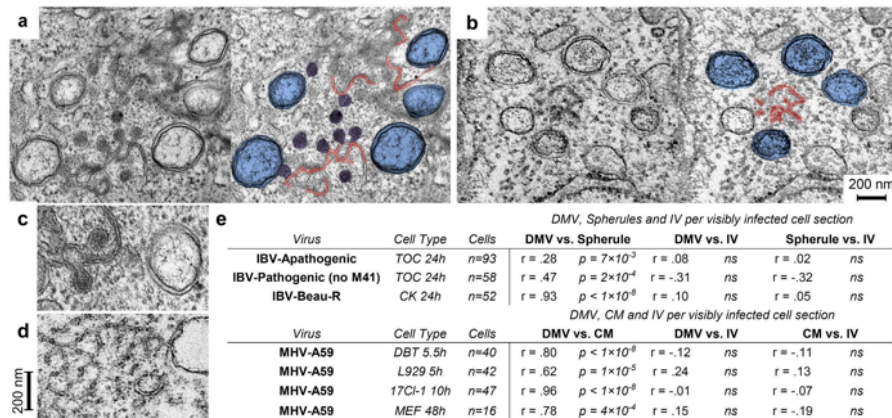


Figure 6. Spatial and temporal correlation between DMVs and other paired membrane structures but not intracellular virions across diverse coronaviruses. Transmission electron micrographs of (a) tracheal organ cultures infected with Beau-R and chemically fixed after 24hours and (b) DBT cells infected with MHV-A59 and chemically fixed after 5.5hours. DMVs (blue), spherules (purple), zippered ER (red in a) and convoluted membranes (red in b) are highlighted. Enlarged images of DMVs and paired membrane structures from (c) IBV and (d) MHV infected cells. (e) Pearson linear correlation coefficients and p values (ns = not significant) for comparisons between the number of DMVs, spherules, convoluted membrane regions and intracellular virions in randomly oriented ultrathin sections through infected cells.

Discussion

In this study we performed a detailed comparison of the membrane rearrangements induced by a range of different strains of IBV. The selected strains covered a wide variety of viral genotypes, lab adapted, field and vaccine strains as well as pathogenic and apathogenic strains of virus. To our knowledge, this study forms the most comprehensive comparison of membrane rearrangements induced by

different virus strains for any coronavirus to date. The ability of each of the selected viruses to replicate in *ex vivo* TOCs was assessed. Indeed, all of the viruses were found to be capable of replication as measured by accumulation of dsRNA in the epithelial cells of the TOC or loss of ciliary activity over the course of infection. All of the strains of IBV inhibited ciliary activity by 96 hpi. Therefore, the ability to inhibit ciliary activity is not associated with the overall pathogenicity of the virus in a bird. Instead, it is more likely, that pathogenicity is linked to the site of virus replication and ability of the virus to spread in the bird. The apathogenic lab adapted and vaccine strains are restricted to sites closer to the site of inoculation and are less capable of spreading to the trachea and other sites within the bird. It was noted, however, that pathogenic field strain 4/91 presented a more gradual inhibition of ciliary activity when compared with the other virus strains, although complete ciliostasis was induced by 96 hpi. It is not possible to titrate this strain by plaque assay in CK cells because this virus does not replicate in CK cells. Therefore, it is possible that the level of infection was lower for this virus. However, the percentage of cells showing signs of virus replication in EM sections and the overall dsRNA accumulation would not indicate that the level of infection was significantly different to any of the other strains of IBV. Therefore, the reason for the difference in the dynamics of inhibition of ciliostasis caused by 4/91 remains unknown.

The ability of each of the selected viruses to induce cellular membrane rearrangements was also determined. When TOCs were infected with each of the virus strains, all three previously identified IBV Beau-R induced membrane structures were identified. This demonstrates that additional, and therefore potentially all, strains of IBV appear to be able to induce zippered ER with associated spherules and DMVs, regardless of viral genotype, lab adaptation or

degree of pathogenicity. Upon further assessment, the average diameter of DMVs and spherules was also consistent between the different virus strains. Therefore, the type and size of membrane structures induced by IBV is likely to be a fundamental requirement for virus replication machinery and is not associated with adaptation to grow in embryonated eggs or cell culture and is not associated with pathogenicity. This finding is significant because such a detailed comparison of different strains of coronavirus has not been established. It was previously unknown whether alterations in either efficiency of induction of membrane rearrangements or variations in the types of structure might account for changes in pathogenicity or tropism for cell culture. The results presented here clearly demonstrate that this is not the case.

In our analysis, it was also found that there is a highly significant correlation between the presence of DMVs and spherules within the same IBV infected cell or DMVs and CM within the same MHV infected cell. This indicates that production of DMVs and either zippered ER with spherules or CMs is a linked and possibly simultaneous process. It also demonstrates that the temporal and spatial link between these structures is conserved among the distantly related *Beta-* and *Gammacoronaviruses*. Although no connections were found between zippered ER or spherules with DMVs in our earlier work (Maier et al. 2013b), when similar experiments were performed in SARS-CoV infected cells, clear connections were found between DMVs, CM and cellular ER (Knoops et al. 2008). Connections between DMVs and paired ER membranes are also present in cells infected with related equine arterivirus (Knoops et al. 2012). In addition, studies using recombinant MHV expressing fluorescently-tagged nsp4 demonstrated that the ER is contiguous with virus replication structures (Hagemeijer et al. 2011). However,

although clearly associated in terms of function and presence in infected cells, data suggests that IBV induced DMVs and spherules are discrete structures formed by different mechanisms (Maier et al. 2013b).

One surprising observation made during this study was that M41 has a low spherule phenotype during replication in both CK cells and TOCs. Although numerous DMVs and virus particles could be detected in M41 infected cells (see Supplementary Fig. 1), very few spherules could be identified. This is despite the fact that virus replication and release of progeny over 96 hours was comparable to Beau-R, consistent with previous work using M41 and Beau-R (Armesto et al. 2009; Casais et al. 2003). In addition, there was no significant difference between the viruses in the overall levels of gRNA at 8 and 24 hpi. This suggests that RNA synthesis and turnover is comparable for the two viruses. Finally, dsRNA accumulation, indicative of viral RNA synthesis and possibly assembly of replication complexes and formation of DMVs was detectable at 4 hpi in Beau-R infected cells but was found earlier in cells infected with M41, at 3 hpi. These results are consistent with previously published results (Kint et al. 2015; Maier et al. 2013b). This indicates that, despite the lower number of visible spherules during M41 replication, there is no effect on virus replication. In fact, earlier dsRNA accumulation may indicate that M41 replication complexes assemble earlier after infection of the cell than during Beau-R infection. Interestingly, we have previously reported that recombinant chimeric viruses containing either gene 1 from Beau-R and the structural and accessory genes from M41, or the coding region for nsp15 to the 3' end from M41 and the remainder of the 5' end from Beau-R both produce easily detectable spherules (Maier et al. 2014). Therefore, the genetic determinants for spherule formation must lie within nsp2 to nsp14. It may be expected that membrane spanning nsps 3, 4 and

6 will play a role in membrane rearrangements, as has been suggested for other coronaviruses (Angelini et al. 2013; Hagemeijer et al. 2014, 2011). However, as other studied coronaviruses do not produce spherules, it cannot be ruled out that further viral proteins may play a role in their formation.

Overall, the data presented here suggests that total spherule number is not associated with level of IBV RNA synthesis and viral fitness, at least in the case of M41. This may be a surprising conclusion because where spherules are induced by other +RNA viruses and are confirmed as sites of viral RNA synthesis, there is a correlation between spherule formation or number and RNA synthesis. Temperature sensitive mutants of Semliki Forest virus (SFV) were found to produce low numbers of spherules at the non-permissive temperature and there was a corresponding reduction in virus replication (Tan 1970). Furthermore, inhibition of spherule formation by tomato bushy stunt virus and brome mosaic virus by inhibition of the endosomal sorting complexes required for transport (ESCRT) pathway results in a reduction in viral RNA synthesis (Barajas et al. 2014; Diaz et al. 2015). Finally, viral RNA synthesis and spherule formation are tightly associated during flock house virus and SFV infection as formation of spherules is only triggered by the process of active RNA synthesis (Kopek et al. 2010; Spuul et al. 2011). Therefore, it is likely that the role played by spherules during IBV replication is somewhat different to other +RNA viruses. However, it is notable that the presence of coronavirus induced DMVs is also not tightly correlated with viral RNA synthesis. Although some work has shown that some MHV temperature sensitive mutants have a reduction in DMV formation or aberrant DMV formation at the non-permissive temperature, associated with reduced viral RNA synthesis (Clementz et al. 2008; Gadlage et al. 2010), recent work suggests that this is not always the case at permissive temperatures. Changes

in DMV number or size were not linked to changes in RNA synthesis (Al-Mulla et al. 2014) and it was not DMV number and morphology but instead glycosylation of one of the viral nsps that was found to be responsible for the reduction in RNA synthesis for another set of viruses (Beachboard et al. 2013). Clearly the induction of membrane rearrangements is critical for virus replication (Lundin et al. 2014) and this process is well conserved amongst all +RNA viruses. However, the precise function of the variety of structures induced by coronaviruses remains a complicated story. It is likely that all of the different structures produced each play a role in virus replication and viral RNA synthesis. In this case, where one type of structure is reduced or not present during infection, another structure would be capable of compensating. During replication of IBV and arteriviruses at least, all virus induced structures are comprised of tightly apposed double membranes. It may be that this feature is the important one in terms of viral RNA synthesis and the precise shape of the membrane is less critical.

An alternative explanation is that the total number of spherules required to allow efficient viral RNA synthesis is very low. In this case, the low number of spherules observed during M41 replication would be sufficient to allow replication complex assembly and viral RNA synthesis. The higher number of spherules present in cells infected with other strains of IBV used here would represent an excess, not strictly required for viral RNA synthesis. Indeed, it has long been reported that viral RNA synthesis can be detected within infected cells at very short times post infection (Maier et al. 2013b; Sawicki et al. 2007; Sawicki and Sawicki 2005, 1986; Ulasli et al. 2010), earlier than any evidence of membrane rearrangements can be observed (Knoops et al. 2008; Maier et al. 2013b; Ulasli et al. 2010). Perhaps low numbers of membrane rearrangements, below levels of detection by electron microscopy, exist

early after infection, but that are sufficient for the levels of RNA synthesis seen at these times. Numerous unanswered questions remain; however, the identification here of two cell culture adapted strains of IBV (Beau-R and M41) that induce variations in membrane rearrangements now provides an exciting opportunity for future work to begin to unravel the complicated story of the mechanism of formation and role of coronavirus induced membrane rearrangements.

Paper two:

Infectious Bronchitis Virus Nonstructural Protein 4 Alone Induces Membrane Pairing

Nicole Doyle ¹, Benjamin W. Neuman ^{2,†}, Jennifer Simpson ¹, Philippa C. Hawes ¹, Judith Mantell ³, Paul Verkade ³, **Hasan Alrashedi** ² and Helena J. Maier ^{1*}

1. The Pirbright Institute, Pirbright, Surrey GU24 0NF, UK
2. School of Biological Sciences, University of Reading, Reading RG6 6AJ, UK
3. School of Biochemistry, University of Bristol, Bristol BS8 1TD, UK

† Current Address: College of STEM, Texas A&M University-Texarkana, Texarkana, TX 75503, USA.

* Correspondence Author:

Published in *Viruses*, 10 (9), 2018

Abstract

Positive-strand RNA viruses, such as coronaviruses, induce cellular membrane rearrangements during replication to form replication organelles allowing for efficient viral RNA synthesis. Infectious bronchitis virus (IBV), a pathogenic avian *Gammacoronavirus* of significant importance to the global poultry industry, has been shown to induce the formation of double membrane vesicles (DMVs), zippered endoplasmic reticulum (zER) and tethered vesicles, known as spherules. These membrane rearrangements are virally induced; however, it remains unclear which viral proteins are responsible. In this study, membrane rearrangements induced when expressing viral non-structural proteins (nsps) from two different strains of IBV were compared. Three non-structural transmembrane proteins, nsp3, nsp4, and nsp6, were expressed in cells singularly or in combination and the effects on cellular membranes investigated using electron microscopy and electron tomography. In contrast to previously studied coronaviruses, IBV nsp4 alone is necessary and sufficient to induce membrane pairing; however, expression of the transmembrane proteins together was not sufficient to fully recapitulate DMVs. This indicates that although nsp4 is able to singularly induce membrane pairing, further viral or host factors are required in order to fully assemble IBV replicative structures. This study highlights further differences in the mechanism of membrane rearrangements between members of the coronavirus family.

1. Introduction

Viruses rely on their host cell to provide most of what they need to replicate and in order to do this, they hijack many cellular processes. A well-studied example is the ability of positive-sense single-stranded RNA viruses (+RNA) to induce cellular membrane rearrangements upon expression of viral proteins (Miller and Krijnse-Locker 2008; Netherton and Wileman 2011). This reorganization of cellular membranes is a critical step in the viral replication cycle since these areas of restructured membranes act as a site for assembly of all components required for viral RNA synthesis as well as offer protection from detection by the host antiviral defenses (den Boon and Ahlquist 2010; Neufeldt et al. 2016). Although the structures of these membranes are relatively well-understood, the mechanisms behind their formation, and particularly the viral and host proteins involved, are often not.

The precise structure of virally induced membrane rearrangements varies between viruses (Harak and Lohmann 2015; Paul 2013), but viruses generally cause proliferation of membranes, forming structures, such as convoluted membranes (CM), as well as distinct types of vesicles. Most common are double membrane vesicles (DMVs), which are discrete from the cytoplasm and are produced by viruses, such as poliovirus (Belov et al. 2012; Bienz et al. 1992), hepatitis C virus (Ferraris et al. 2013; Gosert et al. 2003), human norovirus (Doerflinger et al. 2017), and recently the equine torovirus, Berne virus (Ávila-Pérez et al. 2016). Spherules, which are invaginated vesicles with a channel connecting them to the cytoplasm, have been found in Semliki Forest virus (Kujala et al. 2001), some *Flaviviruses* (Cortese et al. 2017; Gillespie et al. 2010; Welsch et al. 2009; Westaway et al.

1997), as well as Brome mosaic virus (BMV), which is able to induce their formation with the expression of just one viral protein (Schwartz et al. 2002).

An important +RNA virus family, the coronaviruses, include pathogens of both animal and human importance, such as severe acute respiratory syndrome coronavirus (SARS-CoV), Middle East respiratory syndrome coronavirus (MERS-CoV), mouse hepatitis virus (MHV), porcine epidemic diarrhea virus (PEDV), and infectious bronchitis virus (IBV). Within this subfamily of viruses, we see variations in membrane rearrangements formed. DMVs and CM are found in cells infected with the *Alpha-* and *Betacoronaviruses*, such as SARS-CoV, MERS-CoV, and MHV (de Wilde et al. 2013; Goldsmith et al. 2004; Gosert et al. 2002; Snijder et al. 2006; Ulasli et al. 2010; Zhou et al. 2017). In the case of the *Gammacoronavirus* IBV, although DMVs are found, the virus induces little CM and instead induces membrane zippering to form zippered endoplasmic reticulum (zER) as well as double membrane spherules, which are found tethered to the zER (Maier et al. 2013b), producing a much more defined structure when compared to CM. Subsequent to this discovery, MERS-CoV infection has also been shown to produce small circular structures similar in appearance to the spherules seen in IBV infection but less distinct (Oudshoorn et al. 2017).

The coronaviral proteins involved in the production of membrane rearrangements have been recently investigated with the three transmembrane non-structural proteins (nsps) nsp3, 4, and 6, which are the focus of these studies. Nsps 3, 4, and 6 from different coronaviruses are accepted as functional homologues, although amino acid sequence conservation is low (ranging from 13.4 to 25.9% amino acid homology for nsps 3, 4, and 6 between IBV strain BeauR and MHV strain A59).

These proteins do, however, have conserved secondary structure and conserved domains, including enzymatic domains in nsp3, transmembrane domains in all three proteins, and cytoplasmic endo-domains in nsps 4 and 6. For a detailed review of the domain organization and known functions of nsps 3, 4, and 6, see (Neuman 2016). Nsp4 of MHV has been shown to be important for the normal function and stability of DMVs, where mutations in nsp4 resulted in attenuated virus and impairment of DMV formation (Beachboard et al. 2015; Clementz et al. 2008; Gadlage et al. 2010). In addition, nsp3 has been shown to localize to DMVs and CM in SARS-CoV-infected cells (Knoops et al. 2008). In a related group of viruses, the *Arteriviruses*, expression of two nsps (nsps2 and 3) was able to produce DMVs (Pedersen et al. 1999; Posthuma et al. 2008; Roos et al. 2001). These nsps of the arterivirus are considered functional homologs to coronavirus nsp3 and 4 (Gorbalenya et al. 2006). Upon co-expression of nsp3 and 4 from MHV, both proteins located to areas of curved membranes from where they were shown to be able to recruit nsp2 and 6; however, nsp3 and 4 alone were not able to induce the formation of DMVs (Hagemeijer et al. 2014, 2011). Following on from this, it was shown that co-expression of SARS-CoV nsp3 and 4 induced membrane pairing and with the addition of nsp6 the formation of DMV-like structures (Angelini et al. 2013). In a subsequent study by others, it was shown that expression of only nsp3 and 4 from either MERS-CoV or SARS-CoV was able to induce DMV formation, and furthermore, addition of nsp6 made no difference to their shape or size, and did not induce the spherule-like structures seen following infection with whole virus (Oudshoorn et al. 2017). Interestingly, however, a small molecule inhibitor, K22, has been shown to inhibit the replication of several coronaviruses in vitro. In HCoV-229E, K22 impaired DMV formation, while K22 resistance was associated with

mutations in nsp6, emphasizing a role for nsp6 in DMV formation (Lundin et al. 2014).

IBV is a pathogen of poultry, causing significant economic losses to the poultry industry worldwide as well as animal welfare problems. Various strains of IBV cause disease that varies in severity from mild respiratory problems to virulent strains that can cause nephropathology and reproductive organ pathology. In this study, we compared the membrane rearrangements induced by viral proteins from two different strains of IBV, the pathogenic M41 and the apathogenic BeauR. These strains were chosen because BeauR and other strains of IBV induce DMV, zER, and spherule formation; however, M41 produces a low spherule phenotype when compared with other strains of the virus (Maier et al. 2016). As the role in membrane rearrangements for nsp3 and 4 is well-established for several nidoviruses and considering that nsp6 may also play some role, here we investigated the role that these three nsps play in the formation of IBV membrane rearrangements.

2. Materials and Methods

2.1. Cells, Viruses, and Plasmids

Avian DF1 cells were maintained in DMEM (Sigma Aldrich, Gillingham, UK) supplemented with 10% FCS (Sigma Aldrich, Gillingham, UK). IBV strains BeauR and M41-CK (here referred to as M41) have been described previously (Casais et al. 2001; Darbyshire et al. 1979). Plasmids expressing tagged nsps derived from either the apathogenic strain BeauR or the pathogenic strain M41 were generated to produce pEGFP-N1-M41 nsp3, pmCherry-N1-BeauR nsp4, pmCherry-N1-M41

nsp4, pcDNA3.1(-)-BeauR nsp6-3xFLAG, and pcDNA3.1(-)-M41 nsp6-3xFLAG. RNA was extracted from virus-infected cells using an RNAeasy kit (Qiagen, Hilden, Germany) following the manufacturer's protocol. RNA was reverse transcribed using Superscript III (Fisher Scientific, Loughborough, UK) and a random primer following the manufacturer's protocol. PCR was carried out on cDNA using primers specific for each gene, including flanking restriction sites. PCR products were digested and ligated into pEGFP-N1 (Takara Bio Europe, Saint-Germain-en-Laye, France) or pmCherry-N1 (Takara Bio) using XhoI and BamHI restriction sites. Plasmid pcDNA3.1(-) was modified by insertion of a 3xFLAG motif between the KpnI and HindIII sites to generate pcDNA3.1(-)-3xFLAG. The PCR products were then ligated into this backbone using the XhoI and BamHI restriction sites. Plasmid sequences were verified using Sanger sequencing. The ER marker plasmid pYFP-ER was kindly provided by Dalan Bailey.

2.2. SDS-PAGE and Western Blotting

DF1 cells seeded into six-well plates were transfected with pEGFP-N1-M41 nsp3, pmCherry-N1-BeauR nsp4, pmCherry-N1-M41 nsp4, pcDNA3.1(-)-BeauR nsp6-3xFLAG or pcDNA3.1(-)-M41 nsp6-3xFLAG, pEGFP-C2, pmChery-N1, or pcDNA3.1(-)-BeauR nsp7-3xFLAG using lipofectamine 2000 (Fisher Scientific). Cells were transfected with a total of 1000 ng plasmid with a DNA:lipofectamine 2000 ratio of 1:3 following the manufacturer's instructions. After 24 h, cells were lysed in cell lysis buffer (25 mM Tris-HCl (pH 7.4), 150 mM NaCl, 1 mM EDTA, 1% v/v Triton-X100, 5% v/v glycerol, 1× HALT protease inhibitor complex (Fisher Scientific). Cell lysates were heated with 4× sample buffer (Bio-rad Laboratories,

Watford, UK) and separated on 4–20% TGX gels (Bio-rad). Proteins were transferred to a nitrocellulose membrane and blocked in 5% milk in PBS-T. Membranes were incubated with primary antibodies to detect GFP (Biolegend, London, UK), mCherry (Abcam, Cambridge, UK), or FLAG (M2; Sigma Aldrich, Gillingham, UK). After 1 h, membranes were washed with PBS-T and incubated with IRDye conjugated secondary antibodies (LI-COR, Cambridge, UK). Membranes were imaged using an Odyssey CLx Infrared imaging system (LI-COR).

2.3. Immunofluorescence Labelling

DF1 cells seeded onto glass coverslips were transfected with pEGFP-N1-M41 nsp3, pmCherry-N1-BeauR nsp4, pmCherry-N1-M41 nsp4, pcDNA3.1(-)-BeauR nsp6-3xFLAG, and pcDNA3.1(-)-M41 nsp6-3xFLAG alone or in combination using lipofectamine 2000. Cells were transfected with a total of 500 ng plasmid with a DNA:lipofectamine 2000 ratio of 1:2 following the manufacturer's instructions. After 24 h, cells were fixed for 20 min in 4% paraformaldehyde in PBS at room temperature. Cells were then permeabilized in 0.1% Triton X-100 in PBS for 10 min and blocked in 0.5% BSA in PBS for 1 h. Primary anti-FLAG M2 antibody (Sigma Aldrich) and anti-PDI antibody (Enzo Life Sciences, Exeter, UK) were diluted in blocking buffer and cells incubated for 1 h. After three washes in PBS, Alexa fluor conjugated secondary antibodies (Fisher Scientific) were diluted 1/500 and cells incubated for 1 h. After a further three washes in PBS, nuclei were stained using ToPro3 (Fisher Scientific) or DAPI (Sigma Aldrich) and coverslips mounted with Vectashield (Vector Laboratories, Peterborough, UK). Cells were visualized using a Leica SP5 confocal microscope (Leica Microsystems, Milton Keynes, UK).

Quantitation of transfected cells was performed manually on three randomly selected fields of view.

2.4. Transmission Electron Microscopy

DF1 cells in six-well plates were either infected with BeauR and incubated for 1 h at 37 °C when fresh 1× BES medium (MEM, 0.3% tryptose phosphate broth, 0.2% bovine serum albumin, 20 mM *N,N*-Bis(2-hydroxyethyl)-2-aminoethanesulfonic acid (BES), 0.21% sodium bicarbonate, 2 mM L-glutamine, 250 U/mL nystatin, 100 U/mL penicillin, and 100 U/mL streptomycin) was added, or were transfected with plasmids as described above. At 24 hpi, cells were washed once in 0.9% saline and scraped into the saline buffer. Cells were pelleted at 500× *g* for 5 min at 4 °C and 500 µL 2% glutaraldehyde in 0.1 M sodium cacodylate was added to the pellet. Then, the procedure was carried out as stated in material and method chapter, section 2.15.

Alternatively, DF1 cells were seeded onto Thermanox coverslips (Fisher Scientific) and either infected with BeauR and incubated for 1 h at 37 °C, after which time fresh 1× BES medium was added, or cells were transfected with plasmids as described above. After 24 h, cells were fixed in 2% glutaraldehyde for 1 h, incubated in 1% aqueous osmium tetroxide solution for 1 h, then dehydrated in increasing concentrations of ethanol. Cells were embedded into Agar 100 resin and sections of 80 nm were cut, collected on hexagonal 200 thin bar copper grids, and stained with 2% uranyl acetate and lead citrate. Data was recorded on a FEI Tecnai 12 TEM (FEI, Cambridge, UK) used at 100 kV with a TVIPS F214 digital camera.

2.5. *Electron Tomography*

DF1 cells seeded onto Thermanox coverslips were transfected and processed as before. Sections 250 or 300 nm thick were cut from the resin-embedded blocks and collected on 50 mesh copper hexagonal grids coated in formvar or pioloform-coated copper slot grids. Ten or 15 nm gold particles were applied to the grids to serve as fiducial markers for subsequent alignments. Data was recorded on a JEOL 2100 F TEM (Jeol, Welwyn Garden City, UK) used at 200 kV with a TVIPS F416 digital camera, or on a Tecnai 20 TEM (FEI) used at 200 kV with a FEI 4 k × 4 k Eagle CCD camera. Samples were mounted in a JEOL high angle tilt holder or a Fischione double tilt tomography holder, respectively. A single axis tilt series was collected using Serial EM or FEI software. Each single axis tilt series was collected over 100° to 130° in increments of between 1° and 2.5° and subsequently aligned and reconstructed in IMOD (Kremer et al. 1996).

3. Results

3.1. *IBV Induces Typical Membrane Rearrangements in DF1 Cells*

Our previous studies have shown that IBV is able to induce diverse membrane rearrangements in Vero cells, primary chicken kidney cells (CKCs) and tracheal organ cultures (TOCs). These membrane rearrangements include DMVs, zER, and spherules (Maier et al. 2016, 2013b). In order to further characterize membrane rearrangements induced by IBV, we analyzed the membrane rearrangements induced by BeauR in DF1s. Unlike primary CKCs, DF1s are a continuous avian cell

line that are more easily transfected and are therefore used throughout this study. Although the spike protein of BeauR has increased tropism to allow for virus entry into additional cell lines, including DF1 cells, M41 is not adapted to infect these cells (Fang et al. 2005; Promkuntod et al. 2013). DF1 cells were infected with BeauR, fixed after 24 h, processed for EM, and imaged. Consistent with previous work, DMVs, zER, and spherules were all seen in IBV-infected DF1 cells (Figure 1).

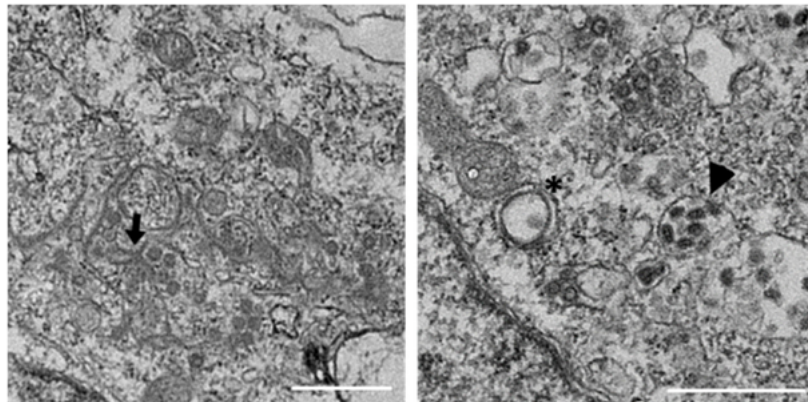


Figure 1. Membrane rearrangements in DF1 cells infected with infectious bronchitis virus (IBV) BeauR. DF1 cells were infected with BeauR for 24 h, fixed, and processed for electron microscopy (EM). Viral particles are indicated with arrowheads, double membrane vesicles (DMVs) with asterisks, and zippered endoplasmic reticulum (zER) and associated spherules with arrows. Scale bar represents 500 nm.

3.2. Non-Structural Proteins 3, 4, and 6 Relocalize upon Co-Expression

Other viruses in the *Nidovirales* order have been shown to require expression of only two or three nsps to induce membrane rearrangements similar to those seen under virus infection conditions (Angelini et al. 2013; Oudshoorn et al. 2017; Roos et al. 2001). To begin to understand the roles of IBV nsps in rearranging cellular membranes, nsps4 and 6 from apathogenic BeauR and nsps3, 4, and 6 from pathogenic M41 were tagged with fluorescent or epitope tags. It was not possible to

generate a plasmid expressing nsp3 from BeauR due to presumed toxic sequences, as has been found for this region in other coronaviruses (Almazán et al. 2000; Yount et al. 2002, 2000). DF1 cells were transfected with these plasmids and after 24 h cells were lysed and proteins separated by SDS-PAGE and detected by Western blot. All fusions proteins were found to be intact with bands detectable at the predicted molecular weights (Figure 2a), although an additional 49 kDa band was present in nsp3-GFP expressing cells, presumably due to a cleavage event within nsp3. It was also noted that nsp6-3xFLAG from M41 migrated at a higher molecular weight than nsp6-3xFLAG from BeauR, most likely due to differences in post-translational modification. Subsequently, DF1 cells were transfected with these plasmids and after 24 h cells were fixed, labelled with an anti-FLAG antibody, and visualized by confocal microscopy. All three nsps showed reticular cytoplasmic labelling consistent with localization to the ER (Figure 2b), as has been observed previously (Baliji et al. 2009; Cottam et al. 2011; Hagemeyer et al. 2011; Kanjanahaluethai et al. 2007; Oostra et al. 2008, 2007; Oudshoorn et al. 2017). In addition to ER localization, nsp4 was found in both small and large puncta in cells where the level of nsp4 expression was higher (comparison shown in Figure 2b). Nsp6 was also found in small cytoplasmic puncta when expressed alone (Figure 2b). To confirm ER localization, DF1 cells were transfected with either the plasmid expressing nsp3-GFP alone or plasmids expressing nsp4 or 6 together with pYFP-ER, as indicated. After 24 h, cells were fixed and labelled with anti-FLAG- and nsp3-expressing cells with anti-protein disulphide isomerase (PDI), a resident ER protein. Colocalization between YFP-ER or PDI and nsp3, 4, and 6 was observed, confirming that these proteins localize to the ER (Figure 2c).

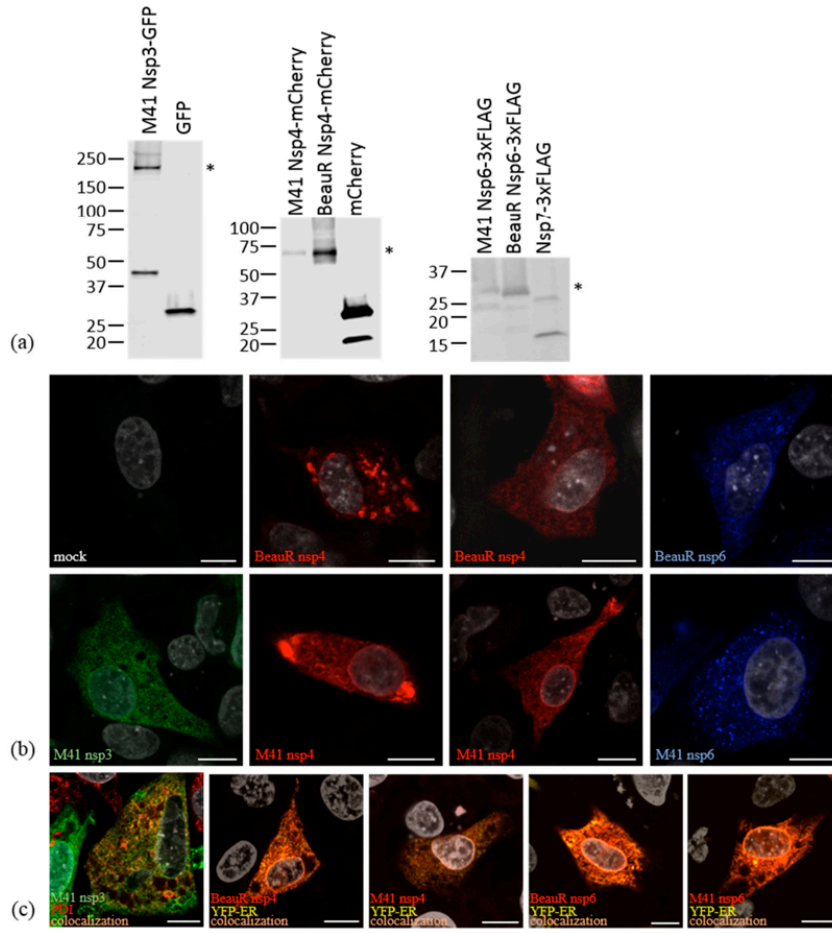


Figure 2. Expression of IBV non-structural proteins (nsps) in DF1 cells. (a) Detection of expression of viral nsps in transfected DF1 cell lysates. Cells were transfected with plasmids expressing tagged nsps, as indicated, or empty vectors or nsp7-3xFLAG as controls. Cell lysates were separated by SDS-PAGE and proteins detected by Western blot. From left to right, nsp3-GFP detected using anti-GFP, nsp4-mCherry detected using anti-mCherry, and nsp6-3xFLAG detected using anti-FLAG, as labelled. Molecular weight markers are shown on the left and asterisks indicate the nsp bands on each blot. (b) DF1 cells were transfected with plasmids expressing nsp4-mCherry and nsp6-3xFLAG from BeauR, and nsp3-EGFP, nsp4-mCherry, and nsp6-3xFLAG from M41. After 24 h, cells were fixed with 4% paraformaldehyde and imaged. Nsp3 (green), nsp4 (red), and nsp6 (blue) were imaged as labelled. Nuclei were stained with ToPro3 (grey) and scale bars indicate 10 μ m. (c) DF1 cells were transfected with plasmids expressing nsp4-mCherry and nsp6-3xFLAG from BeauR, and nsp3-EGFP, nsp4-mCherry, and nsp6-3xFLAG from M41 together with YFP-ER. After 24 h, cells were fixed with 4% paraformaldehyde and imaged. Nsp3 (green) and nsp4 and nsp6 (red) were imaged along with markers for the ER; PDI (red) or YFP-ER (yellow) as indicated. Nuclei were stained with DAPI (grey) and scale bar represents 10 μ m.

Next, to understand whether co-expression of these proteins results in changes in their localization, DF1 cells were transfected with combinations of the plasmids. After 24 h, cells were fixed and labelled with an anti-FLAG antibody. Upon co-expression of some combinations of these viral proteins, this staining pattern changed. Expression of nsp3 with nsp4 resulted in both proteins localizing to cytoplasmic puncta, although some signals for both proteins also remained in the ER (Figure 3). Co-expression of nsp3 with nsp6, or nsp4 with nsp6, did not result in relocalization of either protein, with nsp3 remaining ER-associated, nsp4 remaining both ER-associated and localized in cytoplasmic puncta, and nsp6 remaining both ER-localized and in cytoplasmic puncta (Figure 3). Interestingly, co-expression of nsps3, 4, and 6 resulted in relocalization of all three proteins to cytoplasmic puncta, some containing nsp3 and 4, some nsp6 only, and some puncta containing nsp3, 4, and 6 (Figure 3). Nsps4 and 6 derived from either BeauR or M41 exhibited the same pattern of localization. This demonstrates that co-expression of IBV nsps in the absence of any other viral components can result in their relocalization within the cell, presumably as a result of protein–protein interactions and potentially associated with rearrangement of cellular membranes.

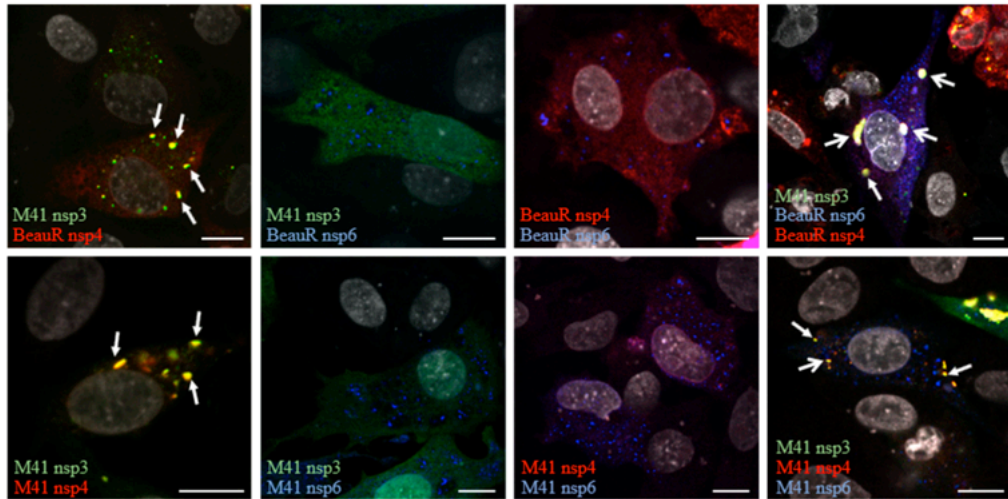


Figure 3. Co-expression of IBV non-structural proteins results in their relocation from the ER to cytoplasmic foci. DF1 cells were transfected with plasmids expressing nsp4-mCherry and nsp6-3xFLAG from BeauR, and nsps3-EGFP, nsp4-mCherry, and nsp6-3xFLAG from M41 in pairs or in a combination of three, as indicated. Solid arrows indicate areas of nsp3 and 4 colocalization, open arrows indicate areas of nsp3, 4, and 6 colocalization. Nuclei were stained with ToPro3 (grey) and scale bar represents 10 μ m.

3.3. IBV nsp4 Alone Is Necessary and Sufficient to Induce Membrane Pairing

To further understand the ability of IBV nsps3, 4, and 6 to rearrange cellular membranes, proteins were expressed in cells and analyzed by electron microscopy (EM). Initially, to assist with subsequent analysis by EM, the percentage of total cells in Figures 2b and 3 that were expressing the nsps of interest, as well as the percentage of cells expressing other combinations of nsps, was quantified (Table S1). DF1 cells were transfected with tagged nsp3, 4, and 6 derived from BeauR or M41 alone and in combination. After 24 h, cells were chemically fixed, embedded in resin, and visualized using an electron microscope. A phenotype common to all transfected cells was small, tight whorl-like structures which stained more strongly than other structures (Figure 4a). These were considered an artefact of transfection.

Transfection of cells with empty pEGFP-N1, pmCherry-N1, or pcDNA3.1(-)-3xFLAG did not result in changes to cellular membranes (Figure 4a). Different types of membrane structures were observed in the transfected cell samples that were absent from mock treated cells, including paired membranes, disordered or piled membranes, and DMV-like structures. Nsp4 in other coronaviruses has been shown to be important in membrane modifications, particularly in the formation of conventional DMVs (Beachboard et al. 2015; Gadlage et al. 2010). Initially, the effect of expression of nsp4 in DF1 cells was investigated. Interestingly, it was observed that expression of BeauR nsp4 alone was capable of forming paired membranes. This the first time this has been observed for any coronavirus nsp4. These paired membranes were observed both as very large areas of extensive accumulations or as small regions of shorter sections of paired membranes. The paired membranes were tightly apposed, often connected to the ER, were largely free of ribosomes, and strongly resembled IBV-induced zER (Figure 4b), although the electron density often surrounding IBV-induced zER was missing here and no spherules were present. Transfection of M41 nsp4 also induced membrane pairing (Figure 4b) with an appearance comparable to that of BeauR nsp4-induced paired membranes. For cells transfected with the BeauR nsp4 expression vector, 31 out of 235 cell sections (13%, percentage of total cells not transfected cells) contained piled membranes, and 3 out of 108 (3%) sections for M41, significant to $p < 0.00001$ by a Fisher's exact test.

It has previously been shown for other coronaviruses that membrane pairing requires co-expression of nsp3 and 4 or that co-expression of these proteins results in DMV accumulation (Oudshoorn et al. 2017). Therefore, the effect of co-expression of nsp3 with nsp4 was investigated. Firstly, the effect of expression of nsp3 alone on cellular membranes was determined. Although over 200 cells were examined from multiple experiments, expression of nsp3 was found to have no striking phenotype with cellular membranes appearing unchanged in the presence of nsp3 derived from M41 when compared with untransfected cells. Furthermore, surprisingly, expression of nsp3 with nsp4 had no effect on the membrane pairing ability of nsp4 (Figure 4c), with membrane rearrangements appearing comparable to cells expressing nsp4 alone, i.e., paired membranes connected to the ER and lacking ribosomes, found covering both large and smaller areas of the cytoplasm. Specifically, the numerous DMV-like structures observed in cells expressing nsp3 and 4 from either MERS-CoV or SARS-CoV were not observed here (Angelini et al. 2013; Oudshoorn et al. 2017). Overall, this data confirms that IBV nsp4 alone is the main driving factor in membrane pairing and co-expression of nsp3 does not alter this function.

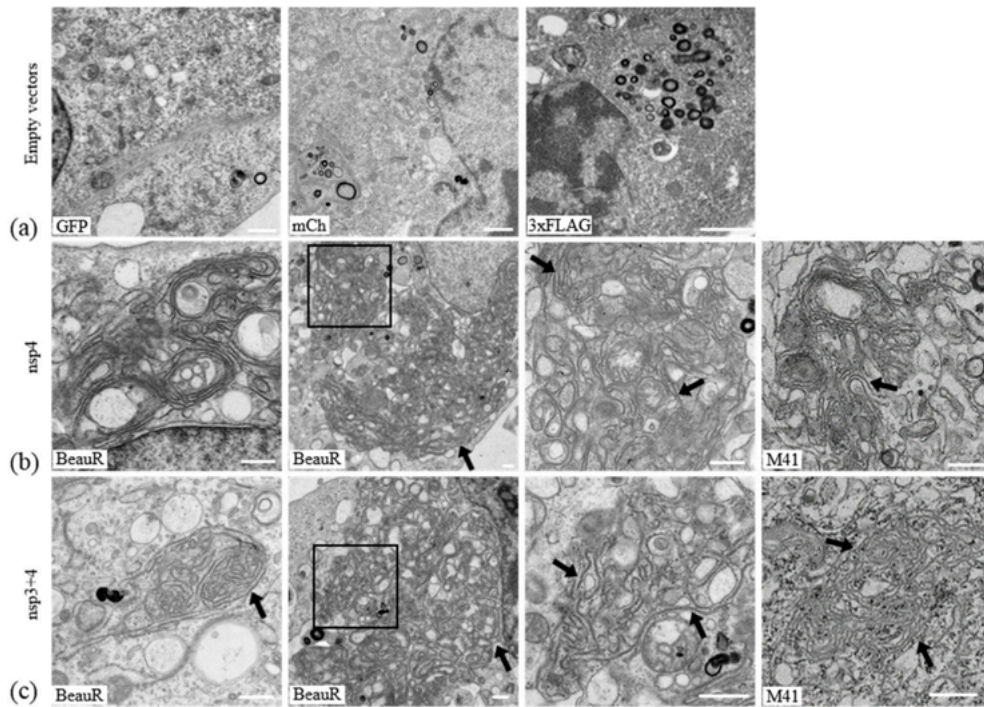


Figure 4. Expression of IBV nsp4 induces pairing of cellular membranes with no additional role for nsp3. DF1 cells were transfected with (a) the empty vectors: GFP, mCherry, and 3xFLAG; with a plasmid expressing BeauR or M41 nsp4-mCherry either (b) alone or (c) with a plasmid expressing M41 nsp3-EGFP, as indicated. After 24 h, cells were fixed and processed for EM. Areas of paired membranes are indicated by an arrow. The third image in (b,c) is a higher magnification of the boxed area in the second image. Scale bar represents 500 nm.

3.4. Nsp6 Induces the Formation of Piled, Disordered Membranes

Coronavirus nsp6 has previously been linked to autophagy induction when expressed alone (Lundin et al. 2014). Nsp6 derived from SARS-CoV has also been shown to induce single membrane vesicle accumulation and microtubule organizing center vesiculation (Angelini et al. 2013). Therefore, the cellular membrane rearrangements induced by expression of IBV nsp6 were analyzed. In cells expressing nsp6 alone from either BeauR or M41, large areas of tangled single membranes, which appear to be derived from the ER, were observed (Figure 5).

These piled, disordered membranes strongly resemble the disordered membrane bodies seen previously upon expression of SARS-CoV nsp3 (Angelini et al. 2013). To determine the effect of expression of nsp6 with other nsps on the formation of disordered membranes or any other structures, samples transfected with plasmids expressing nsp6 and either nsp4 or nsp3 were analyzed. In cells co-expressing nsp3 and 6, it was observed that cells expressing BeauR nsp6 formed disordered membranes while those expressing M41 nsp6 did not. Co-expression of nsp4 and nsp6 produced the paired membranes associated with nsp4 expression (for both BeauR and M41 nsp4). Disordered membranes were only found in cells co-expressing BeauR nsp6 but none when co-expressing M41 nsp6. This indicates that while nsp6 from either BeauR or M41 can induce the formation of disordered membranes when expressed singly, co-expression of nsp6 with either nsp3 or 4 disrupts this mechanism and to a greater extent in M41.

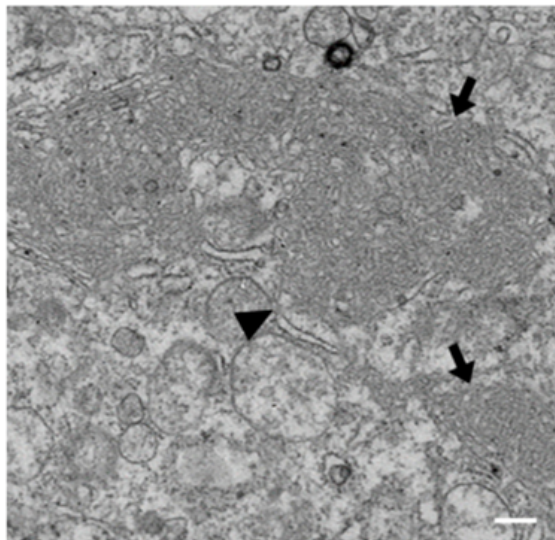


Figure 5. Expression of nsp6 alone induces the formation of piled, disordered membranes. DF1 cells were transfected with plasmids expressing nsp6-3xFLAG from BeauR. After 24 h, cells were fixed and processed for EM. Arrows indicate areas of piled, disordered membranes and the arrowhead indicates the area where piled membranes are derived from ER. Scale bar represents 500 nm.

3.5. *Nsps 3, 4, and 6 Are Not Able to Recapitulate the IBV Replication Organelle*

Finally, the membrane rearrangements induced by co-expression of IBV nsps3, 4, and 6 were investigated by electron microscopy to determine whether co-expression of all three transmembrane nsps could result in the formation of structures comparable to replication organelles in IBV-infected cells. The major phenotype observed following co-expression of all three nsps was the paired membranes induced by expression of nsp4 alone (Figure 6). When nsp4 and nsp6 derived from BeauR were expressed with M41 nsp3, a very limited number of DMV-like structures was observed (3 in 329 cell sections). In cells co-expressing nsp3, 4, and 6 derived from M41, no DMV-like vesicles were found in 489 cell sections with only nsp4-associated paired membranes being detected. In neither combination were the spherules usually found during virus infection observed. Therefore, although co-expression of IBV nsps 3, 4, and 6 may be sufficient for formation of DMVs, this does not seem to be a very efficient process compared with DMV formation by nsp3 and 4 from the *Betacoronaviruses* studied previously (Angelini et al. 2013; Oudshoorn et al. 2017) and nsp6 is unlikely to be the additional nsp required for IBV DMV formation.

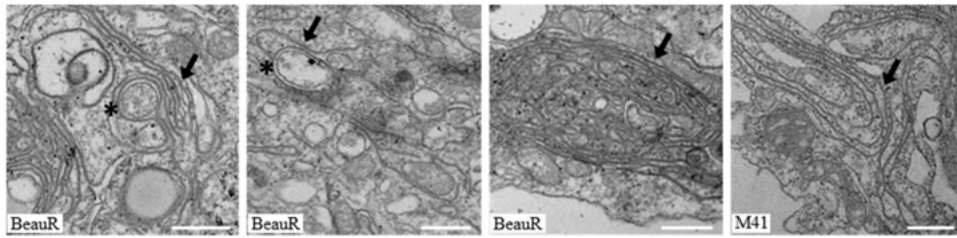


Figure 6. A limited number of DMV-like structures are formed in cells transfected with IBV nsp3, 4, and 6. DF1 cells were transfected with M41 nsp3 and either BeauR nsp4 and 6 or M41 nsp4 and 6. After 24 h, cells were fixed and processed for EM. Paired membranes are indicated with an arrow, DMV-like structures indicated with an asterisk. Scale bar represents 500 nm.

3.6. *IBV nsp3 and 4 Do Not Induce DMVs*

In order to further understand the paired membranes induced by expression of IBV nsp4, electron tomography (ET) was used to visualize membrane rearrangements in three dimensions. In addition, ET was used to confirm that, unlike for other coronaviruses (Angelini et al. 2013; Oudshoorn et al. 2017), co-expression of IBV nsp3 and 4 does not result in the formation of DMVs. DF1 cells were transfected with plasmids expressing either BeauR nsp4 or BeauR nsp4 with M41 nsp3. After 24 h, cells were fixed and processed for ET. The paired membranes produced by nsp4 expression (indicated by arrows) were found to form sheet-like structures with sections of paired membranes dilating in several places (arrowheads) (Figure 7a, Video S1). A comparison with cells expressing nsp3 and 4 showed there is no noticeable difference between the areas of paired membranes induced upon expression of these nsps (Figure 7b, Video S2). Therefore, expression of IBV nsp4 alone results in the formation of paired ER membranes. Addition of nsp3 does not

alter the membrane structures induced with no formation of either DMVs, as seen for other CoVs or spherules.

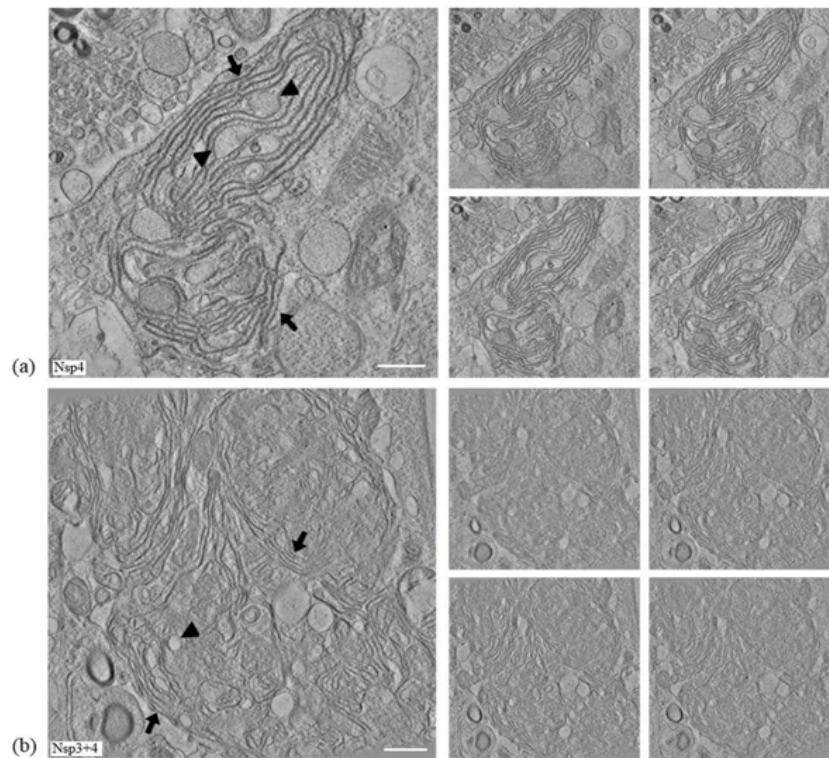


Figure 7. Expression of IBV nsp4 induces the formation of sheet-like areas of paired membranes with no additional role for nsp3. DF1 cells were transfected with a plasmid expressing BeauR nsp4-mCherry either (a) alone or (b) with a plasmid expressing M41 nsp3-EGFP, as indicated. After 24 h, cells were fixed and processed for ET, an average of five slices as well as four individual slices is shown here. Areas of paired membranes are indicated by arrows, areas where paired membranes dilate are indicated by arrowheads. Scale bar represents 500 nm.

4. Discussion

Induction of host cell membrane rearrangements is a tool used by many +RNA viruses, such as coronaviruses (Miller and Krijnse-Locker 2008; Netherton and Wileman 2011). These membrane rearrangements vary between the different members of the family, with the *Alpha* and *Betacoronaviruses* inducing convoluted membranes and DMVs and the *Gammacoronavirus* IBV inducing zippered ER, spherules, and DMVs (de Wilde et al. 2013; Goldsmith et al. 2004; Gosert et al. 2002; Maier et al. 2013b; Oudshoorn et al. 2017; Snijder et al. 2006; Ulasli et al. 2010). The formation of these membrane rearrangements is, however, a well-conserved mechanism used by these viruses in order to provide a site for viral RNA synthesis. Although the pool of knowledge about these structures has been growing, the mechanisms behind their formation remain largely unclear. Some light has been shed in recent years on the specific viral proteins involved in the formation of these structures; however, these studies were lacking in IBV. In this study, we looked at the involvement of nsps3, 4, and 6, which have all been implicated in the formation of membrane rearrangements. As transmembrane proteins, these are likely candidates in reordering the host cell membranes to the advantage of the virus. We showed firstly that DF1 cells are a suitable cell type to use for studying IBV membrane rearrangements in addition to those already tested (Maier et al. 2016).

In order to assess the involvement of nsps 3, 4, and 6 in virus-induced membrane rearrangements, plasmids expressing GFP, mCherry, or 3xFLAG fusion proteins were generated. To confirm expression of full-length fusion proteins, Western blots were performed using antibodies against the tags. For all the constructs, full-length nsp fusion proteins were detected. However, in cells expressing nsp3-GFP, an

additional 49 kDa band was seen indicating that as well as full-length protein, a cleavage product corresponding to the C-terminus of nsp3 plus GFP was also being produced.

Next, we expressed nsps alone or in combination in DF1 cells to assess their ability to rearrange cellular membranes. When expressed alone, all three nsps had a reticular, cytoplasmic localization consistent with previous observations that these nsps localize to the ER (Baliji et al. 2009; Cottam et al. 2011; Hagemeijer et al. 2011; Kanjanahaluethai et al. 2007; Oostra et al. 2008, 2007; Oudshoorn et al. 2017), although nsp4 and nsp6 in addition had a punctate localization with nsp4 in particular forming large foci in some cells. ER localization was subsequently confirmed by colocalization of the three nsps with ER markers. When nsps3 and 4 were co-expressed, both proteins localized to large and small cytoplasmic puncta with some protein also remaining in the ER. This suggests that nsp3 and 4 are able to interact with one another, again consistent with previous findings for other coronaviruses (Hagemeijer et al. 2011; Oudshoorn et al. 2017), resulting in nsp3 moving into the nsp4-containing puncta. Co-expression of nsp3 and 6 or nsp4 and 6 did not result in alteration of their cellular localization. However, when nsp3, 4, and 6 were co-expressed, nsp3 and 4 colocalized as seen before but some puncta now also contained nsp6, although some puncta contained only nsp3 and 4 or nsp6 alone. This suggests that, as seen in other coronaviruses, nsp3 and 4 together, but not alone, are able to direct nsp6 into the nsp3/4 puncta (Hagemeijer et al. 2014, 2011).

Subsequently, EM was used to identify changes to the structure of cellular membranes upon expression of these three proteins. Surprisingly, expression of nsp3 did not induce any notable phenotype. Expression of nsp3 from either SARS-CoV or MERS-CoV results in the production of disordered membrane bodies likely derived from the ER (Angelini et al. 2013; Oudshoorn et al. 2017). It is not clear why nsp3 derived from IBV behaves so markedly differently from nsp3s expressed by other coronaviruses. However, the previously studied nsp3s have all been derived from *Betacoronaviruses* so nsp3 from *Gammacoronaviruses*, including IBV, may function somewhat differently. Indeed, an amino acid sequence comparison between nsp3 sequences from BeauR and the *Betacoronavirus* MHV A59 shows only 13.4% homology and 25.9% similarity. Therefore, although these are accepted as functional homologs, there is scope for these proteins to behave differently from one another. Furthermore, given that we have previously demonstrated that IBV-induced membrane rearrangements are distinct from those induced by *Alpha*- and *Betacoronaviruses* (Maier et al. 2013b), differences in the mechanism of their formation might reasonably be expected.

Interestingly, expression of nsp6 alone induced membrane proliferation and the formation of disordered membranes similar to the disordered membrane bodies (DMBs) induced by SARS-CoV and MERS-CoV nsp3 (Angelini et al. 2013; Oudshoorn et al. 2017). Expression of nsp6 alone did not appear to induce microtubule organizing center vesiculation as seen upon expression of SARS-CoV nsp6 (Angelini et al. 2013) and the presence of autophagosomes was also not apparent (Cottam et al. 2011; Maier et al. 2013a), although this is likely due to differences in experimental approaches, namely the use of EM in this study compared to immunofluorescence of whole cells used previously (Maier et al.

2013a). Therefore, IBV nsp6 also appears to function somewhat differently to nsp6 from SARS-CoV in its ability to rearrange membranes.

The most striking phenotype came upon expression of nsp4; expression of nsp4 alone was sufficient to induce areas of paired membranes. Furthermore, ET demonstrated that these are sheet-like areas of paired ER membranes, highly similar to zER in IBV-infected cells. It was noted that the paired membranes, although resembling zER in infected cells, lacked the electron density often surrounding the membranes (Maier et al. 2013b). This reflects the lack of the other viral proteins making up the replication complex, which, presumably, accumulate on the cytoplasmic surface of the zER. Nsp4-induced paired membranes were observed as both small regions throughout the cytoplasm and also in extensive areas of paired membranes. These two phenotypes potentially reflect the different localizations observed by confocal microscopy with some cells containing nsp4 localized only to the ER and some cells containing large cytoplasmic puncta corresponding to the large areas of paired membranes. Use of correlative light electron microscopy (CLEM) in the future would confirm this. Attempts were made to confirm the nsp4 homotypic interaction by co-immunoprecipitation; however, this was not successful. It has previously been shown for MHV that nsp4 can self-associate (Hagemeijer et al. 2011), although earlier attempts to demonstrate the interaction in SARS-CoV failed (Pan et al. 2008; von Brunn et al. 2007), highlighting that detection of this interaction can be challenging. However, it is likely that self-interaction between nsp4 proteins located in both membranes of the ER zippers the two ER membranes together to generate the paired membranes seen, although it cannot be ruled out that instead an interaction with one or more cellular proteins is

required. Significantly, this is the first time for any coronavirus that, regardless of mechanism, a membrane pairing function for nsp4 alone has been described.

Surprisingly, addition of nsp3 did not alter the membrane rearrangements induced by nsp4 alone. Previous work by others has shown that for other related coronaviruses and arteriviruses, membrane pairing requires the expression of nsp3 and 4 (or their homologs) (Angelini et al. 2013; Hagemeijer et al. 2014, 2011). In addition to this, however, co-expression of nsp3 and 4 for other coronaviruses resulted in the formation of numerous DMV-like structures (Angelini et al. 2013; Oudshoorn et al. 2017). Despite extensive searching and the use of electron tomography to gain three-dimensional information, we were not able to detect any DMVs in cells expressing nsp3 and 4. The reason for this difference is not clear. Here, we used separate plasmids to express nsp3 and 4 but this strategy was also used in previous work and when compared with a cleavable nsp3–4 precursor did not yield different results (Oudshoorn et al. 2017). Therefore, the protein expression strategy is unlikely to be the reason that DMVs were not formed. It is possible that the presence of the shorter nsp3 fragment detected by Western blot prevented the formation of DMVs. However, full-length nsp3 was also present and therefore should have been capable of inducing DMVs in combination with nsp4. In addition, DMVs were not detectable in cells expressing either nsp3 from M41 and nsp4 from BeauR or cells expressing nsp3 and 4 from M41, indicating that the use of proteins from different virus strains was not the reason for the lack of DMVs. Indeed, nsp3 relocalized to both BeauR and M41 nsp4-containing foci suggesting that M41 nsp3 is capable of interacting with both nsp4 proteins. Again, attempts were made to confirm interaction between nsp3 and nsp4 by co-immunoprecipitation, but this was not successful. Interactions between full-length or the C-terminus of nsp3 and nsp4

from other coronaviruses have been shown previously (Hagemeyer et al. 2011; Pan et al. 2008). Interestingly, Sakai et al. showed that just two amino acid residues in nsp4 are necessary for the interaction with nsp3; however, these residues are only conserved in *Betacoronaviruses*, not in *Alpha-* or *Gammacoronaviruses* (Sakai et al. 2017), so it is likely that the mechanism of any nsp3/nsp4 interaction is different in IBV. Overall, the data indicates that DMV formation by IBV requires the presence of additional viral protein(s), either to direct an interaction between nsp3 and nsp4 if it cannot occur directly or because DMV formation is via another mechanism. Co-expression of nsps 3, 4, and 6 did appear to result in the formation of a very small number of DMV-like structures. However, these were significantly less numerous and less easily identifiable than those observed by Oudshoorn et al. (Oudshoorn et al. 2017). Therefore, nsp6 does not appear to be the IBV protein required, in addition to nsp3 and 4, to induce DMVs and other viral proteins must play a role.

Throughout this study, we were unable to detect spherules associated with IBV infection, although we did identify membranes highly similar to zER. In our previous work, we demonstrated that M41 virus has a low spherule phenotype and the region of the genome from the 5' end to nsp13 was responsible for this (Maier et al. 2016). Unfortunately, we were unable to clone nsp3 from BeauR due to toxicity problems in *Escherichia coli*. It was also not possible to clone nsp3 from two further strains of IBV. As the nsp3 used in this study was derived from M41, it is possible that this is the reason that spherules were not detected under any conditions. Nsp3 from BeauR and M41 are highly related with 90.5% amino acid homology and 95.2% similarity with the majority of the differences occurring within the non-functional papain-like protease 1 domain. Despite that fact, it cannot be ruled out that these differences are sufficient to prevent spherule formation. In future, cloning the C-

terminal part of nsp3 from BeauR, as other groups have done for MHV (Hagemeijer et al. 2014), may provide further insight into the role of nsp3 in membrane modifications. An alternative explanation for the lack of spherules could be that the precise molar ratio of nsps to one another, as well as the presence of cleavage intermediates, generated as a result of expression via a polyprotein during virus infection is critical for spherule formation. In that case, the expression approach taken here of transfecting multiple plasmids into cells would not result in the correct ratio of proteins or presence of cleavage intermediates, thereby preventing spherule formation. However, Oudshoorn et al. were also unable to identify CMs and spherule-like structures when combinations of nsps were expressed either from separate plasmids or as a polyprotein (Oudshoorn et al. 2017). Instead, it is more likely that additional viral proteins are required for spherule formation. This is not necessarily surprising. For *Alphaviruses*, spherules are only formed in the presence of all nsps and although they are able to form in the absence of RNA, the length of RNA present directly affects the size of the spherule produced (Hellström et al. 2017; Kallio et al. 2013). Furthermore, in the case of Flock House Virus, spherules only form when RNA synthesis is actively occurring (Kopek et al. 2010). Therefore, spherule formation by IBV may require expression of additional nsps, including those required for RNA synthesis, as well as an RNA template. Alternatively, it may require expression of additional nsps that direct interaction with cellular proteins that facilitate changes to the membrane.

The mechanisms behind the formation of virus-induced membrane rearrangements required for replication organelle formation are doubtlessly complex. Although we have identified a clear role for IBV nsp4 in membrane pairing and the formation of zippered ER, numerous questions remain and further differences between IBV and

members of the *Betacoronavirus* sub-family have been highlighted. The identity of the IBV proteins required for both spherule and DMV formation remain unknown and further study is required to complete our understanding of the critical stage of the virus replication cycle.

Supplementary Materials

The following are available online at <http://www.mdpi.com/1999-4915/10/9/477/s1>,
Table S1: Cells expressing each nsp compared to the total number of cells counted,
Video S1: Electron tomographic reconstruction of paired membranes in an nsp4-expressing cell, Video S2: Electron tomographic reconstruction of paired membranes in an nsp3 and nsp4-expressing cell.

Paper three:

Bioinformatics analysis for L polymerase homology of arenaviruses

Hasan Alrashedi¹, Ian Jones¹, Geraldine Mulley¹, Benjamin W Neuman^{1,2}

1) ¹School of Biological Sciences, University of Reading, Whiteknights, RG6 6AH, UK

2) ² Biology Faculty, Texas A&M University-Texarkana, 7101 University Ave,
Texarkana, TX 75503, USA

*Correspondence Author: Ian Jones: i.m.jones@reading.ac.uk

Submitted to bioRxiv, 2019

Abstract

Many of the deadliest human infectious diseases are zoonotic in origin, meaning they were originally transmitted to humans from an animal reservoir. The emergence of human diseases that cause epidemics with high mortality, such as Arenavirus haemorrhagic fever, drives researchers to investigate the pathogens responsible and develop ways to manage clinical cases and prevent further outbreaks. However, little is currently known about the diversity and prevalence of animal arenaviruses that may have the capacity to become zoonotic in the future. In this paper, sequences of relatively conserved arenavirus L polymerase were used to mine metazoan transcriptome sequence data for the purpose of risk prediction. In essence, bioinformatics was utilized to provide a better understanding of the potential evolution and natural history of uncharacterized virus sequences in the GenBank database. Several matches were identified which, along with a reasoned approach to their phyla, was used to provide a likelihood score of their zoonotic potential.

Introduction

Many of the most dangerous human RNA viruses are zoonotic, transmitted to humans from animal reservoirs, including arenaviruses that cause viral haemorrhagic fever (VHF) e.g. Lassa virus (LASV) or serious neurological damage e.g. lymphocytic choriomeningitis virus (LCMV) that represent a risk to humans (Bonthius 2012; Ehichioya et al. 2010; Fichet-Calvet and Rogers 2009). *Arenaviridae* are a family of viruses composed of four genera, *Mammarenavirus*, *Reptarenavirus*, *Hartmanivirus* and *Antennavirus* (Abudurexiti et al. 2019). Mammarenaviruses are distributed worldwide, with each viral species restricted to the distribution of the animal reservoir host(s), causing febrile diseases in humans and other animals (Buchmeier et al. 2007). More recently, it was discovered that highly divergent arenaviruses in the genera reptarenavirus and hartmanivirus are carried by snakes. It was found that in some European countries such as Netherlands, Finland and Germany, some species of snakes with associated inclusion body disease were infected with reptarenavirus (Aqrawi et al. 2015; Bodewes et al. 2013; Hepojoki et al. 2015b). Recent findings reveal that reptarenavirus infection has also been confirmed in the United States (Chang et al. 2016). Currently, there is no evidence of zoonotic transmission of snake reptarenavirus to humans; their discovery represents only a potential threat to human health because of their prevalence of the infected animals and the fact that many snakes are kept as pets (Zapata and Salvato 2013)

Arenaviruses have a segmented ambisense single strand RNA genome, which is typically grouped as negative sense RNA viruses (Buchmeier et al. 2007). The large (L) segment encodes the viral RNA dependent RNA polymerase (RdRp) or L polymerase and the small zinc finger motif protein (Z), whereas the short (S) segment encodes the nucleoprotein (NP) and glycoprotein precursor (GPC) (Salvato et al. 1989). (Bodewes et al. 2013). The viral RNA dependent RNA polymerase (L polymerase) is the largest protein encoded by arenaviruses with a size of around 6.6 kb in a total genome of ~11kb (Zapata and Salvato 2013). The L polymerase contains an endonuclease domain that plays a significant role in mRNA cap-snatching during viral transcription (Morin et al. 2010). As L polymerase contains several essential catalytic domains it represents a protein which would be expected to be conserved, at least in part, by viruses using a similar mode of replication. Because the L polymerase is highly conserved it provides a useful source of amino acid sequences, for example from the catalytic site and from the endonuclease domain, for homology based searches of the unannotated databases to assess how widespread these conserved features are, and if they are found in virus sequences that may be of pandemic concern.

Material and Methods

Materials and methods of this research was described in detail in section 2.14

Results

Translated blast (tBLASTn) of arenaviruses

The tBLASTn facility on National Center for Biotechnology Information (NCBI) was used to align a query protein sequence to a nucleotide database assuming that any alignment could be in any possible reading frames translatable from any nucleic acid sequence (McGinnis and Madden 2004). As bait, the L polymerase sequences of two species of mammarenavirus, Tacaribe virus (TCRV) and lymphocytic choriomeningitis virus (LCMV), as well as two species of reptarenavirus, Golden Gate virus (GGV) and California Academy of Science virus (CASV) were used to find similarities in the Transcriptome Shotgun Assembly (TSA) database. At least six genes sequences of different species were found to match to some part of the L polymerase of arenavirus species indicating some similarity with the arenaviruses used as the probe (Table 1).

Table 1: Hits identified following tBLASTn of L polymerase of arenaviruses. L polymerase of TCRV: Tacaribe virus (GenBank accession number NP_694848.1), LCMV: lymphocytic choriomeningitis virus (NP_694845.1), GGV: Golden Gate virus (YP_006590089.1), CASV: California Academy of Science virus (YP_006590093.1) were used for searching translated nucleotide in GenBank database by using translated blast (tBLASTn) were Transcriptome Shotgun assembly (TSA) allocated at search set of tBLASTn. The table shows the percentage of protein identity, E-value and accession number.

Virus	Transcribed RNA of TSA alignment	Number of hits (E-value)	Identity	Accession of TSA
TCRV	<i>Channa punctata</i> RP_73146	9e-05	41%	GEKU01073124.1
	<i>Catostomus commersonii</i> Contig_131767	0.001	51%	GECX01131681.1
LCMV	<i>Channa punctata</i> RP_73146	7e-06	43%	GEKU01073124.1
	<i>Asymmetron lucayanum</i> comp27398_c0_seq1	6e-05	26%	GETC01011646.1
	<i>Catostomus commersonii</i> Contig_163647	0.002	36%	GECX01163539.1
	<i>Rhizopus oryzae</i> KNUBEL_RO_010568	0.18	24%	GDUK01010546.1
GGV	<i>Channa punctata</i> RP_73146	5e-15	44%	GEKU01073124.1
	<i>Asymmetron lucayanum</i> comp27398_c0_seq1	4e-04	24%	GETC01011646.1
	<i>Catostomus commersonii</i> Contig_131767	0.002	48%	GECX01131681.1
	<i>Rhopilema esculentum</i> c77127_g1_i1	0.068	23%	GEMS01099264.1
CASV	<i>Channa punctata</i> RP_73146	8e-13	37%	GEKU01073124.1
	<i>Catostomus commersonii</i> Contig_131767	0.001	35%	GECX01131681.1
	<i>Talitrus saltator</i> comp102738_c0_seq1	0.005	27%	GDUJ01083694.1
	<i>Asymmetron lucayanum</i> comp27398_c0_seq1	0.11	24%	GETC01011646.1

The data shows there are transcribed RNA sequences from extant species that align with the bait L polymerase structures including from *Channa punctate* (spotted snakehead fish), *Catostomus commersonii* (white sucker fish), *Asymmetron lucayanum* (lancelet), *Rhizopus oryzae* (fungus), *Rhopilema esculentum* (flame jellyfish) and *Talitrus saltator* (sand hopper). All these candidates had stretches of

homology with similarity given an E-value <1 . As the E-value indicates the number of the hits during database searching that are expected by chance the more significant E-values are less than 1 or zero whilst an E-value equal to 1 is not considered since it indicates only a chance alignment (Pearson 1995; Pearson and Lipman 1988). The target transcripts found (Table 1) were translated to allow further homology detection and structure prediction with other proteins found in the annotated protein database. Subsequently, the translated protein sequences from the TSA database and the sequences of mammarenavirus (TCRV and LCMV) and reptarenavirus (GGV and CASV) used as bait for arenavirus like isolates.

Homology detection and structure prediction of identified proteins

The transcribed RNA of the TSA database (Table 1) were used to deduce protein homology with known proteins or domains using the SIB Bioinformatics Resource Portal (Gasteiger et al. 2003). The largest one or two segments of the open reading frame (ORFs) found were selected and used to find protein homology among other viruses in the database by using the online bioinformatics tool HHpred, version HHsuite-2.0.16mod (Söding et al. 2005). Interestingly, the HHpred output showed all the translated protein fragments of *Channa punctate*, *Catostomus commersonii*, *Asymmetron lucayanum*, *Rhizopus oryzae* and *Talitrus saltator*, identified originally as having homology to the arenavirus L polymerase, to have some homology with the La Crosse bunyavirus polymerase as found in structure 5amr-A in complex with the 3' viral RNA. In some cases, homology was also apparent with Influenza C virus RNA-dependent RNA polymerase (5d98-B), whereas the *Rhopilema esculentum* sequence had homology with the structure of the L polymerase of vesicular

stomatitis virus (5a22-A). The amount of protein homology varied among the translated proteins. For example, the protein homology of the *Rhizopus oryzae* sequence with La Crosse Bunyavirus polymerase (5amr-A) is the longest, reaching 854 amino acids, while the homology between the translated protein of *Catostomus commersonii* with Influenza C virus RNA-dependent RNA polymerase (5d98-B) was only 56 amino acids (Figure 1, 2, 3, and 4). Therefore, ORFs detected in the translated proteins of the transcribed RNA of TSA database showed homology with other viruses of known pathogenicity and could assist in the prediction the phylogenetic relationship among arenaviruses and other viruses archived in the GenBank databases.

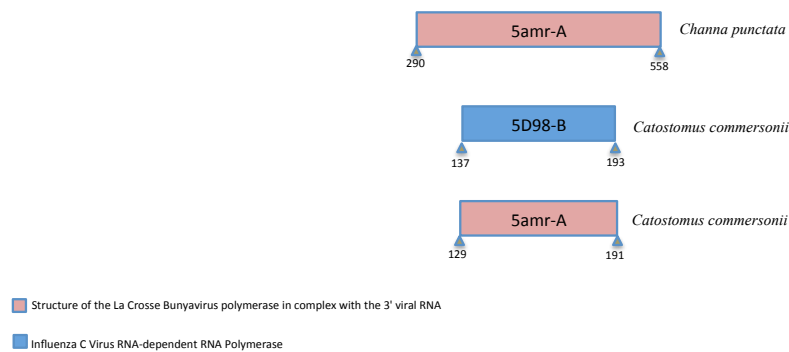


Figure 1: Homology detection of translated L polymerase of Tacaribe virus (TCRV). HHpred bioinformatics tools kit was used for protein analysis, while Microsoft PowerPoint was utilized for drawing the scales. The length of the scale depends on the gene size, the colour depends on virus gene homology. The 5amr-A (darksalmon colour) refers to structure of the La Crosse Bunyavirus polymerase in complex with the 3' viral RNA, 5D98-B (blue colour) refers to Influenza C virus RNA-dependent RNA polymerase.

Appendix: Papers contributions

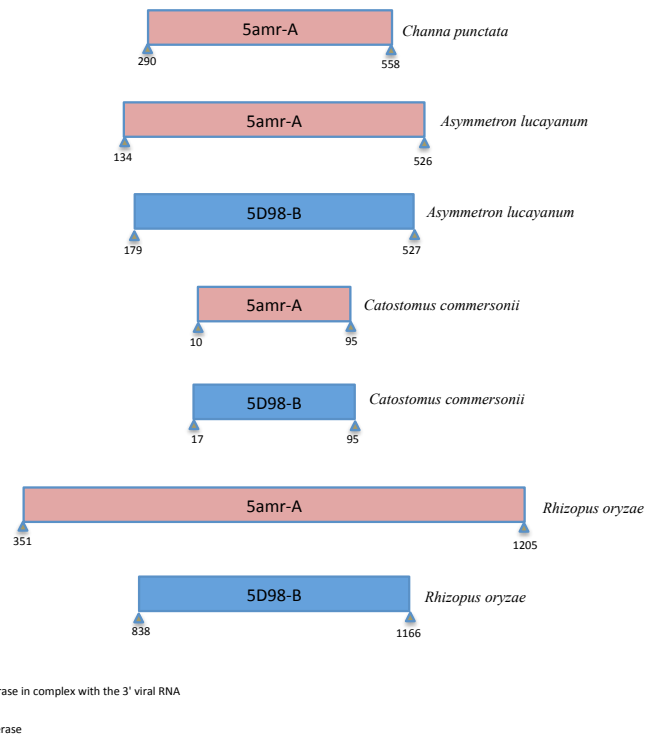


Figure 2: Homology detection of translated L polymerase of lymphocytic choriomeningitis virus (LCMV). HHpred bioinformatics tools kit was used for this purpose were Microsoft PowerPoint was used for drawing the scales. The length and the colour of scale depend on gene size and gene homology of virus. The 5amr-A (darksalmon colour): structure of the La Crosse Bunyavirus polymerase in complex with the 3' viral RNA, 5D98-B (blue colour): Influenza C virus RNA-dependent RNA polymerase.

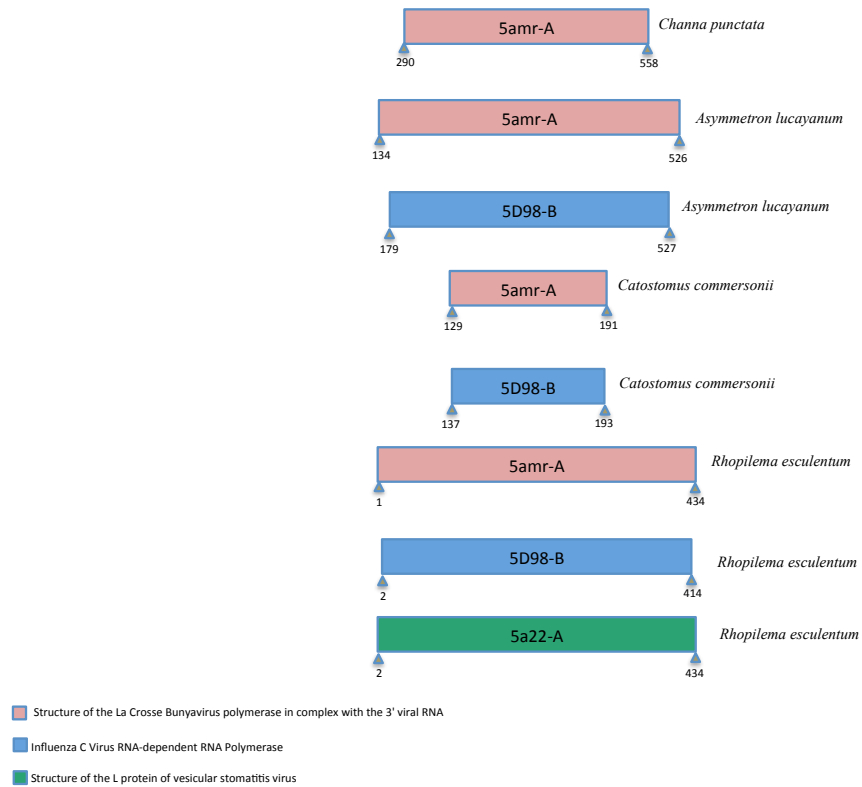


Figure 3: Homology prediction of translated L polymerase of Golden Gate virus (GGV). HHpred bioinformatics tools kit was used for protein analysis and Microsoft PowerPoint was used for drawing the scales. The scale in different colour and length depends on gene homology and gene size of the viruses, were 5amr-A (darksalmon colour) refers to structure of the La Crosse Bunyavirus polymerase in complex with the 3' viral RNA, 5D98-B (blue colour) refers to Influenza C virus RNA-dependent RNA Polymerase, while the 5a22-A (green colour) refers to structure of the L polymerase of vesicular stomatitis virus.

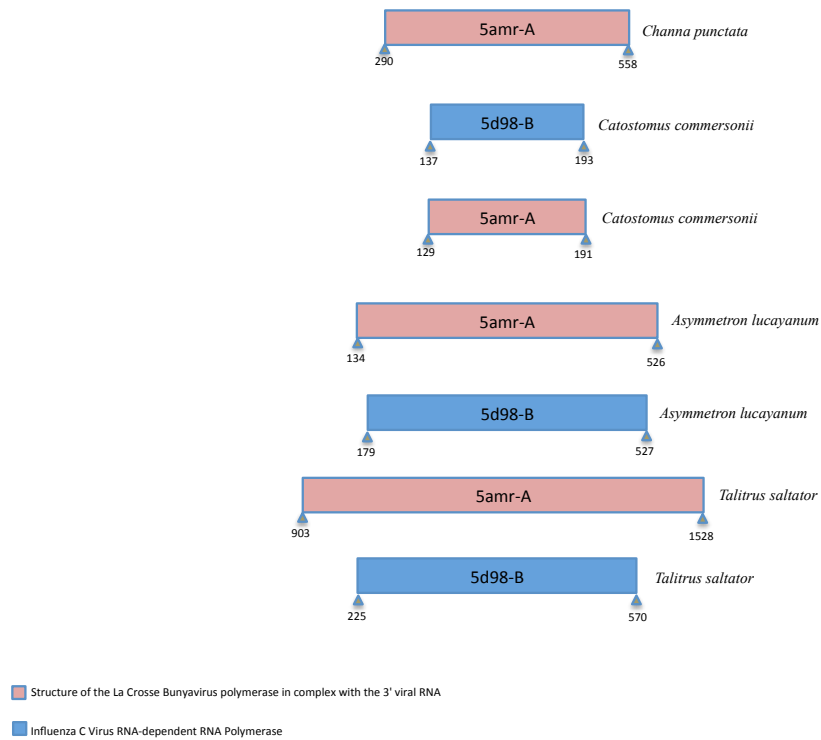


Figure 4: Homology detection and structure prediction of translated L polymerase of California Academy of Science virus (CASV). The translated protein was analysed by using HHpred bioinformatics tools, while the scales were drawn by using Microsoft PowerPoint. The scales showing in different colour and size, the colour refers to the identity of the gene, whereas the length refers to gene size of the target virus. The 5amr-A (darksalmon colour): structure of the La Crosse Bunyavirus polymerase in complex with the 3' viral RNA, 5D98-B (blue colour): Influenza C virus RNA-dependent RNA polymerase.

Multiple Sequence Alignment (MSA) of TSA database and arenavirus proteins

To evaluate the homology and conservation of the proteins found as well as study their phylogeny for the evolutionary relationships among the proteins of the arenaviruses and the TSA database, multiple sequence alignment (MSA) was used (Rani and Ramyachitra 2016). The open reading frames (ORFs) sequence of the TSA database (Table 1) with the L polymerase of Tacaribe virus (TCRV), lymphocytic choriomeningitis virus (LCMV), Golden Gate virus (GGV) and California Academy of Science virus (CASV), were used for MSAs (Blazewicz et al. 2013). To do this, the sequence data of the translated proteins over the region of homology, as described in the results of the HHpred analysis, were aligned with L polymerases of (TCRV), (LCMV), (GGV) and (CASV) using Clustal Omega version (1.2.4). Partial MSAs as shown in Figure 5 were manually edited via Jalview 2.10.1 (Waterhouse et al. 2009).

Appendix: Papers contributions

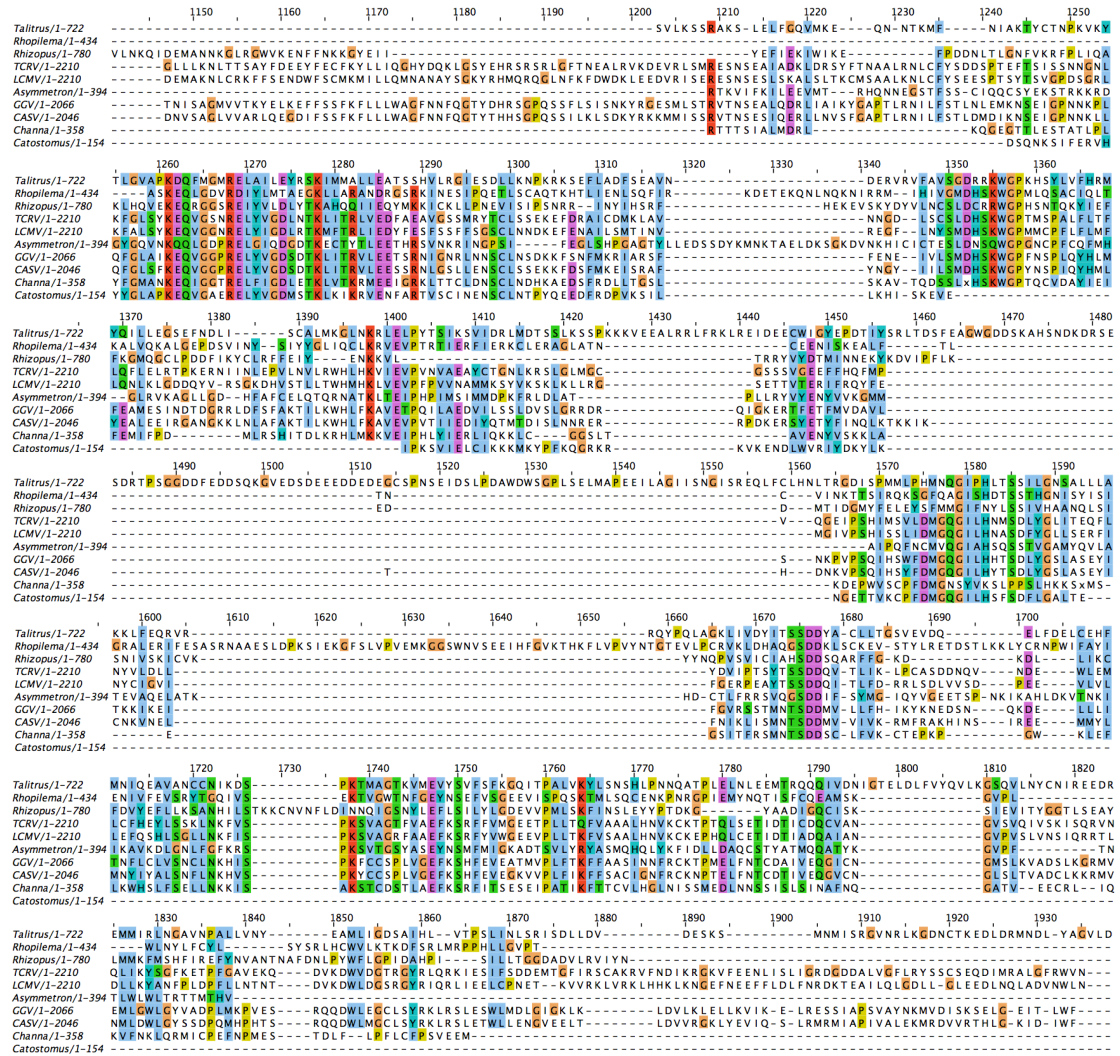


Figure 5: Multiple sequence alignment (MSA) of partial translated protein of TSA database hits with the L polymerase of arenaviruses. The translated proteins of *Channa punctate*, *Catostomus commersonii*, *Asymmetron lucayanum*, *Rhizopus oryzae*, *Rhopilema esculentum* and *Talitrus saltator* were aligned with L polymerase of arenaviruses including Tacaribe virus (TCRV), lymphocytic choriomeningitis virus (LCMV), Golden Gate virus (GGV) and California Academy of Science virus (CASV). The alignment starts around 1230 to 1870 amino acids, as the sequence of translated protein of TSA database matches with L polymerase of the arenaviruses species. Accession number of TRCV, LCMC, GGV and CASV were stated in Table 1. Clustal Omega (1.2.4) was used for the multiple alignments and Jalview 2.10.1 (Waterhouse et al. 2009) was used for manual edition.

Figure 5 shows some shared regions of protein homology following multiple sequence alignments. In particular, two regions of L polymerase appeared to represent the most homologous stretches among the sequences aligned, residues ~1210 to ~1450 and residues ~1560 to ~1880. Interestingly the region 1050 – 1500 has been defined as the core RdRp in the Lassa L structure (Brunotte et al. 2011b) while the later sequence also falls into a conserved region defined as domain IV based on arenavirus sequence analysis (Vieth et al. 2004). That these regions of conservation appear in such diverse targets suggests that it should be possible for design primers that could be used to amplify products from diverse sources as well as from current arenaviruses species by RT-PCR. In fact, RT-PCR was used for identify some species of mammarenavirus (Vieth et al. 2007) and reptarenavirus (Aqrawi et al. 2015). This could provide a diagnostic for the presence of the agents from which the TSA sequences were derived and also find other, related, virus sequences (Lozano et al. 1997; Vieth et al. 2005).

Phylogeny analysis

To present a clear phylogenetic analysis between TSA database and arenaviruses that were used as probes, a phylogenetic tree was constructed that shows the relationship among these species. MrBayes version 3.2.6 (Ronquist et al. 2011) is a command line interface that was used for creating the trees by Bayesian Inference (BI). Bayesian Inference (BI) is based on the concept of probabilities that are based on prior expectation, after the analysis of some of the data. The L polymerase of arenaviruses sequences were aligned with the HHpred sequences from those TSA database hits found by using multiple sequence alignments (MSAs) by Clustal analysis (McWilliam et al. 2013), with some other viruses acting as roots for the phylogeny. The alignment file was then analysed by the MrBayes program. As a result, phylogenetic trees were visualized by a phylogenetic tree viewer program such as FigTree v1.4.3 software, (<http://tree.bio.ed.ac.uk/software/figtree/>) (Hall 2018; Ronquist et al. 2011). In short, phylogenetic trees were successfully created by using Bayesian Inference (BI) facility and presented using FigTree v1.4.3 (Figure 6).

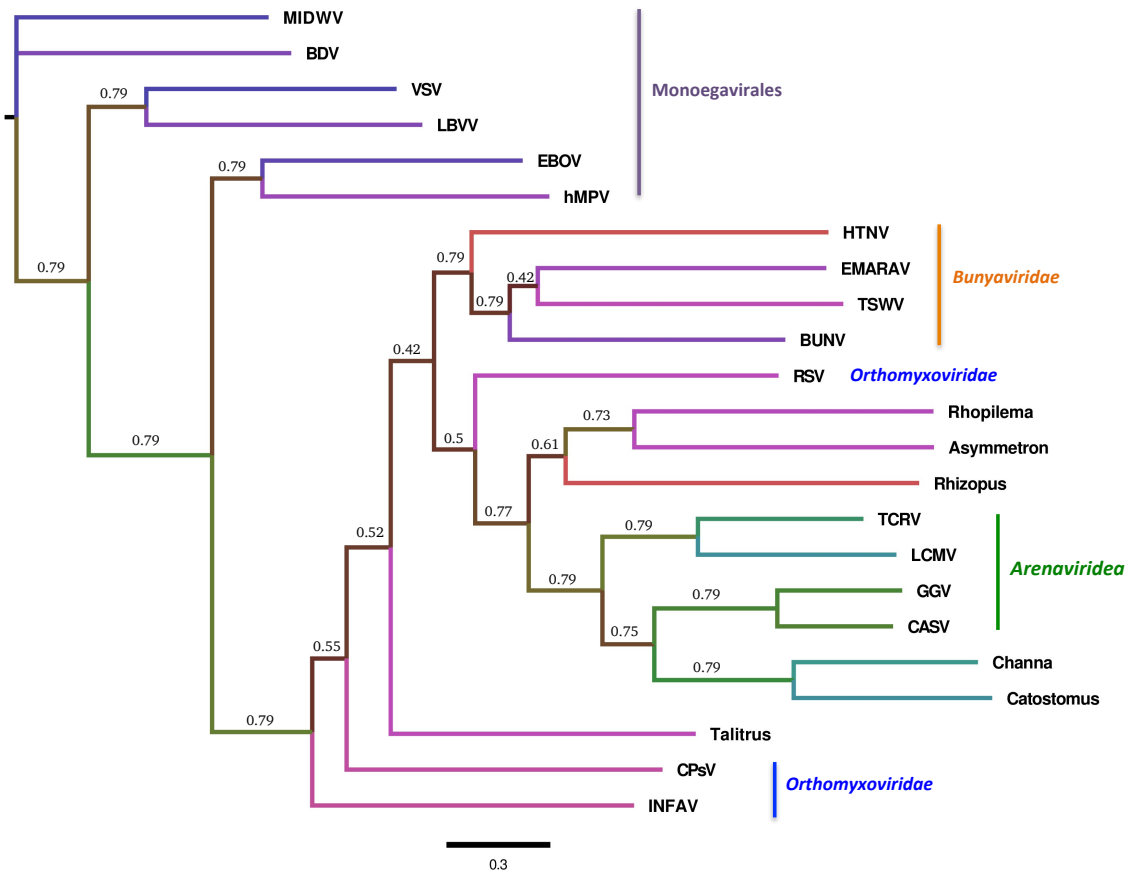


Figure 6: Molecular phylogenetic analysis by Bayesian Inference (BI). The phylogenetic tree was designed by using MrBayes v3.2.6 inference and manually edited by FigTree v 1.4.3. Average standard deviation of split frequencies was less than 0.01. The analysis involved 23 amino acid including translated protein sequences of TSA database, L polymerase sequences of arenaviruses and phylogeny root viruses protein sequences. Accession number of TRCV, LCMC, GGV and CASV were stated in Table 1. Accession number of root viruses, Hantaan virus (HTNV): NP_941982.1, Bunyamwera virus (BUNV): NP_047211.1, Rice stripe virus (RSV): AFM93820.1, Tomato spotted wilt virus (TSWV): AIA24440.1, Vesicular stomatitis virus (VSV): AAA48442.1, Citrus psorosis virus (CPsV): Q6DN67.1, European mountain ash ringspot-associated virus (EMARaV): Q6Q305.2, Lettuce big-vein associated virus (LBVaV): Q8B0U2.1, Influenza A virus: P03433.2, Midway nyavirus (MIDWV): YP_002905331.1, Borna disease virus (BDV): CEK41892.1, Zaire ebolavirus (EBOV), AAG40171.1, Human metapneumovirus (hMPV): AII17600.1.

Viral RNA dependent RNA polymerase (vRdRp) is an ancient enzyme (Černý et al. 2014) which also, via its mutation rate, plays an important role in the evolutionary strategy of RNA viruses, leading to novel emerging viruses (de Farias et al. 2017; Vignuzzi et al. 2006). Viral genes and proteins evolve fast when compared to their cellular counterparts, a function of the vRdRp in driving their evolution (Cabanillas et al. 2013; Pickett et al. 2011; Smith et al. 2012) and Bayesian analysis of RNA viruses, including emerging viruses and others that were archived in GenBank database, is convenient for reconstruction the evolutionary distance between them. As demonstrated in Figure 6, the phylogram generated here suggests some evolution history between arenaviruses and the TSA database hits and with some other viruses that act as phylogeny tree roots including some viruses from *Orthomyxoviridae*, *Bunyaviridae* and *Monoegavirales*. To clarify, the arenaviruses species locate in the middle of the tree between *Rhizopus oryzae* and *Channa punctate*, *Asymmetron lucayanum* and *Rhopilema esculentum*. The bootstrap shows some differences in values between the viruses including arenaviruses and the species found in the TSA, while the values are the same between the other viruses. For instance, the bootstrap values between the arenavirus related TSA sequences from *Channa punctate* and *Catostomus commersonii* are the same and each around 0.79, which could indicate an evolutionary relationship between them.

Discussion

The results of this study shown that when the viral RNA dependent RNA polymerase (L protein) of Tacaribe virus (TCRV), lymphocytic choriomeningitis virus (LCMV), Golden Gate virus (GGV) and California Academy of Science virus (CASV) were utilized for searching the translated nucleotides that are archived in GenBank in the Transcriptome Shotgun Assembly (TSA) database by tBLASTn, some distant homologues were found. The TSA database findings indicated sequences in six living species including *Channa punctate*, *Catostomus commersonii*, *Asymmetron lucayanum*, *Rhizopus oryzae*, *Rhopilema esculentum* and *Talitrus saltator* that have gene homology with the L polymerase of four species of arenavirus used for this study. When the translated proteins of these open reading frames (ORFs) from the TSA data were converted to amino acid sequences the translated proteins of the TSA database were found to have homology with the La Crosse Bunyavirus polymerase (5amr-A), Influenza C virus RNA-dependent RNA Polymerase (5d98-B) and with the L polymerase of vesicular stomatitis virus (5a22-A). Therefore, it was found that the L polymerase of some species of arenaviruses had significant TSA alignment with other species which indicates conserved genes among even distant arenaviruses.

Interestingly, phylogenetic tree alignment of all the protein sequences showed that the four arenavirus sequences located between *Rhopilema esculentum* at the distal end and *Talitrus saltator* at the bottom of the groups of the tree. The tree also shows that the translated protein of *Rhizopus oryzae* located between L polymerase of arenaviruses and the translated proteins of *Rhopilema esculentum* and *Asymmetron lucayanum*.

In summary, an unfiltered screen of the TSA database using conserved domains of known haemorrhagic mammarenaviruses and snake reptarenaviruses, revealed a number of homologies in different species in the database. It is not known if these sequences derive from viable replicating viruses but of the hits found several are unlikely as possible emerging viruses based on the hosts in which the sequences were found. Homologies found in *Rhizopus oryzae* (a fungus) are unlikely to be able to replicate in human cells despite this organism being an opportunistic pathogen. Similarly, sequences found in *Asymmetron lucayanum* (Amphioxides) are too distant to assume replication could occur in human cells. Initially, sequence homologies found in *Talitrus saltator* (a sand fly) might be considered as a possible arbovirus but this is unlikely as this is a non-human biting species so the opportunity for transmission is limited. However, protein sequence homologies found *Channa punctate* (fish), *Rhopilema esculentum* (jellyfish) and *Catostomus commersonii* (fish), could be plausible as components of viruses that at least had the opportunity to cause infection following human contact (by bite, sting and consumption respectively). These studies expand the range of possible viruses associated with new species and offer an indicator of their potential for human transmission. However, the study remains theoretical and experimental evidence for the viruses concerned and for pathogen transmission is yet to be confirmed.

More bioinformatics are recommended to find homology among arenaviruses and other sequences of living species that were archived in GenBank database, particularly from the rapidly growing transcriptome database, in order to monitor future outbreaks by viruses similar to arenaviruses. As a result of next generation sequencing the Transcriptome Shotgun Assembly (TSA) database is updated

continuously, adding more species were reptarenavirus infection could be present. Any homology found can be used to design primers capable of confirming such targets in the lab by cDNA synthesis from the tissues used for the TSA database to help prove the viruses concerned are extant. Only by more RT-PCR on tissue samples, more bioinformatics and more collaboration will the future work of this study be possible.

References

- Abba, Y., Hassim, H., Hamzah, H., Ibrahim, O.E., Ilyasu, Y., Bande, F., Mohd Lila, M.A., Noordin, M.M., 2016. In vitro isolation and molecular identification of reptarenavirus in Malaysia. *Virus Genes* **52**, 640–650.
- Abraham, J., Corbett, K.D., Farzan, M., Choe, H., Harrison, S.C., 2010. Structural basis for receptor recognition by New World hemorrhagic fever arenaviruses. *Nature Structural & Molecular Biology* **17**, 438–444.
- Abraham, J., Kwong, J.A., Albariño, C.G., Lu, J.G., Radoshitzky, S.R., Salazar-Bravo, J., Farzan, M., Spiropoulou, C.F., Choe, H., 2009. Host-Species Transferrin Receptor 1 Orthologs Are Cellular Receptors for Nonpathogenic New World Clade B Arenaviruses. *PLOS Pathogens* **5**, e1000358.
- Abudurexiti, A., Adkins, S., Alioto, D., Alkhovsky, S. V., Avšič-Županc, T., Ballinger, M.J., Bente, D.A., Beer, M., Bergeron, É., Blair, C.D., Briese, T., Buchmeier, M.J., Burt, F.J., Calisher, C.H., Cháng, C., Charrel, R.N., Choi, I.R., Clegg, J.C.S., de la Torre, J.C., de Lamballerie, X., Dèng, F., Di Serio, F., Digiario, M., Drebot, M.A., Duàn, X., Ebihara, H., Elbeaino, T., Ergünay, K., Fulhorst, C.F., Garrison, A.R., Gāo, G.F., Gonzalez, J.-P.J., Groschup, M.H., Günther, S., Haenni, A.-L., Hall, R.A., Hepojoki, J., Hewson, R., Hú, Z., Hughes, H.R., Jonson, M.G., Junglen, S., Klempa, B., Klingström, J., Kòu, C., Laenen, L., Lambert, A.J., Langevin, S.A., Liu, D., Lukashevich, I.S., Luò, T., Lǚ, C., Maes, P., de Souza, W.M., Marklewitz, M., Martelli, G.P., Matsuno, K., Mielke-Ehret, N., Minutolo, M., Mirazimi, A., Moming, A., Mühlbach, H.-P., Naidu, R., Navarro, B., Nunes, M.R.T., Palacios, G., Papa, A., Pauvolid-Corrêa, A., Pawęska, J.T., Qiáo, J., Radoshitzky, S.R., Resende, R.O., Romanowski, V., Sall, A.A., Salvato, M.S., Sasaya, T., Shěn, S., Shí, X., Shirako, Y., Simmonds, P., Sironi, M., Song, J.-W., Spengler, J.R., Stenglein, M.D., Sū, Z., Sūn, S., Táng, S., Turina, M., Wáng, B., Wáng, C., Wáng, H., Wáng, J., Wèi, T., Whitfield, A.E., Zerbini, F.M., Zhāng, J., Zhāng, L., Zhāng, Yànfāng, Zhang, Y.-Z., Zhāng, Yújiāng, Zhou, X., Zhū, L., Kuhn, J.H., 2019. Taxonomy of the order Bunyavirales: update 2019. *Archives of Virology* **164**, 1949–1965.
- Afonso, C.L., Tulman, E.R., Delhon, G., Lu, Z., Viljoen, G.J., Wallace, D.B., Kutish, G.F., Rock, D.L., 2006. Genome of Crocodilepox Virus. *Journal of Virology* **80**, 4978–4991.
- Ahne, W., Juhasz, A., 1995. In-Vitro Replication Of A Reptilian Adenovirus. *Veterinary Research* **26**, 443–448.
- Ahne, W., Thomsen, I., Winton, J., 1987. Isolation of a reovirus from the snake, *Python regius*. Brief report. *Archives of virology* **94**, 135–9.
- Al-Lazikani, B., Jung, J., Xiang, Z., Honig, B., 2001. Protein structure prediction. *Current Opinion in Chemical Biology* **5**, 51–56.
- Al-Mulla, H.M.N., Turrell, L., Smith, N.M., Payne, L., Baliji, S., Züst, R., Thiel, V., Baker, S.C., Siddell, S.G., Neuman, B.W., 2014. Competitive fitness in coronaviruses is not correlated with size or number of double-membrane

References

- vesicles under reduced-temperature growth conditions. *mBio* **5**, e01107-13.
- Almazán, F., González, J.M., Péntes, Z., Izeta, A., Calvo, E., Plana-Durán, J., Enjuanes, L., 2000. Engineering the largest RNA virus genome as an infectious bacterial artificial chromosome. *Proceedings of the National Academy of Sciences of the United States of America* **97**, 5516–21.
- Alvarez, C.P., Lasala, F., Carrillo, J., Muñiz, O., Corbí, A.L., Delgado, R., 2002. C-Type Lectins DC-SIGN and L-SIGN Mediate Cellular Entry by Ebola Virus in cis and in trans. *Journal of Virology* **76**, 6841–6844.
- Andrews, N.C., Fleming, M.D., Levy, J.E., 1999. Molecular insights into mechanisms of iron transport. *Current Opinion in Hematology* **6**.
- Angelini, M.M., Akhlaghpour, M., Neuman, B.W., Buchmeier, M.J., 2013. Severe Acute Respiratory Syndrome Coronavirus Nonstructural Proteins 3, 4, and 6 Induce Double-Membrane Vesicles. *mBio* **4**, e00524-13.
- Anonymous, 2008. Aquatic Animal Health Code. Office International des Epizooties.
- Aqrawi, T., Stohr, A.C., Knauf-Witzens, T., Kregel, A., Heckers, K.O., Marschang, R.E., 2015. Identification of snake arenaviruses in live boas and pythons in a zoo in Germany. *Tierärztliche Praxis. Ausgabe K, Kleintiere/Heimtiere* **43**, 239–247.
- Ariel, E., 2011. Viruses in reptiles. *Veterinary Research* **42**, 100.
- Ariel, E., Holopainen, R., Olesen, N.J., Tapiovaara, H., 2010. Comparative study of ranavirus isolates from cod (*Gadus morhua*) and turbot (*Psetta maxima*) with reference to other ranaviruses. *Archives of Virology* **155**, 1261–1271.
- Ariel, E., Nicolajsen, N., Christophersen, M.-B., Holopainen, R., Tapiovaara, H., Bang Jensen, B., 2009. Propagation and isolation of ranaviruses in cell culture. *Aquaculture* **294**, 159–164.
- Armesto, M., Cavanagh, D., Britton, P., 2009. The Replicase Gene of Avian Coronavirus Infectious Bronchitis Virus Is a Determinant of Pathogenicity. *PLOS ONE* **4**, e7384.
- Armesto, M., Evans, S., Cavanagh, D., Abu-Median, A.-B., Keep, S., Britton, P., 2011. A Recombinant Avian Infectious Bronchitis Virus Expressing a Heterologous Spike Gene Belonging to the 4/91 Serotype. *PLOS ONE* **6**, e24352.
- Armstrong, C., Lillie, R.D., 1934. Experimental Lymphocytic Choriomeningitis of Monkeys and Mice Produced by a Virus Encountered in Studies of the 1933 St. Louis Encephalitis Epidemic. *Public Health Reports (1896-1970)* **49**, 1019–1027.
- Auperin, D.D., Compans, R.W., Bishop, D.H.L., 1982. Nucleotide sequence conservation at the 3' termini of the virion RNA species of new World and Old World arenaviruses. *Virology* **121**, 200–203.
- Ávila-Pérez, G., Rejas, M.T., Rodríguez, D., 2016. Ultrastructural characterization of membranous torovirus replication factories. *Cellular Microbiology* **18**, 1691–1708.
- Baliji, S., Cammer, S.A., Sobral, B., Baker, S.C., 2009. Detection of Nonstructural Protein 6 in Murine Coronavirus-Infected Cells and Analysis of the Transmembrane Topology by Using Bioinformatics and Molecular Approaches.

References

- Journal of Virology* **83**, 6957–6962.
- Barajas, D., Martín, I.F. de C., Pogany, J., Risco, C., Nagy, P.D., 2014. Noncanonical Role for the Host Vps4 AAA+ ATPase ESCRT Protein in the Formation of Tomato Bushy Stunt Virus Replicase. *PLOS Pathogens* **10**, e1004087.
- Barlough, J.E., Matson, D.O., Skilling, D.E., Berke, T., Berry, E.S., Brown, R.F., Smith, A.W., 1998. Isolation Of Reptilian Calicivirus Crotalus Type 1 From Feral Pinnipeds. *Journal of Wildlife Diseases* **34**, 451–456.
- Barrera, O.J., KT Jr, M., 1991. Toward a vaccine against Argentine hemorrhagic fever. *Bull Pan Am Health Organ* **25**, 118–126.
- Beachboard, D.C., Anderson-Daniels, J.M., Denison, M.R., 2015. Mutations across Murine Hepatitis Virus nsp4 Alter Virus Fitness and Membrane Modifications. *Journal of Virology* **89**, 2080–2089.
- Beachboard, D.C., Lu, X., Baker, S.C., Denison, M.R., 2013. Murine hepatitis virus nsp4 N258T mutants are not temperature-sensitive. *Virology* **435**, 210–213.
- Bedossa, P., Ferlicot, S., Paradis, V., Dargère, D., Bonvoust, F., Vidaud, M., 2002. Dystroglycan Expression in Hepatic Stellate Cells: Role in Liver Fibrosis. *Laboratory Investigation* **82**, 1053–1061.
- Belov, G.A., Nair, V., Hansen, B.T., Hoyt, F.H., Fischer, E.R., Ehrenfeld, E., 2012. Complex Dynamic Development of Poliovirus Membranous Replication Complexes. *Journal of Virology* **86**, 302–312.
- Benkö, M., Harrach, B., Both, G., Russell, W., Adair, B., Adám, E., de Jong, J., Hess, M., Johnson, M., Kajon A, et al, 2005. *Virus Taxonomy*, VIIIth Rep. ed. Elsevier, New York.
- Benyeda, Z., Mató, T., Süveges, T., Szabó, É., Kardi, V., Abonyi-Tóth, Z., Rusvai, M., Palya, V., 2009. Comparison of the pathogenicity of QX-like, M41 and 793/B infectious bronchitis strains from different pathological conditions. *Avian Pathology* **38**, 449–456.
- Bernardi, R., Papa, A., Pandolfi, P.P., 2008. Regulation of apoptosis by PML and the PML-NBs. *Oncogene* **27**, 6299.
- Beyer, W.R., Pöppelau, D., Garten, W., von Laer, D., Lenz, O., 2003. Endoproteolytic processing of the lymphocytic choriomeningitis virus glycoprotein by the subtilase SKI-1/S1P. *Journal of Virology* **77**, 2866–2872.
- Bicknese, E.J., Childress, A.L., Wellehan, J.F.X., 2010. A Novel Herpesvirus of the Proposed Genus Chelonivirus from an Asymptomatic Bowsprit Tortoise (*Chersina angulata*). *Journal of Zoo and Wildlife Medicine* **41**, 353–358.
- Bienz, K., Egger, D., Pfister, T., Troxler, M., 1992. Structural and functional characterization of the poliovirus replication complex. *Journal of Virology* **66**, 2740–7.
- Bijlenga, G., Cook, J.K.A., Gelb, Jr, J., Wit, J.J. de, 2004. Development and use of the H strain of avian infectious bronchitis virus from the Netherlands as a vaccine: a review. *Avian Pathology* **33**, 550–557.
- Bishop, D.H.L., 1990. Arenaviruses and their replication. In: *Virology*. Raven Press, New York, pp. 1231–1243.

References

- Blahak, S., 1995. Isolation and characterization of paramyxoviruses from snakes and their relationship to avian paramyxoviruses. *Journal of Veterinary Medicine* **42**, 216–24.
- Blazewicz, J., Frohberg, W., Kierzyńska, M., Wojciechowski, P., 2013. G-MSA - A GPU-based, fast and accurate algorithm for multiple sequence alignment. *Journal of Parallel and Distributed Computing* **73**, 32–41.
- Bodewes, R., Kik, M.J.L., Stalin Raj, V., Schapendonk, C.M.E., Haagmans, B.L., Smits, S.L., Osterhaus, A.D.M.E., 2013. Detection of novel divergent arenaviruses in boid snakes with inclusion body disease in the Netherlands. *Journal of General Virology* **94**, 1206–1210.
- Bonthuis, D.J., 2012. Lymphocytic Choriomeningitis Virus: An Underrecognized Cause of Neurologic Disease in the Fetus, Child, and Adult. *Seminars in Pediatric Neurology* **19**, 89–95.
- Borden, K.L.B., Campbell Dwyer, E.J., Salvato, M.S., 1998. An Arenavirus RING (Zinc-Binding) Protein Binds the Oncoprotein Promyelocyte Leukemia Protein (PML) and Relocates PML Nuclear Bodies to the Cytoplasm. *Journal of Virology* **72**, 758–766.
- Borrow, P., Oldstone, M.B.A., 1994. Mechanism of Lymphocytic Choriomeningitis Virus Entry into Cells. *Virology* **198**, 1–9.
- Bowden, T.A., Crispin, M., Graham, S.C., Harvey, D.J., Grimes, J.M., Jones, E.Y., Stuart, D.I., 2009. Unusual Molecular Architecture of the Machupo Virus Attachment Glycoprotein. *Journal of Virology* **83**, 8259–8265.
- Bowen, G.S., 1977. Prolonged western equine encephalitis viremia in the Texas tortoise (*Gopherus berlandieri*). *The American Journal of Tropical Medicine and Hygiene* **26**, 171–5.
- Bowen, M.D., Peters, C.J., Nichol, S.T., 1996. The phylogeny of New World (Tacaribe complex) arenaviruses. *Virology* **219**, 285–290.
- Briese, T., Paweska, J.T., McMullan, L.K., Hutchison, S.K., Street, C., Palacios, G., Khristova, M.L., Weyer, J., Swanepoel, R., Egholm, M., Nichol, S.T., Lipkin, W.I., 2009. Genetic Detection and Characterization of Lujo Virus, a New Hemorrhagic Fever–Associated Arenavirus from Southern Africa. *PLOS Pathogens* **5**, e1000455.
- Briknarová, K., Thomas, C.J., York, J., Nunberg, J.H., 2011. Structure of a Zinc-binding Domain in the Junín Virus Envelope Glycoprotein. *The Journal of Biological Chemistry* **286**, 1528–1536.
- Brindley, M.A., Hunt, C.L., Kondratowicz, A.S., Bowman, J., Sinn, P.L., McCray, P.B., Quinn, K., Weller, M.L., Chiorini, J.A., Maury, W., 2011. Tyrosine kinase receptor Axl enhances entry of Zaire ebolavirus without direct interactions with the viral glycoprotein. *Virology* **415**, 83–94.
- Brunotte, L., Kerber, R., Shang, W., Hauer, F., Hass, M., Gabriel, M., Lelke, M., Busch, C., Stark, H., Svergun, D.I., Betzel, C., Perbandt, M., Günther, S., 2011a. Structure of the Lassa Virus Nucleoprotein Revealed by X-ray Crystallography, Small-angle X-ray Scattering, and Electron Microscopy. *The Journal of Biological Chemistry* **286**, 38748–38756.
- Brunotte, L., Lelke, M., Hass, M., Kleinstüber, K., Becker-Ziaja, B., Günther, S.,

References

- 2011b. Domain Structure of Lassa Virus L Protein. *Journal of Virology* **85**, 324–333.
- Buchmeier, M.J., 2002. Arenaviruses: Protein Structure and Function BT. In: Oldstone, M.B.A. (Ed.), *Arenaviruses I: The Epidemiology, Molecular and Cell Biology of Arenaviruses*. Springer Berlin Heidelberg, Berlin, Heidelberg, pp. 159–173.
- Buchmeier, M.J., de la Torre, J.C., Peters, C.J., 2007. Arenaviridae: the viruses and their replication. In: *Fields Virology*. Lippincott- Raven, Philadelphia, pp. 1791–1828.
- Buchmeier, M.J., Parekh, B.S., 1987. Protein Structure and Expression Among Arenaviruses. In: Oldstone, M.B.A. (Ed.), *Arenaviruses: Genes, Proteins, and Expression*. Springer Berlin Heidelberg, Berlin, Heidelberg, pp. 41–57.
- Buenviaje, G.N., Ladds, P.W., Melville, L., 1992. Poxvirus infection in two crocodiles. *Australian Veterinary Journal* **69**, 15–16.
- Bui, H.H., Botten, J., Fussedder, N., Pasquetto, V., Mothe, B., Buchmeier, M.J., Sette, A., 2007. Protein sequence database for pathogenic arenaviruses. *Immunome Research* **3**, 1–8.
- Cabanillas, L., Arribas, M., Lázaro, E., 2013. Evolution at increased error rate leads to the coexistence of multiple adaptive pathways in an RNA virus. *BMC Evolutionary Biology* **13**, 11.
- Cajimat, M.N.B., Milazzo, M.L., Borchert, J.N., Abbott, K.D., Bradley, R.D., Fulhorst, C.F., 2008. Diversity among Tacaribe serocomplex viruses (family Arenaviridae) naturally associated with the Mexican woodrat (*Neotoma mexicana*). *Virus Research* **133**, 211–217.
- Cajimat, M.N.B., Milazzo, M.L., Bradley, R.D., Fulhorst, C.F., 2007. Catarina Virus , an Arenaviral Species Principally Associated with *Neotoma micropus* (Southern Plains Woodrat) in Texas. *The American Society of Tropical Medicine and Hygiene* **77**, 732–736.
- Caliendo, A.M., Ingersoll, J., Green, A.M., Nolte, F.S., Easley, K.A., 2004. Comparison of the sensitivities and viral load values of the AMPLICOR HIV-1 MONITOR version 1.0 and 1.5 tests. *Journal of Clinical Microbiology* **42**, 5392–5393.
- Calisher, C.H., Tzianabos, T., Lord, R.D., Coleman, P.H., 1970. Tamiami Virus, a New Member of the Tacaribe Group. *The American Journal of Tropical Medicine and Hygiene* **19**.
- Campbell Dwyer, E.J., Lai, H., MacDonald, R.C., Salvato, M.S., Borden, K.L.B., 2000. The Lymphocytic Choriomeningitis Virus RING Protein Z Associates with Eukaryotic Initiation Factor 4E and Selectively Represses Translation in a RING-Dependent Manner. *Journal of Virology* **74**, 3293–3300.
- Cao, W., Henry, M.D., Borrow, P., Yamada, H., Elder, J.H., Ravkov, E. V, Nichol, S.T., Compans, R.W., Campbell, K.P., Oldstone, M.B.A., 1998. Identification of α -Dystroglycan as a Receptor for Lymphocytic Choriomeningitis Virus and Lassa Fever Virus. *Science* **282**, 2079–2081.
- Carey, D.E., Kemp, G.E., White, H.A., Pinneo, L., Addy, R.F., Fom, A.L.M.D., Stroh, G., Casals, J., Henderson, B.E., 1972. Lassa fever Epidemiological aspects of

References

- the 1970 epidemic, Jos, Nigeria. *Transactions of the Royal Society of Tropical Medicine and Hygiene* **66**, 402–408.
- Carlisle-Nowak, M.S., Sullivan, N., Carrigan, M., Knight, C., Ryan, C., Jacobson, E.R., 1998. Inclusion body disease in two captive Australian pythons (*Morelia spilota variegata* and *Morelia spilota spilota*). *Australian Veterinary Journal* **76**, 98–100.
- Carlton, M., Gillespie, R., Garver, J., Draguljic, D., Vela, E.M., 2012. The Syrian golden hamster as a model to study Flexal virus pathogenesis. *Archives of Clinical Microbiology* **3**, 1–9.
- Carnec, X., Baize, S., Reynard, S., Diancourt, L., Caro, V., Tordo, N., Bouloy, M., 2011. Lassa Virus Nucleoprotein Mutants Generated by Reverse Genetics Induce a Robust Type I Interferon Response in Human Dendritic Cells and Macrophages. *Journal of Virology* **85**, 12093–12097.
- Casabona, J.C., Levingston Macleod, J.M., Loureiro, M.E., Gomez, G.A., Lopez, N., 2009. The RING Domain and the L79 Residue of Z Protein Are Involved in both the Rescue of Nucleocapsids and the Incorporation of Glycoproteins into Infectious Chimeric Arenavirus-Like Particles. *Journal of Virology* **83**, 7029–7039.
- Casais, R., Dove, B., Cavanagh, D., Britton, P., 2003. Recombinant avian infectious bronchitis virus expressing a heterologous spike gene demonstrates that the spike protein is a determinant of cell tropism. *Journal of Virology* **77**, 9084–9.
- Casais, R., Thiel, V., Siddell, S.G., Cavanagh, D., Britton, P., 2001. Reverse Genetics System for the Avian Coronavirus Infectious Bronchitis Virus. *Journal of Virology* **75**, 12359–12369.
- Causey, O.R., Shope, R.E., Bensabath, G., 1966. Marco, Timbo, and Chaco, newly recognized arboviruses from lizards of Brazil. *The American Journal of Tropical Medicine and Hygiene* **15**, 239–43.
- Cavanagh, D., Davis, P.J., Pappin, D.J., Binns, M.M., Bournsnel, M.E., Brown, T.D., 1986. Coronavirus IBV: partial amino terminal sequencing of spike polypeptide S2 identifies the sequence Arg-Arg-Phe-Arg-Arg at the cleavage site of the spike precursor polypeptide of IBV strains Beaudette and M41. *Virus Research* **4**, 133–43.
- Černý, J., Černá Bolfíková, B., Valdés, J.J., Grubhoffer, L., Růžek, D., 2014. Evolution of Tertiary Structure of Viral RNA Dependent Polymerases. *PLOS ONE* **9**, e96070.
- Chang, L.-W., Fu, A., Wozniak, E., Chow, M., Duke, D.G., Green, L., Kelley, K., Hernandez, J.A., Jacobson, E.R., 2013. Immunohistochemical Detection of a Unique Protein within Cells of Snakes Having Inclusion Body Disease, a World-Wide Disease Seen in Members of the Families Boidae and Pythonidae. *PLOS ONE* **8**, e82916.
- Chang, L.-W., Jacobson, E.R., 2010. Inclusion Body Disease, A Worldwide Infectious Disease of Boid Snakes: A Review. *Journal of Exotic Pet Medicine* **19**, 216–225.
- Chang, L., Fu, D., Stenglein, M.D., Hernandez, J.A., DeRisi, J.L., Jacobson, E.R., 2016. Detection and prevalence of boid inclusion body disease in collections of boas and pythons using immunological assays. *Veterinary Journal* **218**, 13–18.

References

- Chao, T.-Y., Raines, R.T., 2011. Mechanism of Ribonuclease A Endocytosis: Analogies to Cell-Penetrating Peptides. *Biochemistry* **50**, 8374–8382.
- Charrel, R.N., de Lamballerie, X., Emonet, S., 2008. Phylogeny of the genus Arenavirus. *Current Opinion in Microbiology* **11**, 362–368.
- Charrel, R.N., Feldmann, H., Fulhorst, C.F., Khelifa, R., Chesse, R. de, Lamballerie, X. de, 2002. Phylogeny of New World arenaviruses based on the complete coding sequences of the small genomic segment identified an evolutionary lineage produced by intrasegmental recombination. *Biochemical and Biophysical Research Communications* **296**, 1118–1124.
- Charrel, R.N., Lemasson, J.J., Garbutt, M., Khelifa, R., De Micco, P., Feldmann, H., De Lamballerie, X., 2003. New insights into the evolutionary relationships between arenaviruses provided by comparative analysis of small and large segment sequences. *Virology* **317**, 191–196.
- Chen, B.J., Lamb, R.A., 2008. Mechanisms for enveloped virus budding: Can some viruses do without an ESCRT? *Virology* **372**, 221–232.
- Cheng, Y., Zak, O., Aisen, P., Harrison, S.C., Walz, T., 2004. Structure of the Human Transferrin Receptor-Transferrin Complex. *Cell* **116**, 565–576.
- Clark, H.F., Karzon, D.T., 1972. Iguana Virus, a Herpes-Like Virus Isolated from Cultured Cells of a Lizard, Iguana iguana. *Infection and Immunity* **5**, 559–569.
- Clegg, J.C., 2002. Molecular phylogeny of the arenaviruses. In: *Arenaviruses I: The Epidemiology, Molecular and Cell Biology of Arenaviruses*. pp. 262, 1–24.
- Clements, D.N., Vaughan-Thomas, A., Peansukmanee, S., Carter, S.D., Innes, J.F., Ollier, W.E.R., Clegg, P.D., 2006. Assessment of the use of RNA quality metrics for the screening of articular cartilage specimens from clinically normal dogs and dogs with osteoarthritis. *American Journal of Veterinary Research* **67**, 1438–1444.
- Clementz, M.A., Kanjanahaluethai, A., O'Brien, T.E., Baker, S.C., 2008. Mutation in murine coronavirus replication protein nsp4 alters assembly of double membrane vesicles. *Virology* **375**, 118–129.
- Coimbra, T.L.M., Nassar, E.S., Burattini, M.N., de Souza, L.T.M., Ferreira, I.B., Rocco, I.M., Travassos da Rosa, A.P.A., Vasconcelos, P.F.C., Pinheiro, F.P., LeDuc, J.W., Rico-Hesse, R., Gonzalez, J.-P., Jahrling, P.B., Tesh, R.B., 1994. New arenavirus isolated in Brazil. *Lancet* **343**, 391–392.
- Cook, J.K., Darbyshire, J.H., Peters, R.W., 1976. The use of chicken tracheal organ cultures for the isolation and assay of avian infectious bronchitis virus. *Archives of Virology* **50**, 109–18.
- Cook, J.K., Orbell, S.J., Woods, M.A., Huggins, M.B., 1996. A survey of the presence of a new infectious bronchitis virus designated 4/91 (793B). *The Veterinary Record* **138**, 178–80.
- Cook, J.K.A., Jackwood, M., Jones, R.C., 2012. The long view: 40 years of infectious bronchitis research. *Avian Pathology* **41**, 239–250.
- Corcoran, J.A., Duncan, R., 2004. Reptilian Reovirus Utilizes a Small Type III Protein with an External Myristylated Amino Terminus To Mediate Cell-Cell Fusion. *Journal of Virology* **78**, 4342–4351.
- Cordey, S., Sahli, R., Moraz, M.-L., Estrade, C., Morandi, L., Cherpillod, P., Charrel,

References

- R.N., Kunz, S., Kaiser, L., 2011. Analytical validation of a lymphocytic choriomeningitis virus real-time RT-PCR assay. *Journal of Virological Methods* **177**, 118–122.
- Cornu, T.I., de la Torre, J.C., 2001. RING Finger Z Protein of Lymphocytic Choriomeningitis Virus (LCMV) Inhibits Transcription and RNA Replication of an LCMV S-Segment Minigenome. *Journal of Virology* **75**.
- Cortese, M., Goellner, S., Acosta, E.G., Neufeldt, C.J., Oleksiuk, O., Lampe, M., Haselmann, U., Funaya, C., Schieber, N., Ronchi, P., Schorb, M., Pruunsild, P., Schwab, Y., Chatel-Chaix, L., Ruggieri, A., Bartenschlager, R., 2017. Ultrastructural Characterization of Zika Virus Replication Factories. *Cell Reports* **18**, 2113–2123.
- Cosset, F.-L., Marianneau, P., Verney, G., Gallais, F., Tordo, N., Pécheur, E.-I., ter Meulen, J., Deubel, V., Bartosch, B., 2009. Characterization of Lassa Virus Cell Entry and Neutralization with Lassa Virus Pseudoparticles. *Journal of Virology* **83**, 3228–3237.
- Cottam, E.M., Maier, H.J., Manifava, M., Vaux, L.C., Chandra-Schoenfelder, P., Gerner, W., Britton, P., Ktistakis, N.T., Wileman, T., 2011. Coronavirus nsp6 proteins generate autophagosomes from the endoplasmic reticulum via an omegasome intermediate. *Autophagy* **7**, 1335–1347.
- Cupp, E.W., Zhang, D., Yue, X.I.N., Cupp, M.S., Guyer, C., Sprenger, T.R., Unnasch, T.R., 2004. Identification Of Reptilian And Amphibian Blood Meals From Mosquitoes In An Eastern Equine Encephalomyelitis Virus Focus In Central Alabama. *The American Journal of Tropical Medicine and Hygiene* **71**, 272–276.
- D'Amato, A.F., Moraes-Neto, M., 2000. First documentation of fibropapillomas verified by histopathology in *Eretmochelys imbricata*. *Marine Turtle Newsletter* 12–13.
- Darbyshire, J.H., Rowell, J.G., Cook, J.K., Peters, R.W., 1979. Taxonomic studies on strains of avian infectious bronchitis virus using neutralisation tests in tracheal organ cultures. *Archives of Virology* **61**, 227–38.
- Davelaar, F.G., Kouwenhoven, B., Burger, A.G., 1984. Occurrence and significance of infectious bronchitis virus variant strains in egg and broiler production in the Netherlands. *The Veterinary quarterly* **6**, 114–20.
- David-Ferreira, J.F., Manaker, R.A., 1965. An electron microscope study of the development of a mouse hepatitis virus in tissue culture cells. *The Journal of Cell Biology* **24**, 57–78.
- Davies, H.A., 1999. General Preparation of Material and Staining of Sections. In: *Electron Microscopy Methods and Protocols*. Humana Press, New Jersey, pp. 1–12.
- Davison, A.J., Harrach, B., 2011. Siadenovirus. In: Tidona, C., Darai, G. (Eds.), *The Springer Index of Viruses*. Springer New York, New York, NY, pp. 49–56.
- de Farias, S.T., dos Santos Junior, A.P., Rêgo, T.G., José, M. V, 2017. Origin and Evolution of RNA-Dependent RNA Polymerase. *Frontiers in Genetics* **8**, 125.
- De La Torre, J.C., 2009. Molecular and cell biology of the prototypic arenavirus LCMV: Implications for understanding and combating hemorrhagic fever

References

- arenaviruses. *Annals of the New York Academy of Sciences*.
- De Voe, R., Geissler, K., Elmore, S., Rotstein, D., Lewbart, G., Guy, J., 2004. Ranavirus-Associated Morbidity And Mortality In A Group Of Captive Eastern Box Turtles (*Terrapene Carolina Carolina*). *Journal of Zoo and Wildlife Medicine* **35**, 534–543.
- de Wilde, A.H., Raj, V.S., Oudshoorn, D., Bestebroer, T.M., van Nieuwkoop, S., Limpens, R.W.A.L., Posthuma, C.C., van der Meer, Y., Barcena, M., Haagmans, B.L., Snijder, E.J., van den Hoogen, B.G., 2013. MERS-coronavirus replication induces severe in vitro cytopathology and is strongly inhibited by cyclosporin A or interferon- treatment. *Journal of General Virology* **94**, 1749–1760.
- de Wit, J.J., Nieuwenhuisen-van Wilgen, J., Hoogkamer, A., van de Sande, H., Zuidam, G.J., Fabri, T.H.F., 2011. Induction of cystic oviducts and protection against early challenge with infectious bronchitis virus serotype D388 (genotype QX) by maternally derived antibodies and by early vaccination. *Avian Pathology* **40**, 463–471.
- Delgado, S., Erickson, B.R., Agudo, R., Blair, P.J., Vallejo, E., Albariño, C.G., Vargas, J., Comer, J.A., Rollin, P.E., Ksiazek, T.G., Olson, J.G., Nichol, S.T., 2008. Chapare Virus, a Newly Discovered Arenavirus Isolated from a Fatal Hemorrhagic Fever Case in Bolivia. *PLOS Pathogens* **4**, e1000047.
- Demby, A.H., Chamberlain, J., Brown, D.W.G., Clegg, C.S., 1994. Early diagnosis of Lassa fever by reverse transcription-PCR. *Journal of Clinical Microbiology* **32**, 2898–903.
- den Boon, J.A., Ahlquist, P., 2010. Organelle-Like Membrane Compartmentalization of Positive-Strand RNA Virus Replication Factories. *Annual Review of Microbiology* **64**, 241–256.
- Denison, M.R., 2008. Seeking Membranes: Positive-Strand RNA Virus Replication Complexes. *PLOS Biology* **6**, e270.
- Diaz, A., Zhang, J., Ollwerther, A., Wang, X., Ahlquist, P., 2015. Host ESCRT Proteins Are Required for Bromovirus RNA Replication Compartment Assembly and Function. *PLOS Pathogens* **11**, e1004742.
- Doerflinger, S.Y., Cortese, M., Romero-Brey, I., Menne, Z., Tubiana, T., Schenk, C., White, P.A., Bartenschlager, R., Bressanelli, S., Hansman, G.S., Lohmann, V., 2017. Membrane alterations induced by nonstructural proteins of human norovirus. *PLOS Pathogens* **13**, e1006705.
- Dolnik, O., Kolesnikova, L., Stevermann, L., Becker, S., 2010. Tsg101 Is Recruited by a Late Domain of the Nucleocapsid Protein To Support Budding of Marburg Virus-Like Particles . *Journal of Virology* **84**, 7847–7856.
- Dolz, R., Vergara-Alert, J., Pérez, M., Pujols, J., Majó, N., 2012. New insights on infectious bronchitis virus pathogenesis: characterization of Italy 02 serotype in chicks and adult hens. *Veterinary Microbiology* **156**, 256–264.
- Domanska-Blicharz, K., Lisowska, A., Minta, Z., Jatczak, J., Mamczur, J., 2012. D1466-like genotype of infectious bronchitis virus responsible for a new epidemic in chickens in Poland. *Veterinary Record* **171**, 351.1-351.
- Downs, W.G., Anderson, C.R., Spence, L., Aitken, T.H.G., Greenhall, A.H., 1963.

References

- Tacaribe Virus, a New Agent Isolated from Artibeus Bats and Mosquitoes in Trinidad, West Indies*. *The American Journal of Tropical Medicine and Hygiene* **12**.
- Drosten, C., Götting, S., Schilling, S., Asper, M., Panning, M., Schmitz, H., Günther, S., 2002. Rapid Detection and Quantification of RNA of Ebola and Marburg Viruses , Lassa Virus , Crimean-Congo Hemorrhagic Fever Virus , Rift Valley Fever Virus , Dengue Virus , and Yellow Fever Virus by Real-Time Reverse Transcription-PCR. *Journal of Clinical Microbiology* **40**, 2323–2330.
- Drury, S.E., Gough, R.E., McArthur, S.D., 2001. Detection and isolation of a flavivirus-like agent from a leopard tortoise (*Geochelone pardalis*) in the United Kingdom. *The Veterinary Record* **148**, 452.
- Edgar, R.C., 2004. MUSCLE: multiple sequence alignment with high accuracy and high throughput. *Nucleic Acids Research* **32**, 1792–7.
- Ehichioya, D.U., Hass, M., Ölschläger, S., Becker-Ziaja, B., Onyebuchi Chukwu, C.O., Coker, J., Nasidi, A., Ogugua, O.O., Günther, S., Omilabu, S.A., 2010. Lassa fever, Nigeria, 2005-2008. *Emerging Infectious Diseases* **16**, 1040–1041.
- Eichler, R., Lenz, O., Garten, W., Strecker, T., 2006. The role of single N-glycans in proteolytic processing and cell surface transport of the Lassa virus glycoprotein GP-C. *Virology Journal* **3**, 41.
- Eichler, R., Lenz, O., Strecker, T., Eickmann, M., Klenk, H.-D., Garten, W., 2003. Identification of Lassa virus glycoprotein signal peptide as a trans-acting maturation factor. *EMPO Reports* **4**, 3–9.
- Eichler, R., Lenz, O., Strecker, T., Eickmann, M., Klenk, H.D., Garten, W., 2004. Lassa Virus Glycoprotein Signal Peptide Displays a Novel Topology with an Extended Endoplasmic Reticulum Luminal Region. *Journal of Biological Chemistry* **279**, 12293–12299.
- Emonet, S.F., de la Torre, J.C., Domingo, E., Sevilla, N., 2009. Arenavirus genetic diversity and its biological implications. *Infection, Genetics and Evolution* **9**, 417–429.
- Fan, L., Briese, T., Lipkin, W.I., 2009. Z Proteins of New World Arenaviruses Bind RIG-I and Interfere with Type I Interferon Induction. *Journal of Virology* **84**, 1785–1791.
- Fang, S.G., Shen, S., Tay, F.P.L., Liu, D.X., 2005. Selection of and recombination between minor variants lead to the adaptation of an avian coronavirus to primate cells. *Biochemical and Biophysical Research Communications* **336**, 417–423.
- Farfán-Ale, J.A., Blitvich, B.J., Marlenee, N.L., Loroño-Pino, M.A., Puerto-Manzano, F., García-Rejón, J.E., Rosado-Paredes, E.P., Flores-Flores, L.F., Ortega-Salazar, A., Chávez-Medina, J., Cremieux-Grimaldi, J.C., Correa-Morales, F., Hernández-Gaona, G., Méndez-Galván, J.F., Beaty, B.J., 2006. Antibodies to West Nile virus in asymptomatic mammals, birds, and reptiles in the Yucatan Peninsula of Mexico. *The American Journal of Tropical Medicine and Hygiene* **74**, 908–14.
- Farkas, S.L., Gál, J., 2009. Adenovirus and mycoplasma infection in an ornate box turtle (*Terrapene ornata ornata*) in Hungary. *Veterinary Microbiology* **138**, 169–

173.

- Farrell, R.E., 2017. Chapter 3 - RNA Isolation Strategies. Academic Press.
- Fehling, S.K., Lennartz, F., Strecker, T., 2012. Multifunctional nature of the arenavirus RING finger protein Z. *Viruses* **4**, 2973–3011.
- Ferraris, P., Beaumont, E., Uzbekov, R., Brand, D., Gaillard, J., Blanchard, E., Roingeard, P., 2013. Sequential biogenesis of host cell membrane rearrangements induced by hepatitis C virus infection. *Cellular and Molecular Life Sciences* **70**, 1297–1306.
- Fichet-Calvet, E., Rogers, D.J., 2009. Risk maps of lassa fever in West Africa. *PLOS Neglected Tropical Diseases* **3**.
- Fields, B.N., Knipe, D.M., Howley, P.M., 2013. Arenaviridae: the viruses and their replication. In: *Fields Virology*. Raven Press, New York.
- Flanagan, M.L., Oldenburg, J., Reignier, T., Holt, N., Hamilton, G.A., Martin, V.K., Cannon, P.M., 2008. New World Clade B Arenaviruses Can Use Transferrin Receptor 1 (TfR1)-Dependent and -Independent Entry Pathways, and Glycoproteins from Human Pathogenic Strains Are Associated with the Use of TfR1. *Journal of Virology* **82**, 938–948.
- Fleige, S., Walf, V., Huch, S., Prgomet, C., Sehm, J., Pfaffl, M.W., 2006. Comparison of relative mRNA quantification models and the impact of RNA integrity in quantitative real-time RT-PCR. *Biotechnology Letters* **28**, 1601–1613.
- Fleming, G.J., Heard, D.J., Jacobson, E.R., Buergelt, C., 2018. Cytoplasmic Inclusions in Corn Snakes, *Elaphe guttata*, Resembling Inclusion Body Disease of Boid Snakes. *Journal of Herpetological Medicine and Surgery* **13**, 18–22.
- Flint, S.J., E.W., R.V.R., K.M., A.M., S., 2000. Principles of Virology. Washington, D.C.
- Foley, A.M., Schroeder, B.A., Redlow, A.E., Fick-Child, K.J., Teas, W.G., 2005. Fibropapillomatosis In Stranded Green Turtles (*Chelonia Mydas*) From The Eastern United States (1980–98): Trends And Associations With Environmental Factors. *Journal of Wildlife Diseases* **41**, 29–41.
- Fölsch, D.W., Leloup, P., 1976. [Fatal endemic infection in a serpentarium. Diagnosis, treatment and preventive measures]. *Tierärztliche Praxis* **4**, 527–36.
- Frame, J.D., Baldwin, J.M., Gocke, D.J., Troup, J.M., Baldwin, J.M., Troup, J.M., 1970. Lassa Fever, a New Virus Disease of Man from West Africa. *The American Journal of Tropical Medicine and Hygiene* **19**, 670–676.
- Franke, J., Essbauer, S., Ahne, W., Blahak, S., 2001. Identification and molecular characterization of 18 paramyxoviruses isolated from snakes. *Virus Research* **80**, 67–74.
- Franke, T.F., 2008. Intracellular Signaling by Akt: Bound to Be Specific. *Science Signaling* **1**, pe29 LP-pe29.
- Freed, E.O., 2002. Viral Late Domains. *Journal of Virology* **76**, 4679–4687.
- Freed, E.O., 2003. The HIV-TSG101 interface: Recent advances in a budding field. *Trends in Microbiology* **11**, 56–59.
- Frye, F.L., Munn, R.J., Gardner, M., Barten, S.L., Hadfy, L.B., 1994. Adenovirus-like

References

- Hepatitis in a Group of Related Rankin's Dragon Lizards (*Pogona henrylawsoni*). *Journal of Zoo and Wildlife Medicine* **25**, 167–171.
- Fulhorst, C.F., Bennett, S.G., Milazzo, M.L., Murray, H.L., Webb, J.P., Cajimat, M.N.B., Bradley, R.D., 2002. Bear Canyon Virus: An Arenavirus Naturally Associated with the California Mouse (*Peromyscus californicus*). *Emerging Infectious Diseases* **8**, 717–721.
- Fulhorst, C.F., Bowen, M.D., Ksiazek, T.G., Rollin, P.E., Nichol, S.T., Kosoy, M.Y., Peters, C.J., 1996. Isolation and Characterization of Whitewater Arroyo Virus, a Novel North American Arenavirus. *Virology* **224**, 114–120.
- Fulhorst, C.F., Bowen, M.D., Salas, R.A., De Manzione, N.M.C., Duno, G., Utrera, A., Ksiazek, T.G., Peters, C.J., Nichol, S.T., De Miller, E., Tovar, D., Ramos, B., Vasquez, C., Tesh, R.B., 1997. Isolation and Characterization of Pirital Virus, a Newly Discovered South American Arenavirus. *The American Journal of Tropical Medicine and Hygiene* **56**.
- Gadlage, M.J., Sparks, J.S., Beachboard, D.C., Cox, R.G., Doyle, J.D., Stobart, C.C., Denison, M.R., 2010. Murine Hepatitis Virus Nonstructural Protein 4 Regulates Virus-Induced Membrane Modifications and Replication Complex Function. *Journal of Virology* **84**, 280–290.
- Gasteiger, E., Gattiker, A., Hoogland, C., Ivanyi, I., Appel, R.D., Bairoch, A., 2003. ExPASy: The proteomics server for in-depth protein knowledge and analysis. *Nucleic Acids Research* **31**, 3784–3788.
- Gebhardt, L.P., Stanton, G.J., De St Jeor, S., 1966. Transmission of WEE virus to snakes by infected *Culex tarsalis* mosquitoes. *Proceedings of the Society for Experimental Biology and Medicine* **123**, 233–5.
- Gebhardt, L.P., Stanton, G.J., Hill, D.W., Collett, G.C., 1964. Natural Overwintering Hosts of the Virus of Western Equine Encephalitis. *New England Journal of Medicine* **271**, 172–177.
- Gelb, J., Ladman, B.S., Pope, C.R., Ruano, J.M., Brannick, E.M., Bautista, D.A., Coughlin, C.M., Preskenis, L.A., 2013. Characterization of Nephropathogenic Infectious Bronchitis Virus DMV/1639/11 Recovered from Delmarva Broiler Chickens in 2011. *Avian Diseases* **57**, 65–70.
- Gillespie, L.K., Hoenen, A., Morgan, G., Mackenzie, J.M., 2010. The Endoplasmic Reticulum Provides the Membrane Platform for Biogenesis of the Flavivirus Replication Complex. *Journal of Virology* **84**, 10438–10447.
- Goldsmith, C.S., Tatti, K.M., Ksiazek, T.G., Rollin, P.E., Comer, J.A., Lee, W.W., Rota, P.A., Bankamp, B., Bellini, W.J., Zaki, S.R., 2004. Ultrastructural Characterization of SARS Coronavirus. *Emerging Infectious Diseases* **10**, 320–326.
- Gonzalez, J.P., McCormick, J.B., Saluzzo, J.-F., Hervé, J.P., Georges, A.J., Johnson, K.M., 1983. An arenavirus isolated from wild-caught rodents (*Pramys* species) in the Central African Republic. *Intervirology* **19**, 105–112.
- Gorbalenya, A.E., Enjuanes, L., Ziebuhr, J., Snijder, E.J., 2006. Nidovirales: Evolving the largest RNA virus genome. *Virus Research* **117**, 17–37.
- Gosert, R., Egger, D., Lohmann, V., Bartenschlager, R., Blum, H.E., Bienz, K., Moradpour, D., 2003. Identification of the hepatitis C virus RNA replication

References

- complex in Huh-7 cells harboring subgenomic replicons. *Journal of Virology* **77**, 5487–92.
- Gosert, R., Kanjanahaluethai, A., Egger, D., Bienz, K., Baker, S.C., 2002. RNA replication of mouse hepatitis virus takes place at double-membrane vesicles. *Journal of Virology* **76**, 3697–708.
- Gramberg, T., Hofmann, H., Möller, P., Lator, P.F., Marzi, A., Geier, M., Krumbiegel, M., Winkler, T., Kirchhoff, F., Adams, D.H., Becker, S., Münch, J., Pöhlmann, S., 2005. LSECtin interacts with filovirus glycoproteins and the spike protein of SARS coronavirus. *Virology* **340**, 224–236.
- Grande-Pérez, A., Martin, V., Moreno, H., de la Torre, J.C., 2016. Arenavirus Quasispecies and Their Biological Implications. *Current Topics in Microbiology and Immunology* **392**, 231–76.
- Greek, T., 2002. Necropsy Examination [WWW Document]. *Chameleons! Online E-Zine*. URL <http://www.chameleonnews.com/02MayGreek.html>
- Greenblatt, R.J., Quackenbush, S.L., Casey, R.N., Rovnak, J., Balazs, G.H., Work, T.M., Casey, J.W., Sutton, C.A., 2005. Genomic Variation of the Fibropapilloma-Associated Marine Turtle Herpesvirus across Seven Geographic Areas and Three Host Species. *Journal of Virology* **79**, 1125–1132.
- Groseth, A., Hoenen, T., Weber, M., Wolff, S., Herwig, A., Kaufmann, A., Becker, S., 2011. Tacaribe Virus but Not Junin Virus Infection Induces Cytokine Release from Primary Human Monocytes and Macrophages. *PLOS Neglected Tropical Diseases* **5**, e1137.
- Günther, S., Hoofd, G., Charrel, R., Röser, C., Becker-Ziaja, B., Lloyd, G., Sabuni, C., Verhagen, R., van der Groen, G., Kennis, J., Katakweba, A., Machang'u, R., Makundi, R., Leirs, H., 2009. Mopeia Virus-related Arenavirus in Natal Multimammate Mice, Morogoro, Tanzania. *Emerging Infectious Diseases* **15**, 2008–2010.
- Hagemeijer, M.C., Monastyrska, I., Griffith, J., van der Sluijs, P., Voortman, J., van Bergen en Henegouwen, P.M., Vonk, A.M., Rottier, P.J.M., Reggiori, F., de Haan, C.A.M., 2014. Membrane rearrangements mediated by coronavirus nonstructural proteins 3 and 4. *Virology* **458–459**, 125–135.
- Hagemeijer, M.C., Ulasli, M., Vonk, A.M., Reggiori, F., Rottier, P.J.M., de Haan, C.A.M., 2011. Mobility and Interactions of Coronavirus Nonstructural Protein 4. *Journal of Virology* **85**, 4572–4577.
- Hagemeijer, M.C., Vonk, A.M., Monastyrska, I., Rottier, P.J.M., de Haan, C.A.M., 2012. Visualizing Coronavirus RNA Synthesis in Time by Using Click Chemistry. *Journal of Virology* **86**, 5808–5816.
- Hall, B.G., 2018. *Phylogenetic Trees Made Easy*, Fifth Edit. ed. Oxford University Press, New York, USA.
- Harak, C., Lohmann, V., 2015. Ultrastructure of the replication sites of positive-strand RNA viruses. *Virology* **479–480**, 418–433.
- Hass, M., Gölnitz, U., Müller, S., Becker-Ziaja, B., Günther, S., 2004. Replicon System for Lassa Virus. *Journal of Virology* **78**, 13793–13803.
- Hastie, K.M., Kimberlin, C.R., Zandonatti, M.A., MacRae, I.J., Saphire, E.O., 2011.

References

- Structure of the Lassa virus nucleoprotein reveals a dsRNA-specific 3' to 5' exonuclease activity essential for immune suppression. *Proceedings of the National Academy of Sciences of the United States of America* **108**, 2396–2401.
- Hayes, R.O., Daniels, J.B., Maxfield, H.K., Wheeler, R.E., 1964. Field and laboratory studies on eastern encephalitis in warm-and cold-blooded vertebrates. *The American Journal of Tropical Medicine and Hygiene* **13**, 595–606.
- Heldstab, A., Bestetti, G., 1982. Spontaneous Viral Hepatitis in a Spur-Tailed Mediterranean Land Tortoise (*Testudo hermanni*). *The Journal of Zoo Animal Medicine* **13**, 113–120.
- Heldstab, A., Bestetti, G., 1984. Virus Associated Gastrointestinal Diseases in Snakes. *The Journal of Zoo Animal Medicine* **15**, 118–128.
- Hellström, K., Kallio, K., Utt, A., Quirin, T., Jokitalo, E., Merits, A., Ahola, T., 2017. Partially Uncleaved Alphavirus Replicase Forms Spherule Structures in the Presence and Absence of RNA Template. *Journal of Virology* **91**.
- Hennion, R.M., Hill, G., 2015. The Preparation of Chicken Kidney Cell Cultures for Virus Propagation. In: Coronaviruses. pp. 57–62.
- Hepojoki, J., Hepojoki, S., Smura, T., Szirovicza, L., Dervas, E., Prähauser, B., Nufer, L., Schraner, E.M., Vapalahti, O., Kipar, A., Hetzel, U., 2018. Characterization of Haartman Institute snake virus-1 (HISV-1) and HISV-like viruses—The representatives of genus Hartmanivirus, family Arenaviridae. *PLOS Pathogens* **14**, e1007415.
- Hepojoki, J., Kipar, A., Korzyukov, Y., Bell-Sakyi, L., Vapalahti, O., Hetzel, U., 2015a. Replication of Boid Inclusion Body Disease-Associated Arenaviruses Is Temperature Sensitive in both Boid and Mammalian Cells. *Journal of Virology* **89**, 1119–1128.
- Hepojoki, J., Salmenperä, P., Sironen, T., Hetzel, U., Korzyukov, Y., Kipar, A., Vapalahti, O., 2015b. Arenavirus Coinfections Are Common in Snakes with Boid Inclusion Body Disease. *Journal of Virology* **89**, 8657–8660.
- Herbst, L.H., Lenz, J., Van Doorslaer, K., Chen, Z., Stacy, B.A., Wellehan, J.F.X., Manire, C.A., Burk, R.D., 2009. Genomic characterization of two novel reptilian papillomaviruses, *Chelonia mydas* papillomavirus 1 and *Caretta caretta* papillomavirus 1. *Virology* **383**, 131–135.
- Hetzel, U., Sironen, T., Laurinmäki, P., Liljeroos, L., Patjas, A., Henttonen, H., Vaehri, A., Artelt, A., Kipar, A., Butcher, S.J., Vapalahti, O., Hepojoki, J., 2013. Isolation, Identification, and Characterization of Novel Arenaviruses, the Etiological Agents of Boid Inclusion Body Disease. *Journal of Virology* **87**, 10918–10935.
- Hoff, G., Trainer, D.O., 1973. Arboviruses in Reptiles: Isolation of a Bunyamwera Group Virus from a Naturally Infected Turtle. *Journal of Herpetology* **7**, 55–62.
- Hoff, G.L., Hoff, D.M., 1984. Herpesviruses of Reptiles. In: Hoff, Gerald L, Frye, F.L., Jacobson, E.R. (Eds.), *Diseases of Amphibians and Reptiles*. Springer US, Boston, MA, pp. 159–167.
- Holopainen, R., Ohlemeyer, S., Schütze, H., Bergmann, S.M., Tapiovaara, H., 2009. Ranavirus phylogeny and differentiation based on major capsid protein , DNA

References

- polymerase and neurofilament triplet H1-like protein genes **85**, 81–91.
- Homer, B.L., Sundberg, J.P., Gaskin, J.M., Schumacher, J., Jacobson, E.R., 1995. Immunoperoxidase detection of ophidian paramyxovirus in snake lung using a polyclonal antibody. *Journal of Veterinary Diagnostic Investigation* **7**, 72–7.
- Huchzermeyer, F., Gerdes, G., Putterill, J., 1994. Viruses and mycoplasmas from faeces of farmed Nile crocodiles. In: 12th Working Meeting of the Crocodile Specialist Group, IUCN - The World Conservation Union. pp. 203–208.
- Huder, J.B., Böni, J., Hatt, J.-M., Soldati, G., Lutz, H., Schüpbach, J., 2002. Identification and Characterization of Two Closely Related Unclassifiable Endogenous Retroviruses in Pythons (*Python molurus* and *Python curtus*). *Journal of Virology* **76**, 7607–7615.
- Huelsenbeck, J.P., Dyer, K.A., 2004. Bayesian Estimation of Positively Selected Sites. *Journal of Molecular Evolution* **58**, 661–672.
- Hurley, J.H., Hanson, P.I., 2010. Membrane budding and scission by the ESCRT machinery: it's all in the neck. *Nature Reviews Molecular cell biology* **11**, 556–566.
- Hyatt, A.D., Williamson, M., Coupar, B.E.H., Middleton, D., Hengstberger, S.G., Gould, A.R., Selleck, P., Wise, T.G., Kattenbelt, J., Cunningham, A.A., Lee, J., 2002. First Identification Of A Ranavirus From Green Pythons (*Chondropython viridis*). *Journal of Wildlife Diseases* **38**, 239–252.
- Hyndman, T., Marschang, R., Bruce, M., Clark, P., Vitali, S., 2019. Reptarenaviruses in apparently healthy snakes in an Australian zoological collection. *Australian Veterinary Journal* **97**, 93–102.
- Imperiali, M., Spörri, R., Hewitt, J., Oxenius, A., 2008. Post-translational modification of α -dystroglycan is not critical for lymphocytic choriomeningitis virus receptor function in vivo. *Journal of General Virology* **89**, 2713–2722.
- Inamori, K., Yoshida-Moriguchi, T., Hara, Y., Anderson, M.E., Yu, L., Campbell, K.P., 2012. Dystroglycan Function Requires Xylosyl- and Glucuronyltransferase Activities of LARGE. *Science* **335**, 93–96.
- Irie, T., Shimazu, Y., Yoshida, T., Sakaguchi, T., 2007. The YLDL Sequence within Sendai Virus M Protein Is Critical for Budding of Virus-Like Particles and Interacts with Alix/AIP1 Independently of C Protein. *Journal of Virology* **81**, 2263–2273.
- Iserte, J.A., Stephan, B.I., Goñi, S.E., Borio, C.S., Ghiringhelli, P.D., Lozano, M.E., 2013. Family-Specific Degenerate Primer Design: A Tool to Design Consensus Degenerated Oligonucleotides. *Biotechnology Research International* **2013**, 1–9.
- Ishii, A., Thomas, Y., Moonga, L., Nakamura, I., Ohnuma, A., Hang'ombe, B., Takada, A., Mweene, A., Sawa, H., 2011. Novel Arenavirus, Zambia. *Emerging Infectious Diseases* **17**, 1921–1924.
- Jacobson, E., Gaskin, J.M., Simpson, C.F., Terrell, T.G., 1980. Paramyxo-like virus infection in a rock rattlesnake. *Journal of the American Veterinary Medical Association* **177**, 796–9.
- Jacobson, E.R., Gaskin, J.M., Clubb, S., Calderwood, M.B., 1982. Papilloma-like virus infection in Bolivian side-neck turtles. *Journal of the American Veterinary*

References

- Medical Association* **181**, 1325–8.
- Jacobson, E.R., Gaskin, J.M., Roelke, M., Greiner, E.C., Allen, J., 1986. Conjunctivitis, tracheitis, and pneumonia associated with herpesvirus infection in green sea turtles. *J Am Vet Med Assoc* **189**, 1020–1023.
- Jacobson, E.R., Ginn, P.E., Troutman, J.M., Farina, L., Stark, L., Klenk, K., Burkhalter, K.L., Komar, N., 2005. West Nile Virus Infection In Farmed American Alligators (*Alligator Mississippiensis*) In Florida. *Journal of Wildlife Diseases* **41**, 96–106.
- Jacobson, E.R., Kopit, W., Kennedy, F.A., Funk, R.S., 1996. Coinfection of a Bearded Dragon, *Pogona vitticeps*, with Adenovirus- and Dependovirus-like Viruses. *Veterinary Pathology* **33**, 343–346.
- Jacobson, E.R., Orós, J., Tucker, S.J., Pollock, D.P., Kelley, K.L., Munn, R.J., Lock, B.A., Mergia, A., Yamamoto, J.K., 2001. Partial characterization of retroviruses from boid snakes with inclusion body disease. *American Journal of Veterinary Research* **62**, 217–224.
- Jacobson, E.R., Telford, S.R., 1990. Chlamydial and Poxvirus Infections of Circulating Monocytes of a Flap-necked Chameleon (*Chamaeleo dilepis*). *Journal of Wildlife Diseases* **26**, 572–577.
- Jancovich, J.K., Mao, J., Chinchar, V.G., Wyatt, C., Case, S.T., Kumar, S., Valente, G., Subramanian, S., Davidson, E.W., Collins, J.P., Jacobs, B.L., 2003. Genomic sequence of a ranavirus (family Iridoviridae) associated with salamander mortalities in North America. *Virology* **316**, 90–103.
- Jiang, Q., Jin, X., Lee, S.-J., Yao, S., 2017. Protein secondary structure prediction: A survey of the state of the art. *Journal of Molecular Graphics and Modelling* **76**, 379–402.
- Johnson, A.J., Pessier, A.P., Jacobson, E.R., 2007. Experimental Transmission and Induction of Ranaviral Disease in Western Ornate Box Turtles (*Terrapene ornata ornata*) and Red-Eared Sliders (*Trachemys scripta elegans*). *Veterinary Pathology* **44**, 285–297.
- Johnson, A.J., Pessier, A.P., Wellehan, J.F.X., Childress, A., Norton, T.M., Stedman, N.L., Bloom, D.C., Belzer, W., Titus, V.R., Wagner, R., Brooks, J.W., Spratt, J., Jacobson, E.R., 2008. Ranavirus Infection Of Free-Ranging And Captive Box Turtles And Tortoises In The United States. *Journal of Wildlife Diseases* **44**, 851–863.
- Johnson, A.J., Pessier, A.P., X. Wellehan, J.F., Brown, R., Jacobson, E.R., 2005. Identification of a novel herpesvirus from a California desert tortoise (*Gopherus agassizii*). *Veterinary Microbiology* **111**, 107–116.
- Johnson, K.M., Wiebenga, N.H., Mackenzie, R.B., Kuns, M.L., Tauraso, N.M., Shelokov, A., Webb, P.A., Justines, G., Beye, H., 1965. Virus isolations from human cases of hemorrhagic fever in Bolivia. *Society for Experimental Biology and Medicine* **118**, 113–118.
- Johnsrude, J.D., Raskin, R.E., Hoge, A.Y.A., Erdos, G.W., 1997. Intraerythrocytic Inclusions Associated with Iridoviral Infection in a Fer de Lance (*Bothrops moojeni*) Snake. *Veterinary Pathology* **34**, 235–238.
- Jones, R.C., Worthington, K.J., Capua, I., Naylor, C.J., 2005. Efficacy of live

References

- infectious bronchitis vaccines against a novel European genotype, Italy 02. *The Veterinary Record* **156**, 646–7.
- Jones, B. V., Hennion, R.M., 2008. The Preparation of Chicken Tracheal Organ Cultures for Virus Isolation, Propagation, and Titration. In: SARS- and Other Coronaviruses. pp. 103–107.
- Just, F., Essbauer, S., Ahne, W., Blahak, S., 2001. Occurrence of an Invertebrate Iridescent-Like Virus (Iridoviridae) in Reptiles. *Journal of Veterinary Medicine, Series B* **48**, 685–694.
- Kallio, K., Hellstrom, K., Balistreri, G., Spuul, P., Jokitalo, E., Ahola, T., 2013. Template RNA Length Determines the Size of Replication Complex Spherules for Semliki Forest Virus. *Journal of Virology* **87**, 9125–9134.
- Kanjanahaluethai, A., Chen, Z., Jukneliene, D., Baker, S.C., 2007. Membrane topology of murine coronavirus replicase nonstructural protein 3. *Virology* **361**, 391–401.
- Keller, S., Hetzel, U., Sironen, T., Korzyukov, Y., Vapalahti, O., Kipar, A., Hepojoki, J., 2017. Co-infecting Reptarenaviruses Can Be Vertically Transmitted in Boa Constrictor. *PLOS Pathogens* **13**, e1006179.
- Kentsis, A., Dwyer, E.C., Perez, J.M., Sharma, M., Chen, A., Pan, Z.Q., Borden, K.L.B., 2001. The RING domains of the promyelocytic leukemia protein PML and the arenaviral protein Z repress translation by directly inhibiting translation initiation factor eIF4E11 Edited by D. Draper. *Journal of Molecular Biology* **312**, 609–623.
- Kerber, R., Rieger, T., Busch, C., Flatz, L., Pinschewer, D.D., Kummerer, B.M., Gunther, S., 2011. Cross-Species Analysis of the Replication Complex of Old World Arenaviruses Reveals Two Nucleoprotein Sites Involved in L Protein Function. *Journal of Virology* **85**, 12518–12528.
- Kernéis, S., Koivogui, L., Magassouba, N., Koulemou, K., Lewis, R., Aplogan, A., Grais, R.F., Guerin, P.J., Fichet-Calvet, E., 2009. Prevalence and risk factors of lassa seropositivity in inhabitants of the Forest Region of Guinea: A cross-sectional study. *PLOS Neglected Tropical Diseases* **3**.
- Kikonyogo, A., Bouamr, F., Vana, M.L., Xiang, Y., Aiyar, A., Carter, C., Leis, J., 2001. Proteins related to the Nedd4 family of ubiquitin protein ligases interact with the L domain of Rous sarcoma virus and are required for gag budding from cells. *Proceedings of the National Academy of Sciences of the United States of America* **98**, 11199–11204.
- Kint, J., Fernandez-Gutierrez, M., Maier, H.J., Britton, P., Langereis, M.A., Koumans, J., Wiegertjes, G.F., Forlenza, M., 2015. Activation of the Chicken Type I Interferon Response by Infectious Bronchitis Coronavirus. *Journal of Virology* **89**, 1156–1167.
- Kitching, A., Addiman, S., Cathcart, S., Bishop, L., Krahé, D., Nicholas, M., Coakley, J., Lloyd, G., Brooks, T., Morgan, D., Turbitt, D., 2009. A fatal case of Lassa fever in London, January 2009. *Euro Surveillance* **14**, 12–14.
- Klewitz, C., Klenk, H.-D., ter Meulen, J., 2007. Amino acids from both N-terminal hydrophobic regions of the Lassa virus envelope glycoprotein GP-2 are critical for pH-dependent membrane fusion and infectivity. *Journal of General Virology* **88**, 2320–2328.

References

- Knoops, K., Barcena, M., Limpens, R.W.A.L., Koster, A.J., Mommaas, A.M., Snijder, E.J., 2012. Ultrastructural Characterization of Arterivirus Replication Structures: Reshaping the Endoplasmic Reticulum To Accommodate Viral RNA Synthesis. *Journal of Virology* **86**, 2474–2487.
- Knoops, K., Kikkert, M., Worm, S.H.E. van den, Zevenhoven-Dobbe, J.C., van der Meer, Y., Koster, A.J., Mommaas, A.M., Snijder, E.J., 2008. SARS-Coronavirus Replication Is Supported by a Reticulovesicular Network of Modified Endoplasmic Reticulum. *PLOS Biology* **6**, e226.
- Kopek, B.G., Settles, E.W., Friesen, P.D., Ahlquist, P., 2010. Nodavirus-Induced Membrane Rearrangement in Replication Complex Assembly Requires Replicase Protein A, RNA Templates, and Polymerase Activity. *Journal of Virology* **84**, 12492–12503.
- Kranzusch, P.J., Schenk, A.D., Rahmeh, A.A., Radoshitzky, S.R., Bavari, S., Walz, T., Whelan, S.P.J., 2010. Assembly of a functional Machupo virus polymerase complex. *Proceedings of the National Academy of Sciences of the United States of America* **107**, 20069–20074.
- Kranzusch, P.J., Whelan, S.P.J., 2011. Arenavirus Z protein controls viral RNA synthesis by locking a polymerase–promoter complex. *Proceedings of the National Academy of Sciences of the United States of America* **108**, 19743–19748.
- Kremer, J.R., Mastronarde, D.N., McIntosh, J.R., 1996. Computer Visualization of Three-Dimensional Image Data Using IMOD. *Journal of Structural Biology* **116**, 71–76.
- Kujala, P., Ikaheimonen, A., Ehsani, N., Vihinen, H., Auvinen, P., Kaariainen, L., 2001. Biogenesis of the Semliki Forest Virus RNA Replication Complex. *Journal of Virology* **75**, 3873–3884.
- Kunz, S., Rojek, J.M., Kanagawa, M., Spiropoulou, C.F., Barresi, R., Campbell, K.P., Oldstone, M.B.A., 2005. Posttranslational Modification of α -Dystroglycan, the Cellular Receptor for Arenaviruses, by the Glycosyltransferase LARGE Is Critical for Virus Binding. *Journal of Virology* **79**, 14282–14296.
- Kurath, G., Batts, W.N., Ahne, W., Winton, J.R., 2004. Complete Genome Sequence of Fer-de-Lance Virus Reveals a Novel Gene in Reptilian Paramyxoviruses. *Journal of Virology* **78**, 2045–2056.
- Lamirande, E.W., Nichols, D.K., Owens, J.W., Gaskin, J.M., Jacobson, E.R., 1999. Isolation and experimental transmission of a reovirus pathogenic in ratsnakes (Elaphe species). *Virus Research* **63**, 135–41.
- Larson, D., Zahradka, P., Sells, B., 1991. Control points in eukaryotic ribosome biogenesis. *Biochemistry and Cell Biology* **69**, 5–22.
- Lecompte, E., Meulen, J., Emonet, S., Daffis, S., Charrel, R.N., 2007. Genetic identification of Kodoko virus, a novel arenavirus of the African pigmy mouse (*Mus Nannomys minutoides*) in West Africa **364**, 178–183.
- Lee, H., Min, B., Lim, Y., 1972. Isolation and serologic studies of Japanese encephalitis virus from snakes in Korea **15**, 69–74.
- Lee, K.J., Novella, I.S., Teng, M.N., Oldstone, M.B.A., de la Torre, J.C., 2000. NP and L Proteins of Lymphocytic Choriomeningitis Virus (LCMV) Are Sufficient for

References

- Efficient Transcription and Replication of LCMV Genomic RNA Analogs. *Journal of Virology* **74**, 3470–3477.
- Lenz, O., ter Meulen, J., Klenk, H.D., Seidah, N.G., Garten, W., 2001. The Lassa virus glycoprotein precursor GP-C is proteolytically processed by subtilase SKI-1/S1P. *Proceedings of the National Academy of Sciences of the United States of America* **98**, 12701–5.
- Levingston Macleod, J.M., D'Antuono, A., Loureiro, M.E., Casabona, J.C., Gomez, G.A., Lopez, N., 2011. Identification of Two Functional Domains within the Arenavirus Nucleoprotein. *Journal of Virology* **85**, 2012–2023.
- Linero, F.N., Scolaro, L.A., 2009. Participation of the phosphatidylinositol 3-kinase/Akt pathway in Junín virus replication in vitro. *Virus Research* **145**, 166–170.
- Liu, J., Gratz, J., Amour, C., Nshama, R., Walongo, T., Maro, A., Mduma, E., Platts-Mills, J., Boisen, N., Nataro, J., Haverstick, D.M., Kabir, F., Lertsethtakarn, P., Silapong, S., Jeamwattanalert, P., Bodhidatta, L., Mason, C., Begum, S., Haque, R., Praharaj, I., Kang, G., Houpt, E.R., 2016. Optimization of Quantitative PCR Methods for Enteropathogen Detection. *PLOS ONE* **11**, e0158199.
- Lole, K.S., Bollinger, R.C., Paranjape, R.S., Gadkari, D., Kulkarni, S.S., Novak, N.G., Ingersoll, R., Sheppard, H.W., Ray, S.C., 1999. Full-Length Human Immunodeficiency Virus Type 1 Genomes from Subtype C-Infected Seroconverters in India, with Evidence of Intersubtype Recombination. *Journal of Virology* **73**, 152–160.
- Lopez, N., Jacamo, R., Franze-Fernandez, M.T., 2002. Transcription and RNA Replication of Tacaribe Virus Genome and Antigenome Analogs Require N and L Proteins: Z Protein Is an Inhibitor of These Processes. *Journal of Virology* **75**, 12241–12251.
- Lozano, M.E., Posik, D.M., Albariño, C.G., Schujman, G., Ghiringhelli, P.D., Calderón, G., Sabattini, M., Romanowski, V., 1997. Characterization of arenaviruses using a family-specific primer set for RT-PCR amplification and RFLP analysis: Its potential use for detection of uncharacterized arenaviruses. *Virus Research* **49**, 79–89.
- Lu, Y.A., Wang, Y., Aguirre, A.A., Zhao, Z.S., Liu, C.Y., Nerurkar, V.R., Yanagihara, R., 2003. RT-PCR detection of the expression of the polymerase gene of a novel reptilian herpesvirus in tumor tissues of green turtles with fibropapilloma. *Archives of Virology* **148**, 1155–1163.
- Ludtke, S.J., Baldwin, P.R., Chiu, W., 1999. EMAN: Semiautomated Software for High-Resolution Single-Particle Reconstructions. *Journal of Structural Biology* **128**, 82–97.
- Lukashevich, I.S., 1992. Generation of reassortants between African arenaviruses. *Virology* **188**, 600–605.
- Lundin, A., Dijkman, R., Bergström, T., Kann, N., Adamiak, B., Hannoun, C., Kindler, E., Jónsdóttir, H.R., Muth, D., Kint, J., Forlenza, M., Müller, M.A., Drosten, C., Thiel, V., Trybala, E., 2014. Targeting Membrane-Bound Viral RNA Synthesis Reveals Potent Inhibition of Diverse Coronaviruses Including the Middle East Respiratory Syndrome Virus. *PLOS Pathogens* **10**, e1004166.

References

- Lunger, P.D., Clark, H.F., 1978. Reptilia-related viruses. *Advances in Virus Research* **23**, 159–204.
- Lunkenheimer K, Hufert FT, S.H., 1990. No Title49. Detection of lassa virus RNA specimens from patients with lassa fever by using the polymerase chain reaction. *J Clin Microbiol. Journal of Clinical Microbiology* **28**, 92.
- Maes, P., Alkhovsky, S. V, Bào, Y., Beer, M., Birkhead, M., Briese, T., Buchmeier, M.J., Calisher, C.H., Charrel, R.N., Choi, I.R., Clegg, C.S., de la Torre, J.C., Delwart, E., DeRisi, J.L., Di Bello, P.L., Di Serio, F., Digiaro, M., Dolja, V. V, Drosten, C., Druciarek, T.Z., Du, J., Ebihara, H., Elbeaino, T., Gergerich, R.C., Gillis, A.N., Gonzalez, J.-P.J., Haenni, A.-L., Hepojoki, J., Hetzel, U., Hò, T., Hóng, N., Jain, R.K., Jansen van Vuren, P., Jin, Q., Jonson, M.G., Junglen, S., Keller, K.E., Kemp, A., Kipar, A., Kondov, N.O., Koonin, E. V, Kormelink, R., Korzyukov, Y., Krupovic, M., Lambert, A.J., Laney, A.G., LeBreton, M., Lukashevich, I.S., Marklewitz, M., Markotter, W., Martelli, G.P., Martin, R.R., Mielke-Ehret, N., Mühlbach, H.-P., Navarro, B., Ng, T.F.F., Nunes, M.R.T., Palacios, G., Pawęska, J.T., Peters, C.J., Plyusnin, A., Radoshitzky, S.R., Romanowski, V., Salmenperä, P., Salvato, M.S., Sanfaçon, H., Sasaya, T., Schmaljohn, C., Schneider, B.S., Shirako, Y., Siddell, S., Sironen, T.A., Stenglein, M.D., Storm, N., Sudini, H., Tesh, R.B., Tzanetakis, I.E., Uppala, M., Vapalahti, O., Vasilakis, N., Walker, P.J., Wáng, G., Wáng, L., Wáng, Y., Wèi, T., Wiley, M.R., Wolf, Y.I., Wolfe, N.D., Wú, Z., Xú, W., Yang, L., Yāng, Z., Yeh, S.-D., Zhāng, Y.-Z., Zhèng, Y., Zhou, X., Zhū, C., Zirkel, F., Kuhn, J.H., 2018. Taxonomy of the family Arenaviridae and the order Bunyavirales: update 2018. *Archives of Virology* **163**, 2295–2310.
- Maier, H.J., Cottam, E.M., Stevenson-Leggett, P., Wilkinson, J.A., Harte, C.J., Wileman, T., Britton, P., 2013a. Visualizing the autophagy pathway in avian cells and its application to studying infectious bronchitis virus. *Autophagy* **9**, 496–509.
- Maier, H.J., Hawes, P.C., Cottam, E.M., Mantell, J., Verkade, P., Monaghan, P., Wileman, T., Britton, P., 2013b. Infectious Bronchitis Virus Generates Spherules from Zippered Endoplasmic Reticulum Membranes. *mBio* **4**.
- Maier, H.J., Hawes, P.C., Keep, S.M., Britton, P., 2014. Spherules and IBV. *Bioengineered* **5**, 288–292.
- Maier, H.J., Neuman, B.W., Bickerton, E., Keep, S.M., Alrashedi, H., Hall, R., Britton, P., 2016. Extensive coronavirus-induced membrane rearrangements are not a determinant of pathogenicity. *Scientific Reports* **6**, 27126.
- Maiztegui, J., Fernandez, N., De Damilano, A., 1979. Efficacy Of Immune Plasma In Treatment Of Argentine Hæmorrhagic Fever And Association Between Treatment And A Late Neurological Syndrome. *The Lancet* **314**, 1216–1217.
- Manire, C.A., Stacy, B.A., Kinsel, M.J., Daniel, H.T., Anderson, E.T., Wellehan, J.F.X., 2008. Proliferative dermatitis in a loggerhead turtle, *Caretta caretta*, and a green turtle, *Chelonia mydas*, associated with novel papillomaviruses. *Veterinary Microbiology* **130**, 227–237.
- Marschang, R.E., Papp, T., Frost, J.W., 2009. Comparison of paramyxovirus isolates from snakes, lizards and a tortoise. *Virus Research* **144**, 272–279.
- Martin, J., Kabat, P., Herniou, E., Tristem, M., 2002. Characterization and Complete

References

- Nucleotide Sequence of an Unusual Reptilian Retrovirus Recovered from the Order Crocodylia. *Journal of Virology* **76**, 4651–4654.
- Martínez-Sobrido, L., de la Torre, J.C., 2016. Reporter-Expressing, Replicating-Competent Recombinant Arenaviruses. *Viruses* **8**, 197.
- Martínez-Sobrido, L., Giannakas, P., Cubitt, B., García-Sastre, A., de la Torre, J.C., 2007. Differential Inhibition of Type I Interferon Induction by Arenavirus Nucleoproteins. *Journal of Virology* **81**, 12696–12703.
- McArthur, S., Wilkinson, R., Meyer, J., 2004. *Medicine and Surgery of Tortoises and Turtles*. Blackwell Publishing Ltd, Oxford, UK.
- McCormick, J.B., Fisher-Hoch, S.P., 2002. Lassa fever. *Current Topics in Microbiology and Immunology* **262**, 75–109.
- McGinnis, S., Madden, T.L., 2004. BLAST: At the core of a powerful and diverse set of sequence analysis tools. *Nucleic Acids Research* **32**, 20–25.
- McLay, L., Ansari, A., Liang, Y., Ly, H., 2013. Targeting virulence mechanisms for the prevention and therapy of arenaviral hemorrhagic fever. *Antiviral Research* **97**, 81–92.
- McNew, R.M., Elsey, R.M., Rainwater, T.R., Marsland, E.J., Presley, S.M., 2007. Survey for West Nile Virus Infection in Free-Ranging American Alligators in Louisiana. *Southeastern Naturalist* **6**, 737–742.
- McWilliam, H., Li, W., Uludag, M., Squizzato, S., Park, Y.M., Buso, N., Cowley, A.P., Lopez, R., 2013. Analysis Tool Web Services from the EMBL-EBI. *Nucleic Acids Research* **41**, 597–600.
- Meulen, J. ter, Badusche, M., Satoguina, J., Strecker, T., Lenz, O., Loeliger, C., Sakho, M., Koulemou, K., Koivogui, L., Hoerauf, A., 2004. Old and New World arenaviruses share a highly conserved epitope in the fusion domain of the glycoprotein 2, which is recognized by Lassa virus-specific human CD4+ T-cell clones. *Virology* **321**, 134–143.
- Milazzo, M.L., Cajimat, M.N.B., Haynie, M.L., Abbott, K.D., Bradley, R.D., Fulhorst, C.F., 2008. Diversity Among Tacaribe Serocomplex Viruses (Family Arenaviridae) Naturally Associated with the White-Throated Woodrat (*Neotoma albigula*) in the Southwestern United States. *Vector Borne and Zoonotic Diseases* **8**, 523–540.
- Miller, D.L., Mauel, M.J., Baldwin, C., Burtle, G., Ingram, D., Hines, M.E., Frazier, K.S., 2003. West Nile Virus in Farmed Alligators. *Emerging Infectious Diseases* **9**, 794–799.
- Miller, S., Krijnse-Locker, J., 2008. Modification of intracellular membrane structures for virus replication. *Nature Reviews Microbiology* **6**, 363–374.
- Monath, T.P., Cropp, C.B., Frazier, C.L., Murphy, F.A., Whitfield, S.G., 1979. Viruses isolated from reptiles: identification of three new members of the family Rhabdoviridae. *Archives of virology* **60**, 1–12.
- Moncayo, A.C., Hice, C.L., Watts, D.M., Travassos de Rosa, A.P.A., Guzman, H., Russell, K.L., Calampa, C., Gozalo, A., Popov, V.L., Weaver, S.C., Tesh, R.B., 2001. Allpahuayo Virus: A Newly Recognized Arenavirus (Arenaviridae) from Arboreal Rice Rats (*Oecomys Bicolor* and *Oecomys Paricola*) in Northeastern Peru. *Virology* **284**, 277–286.

References

- Morin, B., Coutard, B., Lelke, M., Ferron, F., Kerber, R., Jamal, S., Frangeul, A., Baronti, C., Charrel, R., de Lamballerie, X., Vonnrhein, C., Lescar, J., Bricogne, G., Günther, S., Canard, B., 2010. The N-Terminal Domain of the Arenavirus L Protein Is an RNA Endonuclease Essential in mRNA Transcription. *PLOS Pathogens* **6**, e1001038.
- Müller, R., Poch, O., Delarue, M., Bishop, D.H.L., Bouloy, M., 1994. Rift valley fever virus L segment: correction of the sequence and possible functional role of newly identified regions conserved in RNA-dependent polymerases. *Journal of General Virology* **75**, 1345–1352.
- Muro, J., Ramis, A., Pastor, J., Velarde, R., Tarres, J., Lavin, S., 1998. Chronic Rhinitis Associated With Herpesviral Infection In Captive Spur-Thighed Tortoises From Spain. *Journal of Wildlife Diseases* **34**, 487–495.
- Neil, S.J.D., Zang, T., Bieniasz, P.D., 2008. Tetherin inhibits retrovirus release and is antagonized by HIV-1 Vpu. *Nature* **451**, 425-U1.
- Netherton, C.L., Wileman, T., 2011. Virus factories, double membrane vesicles and viroplasm generated in animal cells. *Current Opinion in Virology* **1**, 381–387.
- Neufeldt, C.J., Joyce, M.A., Van Buuren, N., Levin, A., Kirkegaard, K., Gale Jr., M., Tyrrell, D.L.J., Wozniak, R.W., 2016. The Hepatitis C Virus-Induced Membranous Web and Associated Nuclear Transport Machinery Limit Access of Pattern Recognition Receptors to Viral Replication Sites. *PLOS Pathogens* **12**, e1005428.
- Neuman, B.W., 2016. Bioinformatics and functional analyses of coronavirus nonstructural proteins involved in the formation of replicative organelles. *Antiviral Research* **135**, 97–107.
- Neuman, B.W., Adair, B.D., Burns, J.W., Milligan, R.A., Buchmeier, M.J., Yeager, M., 2005. Complementarity in the Supramolecular Design of Arenaviruses and Retroviruses Revealed by Electron Cryomicroscopy and Image Analysis Complementarity in the Supramolecular Design of Arenaviruses and Retroviruses Revealed by Electron Cryomicroscopy and Imag. *Journal of Virology* **79**, 3822–3830.
- Neuman, B.W., Adair, B.D., Yoshioka, C., Quispe, J.D., Orca, G., Kuhn, P., Milligan, R.A., Yeager, M., Buchmeier, M.J., 2006. Supramolecular Architecture of Severe Acute Respiratory Syndrome Coronavirus Revealed by Electron Cryomicroscopy. *Journal of Virology* **80**, 7918–7928.
- Nunberg, J.H., York, J., 2012. The curious case of arenavirus entry, and its inhibition. *Viruses* **4**, 83–101.
- Oldstone, M.B.A., 1987. The Arenaviruses — An Introduction. In: Oldstone, Michael B A (Ed.), *Arenaviruses: Biology and Immunotherapy*. Springer Berlin Heidelberg, Berlin, Heidelberg, pp. 1–4.
- Oostra, M., Hagemeyer, M.C., van Gent, M., Bekker, C.P.J., te Lintelo, E.G., Rottier, P.J.M., de Haan, C.A.M., 2008. Topology and Membrane Anchoring of the Coronavirus Replication Complex: Not All Hydrophobic Domains of nsp3 and nsp6 Are Membrane Spanning. *Journal of Virology* **82**, 12392–12405.
- Oostra, M., te Lintelo, E.G., Deijns, M., Verheije, M.H., Rottier, P.J.M., de Haan, C.A.M., 2007. Localization and Membrane Topology of Coronavirus Nonstructural Protein 4: Involvement of the Early Secretory Pathway in

References

- Replication. *Journal of Virology* **81**, 12323–12336.
- Orenstein, J.M., Banach, B.S., Baker, S.C., 2009. Morphogenesis of Coronavirus HCoV-NL63 in Cell Culture: A Transmission Electron Microscopic Study. *The Open Infectious Diseases Journal* **2**, 52–58.
- Origgi, F.C., Romero, C.H., Bloom, D.C., Klein, P.A., Gaskin, J.M., Tucker, S.J., Jacobson, E.R., 2004. Experimental Transmission of a Herpesvirus in Greek Tortoises (*Testudo graeca*). *Veterinary Pathology* **41**, 50–61.
- Orós, J., Rodríguez, J.L., Déniz, S., Fernández, L., Fernández, A., 1998. Cutaneous poxvirus-like infection in a captive Hermann's tortoise (*Testudo hermanni*). *Veterinary Record* **143**, 508 LP – 509.
- Orosz, S.E., 2006. Proceedings of the North American Veterinary Conference. *The North American Veterinary Conference* **20**, 1560–1562.
- Ortiz-Riaño, E., Cheng, B.Y.H., de la Torre, J.C., Martínez-Sobrido, L., 2012. Self-Association of Lymphocytic Choriomeningitis Virus Nucleoprotein Is Mediated by Its N-Terminal Region and Is Not Required for Its Anti-Interferon Function. *Journal of Virology* **86**, 3307–3317.
- Oudshoorn, D., Rijs, K., Limpens, R.W.A.L., Groen, K., Koster, A.J., Snijder, E.J., Kikkert, M., Bárcena, M., 2017. Expression and Cleavage of Middle East Respiratory Syndrome Coronavirus nsp3-4 Polyprotein Induce the Formation of Double-Membrane Vesicles That Mimic Those Associated with Coronaviral RNA Replication. *mBio* **8**, e01658-17.
- Palacios, G., Druce, J., Du, L., Tran, T., Birch, C., Briese, T., Conlan, S., Quan, P.-L., Hui, J., Marshall, J., Simons, J.F., Egholm, M., Paddock, C.D., Shieh, W.-J., Goldsmith, C.S., Zaki, S.R., Catton, M., Lipkin, W.I., 2008. A New Arenavirus in a Cluster of Fatal Transplant-Associated Diseases. *New England Journal of Medicine* **358**, 991–998.
- Palacios, G., Quan, P.L., Jabado, O.J., Conlan, S., Hirschberg, D.L., Liu, Y., Zhai, J., Renwick, N., Hui, J., Hegyi, H., Grolla, A., Strong, J.E., Towner, J.S., Geisbert, T.W., Jahrling, P.B., Büchen-Osmond, C., Ellerbrok, H., Sanchez-Seco, M.P., Lussier, Y., Formenty, P., Nichol, S.T., Feldmann, H., Briese, T., Lipkin, W.I., 2007. Panmicrobial Oligonucleotide Array for Diagnosis of Infectious Diseases. *Emerging Infectious Diseases* **13**, 73–81.
- Pallister, J., Gould, A., Harrison, D., Hyatt, A., Jancovich, J., Heine, H., 2007. Development of real-time PCR assays for the detection and differentiation of Australian and European ranaviruses. *Journal of Fish Diseases* **30**, 427–438.
- Pan, J., Peng, X., Gao, Y., Li, Z., Lu, X., Chen, Y., Ishaq, M., Liu, D., DeDiego, M.L., Enjuanes, L., Guo, D., 2008. Genome-Wide Analysis of Protein-Protein Interactions and Involvement of Viral Proteins in SARS-CoV Replication. *PLOS ONE* **3**, e3299.
- Papp, T., Fledelius, B., Schmidt, V., Kaján, G.L., Marschang, R.E., 2009. PCR-sequence characterization of new adenoviruses found in reptiles and the first successful isolation of a lizard adenovirus. *Veterinary Microbiology* **134**, 233–240.
- Parodi, A.S., Rugiero, H.R., Greenway, D.J., Mettler, N., Martinez, A., Boxaca, M., De La Barrera, J.M., 1959. Isolation of the junin virus (epidemic hemorrhagic fever) from the mites of the epidemic area (*echinolaelaps echidninus*, barlese).

References

- Prensa Med Argent* 2242–2244.
- Partemi, S., Berne, P.M., Batlle, M., Berruezo, A., Mont, L., Riuró, H., Ortiz, J.T., Roig, E., Pascali, V.L., Brugada, R., Brugada, J., Oliva, A., 2010. Analysis of mRNA from human heart tissue and putative applications in forensic molecular pathology. *Forensic Science International* **203**, 99–105.
- Pasqual, G., Rojek, J.M., Masin, M., Chatton, J.-Y., Kunz, S., 2011. Old World Arenaviruses Enter the Host Cell via the Multivesicular Body and Depend on the Endosomal Sorting Complex Required for Transport. *PLoS Pathogens* **7**, e1002232.
- Paul, D., 2013. Architecture and biogenesis of plus-strand RNA virus replication factories. *World Journal of Virology* **2**, 32.
- Paweska, J.T., Sewlall, N.H., Ksiazek, T.G., Blumberg, L.H., Hale, M.J., Lipkin, W.I., Weyer, J., Nichol, S.T., Rollin, P.E., McMullan, L.K., Paddock, C.D., Briese, T., Mnyalaza, J., Dinh, T.-H., Mukonka, V., Ching, P., Duse, A., Richards, G., de Jong, G., Cohen, C., Ikalafeng, B., Mugero, C., Asomugha, C., Malotle, M.M., Nteo, D.M., Misiani, E., Swanepoel, R., Zaki, S.R., Control, members of the O., Teams, I., 2009. Nosocomial Outbreak of Novel Arenavirus Infection, Southern Africa. *Emerging Infectious Diseases* **15**, 1598–1602.
- Pearson, W.R., 1995. Comparison of methods for searching protein sequence databases. *Protein Society* **4**, 1145–60.
- Pearson, W.R., Lipman, D.J., 1988. Improved tools for biological sequence comparison. *Proceedings of the National Academy of Sciences of the United States of America* **85**, 2444–8.
- Pedersen, K.W., van der Meer, Y., Roos, N., Snijder, E.J., 1999. Open reading frame 1a-encoded subunits of the arterivirus replicase induce endoplasmic reticulum-derived double-membrane vesicles which carry the viral replication complex. *Journal of Virology* **73**, 2016–26.
- Pees, M., Schmidt, V., Marschang, R.E., Heckers, K.O., Krautwald-Junghanns, M.-E., 2010. Prevalence of viral infections in captive collections of boid snakes in Germany. *Veterinary Record* **166**, 422 LP – 425.
- Perez, M., Craven, R.C., de la Torre, J.C., 2003. The small RING finger protein Z drives arenavirus budding: implications for antiviral strategies. *Proceedings of the National Academy of Sciences of the United States of America* **100**, 12978–83.
- Perkins, L.E.L., Campagnoli, R.P., Harmon, B.G., Gregory, C.R., Steffens, W.L., Latimer, K., Clubb, S., Crane, M., 2001. Detection and Confirmation of Reptilian Adenovirus Infection by in Situ Hybridization. *Journal of Veterinary Diagnostic Investigation* **13**, 365–368.
- Pestova, T. V, Kolupaeva, V.G., Lomakin, I.B., Pilipenko, E. V, Shatsky, I.N., Agol, V.I., Hellen, C.U.T., 2001. Molecular mechanisms of translation initiation in eukaryotes. *Proceedings of the National Academy of Sciences of the United States of America* **98**, 7029–7036.
- Peters, C., 2002. Human infection with arenaviruses in the Americas. *Current Topics in Microbiology and Immunology* **262**, 65–74.
- Pickett, B.E., Striker, R., Lefkowitz, E.J., 2011. Evidence for Separation of HCV

References

- Subtype 1a into Two Distinct Clades. *Journal of Viral Hepatitis* **18**, 608–618.
- Pinheiro, F.P., Shope, R.E., de Andrade, A.H.P., Bensabath, G., Cacios, G. V, Casals, J., 1966. Amapari, a New Virus of the Tacaribe Group from Rodents and Mites of Amapa Territory, Brazil. *Proceedings of the Society for Experimental Biology and Medicine* **122**, 531–535.
- Pinschewer, D.D., Perez, M., de la Torre, J.C., 2003. Role of the virus nucleoprotein in the regulation of lymphocytic choriomeningitis virus transcription and RNA replication. *Journal of Virology* **77**, 3882–7.
- Pirger, Z., Rácz, B., Kiss, T., 2009. Dopamine-induced programmed cell death is associated with cytochrome c release and caspase-3 activation in snail salivary gland cells. *Biology of the Cell* **101**, 105–116.
- Plotch, S.J., Bouloy, M., Ulmanen, I., Krug, R.M., 1981. A unique cap(m7GpppXm)-dependent influenza virion endonuclease cleaves capped RNAs to generate the primers that initiate viral RNA transcription. *Cell* **23**, 847–858.
- Posthuma, C.C., Pedersen, K.W., Lu, Z., Joosten, R.G., Roos, N., Zevenhoven-Dobbe, J.C., Snijder, E.J., 2008. Formation of the Arterivirus Replication/Transcription Complex: a Key Role for Nonstructural Protein 3 in the Remodeling of Intracellular Membranes. *Journal of Virology* **82**, 4480–4491.
- Promkuntod, N., Wickramasinghe, I.N.A., de Vrieze, G., Gröne, A., Verheije, M.H., 2013. Contributions of the S2 spike ectodomain to attachment and host range of infectious bronchitis virus. *Virus Research* **177**, 127–137.
- Pythoud, C., Rodrigo, W.W.S.I., Pasqual, G., Rothenberger, S., Martínez-Sobrido, L., de la Torre, J.C., Kunz, S., 2012. Arenavirus Nucleoprotein Targets Interferon Regulatory Factor-Activating Kinase IKK ϵ . *Journal of Virology* **86**, 7728–7738.
- Quackenbush, S.L., Casey, R.N., Murcek, R.J., Paul, T.A., Work, T.M., Limpus, C.J., Chaves, A., duToit, L., Perez, J.V., Aguirre, A.A., Spraker, T.R., Horrocks, J.A., Vermeer, L.A., Balazs, G.H., Casey, J.W., 2001. Quantitative Analysis of Herpesvirus Sequences from Normal Tissue and Fibropapillomas of Marine Turtles with Real-Time PCR. *Virology* **287**, 105–111.
- Quirin, K., Eschli, B., Scheu, I., Poort, L., Kartenbeck, J., Helenius, A., 2008. Lymphocytic choriomeningitis virus uses a novel endocytic pathway for infectious entry via late endosomes. *Virology* **378**, 21–33.
- Radoshitzky, S.R., Abraham, J., Spiropoulou, C.F., Kuhn, J.H., Nguyen, D., Li, W., Nagel, J., Schmidt, P.J., Nunberg, J.H., Andrews, N.C., Farzan, M., Choe, H., 2007. Transferrin receptor 1 is a cellular receptor for New World haemorrhagic fever arenaviruses. *Nature* **446**, 92–96.
- Radoshitzky, S.R., Bào, Y., Buchmeier, M.J., Charrel, R.N., Clawson, A.N., Clegg, C.S., DeRisi, J.L., Emonet, S., Gonzalez, J.-P., Kuhn, J.H., Lukashevich, I.S., Peters, C.J., Romanowski, V., Salvato, M.S., Stenglein, M.D., de la Torre, J.C., 2015. Past, present, and future of arenavirus taxonomy. *Archives of Virology* **160**, 1851–1874.
- Radoshitzky, S.R., Dong, L., Chi, X., Clester, J.C., Retterer, C., Spurgers, K., Kuhn, J.H., Sandwick, S., Ruthel, G., Kota, K., Boltz, D., Warren, T., Kranzusch, P.J., Whelan, S.P.J., Bavari, S., 2010. Infectious Lassa Virus, but Not Filoviruses, Is Restricted by BST-2/Tetherin. *Journal of Virology* **84**, 10569–10580.

References

- Ramos-Vara, J.A., Kiupel, M., Baszler, T., Bliven, L., Brodersen, B., Chelack, B., West, K., Czub, S., Del Piero, F., Dial, S., Ehrhart, E.J., Graham, T., Manning, L., Paulsen, D., Valli, V.E., 2008. Suggested Guidelines for Immunohistochemical Techniques in Veterinary Diagnostic Laboratories. *Journal of Veterinary Diagnostic Investigation* **20**, 393–413.
- Rani, R.R., Ramyachitra, D., 2016. Multiple sequence alignment using multi-objective based bacterial foraging optimization algorithm. *BioSystems* **150**, 177–189.
- Raymond, J.T., Garner, M.M., Nordhausen, R.W., Jacobson, E.R., 2001. A Disease Resembling Inclusion Body Disease of Boid Snakes in Captive Palm Vipers (*Bothriechis Marchi*). *Journal of Veterinary Diagnostic Investigation* **13**, 82–86.
- Raynaud, A., Adrian, M., 1976. Lésions cutanées à structure papillomateuse associées à des virus chez le lézard vert (*Lacerta viridis* Laur). *Comptes rendus de l'Académie des Sciences* **283**, 845–847.
- Rebell, G., Rywlin, A., Haines, H., 1975. Herpesvirus-Type Agent Associated With Skin-Lesions Of Green Sea Turtles In Aquaculture. *American Journal of Veterinary Research* **36**, 1221–1224.
- Regad, T., Saib, A., Lallemand-Breitenbach, V., Pandolfi, P.P., de Thé, H., Chelbi-Alix, M.K., 2001. PML mediates the interferon-induced antiviral state against a complex retrovirus via its association with the viral transactivator. *The EMBO Journal* **20**, 3495–3505.
- Reignier, T., Oldenburg, J., Noble, B., Lamb, E., Romanowski, V., Buchmeier, M.J., Cannon, P.M., 2006. Receptor use by pathogenic arenaviruses. *Virology* **353**, 111–120.
- Reineke, E.L., Kao, H.-Y., 2009. PML: An emerging tumor suppressor and a target with therapeutic potential. *Cancer Therapy* **7**, 219–226.
- Richter, G.A., Homer, B.L., Moyer, S.A., Williams, D.S., Scherba, G., Tucker, S.J., Hall, B.J., Pedersen, J.C., Jacobson, E.R., 1996. Characterization of paramyxoviruses isolated from three snakes. *Virus Research* **43**, 77–83.
- Rivera, S., Wellehan, J.F.X., McManamon, R., Innis, C.J., Garner, M.M., Raphael, B.L., Gregory, C.R., Latimer, K.S., Rodriguez, C.E., Diaz-Figueroa, O., Marlar, A.B., Nyaoke, A., Gates, A.E., Gilbert, K., Childress, A.L., Risatti, G.R., Frasca, S., 2009. Systemic Adenovirus Infection in Sulawesi Tortoises (*Indotestudo Forsteni*) Caused by a Novel Siadenovirus. *Journal of Veterinary Diagnostic Investigation* **21**, 415–426.
- Rodas, J.D., Salvato, M.S., 2006. Tales of mice and men: Natural History of Arenaviruses. *Revista Colombiana de Ciencias Pecuarias* **19**, 382–400.
- Rojek, J.M., Lee, A.M., Nguyen, N., Spiropoulou, C.F., Kunz, S., 2008. Site 1 Protease Is Required for Proteolytic Processing of the Glycoproteins of the South American Hemorrhagic Fever Viruses Junin, Machupo, and Guanarito. *Journal of Virology* **82**, 6045–6051.
- Rojek, J.M., Moraz, M.-L., Pythoud, C., Rothenberger, S., Van der Goot, F.G., Campbell, K.P., Kunz, S., 2012. Binding of Lassa virus perturbs extracellular matrix-induced signal transduction via dystroglycan. *Cellular Microbiology* **14**.
- Rojek, J.M., Spiropoulou, C.F., Campbell, K.P., Kunz, S., 2007. Old World and

References

- Clade C New World Arenaviruses Mimic the Molecular Mechanism of Receptor Recognition Used by α -Dystroglycan's Host-Derived Ligands . *Journal of Virology* **81**, 5685–5695.
- Romanowski, V., 1993. Genetic organization of Jun´ in virus, the etiological agent of argentine hemorrhagic fever. In: *The Arenaviridae*. New York, pp. 51–83.
- Ronquist, F., Huelsenbeck, J., Teslenko, M., 2011. MrBayes Version 3.2 Manual: Tutorials and Model Summaries.
- Roos, N., Pedersen, K.W., Snijder, E.J., van Tol, H., 2001. Non-structural proteins 2 and 3 interact to modify host cell membranes during the formation of the arterivirus replication complex. *Journal of General Virology* **82**, 985–994.
- Rosenthal, M., Gogrefe, N., Vogel, D., Reguera, J., Rauschenberger, B., Cusack, S., Günther, S., Reindl, S., 2017. Structural insights into reptarenavirus cap-snatching machinery. *PLOS Pathogens* **13**, e1006400.
- Rowe, W.P., Murphy, F.A., Bergold, G.H., Casals, J., Hotchin, J., Johnson, K.M., Lehmann-Grube, F., Mims, C.A., Traub, E., Webb, P.A., 1970. Arenoviruses: Proposed Name for a Newly Defined Virus Group. *Journal of Virology* **5**, 651–652.
- Safronetz, D., Lopez, J.E., Sogoba, N., Traore', S.F., Raffel, S.J., Fischer, E.R., Ebihara, H., Branco, L., Garry, R.F., Schwan, T.G., Feldmann, H., 2010. Detection of Lassa Virus, Mali. *Emerging Infectious Diseases* **16**, 1123–1126.
- Sakai, Y., Kawachi, K., Terada, Y., Omori, H., Matsuura, Y., Kamitani, W., 2017. Two-amino acids change in the nsp4 of SARS coronavirus abolishes viral replication. *Virology* **510**, 165–174.
- Sakuma, T., Noda, T., Urata, S., Kawaoka, Y., Yasuda, J., 2009. Inhibition of Lassa and Marburg Virus Production by Tetherin . *Journal of Virology* **83**, 2382–2385.
- Salas, R., Pacheco, M.E., Ramos, B., Taibo, M.E., Jaimes, E., Vasquez, C., Querales, J., de Manzione, N., Godoy, O., Betancourt, A., Araoz, F., Bruzual, R., Garcia, J., Tesh, R.B., Rico-Hesse, R., Shops, R.E., 2017. Venezuelan haemorrhagic fever. *The Lancet* **338**, 1033–1036.
- Salvato, M., Shimomaye, E., Oldstone, M.B.A., 1989. The primary structure of the lymphocytic choriomeningitis virus L gene encodes a putative RNA polymerase. *Virology* **169**, 377–384.
- Salvato, M.S., 1993. Molecular biology of the prototype arenavirus, Lymphocytic choriomeningitis virus. In: *The Arenaviridae*. New York, pp. 133–156.
- Sawicki, S.G., Sawicki, D.L., 1986. Coronavirus minus-strand RNA synthesis and effect of cycloheximide on coronavirus RNA synthesis. *Journal of Virology* **57**, 328–34.
- Sawicki, S.G., Sawicki, D.L., 2005. Coronavirus transcription: a perspective. *Current Topics in Microbiology and Immunology* **287**, 31–55.
- Sawicki, S.G., Sawicki, D.L., Siddell, S.G., 2007. A Contemporary View of Coronavirus Transcription. *Journal of Virology* **81**, 20–29.
- Schilliger, L., Selleri, P., Frye, F.L., 2011. Lymphoblastic Lymphoma and Leukemic Blood Profile in a Red-Tail Boa (*Boa Constrictor Constrictor*) with Concurrent Inclusion Body Disease. *Journal of Veterinary Diagnostic Investigation* **23**, 159–162.

References

- Schlie, K., Maisa, A., Lennartz, F., Ströher, U., Garten, W., Strecker, T., 2010. Characterization of Lassa virus glycoprotein oligomerization and influence of cholesterol on virus replication. *Journal of Virology* **84**, 983–92.
- Schmitt, A.P., Leser, G.P., Morita, E., Sundquist, W.I., Lamb, R.A., 2005. Evidence for a New Viral Late-Domain Core Sequence, FPIV, Necessary for Budding of a Paramyxovirus. *Journal of Virology* **79**, 2988–2997.
- Schroeder, A., Mueller, O., Stocker, S., Salowsky, R., Leiber, M., Gassmann, M., Lightfoot, S., Menzel, W., Granzow, M., Ragg, T., 2006. The RIN: an RNA integrity number for assigning integrity values to RNA measurements. *BMC Molecular Biology* **7**, 3.
- Schumacher, J., Jacobson, E.R., Burns, R., Tramontin, R.R., 1994. Adenovirus-like Infection in Two Rosy Boas (*Lichanura trivirgata*). *Journal of Zoo and Wildlife Medicine* **25**, 461–465.
- Schwartz, M., Chen, J., Janda, M., Sullivan, M., den Boon, J., Ahlquist, P., 2002. A positive-strand RNA virus replication complex parallels form and function of retrovirus capsids. *Molecular cell* **9**, 505–14.
- Sellner, L.N., Turbett, G.R., 1998. Comparison of Three RT-PCR Methods. *BioTechniques* **25**, 230–234.
- Sevilla, N., Kunz, S., Holz, A., Lewicki, H., Homann, D., Yamada, H., Campbell, K.P., de la Torre, J.C., Oldstone, M.B.A., 2000. Immunosuppression and Resultant Viral Persistence by Specific Viral Targeting of Dendritic Cells. *The Journal of Experimental Medicine* **192**, 1249–1260.
- Shao, J., Liang, Y., Ly, H., 2015. Human Hemorrhagic Fever Causing Arenaviruses: Molecular Mechanisms Contributing to Virus Virulence and Disease Pathogenesis. *Pathogens* **4**, 283–306.
- Shibata, N., Yamamoto, T., Karita, M., Kobayashi, M., Kawaguchi, M., Kato, Y., 2004. Expression of genes related to muscular dystrophy with lissencephaly. *Pediatric Neurology* **31**, 183–190.
- Shimajima, M., Ströher, U., Ebihara, H., Feldmann, H., Kawaoka, Y., 2012. Identification of Cell Surface Molecules Involved in Dystroglycan-Independent Lassa Virus Cell Entry. *Journal of Virology* **86**, 2067–2078.
- Shortridge, K., Oya, A., 1984. Arboviruses in reptiles. *The Southeast Asian Journal of Tropical Medicine and Public Health*.
- Shortridge, K.F., Oya, A., Kobayashi, M., Yip, D.Y., 1975. Arbovirus infections in reptiles: studies on the presence of Japanese encephalitis virus antibody in the plasma of the turtle, *Trionyx sinensis*. *The Southeast Asian journal of tropical medicine and public health* **6**, 161–9.
- Shtanko, O., Watanabe, S., Jasenosky, L.D., Watanabe, T., Kawaoka, Y., 2011. ALIX/AIP1 Is Required for NP Incorporation into Mopeia Virus Z-Induced Virus-Like Particles. *Journal of Virology* **85**, 3631–3641.
- Sievers, F., Wilm, A., Dineen, D., Gibson, T.J., Karplus, K., Li, W., Lopez, R., McWilliam, H., Remmert, M., Soding, J., Thompson, J.D., Higgins, D.G., 2014. Fast, scalable generation of high-quality protein multiple sequence alignments using Clustal Omega. *Molecular Systems Biology* **7**, 539–539.
- Simossis, V.A., Heringa, J., 2005. PRALINE: a multiple sequence alignment toolbox

References

- that integrates homology-extended and secondary structure information. *Nucleic Acids Research* **33**, W289-94.
- Simpson, C.F., Jacobson, E.R., Gaskin, J.M., 1979. Herpesvirus-Like Infection Of The Venom Gland Of Siamese Cobras. *Journal of The American Veterinary Medical Association* **175**, 941–943.
- Smith, D.B., McFadden, N., Blundell, R.J., Meredith, A., Simmonds, P., 2012. Diversity of murine norovirus in wild-rodent populations: species-specific associations suggest an ancient divergence. *Journal of General Virology* **93**, 259–266.
- Snijder, E.J., van der Meer, Y., Zevenhoven-Dobbe, J., Onderwater, J.J.M., van der Meulen, J., Koerten, H.K., Mommaas, A.M., 2006. Ultrastructure and Origin of Membrane Vesicles Associated with the Severe Acute Respiratory Syndrome Coronavirus Replication Complex. *Journal of Virology* **80**, 5927–5940.
- Söding, J., Biegert, A., Lupas, A.N., 2005. The HHpred interactive server for protein homology detection and structure prediction. *Nucleic Acids Research* **33**, 244–248.
- Spiropoulou, C.F., Kunz, S., Rollin, P.E., Campbell, K.P., Oldstone, M.B.A., 2002. New World Arenavirus Clade C, but Not Clade A and B Viruses, Utilizes α -Dystroglycan as Its Major Receptor. *Journal of Virology* **76**, 5140–5146.
- Spuul, P., Balistreri, G., Hellstrom, K., Golubtsov, A. V., Jokitalo, E., Ahola, T., 2011. Assembly of Alphavirus Replication Complexes from RNA and Protein Components in a Novel trans-Replication System in Mammalian Cells. *Journal of Virology* **85**, 4739–4751.
- Stacy, B.A., Wellehan, J.F.X., Foley, A.M., Coberley, S.S., Herbst, L.H., Manire, C.A., Garner, M.M., Brookins, M.D., Childress, A.L., Jacobson, E.R., 2008. Two herpesviruses associated with disease in wild Atlantic loggerhead sea turtles (*Caretta caretta*). *Veterinary Microbiology* **126**, 63–73.
- Stauber, E., Gogolewski, R., 1990. Poxvirus Dermatitis In A Tegu Lizard (Tupinambis-Teguixin). *Journal of Zoo and Wildlife Medicine* **21**, 228–230.
- Stenglein, M.D., Sanchez-Migallon Guzman, D., Garcia, V.E., Layton, M.L., Hoon-Hanks, L.L., Boback, S.M., Keel, M.K., Drazenovich, T., Hawkins, M.G., DeRisi, J.L., 2017. Differential Disease Susceptibilities in Experimentally Reptarenavirus-Infected Boa Constrictors and Ball Pythons. *Journal of Virology* **91**, e00451-17.
- Stenglein, M.D., Sanders, C., Kistler, A.L., Ruby, J.G., Franco, J.Y., Reavill, D.R., Dunker, F., DeRisi, J.L., 2012. Identification, Characterization, and In Vitro Culture of Highly Divergent Arenaviruses from Boa Constrictors and Annulated Tree Boas: Candidate Etiological Agents for Snake Inclusion Body Disease. *mBio* **3**, e00180-12-e00180-12.
- Stephen, F., Altschul, Warren, G., Webb, M., Eugene, W.M., Lipman, D.J., 1990. Basic local alignment search tool. *Molecular Biology* **251**, 403–410.
- Stertz, S., Reichelt, M., Spiegel, M., Kuri, T., Martínez-Sobrido, L., García-Sastre, A., Weber, F., Kochs, G., 2007. The intracellular sites of early replication and budding of SARS-coronavirus. *Virology* **361**, 304–315.
- Strecker, T., Eichler, R., Meulen, J. ter, Weissenhorn, W., Dieter Klenk, H., Garten,

References

- W., Lenz, O., 2003. Lassa virus Z protein is a matrix protein and sufficient for the release of virus-like particles. *Journal of Virology* **77**, 10700–5.
- Strecker, T., Maisa, A., Daffis, S., Eichler, R., Lenz, O., Garten, W., 2006. The role of myristoylation in the membrane association of the Lassa virus matrix protein Z. *Virology Journal* **3**, 93.
- Sumi, V., Singh, S.D., Dhama, K., Gowthaman, V., Barathidasan, R., Sukumar, K., 2012. Isolation and molecular characterization of infectious bronchitis virus from recent outbreaks in broiler flocks reveals emergence of novel strain in India. *Tropical Animal Health and Production* **44**, 1791–1795.
- Sun, M., Fuentes, S.M., Timani, K., Sun, D., Murphy, C., Lin, Y., August, A., Teng, M.N., He, B., 2008. Akt Plays a Critical Role in Replication of Nonsegmented Negative-Stranded RNA Viruses. *Journal of Virology* **82**, 105–114.
- Swanepoel, R., Leman, P.A., Shepherd, A.J., Shepherd, S.P., Kiley, M.P., McCormick, J.B., 1985. Identification Of Ippy As A Lassa-Fever-Related Virus. *The Lancet* **325**, 639.
- Tan, K.B., 1970. Electron microscopy of cells infected with Semliki forest virus temperature-sensitive mutants: correlation of ultrastructural and physiological observations. *Journal of Virology* **5**, 632–8.
- Teijaro, J.R., Ng, C., Lee, A.M., Sullivan, B.M., Sheehan, K.C.F., Welch, M., Schreiber, R.D., Carlos de la Torre, J., Oldstone, M.B.A., 2013. Persistent LCMV Infection Is Controlled by Blockade of Type I Interferon Signaling. *Science* **340**, 207–211.
- Ter Meulen, J., Koulemou, K., Wittekindt, T., Windisch, K., Strigl, S., Conde, S., Schmitz, H., 1998. Detection of Lassa virus antinucleoprotein immunoglobulin G (IgG) and IgM antibodies by a simple recombinant immunoblot assay for field use. *Journal of clinical microbiology* **36**, 3143–8.
- Ter Meulen, J., Lukashevich, I., Sidibe, K., Inapogui, A., Marx, M., Dorlemann, A., Yansane, M.L., Koulemou, K., Chang-Claude, J., Schmitz, H., 1996. Hunting of peridomestic rodents and consumption of their meat as possible risk factors for rodent-to-human transmission of Lassa virus in the Republic of Guinea. *The American Society of Tropical Medicine and Hygiene* **55**, 661–662.
- Thierry, E., Guilligay, D., Kosinski, J., Bock, T., Gaudon, S., Round, A., Pflug, A., Hengrung, N., El Omari, K., Baudin, F., Hart, D.J., Beck, M., Cusack, S., 2016. Influenza Polymerase Can Adopt an Alternative Configuration Involving a Radical Repacking of PB2 Domains. *Molecular Cell* **61**, 125–37.
- Trapido, H., Sanmartín, C., 1971. Pichindé Virus. *The American Journal of Tropical Medicine and Hygiene* **20**.
- Trombley, A.R., Wachter, L., Garrison, J., Buckley-beason, V.A., Jahrling, J., Hensley, L.E., Schoepp, R.J., Norwood, D.A., Goba, A., Fair, J.N., Kulesh, D.A., 2010. Short Report: Comprehensive Panel of Real-Time TaqMan™ Polymerase Chain Reaction Assays for Detection and Absolute Quantification of Filoviruses, Arenaviruses, and New World Hantaviruses. *The American Journal of Tropical Medicine and Hygiene* **82**, 954–960.
- Ulasli, M., Verheije, M.H., De Haan, C.A.M., Reggiori, F., 2010. Qualitative and quantitative ultrastructural analysis of the membrane rearrangements induced by coronavirus. *Cellular Microbiology* **12**, 844–861.

References

- Urata, S., Yasuda, J., 2012. Molecular Mechanism of Arenavirus Assembly and Budding. *Viruses* **4**, 2049–2079.
- V'kovski, P., Al-Mulla, H., Thiel, V., Neuman, B.W., 2015. New insights on the role of paired membrane structures in coronavirus replication. *Virus Research* **202**, 33–40.
- Van Damme, N., Goff, D., Katsura, C., Jorgenson, R.L., Mitchell, R., Johnson, M.C., Stephens, E.B., Guatelli, J., 2008. The Interferon-Induced Protein BST-2 Restricts HIV-1 Release and Is Downregulated from the Cell Surface by the Viral Vpu Protein. *Cell Host & Microbe* **3**, 245–252.
- Van Houtan, K.S., Hargrove, S.K., Balazs, G.H., 2010. Land Use, Macroalgae, and a Tumor-Forming Disease in Marine Turtles. *PLOS ONE* **5**, e12900.
- Van Regenmortel, M.H. V, Fauquet, C.M., Bishop, D.H.L., 2000. Virus Taxonomy: Classification and Nomenclature of Viruses: Seventh Report of the International Committee on Taxonomy of Viruses. Academic Press.
- Vancraeynest, D., Pasmans, F., Martel, A., Chiers, K., Meulemans, G., Mast, J., Zwart, P., Ducatelle, R., 2006. Inclusion body disease in snakes: a review and description of three cases in boa constrictors in Belgium. *Veterinary Record* **158**, 757 LP – 761.
- Vennemann, M., Koppelkamm, A., 2010. mRNA profiling in forensic genetics I: Possibilities and limitations. *Forensic Science International* **203**, 71–75.
- Vieler, E., Baumgärtner, W., Herbst, W., Köhler, G., 1994. Characterization of a reovirus isolate from a rattle snake, *Crotalus viridis*, with neurological dysfunction. *Archives of Virology* **138**, 341–344.
- Vieth, S., Drosten, C., Charrel, R., Feldmann, H., Stephan, G., 2005. Establishment of conventional and fluorescence resonance energy transfer-based real-time PCR assays for detection of pathogenic New World arenaviruses. *Journal of Clinical Virology* **32**, 229–235.
- Vieth, S., Drosten, C., Lenz, O., Vincent, M., Omilabu, S., Hass, M., Becker-Ziaja, B., ter Meulen, J., Nichol, S.T., Schmitz, H., Günther, S., 2007. RT-PCR assay for detection of Lassa virus and related Old World arenaviruses targeting the L gene. *Transactions of the Royal Society of Tropical Medicine and Hygiene* **101**, 1253–1264.
- Vieth, S., Torda, A.E., Asper, M., Schmitz, H., Günther, S., 2004. Sequence analysis of L RNA of Lassa virus. *Virology* **318**, 153–68.
- Vignuzzi, M., Stone, J.K., Arnold, J.J., Cameron, C.E., Andino, R., 2006. Quasispecies diversity determines pathogenesis through cooperative interactions within a viral population. *Nature* **439**, 344–348.
- Villafane, F., Roderiguez, G., Martinelli, G., Mantilla, O., 1996. Principales enfermedades que afectan a algunas explotaciones comerciales de Caiman crocodiles fuscus en la costa norte Colombiana. *IUCN World Conservation Congress* 342-346.
- Volpon, L., Osborne, M.J., Capul, A.A., de la Torre, J.C., Borden, K.L.B., 2010. Structural characterization of the Z RING-eIF4E complex reveals a distinct mode of control for eIF4E. *Proceedings of the National Academy of Sciences of the United States of America* **107**, 5441–5446.

References

- von Brunn, A., Teepe, C., Simpson, J.C., Pepperkok, R., Friedel, C.C., Zimmer, R., Roberts, R., Baric, R., Haas, J., 2007. Analysis of Intraviral Protein-Protein Interactions of the SARS Coronavirus ORFeome. *PLOS ONE* **2**, e459.
- Walker, D.H., McCormick, J.B., Johnson, K.M., Webb, P.A., Komba-Kono, G., Elliott, L.H., Gardner, J.J., 1982. Pathologic and virologic study of fatal Lassa fever in man. *The American Journal of Pathology* **107**, 349–356.
- Wallace, D.C., 1999. Mitochondrial Diseases in Man and Mouse. *Science* **283**, 1482–1488.
- Wang, J., Danzy, S., Kumar, N., Ly, H., Liang, Y., 2012. Biological Roles and Functional Mechanisms of Arenavirus Z Protein in Viral Replication. *Journal of Virology* **86**, 9794–9801.
- Wang, Y., Mao, H., Yi, Z., 2017. Protein secondary structure prediction by using deep learning method. *Knowledge-Based Systems* **118**, 115–123.
- Waterhouse, A.M., Procter, J.B., Martin, D.M.A., Clamp, M., Barton, G.J., 2009. Jalview Version 2-A multiple sequence alignment editor and analysis workbench. *Bioinformatics* **25**, 1189–1191.
- Webb, P.A., Johnson, K.M., Hibbs, J.B., Kuns, M.L., 1970. Parana, a new tacaribe complex virus from Paraguay. *Archiv für die gesamte Virusforschung* **32**, 379–388.
- Weinmann, N., Papp, T., de Matos, A.P.A., Teifke, J.P., Marschang, R.E., 2007. Experimental Infection of Crickets (*Gryllus Bimaculatus*) with an Invertebrate Iridovirus Isolated from a High-Casqued Chameleon (*Chamaeleo Hoehnelii*). *Journal of Veterinary Diagnostic Investigation* **19**, 674–679.
- Wellehan, J.F.X., Childress, A.L., Marschang, R.E., Johnson, A.J., Lamirande, E.W., Roberts, J.F., Vickers, M.L., Gaskin, J.M., Jacobson, E.R., 2009. Consensus nested PCR amplification and sequencing of diverse reptilian, avian, and mammalian orthoreoviruses. *Veterinary Microbiology* **133**, 34–42.
- Wellehan, J.F.X., Johnson, A.J., Harrach, B., Benkö, M., Pessier, A.P., Johnson, C.M., Garner, M.M., Childress, A., Jacobson, E.R., 2004. Detection and Analysis of Six Lizard Adenoviruses by Consensus Primer PCR Provides Further Evidence of a Reptilian Origin for the Atadenoviruses. *Journal of Virology* **78**, 13366–13369.
- Welsch, S., Miller, S., Romero-Brey, I., Merz, A., Bleck, C.K.E., Walther, P., Fuller, S.D., Antony, C., Krijnse-Locker, J., Bartenschlager, R., 2009. Composition and Three-Dimensional Architecture of the Dengue Virus Replication and Assembly Sites. *Cell Host & Microbe* **5**, 365–375.
- West, G., Garner, M., Raymond, J., Latimer, K.S., Nordhausen, R., 2001. Meningoencephalitis in a Boelen's python (*Morelia boeleni*) associated with paramyxovirus infection. *Journal of Zoo and Wildlife Medicine* **32**, 360–5.
- Westaway, E.G., Mackenzie, J.M., Kenney, M.T., Jones, M.K., Khromykh, A.A., 1997. Ultrastructure of Kunjin virus-infected cells: colocalization of NS1 and NS3 with double-stranded RNA, and of NS2B with NS3, in virus-induced membrane structures. *Journal of Virology* **71**, 6650–61.
- Westhouse, R.A., Jacobson, E.R., Harris, R.K., Winter, K.R., Homer, B.L., 1996. Respiratory and Pharyngo-Esophageal Iridovirus Infection in a Gopher Tortoise

References

- (Gopherus polyphemus). *Journal of Wildlife Diseases* **32**, 682–686.
- Wolff, S., Ebihara, H., Groseth, A., 2013. Arenavirus budding: A common pathway with mechanistic differences. *Viruses* **5**, 528–549.
- Wozniak, E., McBride, J., DeNardo, D., Tarara, R., Wong, V., Osburn, B., 2000. Isolation and Characterization of an Antigenically Distinct 68- kd Protein from Nonviral Intracytoplasmic Inclusions in Boa Constrictors Chronically Infected with the Inclusion Body Disease Virus (IBDV: Retroviridae). *Veterinary Pathology* **37**, 449–459.
- Wulff, H., McIntosh, B.M., Hamner, D.B., Johnson, K.M., 1977. Isolation of an arenavirus closely related to Lassa virus from Mastomys natalensis in south-east Africa. *Bulletin of the World Health Organization* **55**, 441–444.
- Wyneken, J., 2001. The Anatomy of Sea Turtles, Department of Commerce NOAA Technical Memorandum NMFS-SEFSC-470. Miami.
- York, J., Nunberg, J.H., 2007. A Novel Zinc-Binding Domain Is Essential for Formation of the Functional Junin Virus Envelope Glycoprotein Complex . *Journal of Virology* **81**, 13385–13391.
- Yount, B., Curtis, K.M., Baric, R.S., 2000. Strategy for systematic assembly of large RNA and DNA genomes: transmissible gastroenteritis virus model. *Journal of Virology* **74**, 10600–11.
- Yount, B., Denison, M.R., Weiss, S.R., Baric, R.S., 2002. Systematic assembly of a full-length infectious cDNA of mouse hepatitis virus strain A59. *Journal of Virology* **76**, 11065–78.
- Zapata, J.C., Carrion, R., Patterson, J.L., Crasta, O., Zhang, Y., Mani, S., Jett, M., Poonia, B., Djavani, M., White, D.M., Lukashevich, I.S., Salvato, M.S., 2013. Transcriptome Analysis of Human Peripheral Blood Mononuclear Cells Exposed to Lassa Virus and to the Attenuated Mopeia/Lassa Reassortant 29 (ML29), a Vaccine Candidate. *PLOS Neglected Tropical Diseases* **7**.
- Zapata, J.C., Salvato, M.S., 2013. Arenavirus variations due to host-specific adaptation. *Viruses* **5**, 241–278.
- Zheng, W., Tao, Y.J., 2013. Structure and assembly of the influenza A virus ribonucleoprotein complex. *FEBS Letters* **587**, 1206–1214.
- Zhou, X., Cong, Y., Veenendaal, T., Klumperman, J., Shi, D., Mari, M., Reggiori, F., 2017. Ultrastructural Characterization of Membrane Rearrangements Induced by Porcine Epidemic Diarrhea Virus Infection. *Viruses* **9**, 251.
- Zhou, Xin, Jackson, A.O., Sun, K., Chen, X., Li, Z., Zhou, Xueping, Wang, Q., Qian, S., Ma, X., 2015. Rescue of a Plant Negative-Strand RNA Virus from Cloned cDNA: Insights into Enveloped Plant Virus Movement and Morphogenesis. *PLOS Pathogens* **11**, e1005223.